PILE DRIVING AND LOADING TESTS

Lock and Dam No. 4
Arkansas River and Tributaries
Arkansas and Oklahoma

Prepared by

FRUCO AND ASSOCIATES
1706 OLIVE ST.
ST. LOUIS 3, MISSOURI

For

U. S. Army Engineer District, Little Rock
CORPS OF ENGINEERS
Little Rock, Arkansas
September 1964

199

PILE DRIVING AND LOADING TESTS

Lock and Dam No. 4
Arkansas River and Tributaries
Arkansas and Oklahoma

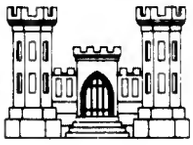

Prepared by

FRUCO AND ASSOCIATES
1706 OLIVE ST.
ST. LOUIS 3, MISSOURI

For

U. S. Army Engineer District, Little Rock
CORPS OF ENGINEERS
Little Rock, Arkansas
September 1964

BLANK PAGE

PREFACE

This report presents the results of a comprehensive pile testing investigation made to develop information regarding the characteristics of different pile driving hammers; the load carrying capacity of different types of piles driven into alluvial sands of the Arkansas River; and the effect of group action on the behavior of laterally loaded piles. The study included field driving and loading tests on bearing piles, model and laboratory tests, driving and extraction tests on steel sheet piling, and evaluation of the test data. The study was performed for the U. S. Army Engineer District, Little Rock, in connection with the design and construction of the locks and dams for the Arkansas River Navigation Project.

This investigation was made by Fruco & Associates, Engineers and Architects, under the direction of C. I. Mansur, Vice President. R. J. Dietrich, Senior Soils Engineer, participated in planning the investigation. Pile driving and field testing were under the supervision of J. C. Hicks, Civil Engineer. Evaluation of the field data was accomplished by A. H. Hunter, Principal Soils Engineer; M. Alizadeh, Senior Structural Engineer; and M. C. Skouby, Soils Engineer. The model studies were made under the direction of M. T. Davisson, Foundation Engineer. J. R. Salley performed the model testing and assisted in evaluation of the data. This report was prepared by C. I. Mansur, A. H. Hunter, and M. T. Davisson. General consultation services for this project were provided by Dr. R. B. Peck and Dr. M. T. Davisson, University of Illinois. H. J. Duffy of Washington University, St. Louis, provided consultation on electric strain instrumentation.

The Raymond Concrete Pile Division, Raymond International, Inc., Kansas City District, drove the piles driven with steam and diesel hammers and was responsible for loading the piles. Driving tests made with the Bodine hammer were subcontracted to the C. L. Guild Construction Company, Providence, Rhode Island. Site grading was accomplished by Steed and Jones, Contractors, Inc., of Pine Bluff, Arkansas. The dewatering wells were installed by the Layne-Arkansas Company.

The Contracting Officer for this investigation was Colonel Charles D. Maynard, District Engineer, U. S. Army Engineer District,

Little Rock. Administrative and technical supervision of the contract was provided by E. F. Rutt, Chief of the Engineering Division; F. W. Sims, Chief of the Foundations and Materials Branch; and H. A. Rabjohn, Assistant Chief of the Foundations and Materials Branch. John W. Gillmore was Project Engineer for the Corps of Engineers.

PILE DRIVING AND LOADING TESTS

Lock and Dam 4

TABLE OF CONTENTS

Page

PART III: FIELD LOAD TESTS

PART IV: MODEL PILE TEST PROGRAM

LIST OF FIGURES

LIST OF TABLES

LIST OF PLATES (Field Tests)

LIST OF PLATES (Model Tests)

PILE DRIVING AND LOADING TESTS

Lock and Dam 4

PART I: INTRODUCTION

Project Description

Navigation project

1. Navigation of the Arkansas River from Catoosa, Oklahoma, near Tulsa to the Mississippi River through a series of low lift locks and dams is currently planned as a part of the multi-purpose program for development of the Arkansas River and tributaries in Arkansas and Oklahoma. The proposed navigation project includes construction of 19 locks and dams, provision of a channel 9 ft in depth and 250 ft in width, together with related channel improvements and stabilization works. Development of the navigation project within the boundaries of the U. S. Army Engineer District, Little Rock, Corps of Engineers, will require the construction of 12 locks and dams in Arkansas, four of which are on the lower Arkansas River below Pine Bluff, Arkansas. The proposed lock chambers will be 110 x 600 ft with dams varying from low fixed weir overflow types to gravity types equipped with tainter gates as required by pool and terrain conditions. A schematic plan of the proposed navigation project in Arkansas is shown on Fig. 1.

Structural foundations

2. Subsurface investigations made for the proposed navigation structures indicate that a deep sand stratum exists at four of the lock and dam sites in the lower Arkansas River Valley downstream from Pine Bluff, Arkansas. At these sites, strata of loose surface silts, sandy silts and clays of variable thickness overlie a stratum of medium to dense sand and silty sand with a thickness ranging from 90 to 150 ft, which in turn overlies a stratum of deeply bedded Tertiary clay.

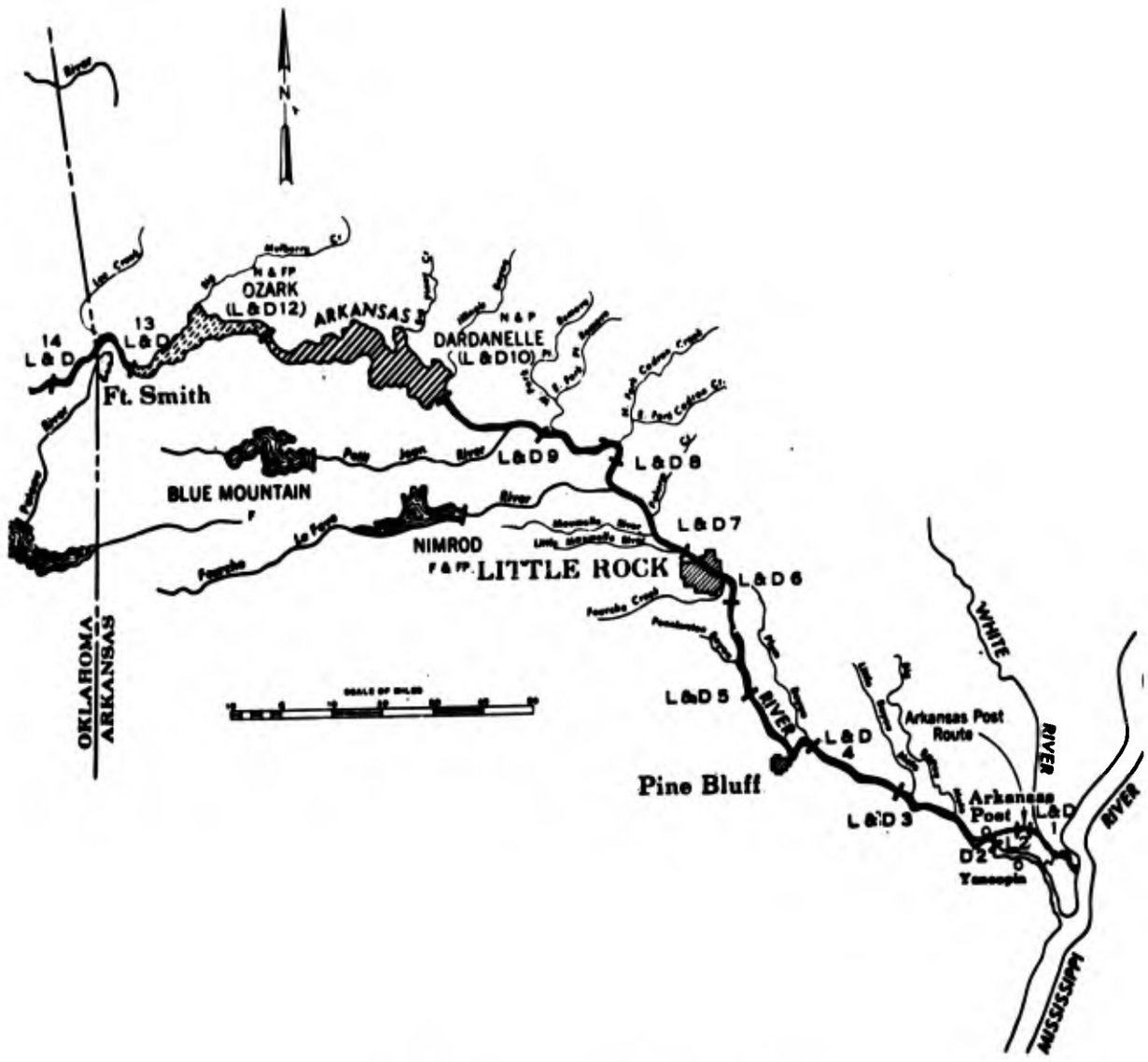

Fig. 1 - ARKANSAS RIVER NAVIGATION PROJECT

Foundation piling were selected to support these structures to insure stability and minimize settlements. The piles will derive their support from combined friction and point bearing obtained from penetration into the deep sand stratum. The piling will be driven in dewatered excavations, but will be submerged during the operational life of the structures. High-capacity piling on relatively close centers will be required for the heavy semi-gravity type lock walls, gate monoliths, and dam piers. Compressive loadings will range from 100 to 165 tons; and tensile loads will range up to 40 tons. Timber piles will be used for bearing and tension piles beneath the stilling basins for Dams 2, 3, and 4. Lateral loadings of vertical piles will approach 15 tons at Locks 1 and 2, where unbalanced lateral forces will be resisted by bending in bearing piles and by struts extending across the lock chamber. Steel sheet piling will be used for seepage and erosion control in the cohesionless sands, for guide wall cells, and for cofferdams.

Pile Investigation

General objectives

3. In view of the magnitude of the proposed construction and the lack of factual information regarding the driving and axial and lateral load carrying capabilities of piles in the lower Arkansas River Valley, a comprehensive pile testing program was initiated by the U. S. Army Engineer District, Little Rock, Corps of Engineers, to develop criteria for design and construction of pile foundations for the locks and dams to be founded on sand. An engineering services contract was awarded to Fruco & Associates, Inc., Engineers-Architects, St. Louis, Missouri, for the investigation work which included development of the test site, driving and testing the piling, and analysis of the test data. The general objectives of the pile investigation were to establish the following criteria:

a. Design and construction criteria for axially loaded piles, including:

(1) Size and penetration of various types of bearing piling required to provide design capacities in compression and tension.

(2) Type and size of pile hammers required for economical driving of suitable bearing piles.

(3) Relationship between driving resistance and compressive capacity of bearing piles.

(4) Effect of jetting on the driving and load carrying characteristics of displacement piles.

b. Design criteria for laterally loaded piles, including:

(1) Behavior of isolated vertical and batter piles subjected to lateral loadings.

(2) Effect of repetitive lateral loading on the deflection of isolated piles.

(3) Relationship between the behavior of isolated piles and pile groups subjected to lateral loadings.

(4) Influence of pile groups on the lateral deformation characteristics of opposed pile groups.

(5) Validity of "Hrennikoff" type analysis for laterally loaded pile groups containing vertical and batter piles.

c. Driving and pulling criteria for sheet piles

Scope

4. The basic pile investigation included field driving and loading tests on a variety of pile types, field driving and pulling tests on sheet piles, and model tests on single and groups of piles. Field driving tests were made on square prestressed concrete piles, steel pipe piles, steel H-piles, and a timber pile, and on medium arch and Z-type steel sheet piles, using different types of hammers. All of the above piling, except the timber pile, were driven with both double-acting steam hammers and a Bodine sonic vibratory hammer. The timber pile was driven with a double-acting (65C) steam hammer only. Supplemental driving tests were made on prestressed concrete piles and a pipe pile using water jets and a double-acting (140C) steam hammer. A prestressed concrete pile was also driven with a DE-40 diesel hammer. The field tests included compression, tension, and lateral loading of single piles. Strain instruments were attached to steel piles to determine the distribution of stress in the piles under compression, tension, and lateral loads.

The lateral load tests were made to measure the horizontal load carrying capacity of a pile, the effect of cyclic loading on deflection, and the soil modulus and its distribution with depth. The scope of the field testing program conducted to achieve the above objectives is summarized below and detailed in Table 1.

Group I - Driving 12-in., 16-in., and 20-in. diameter steel pipe piles, 55 ft in length, using a 140C steam hammer, and load testing to determine the effect of diameter on axial bearing and lateral load capacity, and to determine the soil modulus for displacement type piling. The 16-in. pipe pile was tested in compression, then subjected to cyclic lateral loading, and then retested in compression to determine the effect of repetitive lateral loading on bearing capacity.

Group II - Driving 16-in. square prestressed concrete piles, 45 ft and 55 ft in length, using a 140C steam hammer, and load testing to determine the effect of penetration on capacity of displacement type piling.

Group III - Driving 14BP73 steel H-piling, 42 ft and 55 ft in length, using an 80C steam hammer, and load testing to determine the effect of penetration on capacity of non-displacement type piling. The 42-ft pile was also subjected to 100 cycles of a 20-kip lateral load to measure increase in deflection with repetitive loading.

Group IV - Driving a Class A timber pile with a 65C steam hammer, and load testing to determine the capacity of a timber pile.

Group V - Driving 14BP73 steel H, 16-in. steel pipe, and 16-in. prestressed concrete piles, 55 ft in length, with a Bodine hammer, and load testing for comparison of capacity with similar piles driven with double-acting steam hammers. Comparative driving tests were also made on a 20-in. prestressed concrete pile using a 140C steam hammer and a Bodine hammer. This pile was also subjected to a 100-cycle lateral load test to measure increase in deflection with repetitive loading on a displacement type pile.

Group VI - Driving 14BP73 steel H-piles, 45 ft in length, both vertically and on 3:1 batter with an 80C steam hammer, and testing to determine the lateral capacity of pile and soil reaction to the pile.

Group VII - Jetting a 16-in. steel pipe pile and four surrounding prestressed concrete piles to 38 ft, and driving the five piles to a penetration of 53 ft using a 140C steam hammer, and load testing the 16-in. pipe pile to determine effect of jetting on capacity.

Group VIII - Driving test on a 16-in. prestressed concrete pile with a McKiernan-Terry DE-40 diesel hammer for comparison with driving experience with other hammers used.

Group IX - Driving and pulling tests on MP112 and MZ32 sheet pile using steam hammers and the Bodine hammer to determine driving characteristics and the depth to which these types of sheet piling could be driven with various types of hammers and extracted.

Model tests

5. Model tests were made to determine the relationship between the load-deformation behavior of isolated piles and pile groups. Scaled test piles were embedded in sand in a tank in the laboratory and were subjected to vertical and lateral loadings. Basic tests were made on isolated piles to verify the model and analytical procedures and to determine basic pile and soil constants. Model tests were also performed on idealized groups, and on prototype lock and dam pile groupings to determine the effect of group action and of repetitive loading on lateral deformation, and to check the validity of a Hrennikoff-type analysis for pile groups. The detailed scope of the model testing program in given in Table 2. A general description of the model tests and the specific test objectives are summarized below:

Group I - Compression tests on three sizes each of round and square test piles of variable penetration to determine the effect of size and length on bearing capacity.

Group II - Lateral load tests on single piles of variable flexural stiffness to determine the effect of flexural stiffness of the pile on the lateral subgrade modulus of the soil.

Group III - Lateral load tests to compare the lateral load-deflection characteristics of an isolated pile with those of a rigid wall. The effect of an opposing laterally loaded wall on the deflection of a laterally loaded wall located at a scaled distance equal to 110 ft in the prototype was also evaluated.

Group IV - Load tests on a pair of vertical piles and two pairs of batter piles capped and subjected to vertical and lateral loads. Load distributions were measured and compared with theoretical distributions computed using a Hrennikoff-type analysis. The axial, translational, and rotational stiffnesses of the piles were experimentally determined for utilization in the theoretical analysis.

Group V - Repetitive lateral load tests on a scaled model composed of three lock wall monoliths on vertical piles opposing three lock wall monoliths on batter piles. The walls were located at a scaled distance equal to 110 ft in the prototype. The lateral load versus deflection relationships were evaluated.

Group VI - Repetitive lateral load tests on a scaled model of three monoliths of a typical dam section on battered piles for comparison with similar tests on single piles.

Report

6. The results and analyses of the field and model testing accomplished in this study are presented in this report. They include (a) driving and loading tests on bearing piles, (b) driving and pulling tests on sheet piles, (c) field and model lateral load tests, and (d) criteria for the design and driving of foundation piling for the locks and dams to be founded on sand in the lower Arkansas River Valley. Design criteria presented include curves for selection of size and length of steel pipe piles, prestressed concrete piles, steel H piles, and timber piles subjected to compressive and tensile loads, and general procedures for the design of laterally loaded piles. General driving criteria for bearing and sheet piles are also included. All of the driving data; compression, tension, and lateral load test data; analyses and evaluations; and design and driving criteria presented in this report are based on the foundation soil being cohesionless sand with the water table at or within 2 or 3 ft of the ground surface. However, the results and analyses are also applicable to other water table levels provided appropriate adjustments are made for resulting changes in effective density of the foundation sand.

PART II: TEST PILES AND PILE DRIVING

Pile Test Site

Location

7. The field testing phase of the pile test program was conducted at a site having subsurface conditions similar to the subsurface conditions at the four sites for the proposed locks and dams to be founded on sands in the lower Arkansas River below Pine Bluff, Arkansas. The site was located one mile downstream of the Rob Roy Bridge on the St. Louis and Southwestern Railroad, and about 500 ft east of the east bank of the Arkansas River near the proposed site for Lock and Dam 4. The location and general features of the test site are shown by the aerial photograph on Fig. 2.

Foundation and soil conditions

8. Soil conditions at the pile test site were determined by exploratory borings and laboratory tests made in connection with the foundation investigation for Lock and Dam 4, and by further explorations made specifically for this project. The locations of the borings applicable to the test site are shown on Plate 1. Phase I borings (zero and 100 series) were made to determine the subsurface conditions at Lock and Dam 4. The Phase II borings (200 series) were made to determine the effect of the 20-ft excavation, at the test site, on the relative density of the subgrade as indicated by standard penetration resistance. The supplemental Phase III borings (300 series) were made to determine the effect of pile driving operations on subgrade density and the cause for hard driving of test piles 8 and 11A at penetrations of about 15 ft. The characteristics and physical properties of the foundation soils at the site were determined from classification tests made by the U. S. Army Engineer District, Little Rock, supplemented by detailed testing of selected samples by the U. S. Army Engineer Division, Southwestern, Laboratory, Dallas, Texas.

9. Boring logs depicting the general subsurface conditions at the test site are shown on Plate 2. These logs indicate that three major soil strata exist at the test site: a surface blanket of silt and fine sand which extends from the ground surface at about el 198 to el 185; a deep stratum of relatively dense medium to fine sand which

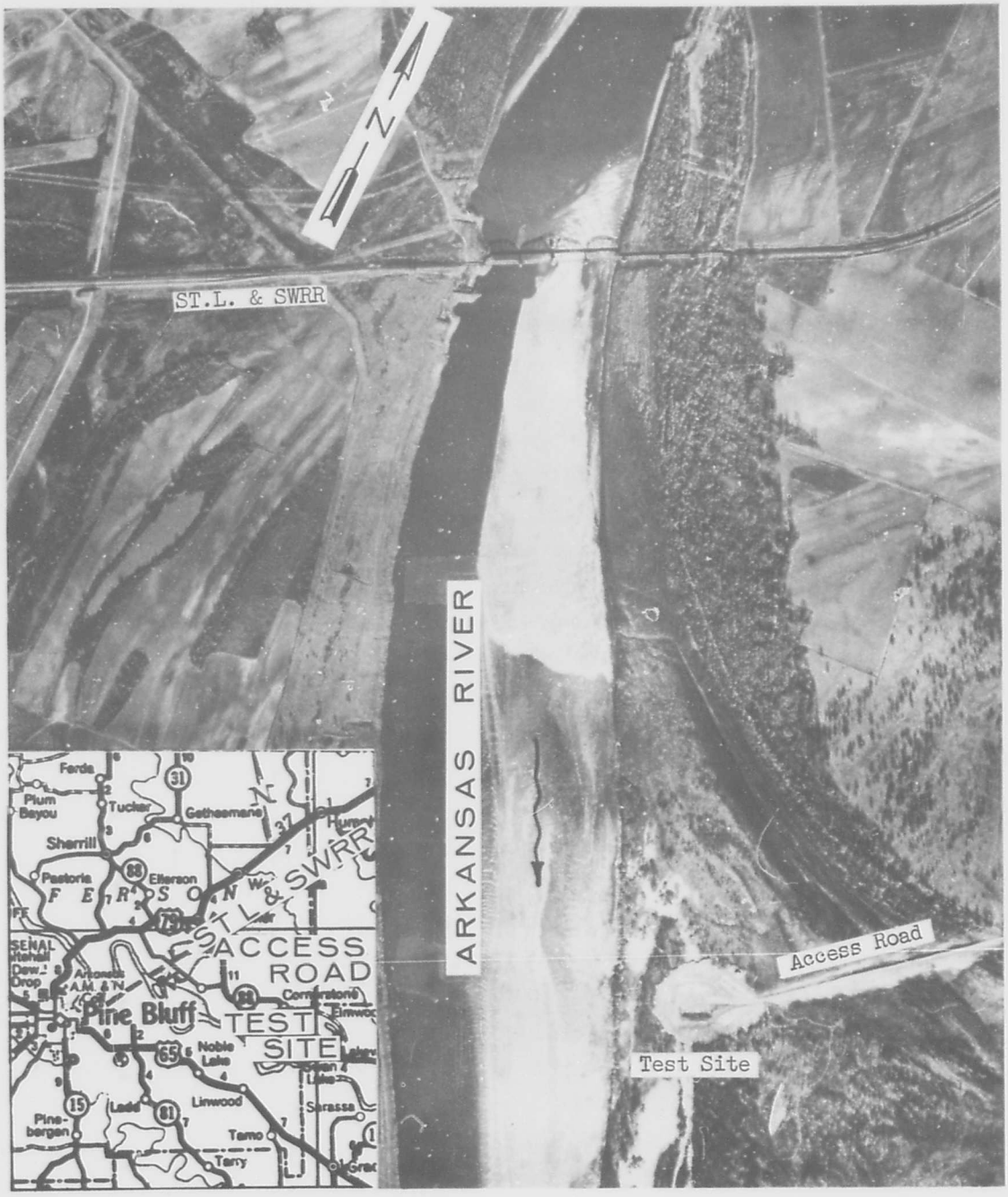

Fig. 2 - PILE TEST SITE LOCATION

extends to about el 92; and a basal stratum of Tertiary clay of undetermined thickness. Some thin seams of silt and clay are present in the deep sand stratum between el 160 and 137. The standard penetration resistance of the upper 60 ft of the deep sand stratum into which the piles were driven generally increases with depth varying from 16 to 67 blows per ft with an average of about 32 blows per ft prior to site excavation. The average dry density ranged from 90 to 109 lbs per cu ft but did not show any significant trend with depth. After the 20-ft excavation for the site was completed, the average penetration resistance of the same zone decreased to about 27 blows per ft with no measurable change in density. No significant change in penetration resistance was noted from the 300 series borings made following the pile driving. Logs were encountered in several of these borings within the top 20 ft of subgrade; these logs may have caused the hard driving of test piles 8 and 11A at about this depth of penetration. Piezometer readings taken during driving and testing are plotted on graph (a), Fig. 3. The ground water table generally varied from 2 to 3 ft below the bottom of the excavation during this period; it was essentially level at the site except for a slight slope riverward.

Laboratory tests

10. Results of mechanical analyses made on samples from the deep sand stratum at the test site are shown on graph (a), Plate 3; shear tests and mechanical analyses on comparable sands from borings made at the initial site for Lock and Dam 4 are presented on graphs (c) and (d), Plate 4. The results of special shear tests made to determine the sliding friction between pile materials and foundation sands are given in Table 3, and are shown graphically on graphs (a) and (b), Plate 4. The physical properties assigned to the deep sand stratum for evaluation of the pile test results are presented below:

Classification - Medium to fine sands and silty sands (SM-SP)
Submerged Unit Weight of Sand - 62.8 lbs per cu ft
Sliding Friction, Steel on Sand - 25° (Range 23°-30°)
Sliding Friction, Mortar on Sand - 30° (Range 28°-36°)
Internal Friction of Sand Subgrade - 32° (Range 31°-35°)

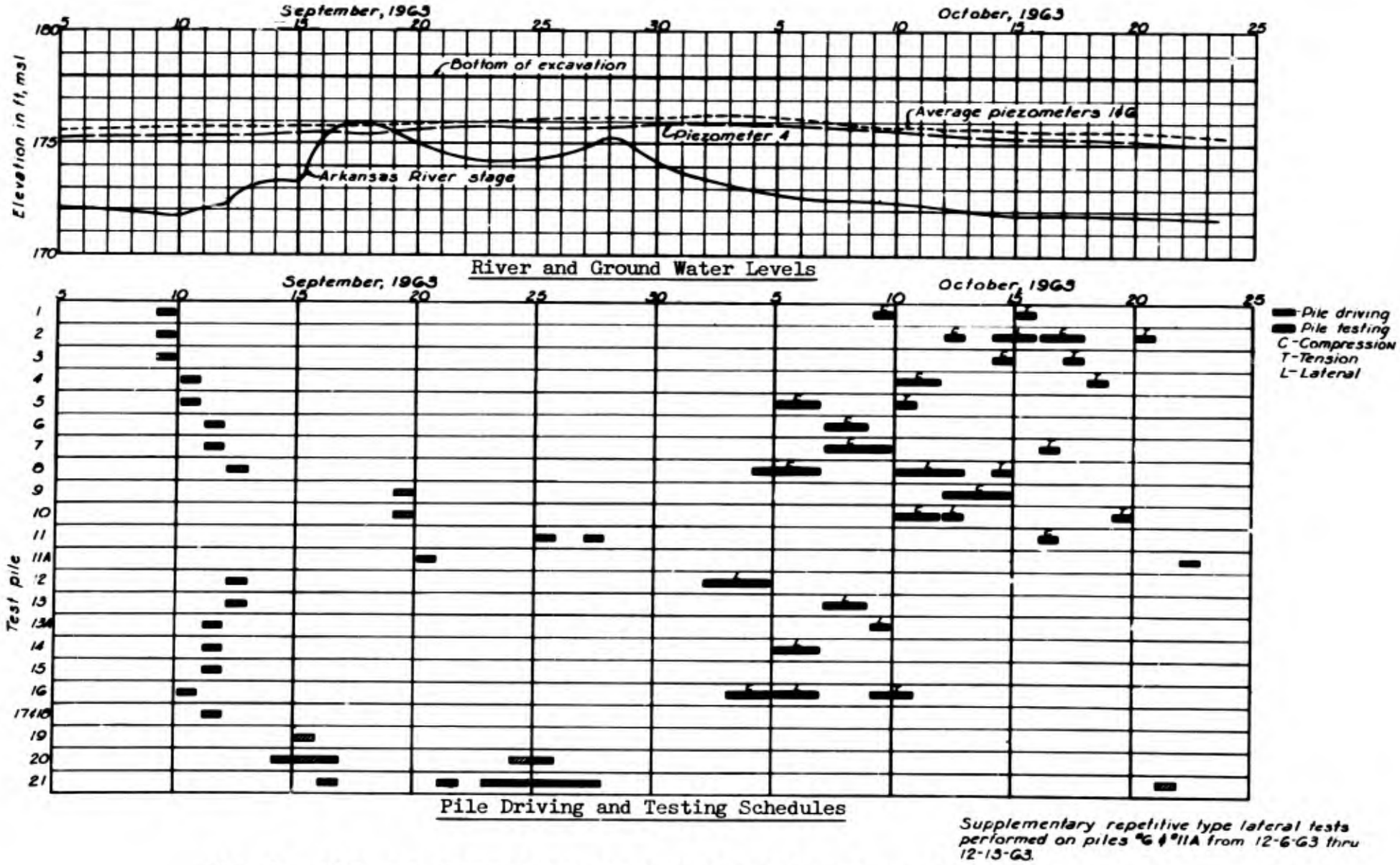

Fig. 3 - RIVER AND GROUND WATER LEVELS DURING FIELD DRIVING AND TESTING

The standard penetration resistance as a function of depth at the test site prior to excavation and at the proposed sites for Locks and Dams 1 through 4 is shown graphically on graph (b), Plate 3. The curves permit comparing the relative density of the subgrades at the various lock sites with that of the pile test site for evaluation of pile behavior at the other sites.

Site development

11. An area was prepared at the pile test site to simulate insofar as practicable the subgrade and overburden stress conditions which will prevail during construction and operation of the locks and dams. Site preparation included excavation of an area 160 ft x 150 ft down to el 178 (20 ft depth), the top of the deep sand stratum and near the minimum ground water elevation expected during the driving and testing period. The excavated material was used to form a protective levee around the site as shown on Plate 5. A dewatering system consisting of five 16-in. diameter wells was installed around the perimeter of the excavation. These wells had a depth of 100 ft and were equipped with 12-in., 1500-gpm deep well turbine pumps manifolded to discharge into a plastic lined ditch and swale leading to the river. Stand-by diesel units were provided for four pumps to insure continuous operation during critical flood periods. The pumping system was capable of maintaining the ground water below the surface of the test area for river stages up to el 198. Eight piezometers were installed within the excavation for observation of ground water levels during driving and testing, and for coordination of pumping. A clay-gravel surfaced road was constructed to the site from county road No. 53 connecting to Arkansas Highway 88 and U. S. Highway 79. Ramps, aprons, and storage areas surfaced with clay-gravel were provided at the site to facilitate all weather operations. Field offices with utilities, telephone, and sanitary services were also furnished. Improvements and dewatering facilities at the site are shown on Plate 5. A general view of the pile testing site is shown by the aerial photograph on Fig. 4.

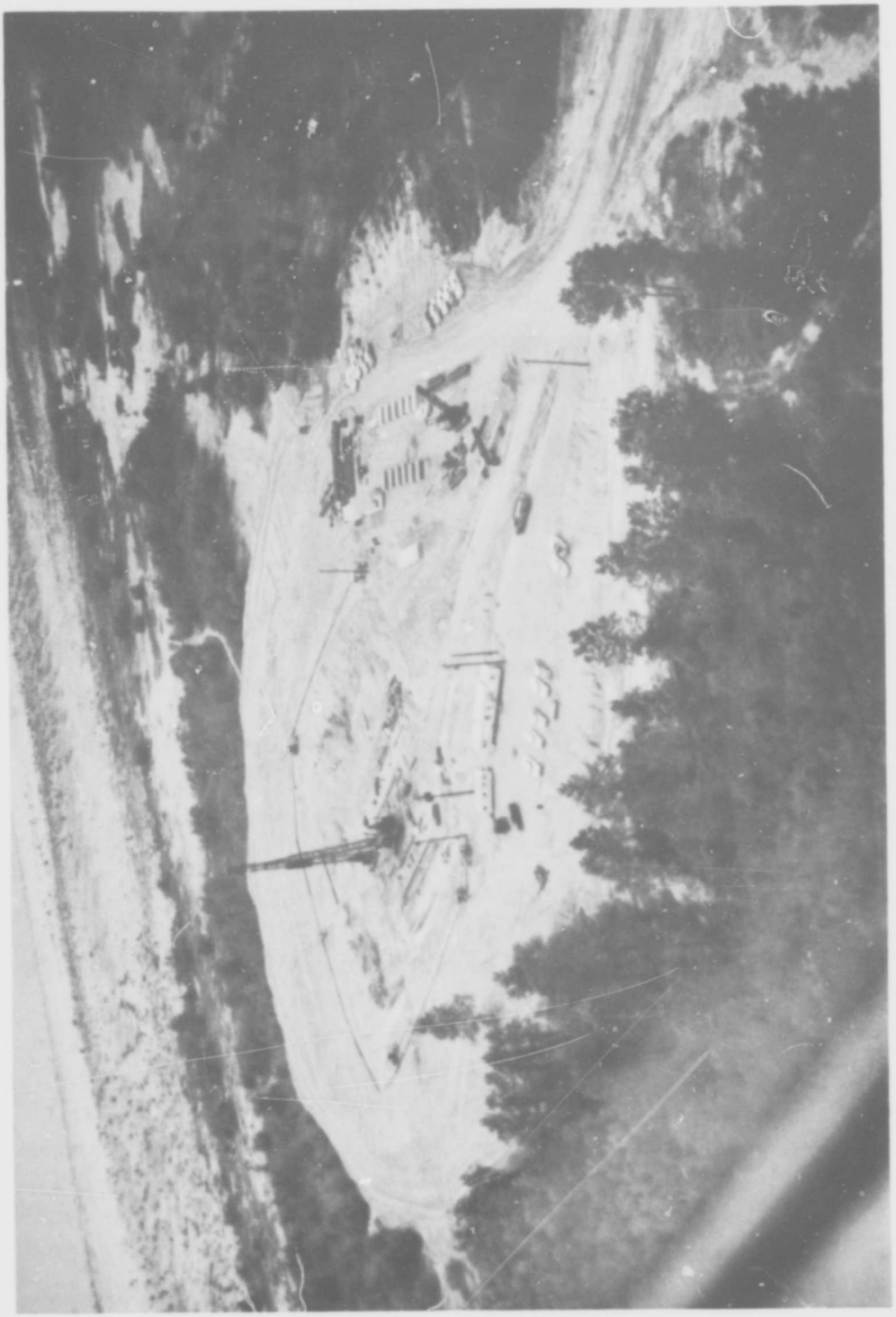

Fig. 4 - PILE TESTING SITE

Test Piling

Pile types

12. The basic types of bearing piles considered suitable for the proposed locks and dams included prestressed concrete piles, steel H-piles (14BP73), and timber piles. Steel pipe piles were driven and tested in order to provide instrumentation for displacement type piles for comparison with concrete piles. MZ32 and MP112 interlocking steel sheet piling will also be used for guide wall cells, cofferdams, scour protection, and seepage cutoffs. Pile sizes and penetrations were initially based on design compression loads and Terzaghi's bearing capacity equation for deep piers supplemented by test data for piling driven into similar soils. The results of these studies indicated that the following types and sizes of piling would be suitable for the navigation structures, and were included in the testing program:

a. Steel H-piles (14BP73)
b. Steel pipe piles (12-, 16-, and 20-in. diameter)
c. Prestressed concrete piles (16- and 20-in. square)
d. Timber piles (Class A)
e. Steel sheet piles (MP112 and MZ32)

Strain instrumentation

13. The steel pipe and H-piles were instrumented with strain gages below ground to determine the distribution of load and bending moments produced by applied axial and lateral loadings. Two types of strain gages were used: steel strain rods, designated as Type 1 instrumentation, and electric-resistance strain gages, designated as Type 2 instrumentation. The strain gages were attached to the outsides of the pipe piles and to the webs of H-piles except for test piles 12, 13, and 13A on which Type 2 gages were also attached to the insides of the flanges. Protective covers, consisting of channels on pipe piles and channels or plates on H-piles, were placed over the instruments to prevent damage during driving and testing. Cover channels and plates were welded to the piles so as to provide a composite structural section. For piles instrumented with electric-resistance type strain gages, welding was limited to within 6 in. of the gages to prevent temperature damage. The space between the welds was filled with epoxy to provide

a water- and sand-proof gage compartment. The addition of the protective channels or plates not only modified the pile section, but for pipe piles also produced an increase in the effective point and wall surface area in contact with the soil. It was assumed that the covers for the H-piles did not change the contact surface as the covers were located inside the assumed minimum perimeter and end failure areas. The location and details of the gages and protective covers are shown on Plates 6 through 9, and on Photo 1, Appendix C.

14. Strain rods. The strain rods extended along the longitudinal axis of a pile to measure its elastic shortening or elongation under compressive or tensile loads. The lower ends of the rods were fastened to the pile with blocks welded to the pile while the upper ends extended above subgrade through guides permitting unrestricted vertical movements. The blocks were tapped and the bottom of the rods threaded to permit placing the rods after the piles were driven. Extensometer gages reading to 0.001-in. were attached to the top of the pile by means of mounting plates welded to the pile. The gage stems rested on the upper end of the strain rods. Fabrication details of the strain rods and mounting plate details are shown on Plate 6. The locations of the gages and details of the protective covers are shown on Plates 7 through 9.

15. Electric-resistance strain gages. The electric-resistance strain gages consisted of Budd-Metalfilm temperature compensated (C6-181-E) gages fastened to the pile using Budd B-3 epoxy cement. The gages were waterproofed by coating them with Thiokol epoxy and enclosing them with a neoprene gasket and a metal coverplate. Belden 8743, #22 vinyl-insulated, 12-wire cable was used for leads in the 3-wire circuits employed. The lead cables were wrapped with asbestos covering and securely attached to the pile by cable clamps. The asbestos covering protected the lead wires when the channels and/or plates were welded to the pile. Gage wires were connected to junction strips for ready and positive attachment to the switch box leading to the strain indicator. The strains were measured using Budd HY-1 strain indicators. Dummy gage and leads were maintained at constant test pile temperatures to minimize drift during testing. The locations of the electric-resistance strain gages are shown on Plates 7 through 9.

Fabrication

16. Steel piles. The steel pipe and H-piles were shop fabricated in accordance with the instrumentation drawings. The basic pipe piles furnished were in conformance with the requirements of ASTM Specification A-252, grade 2, "Welded and Seamless Steel Pipe Piles." The average diameter and wall thickness of the pipe piles determined by actual measurement, conformed to the nominal tabular dimensions for the designated sizes. Mill certificates furnished for the basic H-piles (14BP73) indicated that the steel met the requirements of ASTM Specification A-36, "Steel for Structures." However, measurements made on the H-piles showed that the web and flange dimensions for all but test pile 6, obtained from another source, differed significantly from the assigned standard dimensions for a 14BP73 pile. The average of three measurements made on each H-pile is shown below. These measurements were used in the determination of the pile properties presented hereinafter.

Test Pile	Width (In.)	Depth (In.)	Flange Thick. (In.)	Web Thick. (In.)
7	14.67	13.77	0.580	0.560
9	14.69	13.69	0.528	0.519
12	14.79	13.81	0.532	0.522
13	14.69	13.81	0.562	0.550
13A	14.65	13.56	0.487	0.479

17. Concrete piles. The prestressed concrete piles were commercially manufactured by F-S Prestress Inc., Hampton, Arkansas. These piles were made in accordance with the requirements of the Joint Committee, American Association of State Highway Officials Committee on Bridges and Structures and Prestressed Concrete Institute. The concrete piles were square and had Type SS reinforcement and Type 2 (flat) tips. They were cured for 3 hrs in air and 36 hrs in 135° F steam prior to transfer of the prestress load and removal from the casting bed. The compressive strength of the concrete at release of the prestress as determined by tests on standard 6 x 12-in. cylinders cast from the same batch used for the piles and cured with the piles, was in excess of 4,000 lbs per sq in. Nine supplemental cylinders were cast and cured in the same manner. Seven of these cylinders were shipped to the job site,

stored in air at the site, and ultimately shipped to the U. S. Army Engineer Division, Southwestern, Laboratory for physical testing. The two remaining cylinders were tested by F-S Prestress Inc. before the piles were shipped.

18. Timber pile. An untreated southern yellow pine timber pile was obtained from Southern Wood Treaters, Inc. of El Dorado, Arkansas. The pile conformed with current ASTM Specification D-25, "Round Timber Piles," Class A according to the certificate submitted by the supplier. Field measurements indicated that the dimensional characteristics of the pile met the specifications.

Physical properties

19. Laboratory tests. The physical properties of the steel and concrete piles were determined from external measurements and from tests made on specimens cut from the steel test piles and on the cylinders made from the specific batch used for casting the concrete piling. The results of the tests on the steel piles are tabulated below:

Test No.	Pile Type	Yield Point (Lbs/Sq In.)	Ultimate Tensile Stress (Lbs/Sq In.)	Elongation in 2-In. (%)	Modulus of Elasticity (Lbs/Sq In.)
2	16-in. Pipe	54,500	75,750	28	30.3×10^6
3	20-in. Pipe	44,150	70,510	33	29.8×10^6
7	14BP73	37,150	62,360	39	29.0×10^6
12	14BP73	47,660	75,850	33	29.8×10^6

The results of the tests performed on the concrete cylinders cast with the test piles are summarized below:

Cylinder	Piles Represented	Age[a] (Days)	Compressive Strength (Lbs/Sq In.)	Static Modulus[b] of Elasticity (Lbs/Sq In.)
8-10-A	All but TP 11A	7	5530	--
8-10-B	"	75	4670	6.3×10^6
8-10-C	"	90	6720	6.3×10^6
8-10-D	"	90	5640	6.4×10^6
8-10-E	"	90	5640	6.5×10^6
8-10-F	"	90	6070	6.0×10^6
8-14-A	TP 11A	6	5130	--
8-14-B	"	90	5430	6.6×10^6
8-14-C	"	90	5310	6.9×10^6
			Average -	6.4×10^6

a - All cylinders steam-cured for 36 hrs after casting.

b - Static modulus of elasticity at 0 to 1/3 ultimate strength. No appreciable change noted for static modulus tests at 1/3 to 2/3 ultimate strength.

The sections and physical properties of the test piles used in this program are presented in Table 4.

20. Field flexure tests. Full scale field flexure tests were made on two of the 16-in. square prestressed concrete piles to determine the effect of driving with the 140C steam hammer and the Bodine hammer on the prestress bond. This was done by comparing the load-deflection characteristics of the test piles before and after driving. These tests were made on test piles 5 and 11 which were driven with the 140C steam and Bodine hammers, respectively. The "before-driving" flexure tests were made by applying a single load of about 6 kips at the center of a 32-ft span of each pile when in a horizontal position. After being driven these piles were extracted by jetting and retested in flexure using incremental loadings. A 26-ft span was used in the retest of test pile 5, whereas a 20-ft span was used for test pile 11. The results of these flexure tests are shown on Plate 10; the "after-driving" tests are represented by curves and the "before-driving" tests by points. The deflections were corrected to the corresponding span lengths used in the "after-driving" tests on the basis that the deflections are proportional to the cube of the span. The agreement in deflection at the 6-kip load

indicates that the prestress was not affected by driving with either the 140C steam or the Bodine hammer. The load-deflection curves for test piles 5 and 11 are essentially identical when corrected for the spans used in the tests.

21. A supplemental flexure test was made on an unused 16-in. prestressed concrete pile, designated as test pile 11b, which was cast and cured with the other concrete piles used on this project. The load-deflection curve for this "undriven" pile is shown on Plate 10. The close agreement between the load-deflection characteristics of test piles 11 and 11b, which were tested at the same span, confirms the previous conclusion that driving had no adverse effect on prestress bond. A flexure test was also performed on a 16-in. pipe pile (#2) to check the theoretical computed value of EI.

22. The flexure tests also provided a verification of the EI value computed from the physical properties and used in evaluating the results of the pile tests. A comparison of the adopted EI values, computed from the average test pile measurements and the physical properties of the pile materials, with the values computed from the flexural tests shows fairly close agreement. The adopted theoretical values and those computed from the flexure tests are tabulated below:

Test Pile	Pile Type	Calculated Value of EI in (K in.^{2}) From Flexure Tests Range	From Flexure Tests Average	From Physical Tests Average
2	16" Pipe	22.9 - 23.6	23.0	24.4
5*	16" Conc.	31.2 - 39.2	34.8	34.5
11*	16" Conc.	33.1 - 39.8	35.5	34.5
11b*	16" Conc.	30.4 - 37.1	34.2	34.5

* EI determined for moments below the moment that would crack pile

Pile Driving

Pile hammers

23. Three types of pile-driving hammers were used in the driving tests: double-acting steam hammers, a Bodine hammer, and a diesel hammer. The specific pile hammers used to drive each test pile are

listed in Tables 1 and 5. Operational data for the steam and diesel hammers used in this investigation are given below:

Operational Data	Hammer Manufacturer and Designation					
	Vulcan Iron Works			McKiernan-Terry		
	140C	80C	65C	10B3	9B3	DE40
Weight of ram, lbs	14,000	8,000	6,500	3,000	1,600	4,000
Rated energy per blow, ft lbs	36,000	24,450	19,500	13,100	8,750	32,000
Rated speed, blows per min	103	111	120	105	145	50
Rated steam pressure, lbs per in.^{2}	140	120	120	100	100	--
Stroke, ft	1.3	1.38	1.33	1.58	1.42	8.0

The Bodine sonic vibratory hammer used was a Model B2 having a gross weight of 18,000 lbs. This hammer energizes a pile to its resonant frequency by the use of gear driven mechanical oscillators powered by two gasoline engines. The vibratory energy is transmitted to the soil, temporarily displacing it, allowing the pile to penetrate the soil under the pile and hammer weight. Resonance is assumed to be reached at the maximum rate of pile advance as indicated by driving instruments. Power requirements are determinable using tachometer and manifold pressure data.

Driving bearing piles

24. All of the bearing piles were driven using leads fixed at the top and bottom. Special care was taken to insure proper alignment of the piles in the leads before driving the vertical and batter piles. The driving head and cushion used in driving the test piles are summarized on the next page.

Pile Type	Hammer	Driving Head	Cushion	Cap Block Assembly Weight
Pipe	140C	Aluminum[a] & micarta disks	None	1710 Lbs
Concrete	140C	"	3 to 5 sheets 3/4-in.[d] plywood + 1 pad of 1-in. manila rope	1710 Lbs
H	80C	"[b]	None	1220 Lbs
Timber	65C	"[c]	None	950 Lbs
Concrete	DE40	None	3 sheets 3/4-in. plywood	---
MZ-32	80C	Al-Micarta	None	1220 Lbs
MP-112	10BC	None	None	---
MP-112	9B3	None	None	---

(a) Cap assembly consisted of 10 aluminum alloy disks and 10 Micarta disks 1-in. thick, 17-1/2 in. in diameter, with 4-1/2-in. bore; top steel anvil 4-in. thick, 17-3/4-in. in diameter, with 3-1/2-in. bore; bottom steel anvil 4-1/2-in. thick, same as top anvil; and steel shield 18-in. I.D., 22-in. O.D., and 27-in. high.

(b) Cap assembly consisted of 11 aluminum alloy disks and 11 Micarta disks 1-in. thick, 14-3/8 in. in diameter, with 3-1/2-in bore; top steel anvil 3-1/2-in. thick, 14-3/8-in. in diameter, with 3-1/2-in. bore; bottom steel anvil 6-in. thick, 14-3/8-in. in diameter, with 3-1/2-in. to 5-in. bore; and steel shield 14-1/2-in. I.D., 18-1/2-in. O.D., and 23-3/4-in. high.

(c) Cap assembly consisted of 12 Micarta disks 1-in. thick, 11-3/8-in. in diameter with 4-1/2-in. bore, and 12 aluminum alloy disks 1-in. thick, 11-3/8-in. in diameter, with 4-in. bore; top steel anvil 2-in. thick, 11-3/8-in. in diameter, with 3-1/2-in. bore; bottom steel anvil 6-in. thick, 11-3/8-in. in diameter, with 4-in. bore; and steel shield 12-in. I.D., 16-in. O.D., and 26-in. high.

(d) Manila rope pad used only on test piles 4, 5, 11A, and 19.

Records were maintained for each pile driven and included blows per foot of drive, hammer speed, steam pressure, net driving time, and any other pertinent notes for the steam hammers. The fall of the ram was also

measured for test pile 19 driven with the diesel hammer. For piling driven with the Bodine hammer, the engine speed, manifold pressure, penetration rate, and net driving time were recorded. The results of the driving tests are summarized in Table 5. Pile driving logs showing the blows for each foot of pile penetration for piles driven with steam hammers are plotted on Plate 11. Test piles 14 through 18 were jetted to a depth of 38 to 40 ft using double water jets extending along opposite sides of the pile to the pile tip; the piles were then driven to a penetration of about 53 ft with the 140C hammer. Test pile 16 was driven first in the center of the group of the five jetted piles. Photographs (2 and 3) of typical pile driving operations for both types of hammers are given in Appendix C.

25. Penetration. All of the test piles were driven to the required penetration except for concrete test piles 11A and 11 driven with the Bodine sonic hammer. The initial attempt made to drive test pile 11A, a 20-in. concrete pile, with the Bodine hammer at the originally selected location at the west end of the north pile line (see Plate 1) was unsuccessful as refusal was encountered at a penetration of 16.5 ft. The pile was pulled with the Bodine hammer and redriven to refusal at a penetration of 35.5 ft at a new location on the east end of the north pile line. Several weeks later, test pile 11A was driven with the 140C hammer from a penetration of 35.5 ft to a penetration of 44.4 ft, pulled with the aid of water jets, and redriven with the 140C hammer to a penetration of 52.2 ft at the final location on the east end of the south pile line as shown on Plate 1. Test pile 11, a 16-in. concrete pile, was driven with the Bodine hammer to refusal at a penetration of 38.8 ft. The poor penetration achieved with the Bodine hammer for concrete piles is believed to be due to loss of vibratory energy in the friction clamp used to attach the hammer to the pile head. This attachment, shown in Photograph 4b, Appendix C, was made especially for driving the 16- and 20-in. concrete piles on this project. This attachment consisted of a steel cage which was clamped to the pile by five bolts on each side of the pile. A layer of hard asbestos was placed between the clamp and the pile. As a precaution against the pile accidentally slipping from the clamp, four bolts, two in each direction,

were placed through the clamp and pile. No attempt had previously been made to drive concrete piles of this size with a Bodine hammer. The Bodine head attachment for steel piles consisted of a welded fixture which was bolted to the hammer and provided a rigid connection. The head attachment for H-piles is shown on Photograph 4a, Appendix C. The Bodine hammer tests clearly demonstrated the suitability of this hammer for driving steel bearing piles rigidly attached to the driving head, but the suitability of the Bodine hammer for driving concrete pile is questionable.

26. Pile damage. Damage to piling from driving was minor except for test pile 5, a 16-in. concrete pile, driven with the 140C steam hammer. The head of this pile was damaged at 13 and 54 blows per foot resistance at penetrations of 29 ft and 48 ft, respectively, on account of eccentric driving on the pile head. The pile head was repaired before driving to the scheduled penetration. There was no damage to the head of the H-piles or timber pile. Damage to the pipe piles consisted of some slight bulging at one side of the pile head which is attributed to slight driving eccentricities.

27. Driving time. The net driving time for all the piles driven with the double-acting steam hammers varied from about 5 to 15 minutes except for the 20-in. concrete pile which required 30 min. Partial water jetting reduced driving times to an average of about 4 min. for the jetted pipe and concrete piles. It was possible to drive the steel pipe and H-piles 53 ft deep in 2 to 4 min. with the Bodine hammer whereas the concrete piles, as previously discussed, could not be driven to more than 35 or 40 ft, in about 30 min., with the Bodine hammer. Driving the 16-in. concrete pile with the DE40 diesel hammer required about 45 min. even though the hammer was apparently operating at 85 percent efficiency. The efficiency of the steam hammers is given in Table 5. The results of the field driving tests indicate that bearing and sheet piling of the sizes and penetrations required for the Arkansas River Project can be driven satisfactorily with conventional steam hammers. The time required to drive the individual test bearing piles with the selected double-acting steam hammers was relatively short for piling of the types considered for this project. However, the McKiernan-Terry DE40

hammer appeared inadequate for driving the 16-in., 55-ft concrete pile. The DE40 driving test showed the effect of a lightweight ram on driving; similar piles were driven in less than a third of the time with a 140C hammer which has only a slightly greater energy per blow than the DE40, but has a ram seven times as heavy as that of the DE40. The 140C hammer is considered inadequate for driving 20-in., 50-ft long concrete piles on this project as the blows per foot of penetration were increasing very rapidly at 52-ft penetration. Densification of the sand from driving piles in groups may increase the driving time and/or require heavier hammers with greater energy. Although no driving or load tests were made with a lowered ground water table, such will increase the driving resistance and capacity of a pile for the same penetration into alluvial sands. The tests show that jetting speeded the driving of displacement piles, but it reduced the compression and tension capacity of the pile by approximately 30 percent.

Driving sheet piling

28. Comparable driving tests were made on MZ32 and MP112 steel sheet piling with the Bodine hammer and with the double acting steam hammers. In these tests, a line of eight sheets of each type piling was to be driven to Tertiary clay at a depth of about 95 ft or to refusal. The sheets were 60 ft long and were spliced as required. In the driving tests with the Bodine hammer, the sheets were driven singly to the splicing or final elevation. A hydraulic head clamp was used to grip the sheet piles. With the steam hammers, the piling was initially driven to refusal using a 10B3 hammer; driving was completed using an 80C hammer for the MZ32 sheeting and a 9B3 hammer for the MP112 sheeting. Sheets were driven double with the 80C and 10B3 hammers and singly with the 9B3 hammer. Stage type driving was used for the sheeting driven with steam hammers. Extractor tests were made at the completion of driving. An attempt was made to pull the piles driven with the Bodine hammer with the same hammer as an extractor. Most of the piles driven with the conventional hammers were extracted with a Vulcan 800A extractor, although a few of the Z-piles were pulled with the Bodine hammer.

29. Bodine hammer. The results of the driving tests made with the Bodine hammer are shown on Plates 12 and 13. These results indicate

that MZ32 and MP112 sheet piles could readily be driven to a penetration of about 45 to 50 ft in 2 to 9 min. when each sheet was driven individually. Driving times generally increased with the driving order with interlocks engaged. When the pile lengths were increased by splicing, driving either type of sheet became more difficult and only two sheets of each type piling could be driven to the Tertiary clay. The range of penetrations obtained for the MZ32 piling was 46 to 94 ft, and was 50 to 94 ft for the MP112 sheeting. All but two of the MP112 sheets were damaged at the welds or failed near the pile head from hammer vibrations. With the Bodine hammer, each sheet must be driven to the desired final penetration because of hammer interference or a follower must be used. In general, neither type of sheeting could be reliably extracted by this hammer when penetrations exceeded 60 ft. A summary of extraction information is given in Table 6. Inspection of extracted sheets indicates that heat and vibratory compaction of sand in the interlocks were a deterrent to driving.

30. Steam hammers. Results of the driving tests on sheet piling driven with steam hammers are shown on Plates 14 and 15. These data show that double sheets of MZ32 piling, with interlocks engaged, can be successfully driven to average penetrations of about 55 ft with the 10B3 hammer in driving times ranging from 17 to 30 min. The MZ32 piling was driven from 55 ft to depths ranging from 85 to 104 ft in about 20 min. additional driving time with the 80C hammer. All of these piles could have been driven to greater penetrations if desired. However, the MP112 piling could not be driven as double sheets with the 10B3 hammer more than about 30 ft; all of the piling were damaged by curling even though driving resistances were relatively low. The MP112 sheeting was subsequently driven to penetrations of from 86 to 95 ft with a 9B3 hammer driving on single sheets with interlocks engaged; these sheets could have been driven deeper. Neither type of piling could be extracted using an 80OA extractor if the penetration exceeded 60 ft. Extraction test data are summarized in Table 6.

PART III: FIELD LOAD TESTS

Compression Tests

Test procedure

31. Compressive loads were applied to the test piles by means of a calibrated hydraulic jack reacting against a loaded test frame. The test frame consisted of a steel platform supported on spread foundations straddling the line of test piles. The supporting foundations were continuous and consisted of bolted crane timbers with 12- x 12-in. timber cross ties capped with a longitudinal steel beam. This arrangement permitted movement of the test frame on rollers along the line of test piles and expedited the test set-up. The mats were spaced 16 ft on centers with 5 ft lateral clearance provided from all piles under test. The platform was loaded with 5.5- and 11-ton concrete blocks. Loads were applied to the platform in two increments at the start of a test and at one-half the estimated pile capacity, to minimize the surcharge delivered to the subgrade by the frame reactions. A compression test frame having a capacity of 500 tons was provided for each test pile line. Compression frame fabrication details are shown on Plate 16 and by Photo 5a, Appendix C.

32. The test loads were applied in approximately 10 equal increments selected on the basis of the estimated pile capacity as determined from driving information and static calculations. All loads were applied and released at a rate of 2 tons per min. Each load increment was maintained for a minimum period of one hour; no new loading was applied until the pile head movement was less than 0.010 in. per hr. Gas regulating equipment was used to apply and maintain the test load constant. At the estimated design load, no additional loads were applied until the pile head movement was less than 0.005 in. per hr. All piles were loaded to plunging failure (gross pile head deflection exceeded 0.01 in. per ton). The movement of the pile head was measured by three dial indicators, reading to 0.001 in., attached to the pile head with the dial stems resting on an independently supported reference beam. The reference beam was supported on adjacent piling when feasible or on posts securely driven into the subgrade at a minimum distance of 5 ft laterally

from the test pile. During testing, the elevation of the beam was periodically checked with a sensitive level to provide a basis for correction of pile head movement if there was any movement of the reference beam. The dial indicators at the pile head were read before application of loads and at elapsed times of 1, 5, 10, 20, 30, 45, and 60 min. thereafter or until the rate of settlement did not exceed the established limits. Strain measurements were made before application of loads and after pile head movements were stabilized under a specific load. Testing was continued around the clock, and any test started was carried to completion without interruption. Protective covers were provided for the jacking, instrumentation, and reaction beam systems to minimize thermal effects on test measurements.

Test data and analysis

33. Applied load vs gross pile head settlement curves were plotted for each compression test. The gross settlement of the pile head was considered to be the average of the three dial indicator readings corrected for movement of the reference beam when required. Curves were also plotted showing the net pile head settlement vs applied compressive load for tests performed using cyclic loading procedures, and pile tip movements vs applied compressive load for piles instrumented with strain rods. Pile tip movement was considered to be the difference between the gross pile head settlement and the elastic shortening of the pile as indicated by the lower strain rod located one ft above the pile tip. These settlement curves are presented on Plates 17 through 27.

34. The distribution of load in the instrumented piles was computed for selected applied loadings from the pile strain measurements. Loads were computed from the following formula:

$$P = A E \Delta e/L$$

where

P = Average load in lbs at the center of the gage span

A = Cross-sectional area of the pile in sq in.

E = Modulus of elasticity of pile material in lbs per sq in.

Δe = Strain over the gage span

L = Gage length in in.

For strains measured with strain rods, $\Delta e/L$ = difference in movement of adjacent strain rod anchors divided by the distance between the adjacent anchors. Electric resistance strain gages measured $\Delta e/L$ directly in microinches per in. Properties of the test piles used in the stress analysis are given in Table 4. In the calculation, it was assumed that no residual stresses existed in the pile at the start of testing. The computed load distribution curves are included as graphs (b) on the plates showing the results of the compression tests on the steel test piles. Applied loadings on the piles are depicted on the graphs by a solid symbol whereas loads determined from strain rods and electric resistance strain gages are depicted by open circles and triangles, respectively. Extrapolation of these curves to the ground elevation indicates the load applied to the pile and provides a check on the jack calibration. Extrapolation to the pile tip permitted estimating the point load. Curves showing the variation in point load with applied load are presented as graphs (c) on the "Compression Test Results" plates. The wall friction load, considered to be the difference between the applied load and the tip load, is also plotted on the (c) graphs.

35. Compressive failure loads were determined from the applied load vs pile head settlement curves by means of the four criteria described below:

a. Load on the gross settlement curve where the slope equals 0.01 in. per ton.

b. Load on the net settlement curve where the pile settlement equals 0.25 in.

c. Load depicted by the intersection of tangents to the initial and final portions of the gross settlement curve.

d. Load where the slope of the gross settlement curve became disproportionate to the load applied. This method was limited to tests wherein the load - pile settlement curve had a pronounced change in slope.

The failure load for each pile test was considered to be the average of the loads obtained for the above methods. A summary of the compressive failure loads for the various piles tested is presented on Table 7.

36. The results of the compression tests were analyzed, and general design curves for pipe, concrete, timber, and H-piles were

developed for determining the size and penetration required to support loadings within the range necessary for this project. The Terzaghi expression for deep piers (Ref. 1) was used in the analyses wherein the tip and wall friction portions of the failure load were equated to the corresponding term in the general expression. The Terzaghi expression is presented below:

$$Q_u = A_t \gamma' (D N_q + \S r N_\gamma) + 1/2 A_f K D^2 \gamma' \tan \delta$$

where

Q_u = Pile failure load in tons

A_t = Area of pile tip in sq ft

γ' = Bouyant density of sand - 0.031 tons per cu ft (water table at ground surface)

D = Pile penetration in ft

N_q & N_γ = Terzaghi bearing capacity factors

$\S$ = Pile shape factor - 0.8 for square piles
0.6 for round piles

r = Radius of circular section or 1/2 side dimension of square section

A_f = Circumferential area of pile in sq ft/ft of pile length

K = Lateral earth pressure coefficient

δ = Material friction angle - 32° sand on sand
25° steel on sand
30° concrete and wood on sand

For piles in compression, the first term of the general bearing capacity equation defines the point bearing whereas the second term defines the portion of the pile capacity due to skin or wall friction.

37. Pipe piles. The distribution of load in the pipe piles was determined from the load distribution curves presented on Plates 17 through 22. From the load distribution obtained, the point bearing capacity factor (N_q) and the lateral earth pressure coefficient (K) were calculated for each test using the Terzaghi static bearing capacity expression. The following assumptions were made in these calculations: (a) the term containing $N_\gamma = 0$; (b) K constant over the embedded portion of the pile; and (c) the sliding coefficient of friction between steel and sand = 25° as determined from laboratory tests. Point and

wall areas were adjusted to account for increases produced by the protective channels shielding the instrumentation. The load distribution, together with the calculated bearing capacity factor (N_q) and lateral earth pressure coefficient (K) as determined from the pipe pile tests, are presented below. The load distributions and values of N_q and K shown are those computed for applied load at the time of failure.

Test Pile	Nominal Diameter (In.)	Penetration (Ft)	Average Failure Load (Tons)	Load Distribution: Point Bearing Tons	Point Bearing %	Wall Friction Tons	Wall Friction %	Computed Values: N_q	Computed Values: K
1	12	53.1	140	34	24	106	76	22	1.31
2	16	52.8	195	58	30	137	70	21	1.29
2*	16	52.8	210	67	32	143	68	25	1.32
3	20	53.0	215	77	36	138	64	20	1.17
10	16	53.1	180	46	26	134	74	18	1.23
16**	16	52.7	140	41	29	99	71	17	0.99
Average		53.0			30		70	21	1.26

* Retested after subjecting pile to 5 cycles of lateral load producing a deflection of 0.5 in.

** Not included in average

These test results are also presented graphically on Fig. 5 wherein the total, wall, and point loads at failure are plotted vs the effective or equivalent pile diameter for the various pipe piles tested. The effective diameter for the point and wall portions of the load was computed for the pile section as modified by the addition of the protective channels. The effective diameter for the total load condition was assumed to be the weighted average of the point and wall loads. These curves are valid for pipe piles having a penetration of about 53 ft. The results of the load test on test pile 16 were not used in the curve fitting as this pile was jetted prior to final driving and was located at the center of a group of jetted piles. The jetting apparently produced a significant reduction in wall friction by loosening the sands adjacent to the pile and also caused some reduction in point bearing. It will be noted that test pile 10, which was driven with the Bodine hammer, had comparable load carrying characteristics to those of the piles

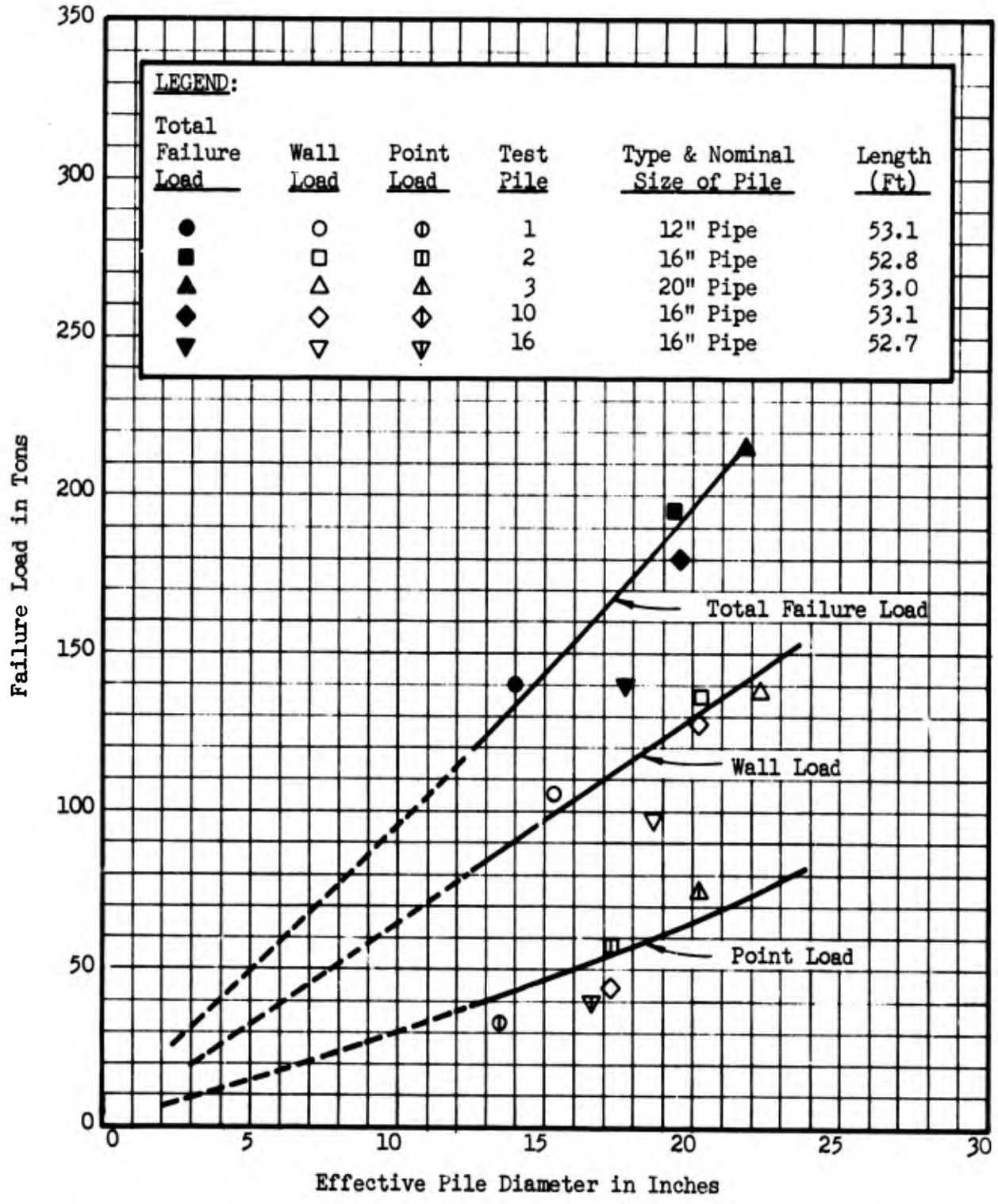

Fig. 5 - COMPRESSIVE FAILURE LOAD VERSUS PIPE PILE DIAMETER

driven with the 140C steam hammer. The compression test on test pile 2, after it was subjected to five cycles of repetitive lateral loading, indicates that the lateral loading had no significant effect on the compressive capacity. The failure and ultimate (plunging) loads were essentially the same for both tests.

38. Concrete piles. The results of the compression tests on the square prestressed concrete piles are shown on Plates 23 and 24. A summary of the field test results is tabulated below:

Test Pile	Size (In.)	Penetration (Ft)	Average Failure Load (Tons)	K	Driving Hammer
4	16	40.2	170	1.59	140C
5	16	51.0	240	1.45	140C
11	16	38.8	150	1.45	Bodine
	Average			1.50	

An evaluation of the above compression tests was made by means of the Terzaghi equation. The tip capacity of the concrete pile was computed by assuming the bearing capacity factor of the sand at the pile tip (N_q) to be 21 as determined from the tests on the pipe piles. The wall friction was assumed to equal the failure load minus the computed tip load. An average lateral earth pressure coefficient (K) of 1.50 was obtained for the skin friction portion of the load; the friction angle between concrete and sand was considered equal to 30° as determined from laboratory tests.

39. Steel H-piles. Pile settlement vs load and load distribution curves obtained from the field tests on 14-in. steel H-piles are presented on Plates 25 through 27, A summary of the test results is tabulated below:

Test Pile	Penetration (Ft)	Average Failure Load (Tons)	Load Distribution: Point Bearing Tons	Point Bearing %	Wall Friction Tons	Wall Friction %	Computed Value: Nq	Computed Value: K
6	40.0	140	21	15	119	85	12	1.88
7	52.1	190	39	21	151	79	17	1.41
9	53.2	210	25	12	185	88	11	1.66
	Average			16		84	13	1.65

Theoretical calculations made following the methods described for pipe piles in paragraph 37 indicate that the bearing capacity factor at the pile tips had an average value of 13 and that the lateral earth pressure coefficient (K) had an average value of 1.65, based upon the assumption that the failure surface between the pile and foundation sand followed the minimum perimeter of the H-pile. The difference in values of N_q and K computed for the H-piles from the values computed for the pipe and concrete piles can probably be attributed to unreliability of the assumptions made regarding the point and wall failure surfaces for this non-displacement type of pile. In the development of a general design curve for a constant size H-pile, the actual failure surfaces are of academic interest only as the developed design curves would not be affected within the penetration ranges tested.

40. Timber piles. The load vs settlement curves for the compression test on the Class A timber pile is shown on Plate 24. The failure load for this pile was 80 tons. The timber pile tested had a 15.2-in. butt and a 10.7-in. tip. Load distribution in the pile was estimated assuming that the bearing capacity factor (N_q) at the tip was 21 as previously determined for the displacement type pipe piles having flat tips. A lateral earth pressure coefficient of 1.25 was calculated for the wall friction portion of the failure load on the assumption that the sliding friction between timber and sand was 30°.

Discussion of results

41. The field driving and loading tests show that it is feasible to drive 12- to 20-in. concrete, pipe, or steel H piles into the alluvial sands of the lower Arkansas River Valley that will have compressive capacities of about 150 to 250 tons at penetrations of 50 to 55 ft. The test results also show that pile behavior can be reasonably predicted from the Terzaghi expression for deep piers using reasonable values of lateral earth coefficient (e.g. 1.5±), tip bearing factor (e.g. $N_q = 21\pm$), and coefficient of friction ($\delta = 25°$ to 30°). Computed capacities of various types of piles were based on lateral earth coefficients (K), as determined from the field tests, of about 1.25 for the pipe and timber piles, 1.5 for the concrete piles, and 1.65 for the steel H piles; $N_q = 21$; $\delta = 25°$ to 30° depending on type of pile, water table at the ground surface; and $\gamma' = 62$ pcf.

42. Load distribution and residual stresses. The distribution of compressive load in the steel piles was computed from the change in strain produced by the applied compressive loads. This procedure neglected any residual loads in the piling which may have been induced during driving. An approximate estimate of residual loads produced by pile driving was made by comparing strain readings before and after compression and tension tests. The results of this supplementary study are presented in Appendix D. The analyses presented in Appendix D indicate that significant residual compressive stresses exist in piles after driving with conventional steam hammers and that such stresses also remain after testing in compression. It appears that very little residual stress remained in the steel piles driven with the Bodine hammer. This is to be expected as sonic pile driving temporarily displaces the soil by an energy wave, and penetration of the pile is achieved under the static weight of the pile and hammer. Residual stresses in the pile (16) that was partially jetted, with other surrounding jetted piles, were appreciably less than the residual stresses produced in the piles driven with steam hammers without the aid of jetting.

43. Design loads. Theoretical design curves showing the relationship between penetration and compressive failure load for a range of sizes of steel pipe piles, prestressed concrete piles, and steel H-piles, and a timber pile are presented on Plate 28. These curves were prepared on the basis of the Terzaghi expression and the load distribution in the pile as computed neglecting residual driving stresses. The failure loads from the field tests are plotted on the curves for concrete and H-piles which had sections conforming closely to the prototype piles. It should be recognized that these curves could be modified using the load distribution corrected for residual driving stresses which would result in a slight change in the shape of the curve without altering the total load capability within the range of pile penetrations used in the field testing.

44. Jetted piles. The compressive capacity of test pile 16, which was jetted to a depth of 40 ft and was surrounded by partially

jetted piles, was about 70 percent of the compressive capacity of similar piles driven without jetting. The design curves presented on Plate 28 are not valid for jetted piles. It is, however, recognized that the foundation sands will be densified by driving large displacement piles on relatively close centers making it more difficult to drive the piles to the desired penetration. This increase in driving resistance could necessitate some jetting of piling in construction. However, as jetting reduces the capacity of piles, no jetting of piles should be permitted unless field experience indicates that the piles cannot be practically driven to the required minimum penetration, and until load tests have been made and evaluated to determine the effect of jetting on the load carrying capacity. If the capacity of the pile has been reduced significantly by jetting, it may be necessary to redesign the pile foundation.

Tension Tests

General test procedures

45. Tension loads were applied to the test piles by jacking against each end of a loading frame which was attached to the pile head by steel rods. The rods were welded directly to the steel piles, and to steel collars pinned to the concrete and timber piles. Details of the frame are shown on Plate 29. The test loads were applied in approximately 10 increments based on the estimated ultimate load as computed from static equations. Pile head movements and strain gage observations were recorded for each test load applied. The instrumentation of the pile head was similar to that used for the compression tests. All of the tensile tests were carried to ultimate failure. The testing procedure resembled closely the procedure described for the compression tests. A typical tension test setup is shown in Photograph 6a, Appendix C.

46. Curves showing the load as a function of gross rise of the pile heads were prepared for each tension test. Moreover, curves showing load vs net rise of the pile head were prepared for the test piles subjected to cyclic loadings. For test piles instrumented with

strain rods, curves were also plotted showing load vs movement of the pile tip. These curves are presented on Plates 30 through 36. The gross pile head movements plotted on the curves are the average of the measurements made by the three dial indicators. The net rise of the pile head was considered to be the gross movement minus the rebound at zero load. Pile tip movement was considered to be the gross movement of the pile head minus the total movement of the lowest strain rod. The curves showing pile tip movements and the curves showing the net rise of the pile head are essentially the same.

47. The distribution of load in the instrumented piles was determined for the tension tests in the same manner as for the compression tests. It was assumed that at the start of the test that no residual stresses or loads existed in the piles from the preceding compressive loadings. The load distribution curves for the instrumented piles are included along with the curves showing the pile head load vs deformation on Plates 30 through 36. The influence of the residual stresses remaining in the piles from driving and/or the compression test is indicated by the apparently high tensile load existing near the pile tips on the load distribution curves. These apparent high tip loads are the result of a relaxation in strain from compression to tension in the pile and of residual tensions. The load distribution in tension becomes more rational when the load distribution is computed on the basis of the change in strain from the final unloading at the end of testing (see Appendix D).

Test data and analyses

48. Tension failure loads were determined from the curves of applied load vs rise of pile head by means of the four methods previously described for evaluating compression tests. In determining the failure load at a net set of 0.25 in., the net rise curves and tip movement curves were used interchangeably. Tension failure loads are presented in Table 8.

49. The tension test data were analyzed to develop general design curves for the four basic types of piles tested. Lateral earth pressure coefficients were computed from the test failure loads by means of the second term of the Terzaghi equation ($Q_u = 1/2\ A_f\ K\ D^2\ \delta' \tan \delta$), presented in paragraph 36. The lateral earth pressure coefficient was assumed to be constant over the full length of the pile. Modifications

to the piling for protection of instrumentation were considered in computing the surface area of the pipe piles. The failure surface for the steel H-piles was assumed to be the perimeter of the circumscribing rectangle. A summary of the tension test analyses showing the average failure load, computed values of K tan δ, the assumed sliding friction angle between the pile and the foundation sand, and the computed average K for each pile is presented below:

Test Pile	Pile Type	Failure Load (T)	Computed K tan δ	Assumed δ	Computed K
1	12" Pipe	70	0.410	25°	0.88
2	16" Pipe	91	0.394	25°	0.84
3	20" Pipe	90	0.356	25°	0.76
4	16" Conc.	71	0.532	30°	0.92
7	14BP73	41	0.207	28.5°*	0.38
8	Timber	25	0.346	30°	0.60
10	16" Pipe	87	0.370	25°	0.79
16	16" Pipe	63	0.308	25°	0.66

*Average of tan δ for minimum perimeter of H-pile

The tension failure loads for the pipe piles, with about 53-ft penetration, are plotted vs effective diameter on Fig. 6. The effective diameter of a pipe pile was considered to be the diameter of a circle with a perimeter equal to the actual perimeter of the pile as modified. The data shown on Fig. 6 indicate that the tension capacity of pipe piles is directly proportional to the diameter of the pipe except for test pile 16, for which the capacity was considerably lower (30%) than that of the other 16-in. diameter piles. The low failure load of test pile 16 was probably caused by the jetting of the test pile and adjacent piles which loosened the sand and reduced the lateral earth pressure coefficient.

Discussion of results

50. Evaluation of the tabulation presented in paragraph 49 summarizing the tension test results shows that the computed lateral earth pressure coefficient for all straight sided piles averaged 0.84 and ranged between 0.76 and 0.92, excluding the H- and jetted pipe piles.

51. Design curves for the four types of piles tested in tension were prepared on the basis of the average computed lateral earth

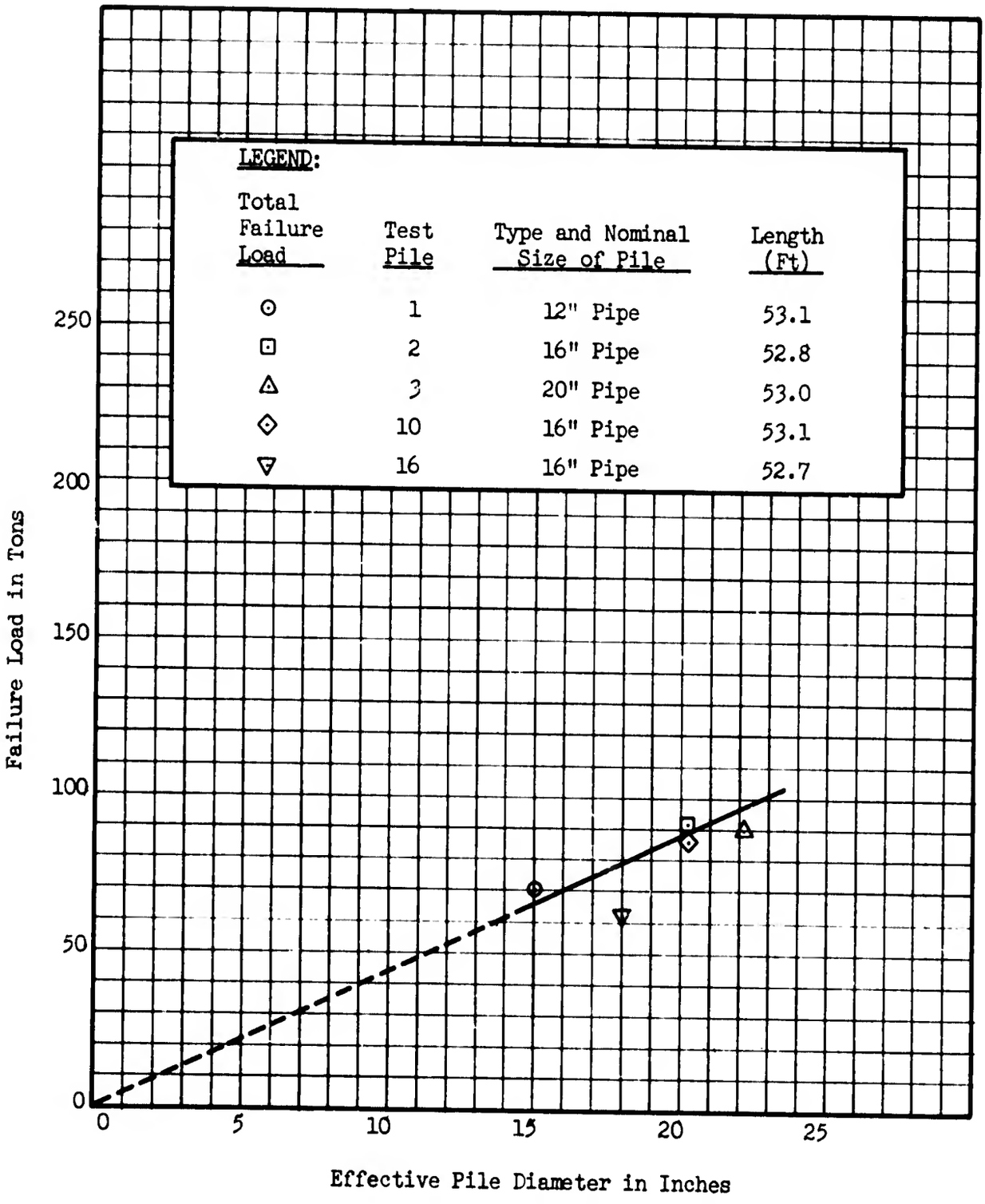

Fig. 6 - TENSILE FAILURE LOAD VERSUS PIPE PILE DIAMETER

pressure coefficient and sliding friction values shown in the tabulation in paragraph 49. These design curves are presented on Plate 37. Individual test capacities for the concrete and steel H-piles are plotted on the applicable curves for comparison with the design curves.

52. The very good agreement among the individual test results for pipe piles indicates that the design curves presented are reasonably valid and can be used for the design of tension pipe piling for this project. Similarly, the tension test results for the concrete and tapered timber piles also appear reasonable, and the design curves presented can be used for the design of concrete and timber piles in tension. However, the design curve for H-piles appears quite conservative and additional tests are recommended to check its validity. The design curves are not considered valid for jetted piles.

Lateral Load Tests

General test procedures

53. The lateral load tests were accomplished in general accordance with the schedules set forth in Table 1. The test piles were loaded normal to the longitudinal and major axis of the pile as close to the ground line as feasible by means of hydraulic jacks. Adjacent piles were used for reactions, except for test pile 12 where the reaction was provided by concrete blocks. Pile head deflections were measured by extensometers located near the ground line and approximately 18 in. above the ground line. Drawings of the testing frames and head instrumentation for lateral loading tests are shown on Plate 38. A typical test setup is shown by photograph 6b, Appendix C. Loads were applied in about 10 equal increments for all tests except for the special repetitive load tests on piles 6 (14" H) and 11A (20" concrete). The lateral loads were applied and released at the rate of 2 tons per min., and were held constant for a minimum period of one hour and until the pile head movement was less than 0.010 in. per hr. Tests were carried to lateral deflections approaching 2 in. except for piles scheduled for subsequent tensile tests and special repetitive load tests; in these instances the lateral deflection at the ground surface was limited to 0.50 in. In the repetitive tests, test piles 6 and 11A were subjected to 100 repetitions of loads of 20.3 kips and 30.6 kips, respectively. These loads

were applied as single increments except for the first, fourth, tenth, fortieth, and hundredth applications wherein the loads were applied in three increments. Ground water levels during the lateral load tests varied from 2 to 3 ft below ground surface as shown on Fig. 3, except for test piles 6, 11A, and 12, where the area surrounding the pile was flooded to a height of 1 in. above the ground line in an attempt to simulate the ground water conditions which would occur in the prototype construction. Field experiments indicated, however, that seepage pressures produced in the subgrade by the ponding approached the additional static pressure caused by the moist weight of the top 2 to 3 ft of subgrade for the depressed ground water condition. Some reduction in the seepage pressures was obtained by introducing water below grade through wellpoints penetrating about 8 ft into the subgrade around the pile. It was concluded that the small reduction in surcharge on the subgrade did not warrant use of the flooding procedure and the disturbances associated with it.

Load test data and analyses

54. A summary of the lateral load test results is shown in Table 9, together with information regarding the method of loading, loading point, lower measurement point, and the lateral load carried by the piles at ground line deflections of 0.25 in. and 0.50 in. Plots of load vs pile deflection at the ground surface are shown for all tests on graph (a), Plate 39, for the first cycle of loading. Load vs deflection curves for the repetitive tests on test piles 6 and 11A are shown on graph (b), Plate 39.

55. Theoretical expressions. The results of the field tests on laterally loaded piles were analyzed by means of the theoretical expressions and non-dimensional coefficients presented by Reese and Matlock (Ref 3) for single piles in cohesionless soil. These expressions are based on a triangular distribution of horizontal subgrade modulus (k) with depth (x) wherein $k = n_h x$. Non-dimensional coefficients are available to simplify computation of deflections, shears, slopes, and bending moments for various conditions of head fixity and pile penetrations for vertical piles loaded normal to their longitudinal axes. These coefficients involve the flexural stiffness of the pile relative to the

soil modulus for varying conditions of pile embedment. The relative stiffness factor T, in in., is defined as:

$$T = \sqrt[5]{\frac{EI}{n_h}} \quad \text{or} \quad n_h = \frac{EI}{T^5}$$

where

EI = Flexural stiffness of the pile in lb in.^{2}

E = Static modulus of elasticity in lbs per sq in.

I = Moment of inertia in in.^{4}

n_h = Coefficient of horizontal subgrade reaction in lb per in.^{3}

T has a unit of length and, if divided by the embedded length of the pile, a non-dimensional depth coefficient can be defined. A study of these coefficients shows that a pile having a length of 5 T or greater behaves the same as a pile of infinite length. As all of the test piles had lengths in excess of 5 T, the following theoretical expressions are applicable for evaluation of the lateral load test data:

Case I - For a moment M_g in in. lbs, applied to the pile at the ground surface (x = 0), the deflection, Y_g, at the ground surface in in. is:

$$Y_g = 1.623\ M_g \frac{T^2}{EI}$$

The slope of the pile, θ_g, at the ground surface in radians is:

$$\theta_g = 1.75\ M_g \frac{T}{EI}$$

The maximum moment occurs at the ground surface, but the maximum soil reaction (w) in lbs per in. occurs at x = 0.65 T. The magnitude of the maximum soil reaction is:

$$w_{max} = 0.45 \frac{M_g}{T^2}$$

Case II - For a shear (Q_g) in lbs, applied normal to the axis of the pile at the ground surface, the deflection (Y_g) at the ground surface in inches is:

$$Y_g = 2.435\ Q_g \frac{T^3}{EI} \quad \text{or} \quad T = \sqrt[3]{\frac{Y_g\ EI}{2.435\ Q_g}}$$

The slope of the pile (θ_g) at the ground surface in radians is:

$$\theta_g = 1.623\, Q_g \frac{T^2}{EI}$$

The moment is zero at the ground line but reaches a maximum at $x = 1.4\ T$. The magnitude of the maximum moment in in. lbs is:

$$M_{max} = 0.772\, Q_g\, T$$

Similarly the maximum soil reaction occurs at $x = 0.85\ T$ and has a maximum value:

$$w_{max} = 0.96\, \frac{Q_g}{T}$$

For piling subjected to combined moments and shears, ground line deflections and slopes may be added algebraically.

56. Coefficient of horizontal subgrade reaction. Values of n_h were computed for the initial loading cycle from the following equation using loads and deflections obtained from graph (a), Plate 39.

$$n_h = \frac{4.42\, Q_g^{1.667}}{Y_g^{1.667}\, (EI)^{0.667}}$$

Plots of n_h vs deflection are shown on graph (c), Plate 39. A recommended design curve for n_h vs deflection for one cycle loading for piles driven into submerged, alluvial Arkansas River sands is also shown on graph (c), Plate 39.

57. Moment. The theoretical moment distribution was computed, using the previous expressions and non-dimensional coefficients from Ref 3, for test piles 2, 10, 12, 13, 13A, and 16 for one of the applied lateral loads on each of these piles using the n_h value determined from the pile head deflection at the corresponding load. These theoretical moments are shown on Plates 40 and 41 as plotted points for comparison with the moments computed from the strain gage readings for the same lateral load. For vertical piles, test piles 2, 10, 13A, and 16, the theoretical and computed moments verify the theoretical assumption regarding the distribution of subgrade modulus. However, for the battered piles, test piles 12 and 13, the theoretical moments are greater than the measured moments. A closer agreement is obtained for batter piles

if the theoretical moments are computed using a parabolic distribution for the modulus of subgrade. Reese and Matlock (Ref 4) have given procedures for the theoretical incorporation of various distributions of subgrade moduli.

58. Repetitive loading. The effect of repetitive lateral loading on pile head deflection at the ground line was determined using the data from the field tests made on test pile 6, a steel H-pile, and test pile 11A, a 20-in. square prestressed concrete pile. The increase in deflection of the pile head with repetition of load is shown by graph (b), Plate 39. The data plotted on graph (b) show that the deflection of the H-pile at the ground surface for the initial load application was increased 190 percent by 100 repetitive loadings; for the concrete piles the increase was 170 percent.

Discussion of results

59. The results of the lateral loading tests demonstrate the validity of the theoretical expressions contained in Ref 3 by Reese and Matlock based on a linear variation of lateral subgrade modulus with depth. Isolated piling subjected to a single lateral load application may be designed by means of the above equations and the coefficient of horizontal subgrade reaction presented on graph (c), Plate 39. For isolated piles subjected to repetitive lateral loadings, the lateral deflections will, however, be about twice the computed value for isolated piles. The relative lateral load capabilities of the test piles are evident from the data presented in Table 9 and from inspection of the load deflection curves presented on graph (a), Plate 39. In general, these curves illustrate that for a given deflection, the lateral load capacity increases with the flexural stiffness of the pile. It appears that except for the timber pile, any of the pile types tested can develop the required maximum lateral capacity if the proper flexural stiffness is provided. As the tests were conducted with the water table near the ground surface, the values of n_h shown on graph (c), Plate 39, are applicable for a water table at or near the ground surface. Values of n_h for an unsubmerged condition can be approximately obtained by multiplying the plotted values of n_h by the ratio of the moist unit weight of the sand to its submerged unit weight (Ref 13).

Pile Driving Criteria

Dynamic equations

60. The compressive failure loads obtained from the tests were compared with ultimate pile capacities computed using the Pacific Coast Uniform Building Code, Janbu, and the Engineering News dynamic equations. Dynamic capacities were computed for each test pile using the actual pile dimensions and physical properties, together with the driving resistance and efficiency for the last foot of penetration and driving characteristics of the hammer employed. The dynamic equations used in the capacity comparisons, as modified to include an efficiency factor, are given below:

Pacific Coast Uniform Building Code:

$$R_u = \frac{12\, e_f\, E_h \dfrac{W + K_r P}{W + P}}{s + \dfrac{R_u L}{A E}}$$

Janbu:

$$R_u = \frac{12\, e_f\, E_h}{K_u\, s}$$

Engineering News:

$$R_u = \frac{12\, e_f\, E_h}{s + 0.1}$$

where

R_u = Ultimate pile capacity in lbs

E_h = Rated hammer energy in ft lbs per blow

e_f = Hammer efficiency

W = Weight of driving ram in lbs

P = Weight of pile in lbs

L = Length of pile in in.

A = Average cross-sectional area of pile in sq in.

s = Average pile set in in. per blow for last 20 blows (s based on average for last foot of driving in this report)

E = Modulus of elasticity of pile material in lbs per sq in.

K_r = Coefficient of restitution: 0.25 for steel piles; 0.10 for all other type piles

$$K_u = c_d \left[1 + \sqrt{1 + \frac{\lambda e}{c_d}} \right]$$

$$c_d = 0.75 + 0.15 \frac{P}{W}$$

$$\lambda e = \frac{e_f E_h L}{A E s^2}$$

The efficiency of the steam hammers was considered to be 84 percent for a hammer in first rate condition operating at the required speed at the rated steam pressure as recommended by the manufacturer. Where the steam pressure at the ultimate pile penetration was less than the rated value, the energy was adjusted downwards in accordance with the following ratio:

$$e_f = 0.84 \times \frac{E_{h(adjusted)}}{E_{h(rated)}}$$

where

$E_{h(adj)} = d\ (W + a\ p)$

d = Hammer stroke in ft

W = Weight of driving ram in lbs

a = Effective downward hammer piston area in sq in.

p = Steam pressure in lbs per sq in.

The average computed efficiencies for the hammers used to drive the test piles on this project were: 0.78 for pipe piles; 0.81 for concrete piles; and 0.84 for H-piles. The capacities computed from the above formulas and the compressive failure loads for the test piles driven with the steam and diesel hammers are shown in Table 11. The ratio between the test failure load and the pile capacity computed from the dynamic formulas are also shown in this table for each pile. These ratios indicate that pile capacities computed from the Pacific Coast equation generally agree with the actual test failure loads better than

those computed from the other equations considered, although the Janbu equation did have good agreement for several piles. For the pipe and concrete piles driven with the 140C hammer and the timber pile driven with the 65C hammer, the test failure loads were all within eight percent of the computed capacity. The ratios of the test failure loads for the steel H-piles driven with the 80C hammer to the computed capacity from the Pacific Coast equation ranged from 1.25 to 1.34. A ratio of 1.5 was similarly obtained for the 16-in. concrete pile driven with the DE40 diesel hammer. The agreement between the dynamic pile capacity curves computed from the Pacific Coast equation and the test failure loads plotted at the recorded final field driving resistance for the last foot of drive is graphically illustrated on Plate 42 for pipe, concrete, timber, and steel H-piles.

Hammer selection

61. The dynamic driving curves may also be used for evaluating the construction capabilities of various pile and hammer combinations. From the shape of the dynamic curves, it is apparent that there is a limiting compressive capacity obtainable for any specific pile and hammer. The flattening of the curve as the number of blows per foot increases indicates that beyond a certain point a considerable increase in the number of blows has little effect on the pile capacity. When this point is reached, driving becomes uneconomical. A comparison of driving curves for several hammers will readily demonstrate the desirability of using a heavy hammer which has a reasonable margin of energy over and beyond that needed to produce the desired capacity. Working capacities up to about 80 percent of the ultimate capacity as determined from the dynamic equation are generally readily obtained.

62. Example. An example of the use of the Pacific Coast dynamic equation to evaluate the driving potential of several pile hammers is shown on graph (a), Plate 43. In this example, it was assumed that the water table is at the ground surface and that a 16-in. diameter steel pipe pile was to have a compressive capacity of 160 tons. Inspection of the graph shows that all of the hammers considered will theoretically drive this pile to the desired capacity although the 80C steam hammer is marginal and would not be conducive to economical driving. Dynamic curves have also been used to determine the maximum

size hammer that can be used without damaging the pile by overstressing it in compression either at the pile head for straight sided piles or at the center of load capacity for tapered piles. Chellis (Ref 5) suggests correlating pile behavior with compressive stresses produced by the hammer. Stress magnitudes would be obtained by dividing the dynamic capacity by the cross-sectional area of the pile. For convenience, the fiber stress produced by driving may be plotted as duplicate ordinates with capacity on the dynamic curve as shown on graph (a), Plate 43. Stresses produced by the hammer would be limited to the working stress of the pile materials or the hammer blows restricted to an allowable maximum.

63. Driving stresses. While the magnitude of compressive and tensile driving stresses developed in prestressed concrete piles is controversial, comparison of field measurements with stresses calculated by means of wave equations, Hirsch, Sampson, and Lowery (Ref 6), show fair agreement. Conclusions reached from the above study regarding the development of driving stresses in concrete piling are listed below:

a. For a given ram energy, a heavy ram produces lower stresses and more permanent set than does a light ram.

b. A light or weak soil resistance produces larger tensile stresses in a pile than a high soil resistance.

c. In general, long piles have higher tensile stresses than short piles.

d. The cross-section of a pile has little effect on the tensile stress.

e. In general, tensile stresses are greater for friction piles than for point bearing piles.

f. A proper cushion is effective in the reduction of both tensile and compressive stresses.

Inasmuch as the piling for this project will be driven in a high resistance soil and hammer weights and energies carefully selected, it is unlikely that the tensile stresses produced during driving will be detrimental to the pile behavior. It should be noted that an examination of test piles 5 and 11, which were pulled following completion of testing, revealed that discontinuous cracks had developed in the middle third of the pile either during driving or handling. The cracking was

essentially the same for both piles despite the fact that one pile was driven with the 140C hammer and the other with the Bodine hammer. Flexure tests made on these piles and on an undriven pile, previously discussed, showed that all three piles had essentially identical load-deformation characteristics. It was therefore concluded that the cracks were superficial and would not affect the structural behavior of the concrete piles. However, for production piles, it may be beneficial to pull and examine several piles for crack development at the initiation of the project, particularly if very heavy hammers are used.

64. Driving limitations for the prestressed concrete piling were established using criteria developed from a literature study made by the U. S. Army Waterways Experiment Station in connection with the driving of long and heavily loaded piling for the Morganza Control Structure (Ref 7). Conclusions reached from this study supplemented by construction experience on the project (Ref 8) indicate that no material damage to the piling will occur if the driving energy per inch of penetration does not exceed 5,000 ft lbs per square inch of pile cross-section. This assumes that local overstress from eccentric driving or irregular pile surfaces will be prevented by using proper alignment and a suitable cushion in the driving head.

Discussion of results

65. The results of the pile driving studies provide a guide for selection of pile driving equipment and establishment of field driving criteria for the locks and dams to be founded on sands in the lower Arkansas River Valley. Correlations between driving resistance and compressive capacity provided by the Pacific Coast Unified Building Code dynamic equations can be used as a guide for selection of pile driving hammers and for determination of pile capacity at penetrations in excess of minimums established after consideration of scour and tensile capacity, e.g., see Plates 43 and 44 for hammer selection and pile driving criteria for ground water table at or near ground surface.

PART IV: MODEL PILE TEST PROGRAM

66. The early techniques used for analyzing pile foundations subjected to lateral loads completely ignored the soil resistance; the ends of the piles were treated as either pinned or fixed, and the problem became strictly an exercise in structural mechanics. It was generally recognized that these techniques were extremely conservative in many cases and attempts were made to modify them to take into account the effect of the soil resistance. Empirical techniques employing the results of field load tests (Ref 9 and 10) on groups of piles were also used to determine the lateral load capacity of piles under structures. More recently, design procedures, e.g. the one developed by Hrennikoff (Ref 11), take the soil resistance into account by assuming that the pile acts as a beam on an elastic foundation. The history of the development of theories for laterally loaded pile groups is given by Prakash (Ref 12).

67. Although the design procedure developed by Hrennikoff accounts for the properties of both the soil and the pile, the answers given by these theories cannot be better than the data used regarding the soil properties. The most important items not generally considered by the presently available design techniques are:

a. Variation of the subgrade modulus along the embedded portion of the pile.

b. Group effect, i.e., the effect of piles on the lateral resistance of adjacent piles.

c. Effect of repeated loading.

d. Shearing resistance offered by the soil to the lateral movement of the pile cap.

If a theory is to predict the behavior of a laterally loaded pile group with a satisfactory degree of accuracy, the above items must be taken into account. Hrennikoff's procedure can be modified to include the foregoing factors provided that information regarding these factors is available. The following paragraphs describe briefly the effects that these factors may have on the behavior of a laterally loaded pile foundation.

68. The lateral subgrade modulus is usually assumed to have a constant value with respect to depth regardless of the soil type. Terzaghi (Ref 13) has shown that the actual variation of the subgrade modulus with respect to depth for preloaded cohesive soils is considerably different, having a value near zero at the ground surface and transitioning smoothly to nearly a constant value at some depth. Therefore, in using the theories now available, it is possible to make a mistake both with respect to the magnitude of the subgrade modulus and with respect to its variation along the pile. The error may result in an underestimate of the deflections and moments by a factor of two (Ref 14). Furthermore, for granular soils, Terzaghi has shown that the subgrade modulus is about zero at the ground surface and increases in a nearly linear fashion with depth.

69. In designing friction pile foundations, it is common to take into account a reduction factor for group loading. This accounts for the fact that a group of piles may not have the same capacity as the capacity of an individual pile multiplied by the number of piles in the group. A similar approach is required for groups of piles subjected to lateral loads. It has been shown by Prakash (Ref 12) that pile spacings on the order of 6 to 8 diameters are required before group action is eliminated with respect to lateral loading. Because pile spacings are generally on the order of three diameters, it is clear that group action should be considered. The effect of ignoring group action is to underestimate the deflection for a given lateral load by a factor of approximately two.

70. Very little definitive information is available regarding the effect of repeated loadings on laterally loaded piles in sand. The information that is available indicates that for a given lateral load the deflection observed at the end of the first load cycle is approximately doubled under the action of repeated loads.

Objective

71. The relationship between the behavior of a single, isolated, laterally loaded pile and the behavior of various piles in a group of similar piles can hardly be determined from field tests because physical and economical considerations preclude testing full scale structures. However, the results of lateral load tests performed on single piles in

the field can be obtained economically. If a practical design procedure is to be developed, it should use the results of lateral load tests on single piles along with some relationship between the behavior of a single pile and the behavior of groups of piles. Therefore, the primary objective of the model test program was to develop for lateral loads the relationship between the load-deflection behavior of a single pile and the various piles in a pile group.

72. Some information is available regarding the behavior of model pile groups consisting of up to nine piles (Ref 12). However, the foundations involved in the Arkansas River Project have on the order of 100 piles per monolith; the extrapolation from nine model piles to 100 prototype piles was considered too speculative without further tests. The model testing program was carried out as an extension of the work presented in Ref 12 in order that the previous experience could be utilized as background information.

73. Another important object of the model pile test program was to check the validity of a Hrennikoff-type analysis. This was carried out by using, as input data to the Hrennikoff-type analysis, coefficients that were determined experimentally rather than analytically. In this manner a check was obtained between the experimental and analytical results wherein the comparison of the two indicated the applicability of Hrennikoff's procedure. An experimental check of the Hrennikoff analysis had never been performed previously.

74. The model pile test program also had several secondary objectives. A series of tests was performed to illustrate the variables affecting the bearing capacity of vertical steel piles. Lateral load tests were performed on both steel and aluminum piles to show the effect of pile size, length, and stiffness on the lateral soil resistance. The lateral load tests also illustrate the variation of the subgrade modulus with respect to depth. Another series of tests was performed to illustrate whether or not one lock wall affected the behavior of an opposing lock wall.

Scope

75. The scope of the model pile test program is set forth in Table 2. Five series of tests were performed; each test series was performed in separate beds of sand. Those tests that were to be compared

directly with each other should have relatively minor variations in the soil properties because they were performed in the same bed of sand. The five beds of sand used in these tests have been designated A through E. The tests are numbered numerically within each sand bed designation, for example, Tests A1 through A22.

76. Tests A1 through A18 were made to evaluate the effect of varying the size, shape, and length of a pile on the vertical bearing capacity of the pile. Tests A19 through A22 were made to evaluate the effect of the flexural stiffness of the pile on the soil resistance offered by the soil to the pile.

77. Tests B1 through B3 were made to compare the soil resistance offered to a single isolated laterally loaded pile with that offered to a wall. The tests also illustrate the influence that one lock wall may have on the movement of an opposing lock wall.

78. Test C1 was made to verify those aspects of the Hrennikoff analysis related to structural mechanics. Three pairs of piles were capped to form a group; one pair was vertical, one was battered with the direction of the lateral load, and one was battered against the direction of the lateral load. The group was then subjected to both vertical and lateral loading. The test results were compared with theoretical predictions from the Hrennikoff analysis using the experimentally determined axial and translational stiffnesses at the pile heads.

79. Tests D1 through D3 were made on two carefully scaled model walls, each consisting of three lock wall monoliths; the walls were placed opposite each other at a scaled distance of 110 ft, the width of the locks in the Arkansas River project. One wall was supported on vertical piles only (Test D1), and the other wall supported by batter piles only (Test D2). In Tests D1 and D2, the walls were loaded individually and the lateral deflection measured for various lateral loads. In Test D3, the walls and foundation piling for Tests D1 and D2 were loaded simultaneously with repetitive lateral loads.

80. Test E1 was made on a scaled model of three monoliths of a typical dam section supported on batter piles. Repetitive lateral loadings were applied to each monolith and the deflections measured.

Test Series A

Purpose

81. The general purpose of Test series A was to gain experience with the model materials that had been selected and to define numerically the parameters controlling their behavior. The test series also had as its purpose the verification of the model techniques. Tests A1 through A18 show the effect on the vertical bearing capacity of varying the width, shape, and length of the pile. A consistent pattern of results was obtained, which indicated that model techniques could be used to determine the effect of these variables on the bearing capacity of a pile in sand. Tests A19 through A22 show the effect of varying the flexural stiffness of the pile on the soil resistance offered to the pile. These tests illustrated that the flexural stiffness of the pile has a minor effect on the soil resistance, and confirm that the subgrade modulus for granular materials has a triangular variation with respect to depth.

Description of model

82. Tests A1 through A18 consisted of applying compression loads on 1/2-in., 3/4-in., and 1-in. diameter model piles with embedded lengths of 12 in., 24 in., and 36 in. for each of the three different diameters. A similar series was performed on square piles having dimensions of 1/2 in., 3/4 in., and 1 in. The pile size and the embedded length for Tests A1 through A18 are given in Table 13. All the piles were made of steel and had a length 6 in. longer than the embedded length; the tips were flat. The extra length was required for instrumentation purposes. Lateral load tests were performed on piles in Tests A19 through A22. Test A19 consisted of an instrumented, 1/2-in. square, hollow, steel pile; the strain gage configuration was the same as that for the aluminum piles. Tests A20 and A21 were solid steel bars, 1/2 in. square and 1/2 in. x 1 in., respectively. Test A22 was an aluminum monitor pile.

83. The location in plan of each test in Series A is shown on (a), Plate 45. The tests were performed in a bin 4 ft in diameter with a depth of 4 ft. The pile spacing in plan was chosen so that neither an adjacent pile nor the wall of the tank was closer than 6 in. to the pile being tested. In addition, no two adjacent piles had the same length; this avoided disturbance of one pile by the soil motions that occur at

the tip of an adjacent pile. A photograph (b) of the test set-up is shown on Plate 45.

84. All the piles were supported initially from cross members placed across the soil tank. The sand was then rained into the bin as described in Appendix A. After the tips of the piles of each of the three different lengths were embedded from 3 to 6 in. during the raining process, the piles were given a slight axial load to insure that they seated properly in the sand. The remainder of the sand was then placed and the falsework supporting the piles removed.

Procedures

85. Bearing capacity tests. The arrangement that was used to apply the axial loads to the piles and to measure the axial deflections is shown on (b), Plate 45. A hydraulic ram was mounted over the piles in series with a sensitive proving ring. A cantilever arm attached to the pile head served as a reaction for the dial indicator that was used to measure the axial deformation. The piles were loaded to failure in approximately 10 min.

86. The observed test data consisted of the load applied to the pile and the corresponding deflection. The test data were plotted as the test progressed to insure that a sufficient quantity of data was taken. In general, the quantity of observations taken was more than double that needed to define the relationship between load and settlement. The proving ring had a sensitivity of approximately 0.0008 in. per lb of load. The axial settlements were measured with an extensometer with a 0.001-in. per division dial indicator.

87. Lateral load tests. Lateral loads were applied to piles A19 through A22 at the ground surface. This was accomplished by placing a string around the pile and carrying it horizontally over a pulley from which a hanger-and-weight system was suspended. The deflections were measured at the ground surface by means of a 0.0001-in. per division dial indicator. The loads were applied in 1-lb increments up to a total of 6 lbs; the deflection was observed for each load increment. For Tests A19 and A22, the bending moments were observed along the embedded portion of the piles by means of SR-4 strain gage instrumentation for each applied load.

Analysis of data

88. Bearing capacity tests. The observed load-settlement relationships for Tests A1 through A18 are plotted on graphs (c) and (d) on Plate 45 and graphs (a) through (d) on Plate 46. Failure was defined by arbitrarily selecting a point on the load-settlement curve where it appeared to become tangent to a steep and straight line approaching ultimate failure. After the failure load had been defined, it was corrected for the weight of the pile and attached equipment. All tests were treated in a similar manner to arrive at the corrected failure loads listed in Table 13.

89. A lateral earth pressure coefficient of 0.33 was arbitrarily assumed in analyzing the test data; however, this coefficient of earth pressure takes into account the fact that sand was placed around the pile instead of the piles being driven into the sand. The sliding friction angle for steel on sand was determined in the soils laboratory of the University of Illinois to be 23°. By use of the Terzaghi formula, Ø-values were determined which make the theory and the test results compatible; this was accomplished by substituting the experimentally determined components and solving for Ø at the pile tip. The Ø-values were consistent and ranged from 36° to 38°. For comparison, the Ø-value of the sand used in the model as obtained from a triaxial test was 36.4°. The ultimate capacity of the model piles as a function of the embedded depth is shown for round piles (a) and square piles (b) on Plate 47. The curves through the points indicate the theoretical values computed from the Terzaghi formula for the Ø-value indicated. Therefore, the theory accounts satisfactorily for variations in size, shape, and length of the piles.

90. Lateral load tests. The load-deflection relationship observed at the ground surface for the 1/2-in. diameter aluminum monitor pile (A22) was analyzed according to the procedures described in Appendix B. The observed moments for lateral loads of 2, 4, and 6 lbs have been plotted vs depth on graph (a), Plate 48; the deflections corresponding to these loads are given in the accompanying tabulation. The coefficient of horizontal subgrade reaction (n_h) was determined for each of the loads applied to the pile; n_h has been plotted vs deflection on graph (b), Plate 48. It is clear that n_h is dependent on deflection. The

dependence is not as serious as it might appear because the deflections and moments depend on approximately the square root of the absolute magnitude of n_h; therefore, variations in n_h have a relatively small effect on design calculations. From the relationship on graph (b), Plate 48, it is clear that high values of n_h exist at small deflections (0.01 in.), presumably corresponding to elastic behavior of the soil near the ground surface. The soil near the ground surface tends to become plastic at larger deflections (0.05 in.) with a resulting decrease in n_h. Beyond the region of relatively low deflections, the n_h vs deflection relationship is nearly constant; for the pile tested, the minimum value of n_h is approximately 8.5 lbs per cu in. Theoretical moments were computed as described in Appendix B and are plotted as curves with the test data on graph (a), Plate 48. An excellent correlation between the theoretical and experimental results was obtained indicating that the assumption of a triangular variation of subgrade modulus in granular materials with respect to depth is correct.

91. On the assumption that the n_h vs deflection relationship for the monitor pile (A22) is valid, theoretical moments were computed for test pile A19 and the moments plotted on graph (a), Plate 49, along with the experimental data. In the calculations for moment at a given load (Q_g) and deflection (Y_g), n_h was taken from graph (b), Plate 48, as the value corresponding to the deflection (Y_g). Again, an excellent correlation of theoretical and observed moments was obtained. It should be noted that the pile used in the test, test pile A19, had a flexural stiffness of 7.30×10^4 lb-in.^{2} which is approximately five times that of the hollow aluminum monitor pile (1.5×10^4 lb-in.^{2}). Therefore, if the coefficient of horizontal subgrade reaction is dependent on the flexural stiffness of the pile, the dependency is minor and of no consequence.

92. The theoretical deflections for test piles A20 (0.5 in. wide) and A21 (1.0 in. wide) were predicted using the n_h vs deflection relationship for the monitor pile on graph (b), Plate 48. The values of n_h were taken from graph (b), Plate 48, at corresponding deflections, as for pile A19. A theoretical load-deflection curve for each pile has been plotted on graph (b), Plate 49, along with the observed data. As the correlation between the theoretical and experimental results is

satisfactory, it may be reasoned that a variation in the width of the pile (from 1/2 in. to 1 in.) does not significantly alter the subgrade modulus.

93. The values obtained for the coefficient of horizontal subgrade by evaluation of the monitor pile test data can be used with piles of different flexural stiffnesses and different widths. This allows the computation of deflections and moments for other types of piles embedded in the same soil. The tests also indicate the validity of the assumption that the subgrade modulus is essentially zero at the ground surface and increases linearly with depth. Therefore, it is concluded that the assumed variation of subgrade modulus with respect to depth is appropriate for granular soils and that the coefficient of horizontal subgrade reaction does not vary significantly with changes in the width or flexural stiffness of the pile. Furthermore, the model materials and techniques selected give a reasonable representation of prototype behavior.

Test Series B

Purpose

94. This test series had two purposes: (1) to compare the soil resistance offered to a pile with that offered to a wall, (2) to demonstrate whether or not one lock wall can influence the deformation of an opposing lock wall. The influence of opposing lock walls was to be determined by comparing the load-deflection curves for two walls when loaded individually with those for simultaneous loading.

Description of model

95. A plan and section of the model walls are presented on drawings (a) and (b), Plate 50. The tests were performed in a tank 9 ft-4 in. by 10 ft-6 in. by 2 ft-6 in. deep. Two walls were manufactured from steel plate 10 in. x 36 in. x 3/4 in.; they were embedded 6 in. and spaced 33 in. apart, corresponding to 110 ft in the prototype. In addition, two 1/2-in. square x 10-in. long steel bars were used as individual piles; they were also embedded 6 in. The walls were loaded at approximately their lower third point to reduce the tendency of the walls to rotate as they were translated. A hydraulic ram was used to supply the

load to a 2-ft long arm welded to the back of the wall. The force was measured by means of an SR-4 strain gage dynamometer on the head of the ram. Deflections were measured by means of dial indicators reading to 0.0001 in. per division. Three dial indicators were used for each wall; one at each end of the wall and the other approximately 6 in. above one of the lower dials. Because the distance between the dials was known, the data could be converted to horizontal and vertical rotations in addition to the translation. A photograph of the test apparatus is shown (c) on Plate 50.

96. The piles were loaded laterally at the ground line by means of weights suspended on a string running over a pulley to the piles. The movement of the piles was recorded at the ground surface by means of a dial indicator reading to 0.001 in. per division.

Procedure

97. The tests on the two piles were carried out by adding loads in increments and recording the deflection for each load. A preliminary test indicated that the wall models had an ultimate capacity of approximately 250 lbs. The test loads were, therefore, limited to approximately 150 lbs. Each wall was loaded up to 150 lbs and unloaded four times. The fourth load cycle gave essentially the same behavior as the second and third load cycles; therefore, it was concluded that the behavior under the fifth load cycle could be predicted from the fourth load cycle. By this procedure, the effect of the opposing wall could be determined when both walls were loaded together. After the cyclic loading of each wall, both walls were loaded simultaneously.

Analysis of data

98. In order to compare the data for both the piles and the walls, the load on the walls has been expressed as that acting on a 1/2-in. width. In this manner, a direct comparison is obtained between the soil resistance offered to an isolated pile 1/2-in. wide and that offered to a wall that is essentially infinitely long. The load for a 1/2-in. width has been plotted vs the corresponding deflection on graph (d), Plate 50. The load-deflection relationships for the individual walls are those for the fourth cycle which is presumed to be nearly that which would have been observed for the fifth loading cycle for each wall when loaded individually. The walls encountered more resistance when loaded

simultaneously than when loaded separately; this resulted in a 10% to 15% reduction in deflection for a given load. For a given load per unit of width, the walls deflect approximately 10 to 15 times as much as the piles.

99. The tests clearly illustrate the striking difference in the behavior of a wall as compared to that of a single isolated pile. The reduced deflection observed under a given load when both walls were loaded simultaneously, as opposed to when they were loaded individually, is to be expected on theoretical grounds. However, the reduction in deflection is not significant enough to warrant a change in design procedures.

Test Series C

Purpose

100. Test series C was designed to compare the behavior of a pile group, containing vertical piles and batter piles oriented in different directions with respect to the load, with the behavior theoretically predicted according to a Hrennikoff-type analysis. The axial and translational stiffnesses of the pile head were determined experimentally. On the basis of these measurements, the rotational stiffness of the pile head could be computed. The experimental data supply the information required for the structural mechanics aspects of the Hrennikoff analysis.

Description of model

101. The piles in Test C were located in the same 4-ft diameter tank used for Test series A. The layout of the pile group is shown (a) on Plate 51, which also shows the location of the monitor pile. Two rows of three piles each were oriented in the direction of the horizontal loading; the space between the rows was 3 in. center to center. In the direction of loading, the piles were spaced 5 in. center to center. According to Ref 12, these pile spacings should assure that the behavior of one pile does not interfere with the behavior of an adjacent pile; therefore, group action under lateral loading was eliminated as a variable. The six piles were divided into a pair of vertical piles at the center of the group, a pair of piles on a 3:1 batter in the direction of the lateral load, and a similar pair battered away from the load

(shown on (b), Plate 51). The piles were embedded 21 in. into the sand and extended 4 in. above the sand surface. A 9 x 15 x 2-1/2-in. thick pile cap was poured around the piles; the cap material was "hydrocal."

102. Vertical loads were added to the pile group by placing weights directly on the cap. A photograph of the loaded pile cap with the attached instrumentation and horizontal loading equipment is shown (c) on Plate 51. Two dial deflection indicators reading to 0.0001 in. per division were placed behind the group; these indicators measured horizontal rotation as well as translation. A level bubble with a sensitivity of 5 sec per division was placed on the pile cap to measure rotation in a vertical plane. The horizontal load was applied with dead weights and a pulley system.

Procedure

103. The pile group was tested under two different loading conditions. First, vertical and horizontal loads were added up to loads of 50 lbs vertically and 51 lbs horizontally (see loading schedule, Table 14). In this case, the pile cap was in contact with the sand which offered some resistance to both vertical and horizontal movements. A second loading condition was produced by removing approximately 1/8 in. of sand from beneath the pile cap. In this case the pile cap and the loads added to the cap were supported entirely by the piles. A maximum vertical load of 50 lbs and a maximum horizontal load of 31 lbs were applied. The rotations and horizontal deflections of the pile cap were measured for each loading condition along with the bending and axial strains acting in the piles.

104. Before the piles were capped, the axial and lateral stiffnesses of each pile were determined by measurement. These values were used to determine the input data to a Hrennikoff-type analysis. The axial stiffness was obtained by adding axial loads up to 6 lbs, repetitively; the load-deflection relationship for each cycle was observed until it became clear that the behavior was essentially elastic and that the relationship for the next cycle of loading could be predicted. The lateral modulus was obtained by applying a 4-lb load at the ground line, and measuring the deflection at the same point. Generally from four to five cycles of loading were required before the behavior became nearly elastic and the

load-deflection relationship for the next cycle could be predicted. Both moduli were determined for the last loading cycle; these moduli were expected to apply after the piles were capped and loaded as a group.

Analysis of data

105. The load-deflection relationships at the sand surface and the moment vs depth relationships have been treated in the manner described in Appendix B. The moment vs depth relationship for a 4-lb load applied to the single isolated monitor pile is shown on graph (a), Plate 52. It should be noted that this pile is useful for judging the relationship of Test series C to any other test series performed in this investigation, but it is not applicable directly to the pile group for the reasons given below. The moment vs depth curves for a 4-lb normal load applied to each of the pairs of piles tested are given on graphs (b), (c), and (d), Plate 52. It was assumed that batter piles could be treated in the same manner as vertical piles. The deflections and T-values are also given for each pile in the accompanying tabulation. The T-value for the monitor pile is approximately 40% higher than that for the pair of vertical piles because the T-value for the pair of vertical piles is for the fourth or fifth load cycle, whereas that for the monitor pile is for the first cycle. If a standard of comparison is desired for the six piles in the group, it is suggested that the two vertical piles be used as the standard.

106. The horizontal load has been plotted vs the horizontal deflection on Plate 53 for each of the two pile cap conditions (resting on the sand and clear of the sand). The solid line represents the case with the pile cap resting on the sand; the numbers preceding the letter V represent the total vertical load in lbs that is on the pile group at the point in question. In this manner, a complete load-deflection history of the pile cap is given. The dashed line represents the load-deflection relationship when the pile cap was not touching the sand. This has been plotted as though it started from the same zero point as the first load test. Note that considerably more deflection is observed when the pile cap does not touch the sand than when it rests on the sand.

Hrennikoff theory

107. The experimentally determined pile constants have been inserted into the Hrennikoff-type analysis for the purpose of predicting the

deflection of the pile cap and the moments at the pile heads. Table 15 lists the pertinent information regarding the pile stiffnesses. By using the T-value and the expressions in par. 55, the translational and rotational stiffnesses of the piles have been computed as recommended by Hrennikoff (Ref 11); the stiffnesses have been divided by the axial stiffness to get the Hrennikoff ratios, r_1, r_2, and r_3. For the condition where the pile cap was not touching the sand, and for a horizontal load of 31 lbs and a vertical load of 50 lbs, the moment, shear, and axial loads at the pile head were computed by a Hrennikoff-type analysis and are listed in Table 15. The experimentally determined moment, shear, and axial loads are also listed in Table 15 for comparison. The comparison of moments is remarkably good and the comparison of the shears is quite acceptable. However, the axial loads in the pair of piles battered away from the horizontal load is approximately 2.5 lbs higher than the computed values of 0.4 lb, whereas the axial load in the pair of vertical piles is approximately 3.5 lbs lower than the computed value of 9.5 lbs. A good check was obtained for the pair of piles battered with the load (15.4 lb compared to 16.1 lb computed). If the pile cap was not perfectly rigid the observed discrepancies would be anticipated. Considering that the possible experimental error in determining the smaller axial loads (described in Appendix A) is near the magnitude of the actual loads under consideration, the comparison of the axial loads can be classified as acceptable. For the maximum pile load, which is the load upon which a design is usually based, the discrepancy is less than 5%. A lateral deflection of 0.0074 in. was predicted theoretically whereas the measured value was 0.0088 in., or 19% more than the predicted value.

108. Test C demonstrates clearly that a triangular variation of the subgrade modulus is appropriate for computing the pile head constants for use in a Hrennikoff-type analysis. Furthermore, the fixity of the pile head should be considered in the analysis (the foregoing comparison between experiment and theory assumed that the pile head was fixed). If these refinements are accounted for, then a Hrennikoff-type analysis will probably give results that are sufficiently accurate for design purposes.

Test Series D

Purpose

109. The purpose of Test series D was to perform lateral load tests on scaled models of the actual pile groupings under consideration for two of the lock wall monoliths. Two walls, consisting of three monoliths each, were constructed opposing each other as they would in an actual lock; the distance between them was equal to 110 ft in the prototype, or 44 in. in the model. The influence of the piles beneath one lock wall on the deformation of the piling beneath an opposing lock wall was to be determined by testing both walls at the same time. The lock walls were also to be subjected to repetitions of load to evaluate the influence of cyclic loading. In addition, the behavior of single isolated piles was to be determined for comparison with the behavior of piles within the groups.

Description of model

110. Pile groups. A plan of the model used for Test series D is shown (a) on Plate 54. The three monoliths labeled V1, V2, and V3 comprise the wall founded on vertical piles. Similarly, the three monoliths labeled B1, B2, and B3 comprise a wall supported by batter piles. Two single isolated monitor piles were placed near monoliths V3 and B3; these were tested and removed before the monoliths were tested. A photograph of the pile caps on the piling for the two model walls is shown (a) on Plate 54. All tests were performed in the same tank used for Test Series B.

111. The scale factor for the pile group is the width of the model pile (1/2-in.) compared to the width of a prototype pile. For a 14-in. wide pile the scale factor is approximately 1:28; the scale factor for other piles can be determined similarly. The center to center pile spacing in terms of pile width is the important variable with respect to group loading. The B monoliths contained 96 piles each, part of which are battered 3:1 towards the lock chamber while the remainder were battered 5:1 away from the lock chamber. A plan is shown (a) on Plate 55 of the pile layout for the B-monoliths which are essentially models of the land wall monoliths for Lock 3. The V-monoliths had 99 piles each with a pile spacing of four diameters in both directions (see (b),

Plate 55). This contrasts to the pile spacing of four diameters laterally in the battered pile groups, and 3.2 diameters parallel to the load. For the batter pile groups, the significant spacing is the 3.2-diameter spacing parallel to the load.

112. Construction of models. Sand was placed in the tank up to a level 16 in. below grade. Then a jig was placed that would hold the model piles in position while the sand was placed around them. The piles were put into position at their proper location in plan and given the proper batter; they were then tapped to grade with a small hammer. Photographs of the piling for the two lock walls during construction are shown on (a) and (b), Plate 56. After the piles were positioned, the sand was placed as described in Appendix A. Forms were made with 3/8-in. plywood and the pile caps were poured using "hydrocal." The pile caps were separated by 3/8-in. and had a height of 8 in. at the rear and 4 in. on the lock chamber side. Masonite strips 1/8-in. thick had been placed between the pile rows beneath the pile cap before the cap was poured. These strips were removed after the forms had been stripped in order to separate the pile cap from the subsoil. This allowed the entire weight of the pile cap to be carried by the piles.

113. Loading and instrumentation. Six hydraulic jacks, each having SR-4 strain gage dynamometers mounted on the head, were used to load the model monoliths (see (b), Plate 54). The load was applied 6 in. above the sand surface, thus applying a moment as well as a lateral load. Each monolith had three dial indicators mounted on the back; two of the dial indicators were near the sand surface whereas the third was 6 in. above one of the lower dials. Because the distance between the dials was known, both the vertical and horizontal rotations could be computed in addition to the horizontal translation. A total of twelve instrumented piles were installed in the monoliths. Five of the vertical piles were instrumented, three in monolith V2 and two in monolith V3. Seven of the batter piles were instrumented, five in monolith B2 and two in monolith B3. The instrumented piles were located as shown on (a) and (b), Plate 55.

Procedure

114. The procedure for loading the model foundation piling was to load each monolith individually for two or three cycles before loading

all three monoliths simultaneously. This procedure gave an indication of the difference in behavior for one pile group acting by itself compared to all three pile groups loaded together. After loading the monoliths for each wall individually, both walls were loaded simultaneously. The details of the loading sequence are given in Table 16.

115. Monoliths V1 and V3 were loaded simultaneously on the assumption that they acted individually because of their wide separation. The loading proceeded from zero to 1 and 2 lbs per pile, returned to zero, and then increased to 2 lbs; the load was finally returned to zero. While monoliths V1 and V3 were being loaded, the deflections were recorded for each load increment, whereas the strains in the instrumented piles were recorded only for the second application of the 2-lb per pile load. After monoliths B1 and B3 were tested, monolith B2 was loaded. This monolith was subjected to three cycles of load up to 2 lbs per pile; the strains in the instrumented piles were recorded on the first application of the 2-lb per pile load. The deflections were recorded at each load interval.

116. After the individual monoliths had been tested, all three monoliths, V1, V2, and V3, were loaded simultaneously up to 4 lbs per pile; the load was cycled three times. The deflections were recorded for each load increment whereas the strains in the instrumented piles were recorded only for the initial application of the 2- and 4-lb per pile load. A similar loading procedure was used for the B series monoliths as indicated in Table 16. When both lock walls were loaded simultaneously, the deflections and strains in the instrumented piles were recorded for the initial application of the 2- and 4-lb per pile load. This was followed by eight cycles of loading to 4 lbs per pile for which the deflection was recorded for each monolith. The load was not reduced to zero after the 4-lb loading; however, the load was reduced to that corresponding to the hydraulic ram friction, or approximately 0.5 lbs per pile. On the tenth cycle of loading to the 4-lb per pile load, all of the strains and deflections in the instrumented piles were recorded. The cycling was continued until 50 cycles of the 4-lb per pile load had been applied; deflections and strains were recorded for the cycles indicated on Table 16.

Analysis of data

117. The relationships between lateral load and lateral deflection for monoliths V2 and B2 are shown on graphs (a) and (b), respectively, Plate 57. In order to have a standard of comparison throughout the test program, the lateral load has been plotted in terms of pounds per pile. The lateral deflection at the surface of the sand was determined by averaging the two deflection dial readings and then correcting them for the observed vertical tilt of the monolith, taking into account the distances that the gages were located above the sand surface.

118. The load-deflection curves show the loading history of each monolith. The cycle numbering sequence begins with the 4-lb load; these are labeled 1 through 3 on Plate 57. Under the cyclic loading, when both walls were loaded together, the numbering sequence for the 4-lb loading continued consecutively starting with cycle 4.

119. It should be noted that end monoliths V1, V3 and B1, B3 were included in the test program for the sole purpose of assuring that the center monoliths, V2 and B3, behaved as typical interior monoliths. Considerable distortion of the end monoliths was observed during testing. As was anticipated, more resistance to movement was observed along the outer edges of the end monoliths than occurred at the edges adjacent to the center monoliths. Because of this, the end monoliths twisted in the horizontal plane. No proven analytical techniques are available for pile groups in torsion; therefore, the analysis of the end monoliths is outside the scope of this investigation and the data are not presented herein.

120. The moment vs deflection relationships for the two monitor piles (1 and 6) are given on graphs (a) and (b), Plate 58. Moments have been plotted for loads of 2, 4, 4 lb after 5 cycles of loading, and for zero load at the end of the test. Some increase in both deflection and maximum moment was observed under the cyclic loading in monitor pile 1. However, the first 4-lb load on monitor pile 6 was accidentally applied with impact; therefore, the deflection and moments on the first cycle exceeded those for the fifth cycle. As in previous tests, the comparison of theoretical moments with the observed moments supports the assumption of a triangular variation of subgrade modulus with respect to depth.

121. The moment vs depth relationships for the eight instrumented piles under monoliths V2 and B2 are shown on graphs (a) through (d) of both Plates 59 and 60 for the initial 2-lb loadings when the monoliths were loaded individually and also when they were loaded as part of a wall. In addition, a theoretical curve has been plotted for one of the loads for each pile. The theoretical curves support the conclusion that a triangular variation of the subgrade modulus with respect to depth is appropriate, regardless of the wide variation in the behavior of different piles in the pile group. Large variations between the theoretical curves and the experimental data occurred for several piles in the end monoliths because they were subjected to torsion in addition to lateral load. Pile 4, which was located in the center of monolith V2 attracted approximately twice the shear anticipated. The cause of this unexpected stiffness is unknown. However, piles 3 and 5 in monolith V2 behaved as anticipated and may be considered representative of the piles in the group. Generally, for the batter piles, the maximum theoretical moment exceeded that observed experimentally; this is consistent with the remainder of the test program, including the field tests.

122. Group action. Before group action is considered, the effect of one lock wall upon an opposing lock wall deserves some comment. The load deflection histories for the center monoliths, V2 and B2, show three cycles of the 4-lb per pile loading while each wall was being tested individually. The fourth cycle is the first 4-lb per pile loading when both walls were loaded together. An insignificant reduction in deflection was observed for monolith V2. The change in deflection between cycle 2 and cycle 3 is several times that observed between cycle 3 and cycle 4. However, for monolith B2 only a very small change was noted. It was concluded from Test Series B that the influence of one lock wall on an opposing wall would be negligible for design purposes. The foregoing interpretation of the load deflection relationships for Test Series D supports this conclusion.

123. In the analysis of group action, only monoliths V2 and B2 will be discussed. It can be noted from Plate 57 that the behavior of monoliths V2 and B2, when loaded individually, is very similar to that when loaded as part of a wall. Therefore, the conclusions drawn for the center monoliths as individuals will apply when they are loaded as part of a wall.

124. A Hrennikoff-type analysis was performed for monolith V2 when subjected to a lateral load of 2 lbs per pile. The analysis indicated that tension loads in several of the piles exceeded the tension capacity of the piles. In a supplementary test, it was determined that the axial stiffness in tension was 1000 lbs per inch and that a failure occurred at approximately 6 to 7 lbs per pile. Therefore, the test results at a lateral load of 2 lbs per pile would be expected to give deflections that are higher than would be the case if the tension capacity were not exceeded. To avoid this difficulty an analysis was made for a load of 1 lb per pile. An average T-value of 4.4 in. was computed for monolith V2 assuming that the pile heads were fixed at the pile cap and making an allowance for tilt of the pile group (0.0005 rad). If this T-value is compared to that for the monitor piles (T = 3.39), the T-multiplier (T for the group/T for an individual) becomes 1.30. However, the T-values for the monitor piles were somewhat less than those for certain individual piles that were tested around the periphery of monolith V2 because the sand adjacent to the piles within the pile group was less dense than that around the isolated individual piles. It is believed, therefore, that a more reasonable comparison can be made using the T-values for the piles tested at the periphery of monolith V2 as individuals than by using the monitor piles. The T-value for the individual piles in monolith V2 was 3.53 in.; on this basis, a T-multiplier of 1.25 is obtained. The T-multiplier of 1.25 obtained for a pile spacing of four pile widths equals the value for a spacing of three pile widths observed by Prakash (Ref 12). Therefore, the T-multiplier for large groups is slightly higher than that for the smaller groups tested by Prakash.

125. A Hrennikoff-type analysis for pile group V2 was performed using T = 4.4 in., EI = 1.5×10^4 lb-in.^{2}, an average load of 1 lb per pile, and an axial stiffness of 1600 lbs per in. as determined by calibration of several piles in the pile group. A theoretical lateral deflection of 0.0062 in. was computed using these data compared to the 0.0075 in. actually observed. Therefore, a Hrennikoff-type analysis gives a reasonable prediction of the actual deflections.

126. A Hrennikoff-type analysis was performed for monolith B2 with the same input data as for monolith V2. No tension loads were computed

that exceeded the tension capacity of the piles. The observed lateral displacement was 0.0038 in., whereas the computed displacement was 0.0033 in. It is probable that the discrepancy between these two values could be reduced considerably if a T-value higher than 4.4 in. were used. It should be noted that the pile spacing in group B2 is 3.2 pile widths compared to 4.0 pile widths for group V2. Under these conditions, a higher T-multiplier number should be expected; this corresponds to a higher T-value. Therefore, a higher computed displacement would result if this correction were made. The comparison is considered satisfactory without the correction. It is concluded that a Hrennikoff-type analysis provides a reasonable method for predicting the deflection of a laterally loaded pile group provided that the proper axial stiffnesses and the proper variation of the subgrade modulus with respect to depth are used in the analysis.

127. Repetitive loading. The aforementioned considerations, including the fact that the tension capacities of the piles were exceeded in the vertical pile monoliths at 2 lbs per pile load, and in the batter pile monoliths at 4 lbs per pile load have obscured somewhat the results obtained from the cyclic loading portion of the test program. An inspection of the load-deflection curves on graph (a), Plate 57, for monolith V2 indicates that at the 4-lb load the ratio of the deflection for the last cycle of loading to that for the first cycle of loading is 1.5. An extremely large deflection was noted under the first cycle of 4-lb loading. The cyclic loading produced an increase in deflection of approximately 50 percent, whereas a value of approximately 100 percent was anticipated (Ref 12). It is clear that this behavior must be related to the fact that the tension piles were not fully effective and that the compression piles were apparently becoming more effective.

128. An inspection of the load-deflection curves on graph (b), Plate 57, for monolith B2 shows that the ratio of the deflections for the last cycle of 4-lb per pile loading to the first cycle is 2.87. This behavior probably was caused by tension piles that were failing progressively, thereby increasing the deflection of the monolith. Therefore, the deflection ratio of the last cycle to the first cycle should be interpreted downwards from 2.87. It is probable that the deflection ratio has a value between 1.5 and 2.87.

129. Tension pile behavior. In both of the aforementioned Hrennikoff-type analyses, 1600 lbs per in. was used for the axial stiffness of the piles. If those piles that were in tension were treated as though they had a stiffness of 1000 lbs per in. as determined by test, the computed deflections would have been somewhat higher and would have agreed more closely with the observed deflections.

Test Series E

Purpose

130. The purpose of Test series E was to perform lateral load tests on a scaled model of the piling beneath three dam monoliths. The dam monoliths were to be subjected to repetitions of load to evaluate the influence of cyclic loading. In addition, the behavior of single isolated piles was to be determined and compared to the behavior of piles within the group.

Description of model

131. Pile groups. A plan (a) and photograph (b) of the model used for Test series E are shown on Plate 61. The three monoliths, labeled M1, M2, and M3, represent a pier monolith and two sill monoliths on either side of the pier. The pier monolith was chosen as the center section because it has the largest number of piles and, therefore, should be subject to the greatest effects from group action. A single isolated pile was placed near monolith M2 as shown on (a), Plate 61.

132. A plan (a) and photograph (b) of the piles in monoliths M1 through M3 are shown on Plate 62 on which the directions of the batter of each row of piles are indicated. A total of 245 piles was used for test E. The sill monoliths had 47 piles each, whereas the pier monolith had a total of 150 piles. All piles in the group were battered 3:1. The pile spacing was approximately three pile widths in the direction of the loading, but somewhat greater in the sill monoliths in the direction normal to the loading. For pier monolith M2, the spacing was three pile widths in both directions. For 14-in. wide piles, the scale factor is approximately 1:28; for other sizes of prototype piles the scale factor would be proportional.

133. Construction of models. Sand was placed up to a level 12 in. below grade. Then a jig was placed to hold the model piles in position while sand was placed around them. The piles were put into position at their proper location in plan, given the proper batter, and then tapped to grade with a small hammer. It should be noted that the piles were tapped a greater distance into the sand in these tests than was the case in Test series D. Therefore, their axial stiffness should be expected to be somewhat higher. After the piles were in position, sand was placed as described in Appendix A. The tank was the same one used for Test series B and D. Forms were made for the pile cap and the construction generally proceeded as described for Test series D. The pile caps had a height of 8 in. at the rear and 4 in. at the front.

134. Loading and instrumentation. The loading equipment and deflection measuring equipment used on Test series E was identical to that used in Test series D. Eight instrumented piles were used in this test series, a monitor pile and seven within the pile groups. The locations of the instrumented piles are shown on (a), Plate 62. Three of the instrumented piles were located in monolith M1; the other four were located in monolith M2.

Procedure

135. The test procedure was generally similar to that used for Test series D. All the monoliths were tested individually before they were loaded simultaneously as a wall. Monoliths M1 and M3 were subjected to two cycles of 2-lb per pile loading, whereas monolith M2 was subjected to three cycles (see Table 17). Then all three monoliths were loaded simultaneously up to 4 lbs per pile. An additional 25 cycles of the 4-lb per pile load were applied as indicated in Table 17.

Analysis of data

136. The load-deflection relationships observed for monolith M2 is presented on Plate 63. In all cases the lateral load has been converted to pounds per pile, and the deflections have been corrected for tilt to arrive at the lateral deflection at the sand surface. As for Test series D, the data from the end monoliths were not used in the analysis and, therefore, the data are not presented herein.

137. The moment vs depth relationship for the single monitor pile is presented on Plate 64. The moments were computed for lateral

loads of 2 lbs and 4 lbs. In addition, the moment relationship for the fifth and one-hundredth cycles of 4-lb loading are shown. The moment vs depth relationships for the four instrumented piles included in monolith M2 are presented on graphs (a) through (d), Plate 65. The data points are for the initial 2-lb loadings on the monoliths when loaded individually and when loaded as part of a wall. A theoretical moment curve has been computed for one of the pile loadings for each of the instrumented piles, assuming that the subgrade modulus has a triangular variation with depth. A reasonable check is obtained, although the theoretical moments are usually higher than the observed moments. This agrees with the observations made in the field on batter piles.

138. Group action. In order to perform a Hrennikoff-type analysis for a pile group, information regarding the behavior of batter piles loaded normal to their axes is required. A T-value of 3.67 was measured for piles loaded in a direction tending to pull the pile upwards, and 3.04 for piles loaded downwards towards the sand. In the analysis, the piles were assigned T-values corresponding to their batter; a T-multiplier of 1.3 was used. Because the piles were tapped further into the sand in the preparation of Test series E than they were in Test series D, higher axial stiffnesses were observed; this stiffness was 2300 lbs per inch. However, the modulus in tension is not likely to be significantly more than 1000 lbs per inch determined for the other tests. A Hrennikoff-type analysis was performed for a load of 2 lbs per pile and a flexural stiffness of 1.5×10^4 lbs in.^{2} (Appendix A). A theoretical deflection of 0.0056 in. was computed which is much less than the 0.0130 in. that was observed. However, several of the piles had computed tensions exceeding the tension capacity of the piles. In order to make comparisons in the elastic range of behavior an analysis was performed at a load of 1 lb per pile. On this basis the observed deflection is 0.0030 in., which compares favorably with the 0.0028 in. that was computed.

139. The analysis of the dam monoliths using a Hrennikoff-type analysis indicates that a T-multiplier of 1.3 is appropriate for a pile spacing on the order of three pile widths. Furthermore, the deflections computed with the analytical procedure check very closely with the observed deflections, providing the proper axial stiffnesses and the

proper variation of the subgrade modulus with respect to depth is used to obtain the Hrennikoff ratios.

140. Repetitive loading. For monolith M2 the ratio of the deflections for the twenty-sixth cycle of 4-lb per pile loading compared to the first cycle was 2.1. This is likely to be higher than would have been observed if the tension capacity of some of the piles in the pile group had not been exceeded. Therefore, the ratio of 2.1 can be interpreted downwards. Additional information on repetitive loading is available from the monitor pile (Plate 64). The deflection for the one-hundredth cycle of 4-lb loading was 1.7 times that obtained for the first cycle.

141. Tension pile behavior. The same discussion given in paragraph 129 for Test series D will apply in this case.

PART V: SUMMARY OF FIELD AND MODEL TESTS

142. The results of this investigation relevant to driving and the load-carrying capacity of single piles penetrating the alluvial sands at the pile test site are summarized in the following paragraphs. The results are considered applicable to other sites in the alluvial valley of the Arkansas River where the foundation sands are comparable and the water table is at or close to the ground surface. Appropriate allowance must be made in relating the test results to driving and load capacities of groups of piles.

Pile Driving

Bearing piles driven with steam or diesel hammers

143. Single piles were driven into the alluvial sands at the test site with the indicated hammers in the following net driving times:

Pile	Size	Hammer	Driving Time (Min.)	Penetration	Remarks
Steel pipe	12 in.	140C	10 to 15	53 ft	
"	16 in.	"			
"	20 in.	"			
Concrete	16-in. sq	"			
"	20-in. sq	140C	30	52	
Steel H	14BP73	80C	10	52	
Timber	11- to 15-in.	65C	8	39	
Concrete	16-in. sq	DE40	45	53	
Steel pipe	16-in.	140C	4	53	Jetted 40 ft
Concrete	16-in. sq	140C	4	53	Jetted 38 ft

144. A comparison of the results of flexure tests made before and after driving a 16-in. prestressed concrete pile with the 140C double-acting steam hammer indicates that the prestress bond was unaffected by the driving stresses.

Bearing piles driven with the Bodine hammer

145. Steel H and pipe piles were driven to a penetration of 53 ft in 2 to 4 min., respectively, with the Bodine Model B-2 sonic vibratory hammer. The Bodine hammer, equipped with the friction-type head attachment used in this testing program, required about 30 min. to drive 16- and 20-in. prestressed concrete piles to refusal at a penetration of about 35 ft. This hammer, with the head attachment used, is not considered suitable for driving heavy concrete piles for this project.

146. A comparison of flexure tests made on a prestressed concrete pile before and after driving with the Bodine hammer indicates that the driving stresses had no effect on the prestress bond.

Sheet piling driven with steam hammers

147. Double sheets of MZ32 piling were successfully driven to an average penetration of about 55 ft with a McKiernan-Terry 10B3 double-acting steam hammer in driving times ranging from 17 to 30 min. Double sheets of MZ32 piling were driven to an average penetration of about 100 ft with a Vulcan 80C double-acting steam hammer in net driving times ranging from 35 to 50 min.

148. Double sheets of MP112 piling could be driven with a McKiernan-Terry 10B3 double-acting steam hammer to a penetration of only 30 ft; the sheets were also damaged by rolling and bending at low driving resistances. Single sheets of MP112 piling were successfully driven with a McKiernan-Terry 9B3 double-acting steam hammer to a penetration in excess of 90 ft at a rate of about 3 ft per min.

149. Sheet piling having a penetration in excess of 60 ft could not be pulled with a Vulcan 800A extractor.

Sheet piling driven with Bodine hammer

150. Single sheets of MZ32 and MP112 steel sheet piling were driven to a penetration of about 45 ft in 2 to 9 min. with the Bodine hammer. This sheeting could not be driven more than about 50 ft with the sheets in interlock with the Bodine hammer driving the sheets individually. A follower is necessary to permit stage driving of sheeting with the Bodine hammer. Under hard driving conditions the Bodine hammer damaged the top and welds of MP112 sheet piling.

151. Four of the sheet piles having a penetration in excess of 60 ft were extracted with the Bodine hammer.

Bearing Capacity of Isolated Piles

Compressive capacity

152. On the basis of the field tests made at the site, compressive and tensile capacities of single piles driven to a penetration of 50 ft would be approximately as follows for the water table at the ground surface.

Pile	Size	Capacity (Tons) Compressive	Tensile
Pipe	12-in.	100	45
"	16	140	68
"	20	190	80
Concrete	12-in. sq	170	80
"	16	235	112
"	20	300	135
H	14BP73	190	37
Timber	11-in.	105	37

There is no appreciable difference in the compressive capacity of piles driven to the same penetration using either double-acting steam hammer or the Bodine hammer.

153. Partial jetting of piling with double jets during driving causes a reduction in compressive capacity. The compressive capacity of a pipe pile jetted to 40 ft and driven to a penetration of 53 ft was 70 percent of the capacity of similar piles driven to the same penetration without jetting. The reduction in capacity is attributed to a lesser driving resistance at the completion of driving and the loosening of the sand caused by jetting the test pile and four surrounding piles.

154. The compressive capacity of piling driven into the alluvial sands at the test site may be predicted reasonably accurately by means of the Terzaghi expression for deep piers. The sliding friction angle between pile materials and the sand, as determined from laboratory tests, ranged from about 25° to 30°. Lateral earth pressure coefficients in the range of 1.25 to 1.50 were indicated by the field tests.

155. The compressive capacity of displacement type bearing piles driven with the double-acting steam hammers may be estimated from the Pacific Coast Uniform Building Code dynamic pile driving equation. The compressive load capacity of H-piles may be estimated from the above pile driving formula by adding 25 percent to the computed capacity.

Tension capacity

156. Tensile capacities of piles driven to a penetration of 50 ft are summarized in paragraph 152. For any given design load, the required penetration for any size of the four types of piles tested can be selected from the general tension design curves presented on Plate 37. A factor of safety of 1.75 to 2.0 should be applied to the general design curves for selection of pile penetration requirements. The higher factor of safety should be used for piles located adjacent to channels where loss in surcharge from scour is possible.

157. There was no significant difference in the tensile capacity of piles driven with double-acting steam hammers or the Bodine hammer.

158. Partial jetting the test piles, using double jets during driving, reduced significantly the tensile capacity. A comparison of the tensile capacities of pipe piles driven to a penetration of about 53 ft without jetting and with double jetting to 40 ft showed that the jetted pile capacity was only 70 percent the capacity of piles driven without jetting. This reduction in tension capacity is attributed to the loosening of the sand caused by jetting the test pile and four surrounding piles.

159. The tensile capacity of piles in sands may be reasonably predicted by means of the frictional term of the Terzaghi expression for deep piers. Lateral earth pressure coefficients of about 0.80 were measured for the straight-sided displacement piles driven without jetting. The indicated lateral earth pressure coefficient for the H-piles was 0.40. The lateral K value for the jetted pile was 0.66.

Lateral capacity

160. The lateral capacities of the piles tested (single pile and first application of load) were about as follows:

Pile	EI (10^6 K In.^{2})	Lateral Load (K) Deflection = 0.125"	Lateral Load (K) Deflection = 0.25"
20-in. Concrete	84	28	44
Timber	3.2	6	10
All others tested	22 to 35	12 to 18	20 to 32

161. The coefficient of horizontal subgrade reactions decreases with pile deflection to an essentially constant value at deflections in excess of about 0.5 in. The subgrade modulus vs deflection curves for a single load application shown on Plate 39 are considered valid for submerged alluvial sands. The lateral subgrade modulus is essentially a property of the soil and is not affected significantly by the width and flexural stiffness of the pile.

162. Repetitive lateral loading of piling (to a given load level) increased the deflection to 1.7 to 1.9 times the deflection produced by the initial load application

Bearing Capacity of Pile Groups

Axially loaded piles

163. The compressive and tensile capacities of piles of the same penetration in groups may be some greater than the capacities indicated by the field load tests due to the increase in subgrade density produced during group driving. Therefore, the effect of group driving on the capacity should be checked by field load tests performed on typical piles within driven groups at each site where piles are to be driven.

164. The increase in density produced by driving displacement piles on relatively close centers may increase the driving resistance to the extent that it would be impractical to drive the piles to the minimum penetration required for scour or tension without damage to the piles. If jetting is required, it should be of a minimal nature, and its effect on compression, tension, and lateral load capacities should be determined by supplemental field tests. If the jetting reduces the pile capacities significantly, the piling should be redesigned to allow for the reduction in capacity caused by the jetting.

Laterally loaded piles (model tests)

165. For a given load per unit of width, a wall in the model tests deflected approximately 10 to 15 times as much as an isolated pile. Simultaneous loading of two opposing walls located a scalar distance of 110 ft apart, as in the prototype, results in a deflection which is 10 to 15 percent less than the deflection of an individually loaded wall. The reduction in lateral deflection resulting from simultaneous loading of opposed walls is not of sufficient magnitude to warrant consideration in wall design for walls located 110 ft apart.

166. The behavior of laterally loaded piles in groups can be predicted by means of a Hrennikoff-type analysis wherein the pile constants are computed using a triangular variation of subgrade modulus for sands, together with consideration of the fixity of the pile head.

167. For pile groups wherein the center-to-center spacing in the direction of loading is less than six pile widths, the expressions used to determine the pile head constants for the Hrennikoff-type analysis should be modified by the introduction of a T-multiplier. The experimental values of the T-multiplier determined from the model tests on typical lock and dam monoliths were 1.30 and 1.25 for pile centers of 3 and 4 widths, respectively.

PART VI: DESIGN AND CONSTRUCTION RECOMMENDATIONS

168. The findings of the field and laboratory phases of this investigation clearly demonstrate that it is feasible to support the lock and dam structures in the lower Arkansas River Valley on piling penetrating the deep stratum of alluvial sand. Recommendations relevant to the design and construction of the pile foundations for this project are summarized hereinafter.

Compression and tension capacity

169. The size and penetration requirements for bearing piles in compression and tension can be determined from the general design curves presented on Plates 28 and 37, respectively. These curves are applicable for isolated piles driven without jetting with the water table 2 to 3 ft below the ground surface.

170. A factor of safety of 1.5 applied to the compression design curves is considered adequate for selecting pile sizes and penetrations due to the similarity of the foundation sands at the proposed lock and dam sites, and because the sands at the sites have somewhat higher (sample) driving resistances than the sands at the test site. For piles subjected to tensile loadings, a factor of safety of 1.75 is suggested for Lock and Dam 1 and Lock 2, whereas a factor of safety of 2.0 is recommended for Dam 2 and Lock and Dam 3 and 4 located in the Arkansas River.

171. When bearing piles are subjected to both compression and tension loadings, the greater length required by either type of loading should be provided.

172. All bearing piles, except tension piles, should be driven to a minimum penetration of 35 ft as a precaution against the possibility of a reduction in capacity from scour, except at Lock and Dam 3 and 4 where a minimum penetration of 40 ft should be required for piles supporting the river walls. Tension piles should be driven to the design length.

173. The general design curves may require some adjustment for displacement piles located in groups on relatively close spacings because of the possible increase in density which may take place during driving. The effect of group driving on bearing capacity should be evaluated by

supplemental load tests performed during construction as indicated by driving conditions.

Lateral load capacity

174. The design of laterally loaded piles can be accomplished by trial and error methods involving comparison of permissible and theoretical stresses and deflections for a selected pile system. Theoretical pile stresses and deflections can be determined using the following methods which utilize the experimentally measured subgrade modulus and axial pile stiffness, together with indicated modifications for group effect and load repetition:

a. Isolated piles.

(1) Single load application - Determine the coefficient of horizontal subgrade reaction (n_h) at the permissible lateral deflection from Plate 39, and calculate the load vs stress relationships using the expressions presented in paragraph 55.

(2) Repetitive loading - Calculate load vs stress relationships as for (1) above, except that n_h should be determined at one-half the permissible deflection value. The ultimate deflection will be double the deflection calculated from the expressions presented in paragraph 55 for repetitive loading.

b. Pile groups (spacings less than eight pile diameters in direction of loading)

(1) Single load application - Calculate loads, stresses, and deflections using a Hrennikoff-type analysis wherein the axial and translational stiffness of the pile head are determined from the experimental data. The relative stiffness factors for the pile (T) should be multiplied by 1.25 and 1.30 for a four and three pile diameter or width spacing in the direction of loading, respectively. The coefficient of horizontal subgrade reaction should be selected from Plate 39 at the permissible lateral deflection and the axial stiffness in compression evaluated from Table 10 for the type and size of pile to be used.

(2) Repetitive loadings - Calculate loads, stresses, and deflections as for single load application above, except that n_h should be selected at one-half the permissible deflection. The ultimate

deflection computed from the Hrennikoff-type analysis will be approximately double that computed for repetitive loading.

Pile driving

175. Field driving criteria for compressive piles having penetrations in excess of the minimum penetration set forth in paragraph 172 should be based on the Pacific Coast Uniform Building Code dynamic equation. For piles driven with steam hammers, the steam pressure at the hammer should be used in the computation of the field driving curves. The computed dynamic capacities for H piles may be increased by 25 percent for field usage. The depth of the water table below the ground surface should be taken into account in preparing field driving criteria curves.

176. The following factors of safety are suggested for determination of required driving resistance for the last foot of pile penetration.

a. For piles having penetrations between the minimum and that required by the compressive design curves, the compressive design load should be multiplied by 1.5 or 1.6.

b. For piles having penetrations equal to or greater than that required by the compressive design curves, the compressive design load should be multiplied by 1.25.

177. The permissible maximum number of hammer blows to be applied to bearing piles should not exceed the values determined using the criteria presented in paragraphs 63 and 64 of this report.

178. No jetting of piles should be permitted unless field experience indicates that the piles cannot be driven to the required minimum penetrations previously specified without damaging the piles or requiring excessive driving time. Pile loading tests indicate that jetting reduces the compression, tension, and lateral load capacity not only of a pile being driven but also of adjacent piles previously driven; therefore, no jetting should be permitted until load tests have been made and evaluated to determine the effect of jetting on the load carrying capacity of the pile. Any jetting procedures permitted must not reduce the compression, tension, and/or lateral load capacity below minimum values required by design unless the pile foundation is redesigned to allow for such reduction.

NOTATIONS

A	Cross-sectional area of pile, $in.^2$
A_t	Area of pile tip, ft^2
A_f	Circumferential area of pile, ft^2/ft of pile length
a	Effective downward hammer piston area, $in.^2$
C_u	Uniformity coefficient
D	Pile penetration, ft
δ	Material friction angle
d	Hammer stroke, ft
D_{10}	Effective grain size, mm
E	Modulus of elasticity, psi, unless otherwise noted
Δ_e	Strain over gage length
E_h	Rated hammer energy, ft lbs per blow
EI	Flexural stiffness, lb $in.^2$
e_f	Hammer efficiency
γ'	Buoyant or submerged density of sand, T/ft^3
I	Moment of inertia, $in.^4$
K	Lateral earth pressure coefficient, or kips
k	Horizontal subgrade modulus, lbs per $in.^2$
K_r	Coefficient of restitution
L	Length, in.
M	Pile moment, in. lbs

M_g	Pile moment at ground surface, in. lbs
N_q, N_γ	Terzaghi bearing capacity factors
n_h	Coefficient of horizontal subgrade reaction, lbs per $in.^3$
P	Load or weight of pile, lbs
p	Steam pressure, psi
Q_u	Pile failure load, T
Q_g	Load normal to pile axis at ground surface, lbs
Q	Load normal to pile axis above ground surface, lbs
r	Radius of circular section or 1/2 side dimension of square section
R_u	Ultimate pile capacity, lbs
s	Average pile set, in. per blow
T	Relative stiffness factor
θ_g	Slope of pile at ground surface, radians
W	Weight of driving ram, lbs
w	Soil reaction, lbs per in.
x	Depth below ground surface, in.
Y_g	Lateral deflection of pile at ground surface, in.
Y_{zm}, Y_{zq}	Non-dimensional coefficients
ϕ	Pile shape factor

REFERENCES

1. Terzaghi, K. (1943), "Theoretical Soil Mechanics," John Wiley and Sons, New York.

2. Nordlund, R. L. (1963), "Bearing Capacity of Piles in Cohesionless Soils," ASCE Proceedings.

3. Reese, L. C. and Matlock, H. (1956), "Non-Dimensional Solutions for Laterally Loaded Piles with Soil Modulus Assumed Proportional to Depth," Proceedings, Eighth Texas Conference on Soil Mechanics and Foundation Engineering, Austin.

4. Reese, L. C. and Matlock, H. (1960), "Generalized Solutions for Laterally Loaded Piles," ASCE Proceedings, Vol. 86, No. SM5, Part I.

5. Chellis, R. D. (1961), "Pile Foundations," McGraw-Hill, New York.

6. Hirsch, T. J., Sampson, C. H. and Lowery, L. L. (1963), "Driving Stresses in Prestressed Concrete Piles," ASCE Annual Meeting, San Francisco.

7. "Review of Use of Long and Heavily Loaded Piles," Morganza Control Structure, Waterways Experiment Station, 1950.

8. "Review of Soils and Foundation Design and Field Observations," Morganza Floodway Control Structure, Waterways Experiment Station, 1954.

9. Feagin, L. B. (1937), "Lateral Pile Loading Tests," Transactions, ASCE, Vol. 102, pp 236-254.

10. Feagin, L. B. (1948), "Performance of Pile Foundations of Navigation Locks and Dams on the Upper Mississippi River," Proceedings, Second International Conference on Soil Mechanics and Foundation Engineering, Rotterdam, Vol. IV, pp 98-106.

11. Hrennikoff, A. (1950), "Analysis of Pile Foundations with Batter Piles," Transactions, ASCE, Vol. 125, pp 351-374.

12. Prakash, S. (1962), "Behavior of Pile Groups Subjected to Lateral Load," Ph.D. Thesis, University of Illinois.

13. Terzaghi, K. (1955), "Evaluation of Coefficients of Subgrade Reaction," Geotechnique, Vol. 5, pp 297-326.

14. Davisson, M. T. and Gill, H. L. (1963), "Laterally Loaded Piles in a Layered Soil System," Proceedings, ASCE, Vol. 89, No. SM3, pp 63-94, May.

15. Kolbuzweski, J. J. (1948), "An Experimental Study of the Maximum & Minimum Porosities of Sand," Proceedings, Second International Conference on Soil Mechanics & Foundation Engineering, Rotterdam, Vol. 1, pp 158-165.

BLANK PAGE

Table 1

FIELD DRIVING AND TESTING PROGRAM

Test Pile	Pile Type	Pile Size	Length (Ft)	Driving Hammer	Type Load Test C	H	T	Type Instrumentation 1	2	Remarks
GROUP I - Effect of Diameter on Bearing Capacity - Steel Pipe Piles										
1	Pipe	12"	55	140C	X	-	X	X	-	
2	Pipe	16"	55	140C	X	X	X (R)	X	X	Test C, H 5 cycles to 1/2" deflection, C and T
3	Pipe	20"	55	140C	X	-	X	X	-	
GROUP II - Effect of Length on Bearing Capacity - Prestressed Concrete Piles										
4	Concrete	16"	45	140C	X	-	X (R)	-	-	
5	Concrete	16"	55	140C	X	X	- (Flexure)	-	-	Jet-pull for flexure
GROUP III - Effect of Length on Bearing Capacity - Steel H-Piles										
6	Steel "H"	14BP73	42	80C	X	X	- (R)	X	-	Test H 100 cycles under 20 kip load
7	Steel "H"	14BP73	55	80C	X	-	X (R)	X	X	
GROUP IV - Capacity of Timber Pile										
8	Timber	Class A	40	65C	X	X	X (R)	-	-	
GROUP V - Behavior of Piles Driven with a Bodine Hammer										
9	Steel "H"	14BP73	55	Bodine	X	-	-	X	-	
10	Pipe	16"	55	Bodine	X	X	X	X	X	
11	Concrete	16"	55	Bodine	X	-	- (Flexure)	-	-	Jet-pull for flexure
11A*	Concrete	20"	55	Bodine, 140C	-	X	- (R)	-	-	Test H 100 cycles under 30 kip load
GROUP VI - Lateral Load Capacity of Battered H Piles										
12	Steel "H"	14BP73	45	80C	-	X	-	-	X	3 on 1 batter to north
13	Steel "H"	14BP73	45	80C	-	X	-	-	X	3 on 1 batter to north
13A	Steel "H"	14BP73	45	80C	-	X	-	-	X	Drive vertically for comparison with 12 and 13
GROUP VII - Effect of Jetting on Pipe Pile Capacity										
14	Concrete	16"	55	140C	-	X	-	-	-	Drive in following order:
15	Concrete	16"	55	140C	-	-	-	-	-	16, 14, 15, 17 and 18.
16	Pipe	16"	55	140C	X	X	X	-	X	Jet w/double jets to 38-ft
17	Concrete	16"	55	140C	-	-	-	-	-	penetration, drive to
18	Concrete	16"	55	140C	-	-	-	-	-	final penetration w/o jets.
GROUP VIII - Driving Concrete Pile Using a Diesel Hammer										
19	Concrete	16"	55	DE-40	-	-	-	-	-	
GROUP IX - Tests with Steel Sheet Piling										
20A	Sheet Piling	MZ-32	60-120	10B3 & 80C	Drive & Pull					Drive with 10B3 first, then 80C
20B	Sheet Piling	MZ-32	60-120	Bodine	Drive & Pull					Drive to maximum depth or to Tertiary clay
21A	Sheet Piling	MP-112	60-120	10B3,80C & 9B3	Drive & Pull					Drive with 10B3 first, then 80C, finally 9B3
21B	Sheet Piling	MP-112	60-120	Bodine	Drive & Pull					Drive to maximum depth or to Tertiary clay

C - Compression Test
H - Lateral Test
T - Tension Test
(R) - Cyclic Loading

* After driving with Bodine, pull using jets and redrive with 140C at new location.

Table 2

MODEL TESTING PROGRAM

Sand Bed	Test	Pile Description: Size	Length	Section	Prototype Size: Size	Length	Pile Orientation	Test Type	Remarks
GROUP I - Effect of Size and Length on Bearing Capacity									
A	1, 7 & 13	1/2" Rd	12"-24"-36"	Solid	14"	28'-56'-84'	Vertical	Vertical Load	
	2, 8 & 14	3/4" Rd	12"-24"-36"	Solid	21"	28'-56'-84'	Vertical	Vertical Load	
	3, 9 & 15	1" Rd	12"-24"-36"	Solid	28"	28'-56'-84'	Vertical	Vertical Load	
	4, 10 & 16	1/2" Sq	12"-24"-36"	Solid	14"	28'-56'-84'	Vertical	Vertical Load	
	5, 11 & 17	3/4" Sq	12"-24"-36"	Solid	21"	28'-56'-84'	Vertical	Vertical Load	
	6, 12 & 18	1" Sq	12"-24"-36"	Solid	28"	28'-56'-84'	Vertical	Vertical Load	
GROUP II - Effect of Pile Flexural Stiffness on Lateral Subgrade Modulus									
A	19	1/2" Sq	19"	Hollow	14"	44'	Vertical	Lateral Load	
	20	1/2" Sq	24"	Solid	14"	56'	Vertical	Lateral Load	
	21	1/2"x1" Rect	24"	Solid	14"	56'	Vertical	Lateral Load	
	22	1/2" Rd	21"	Hollow	14"	49'	Vertical	Lateral Load	
GROUP III - Comparison of Lateral Soil Resistance Offered to an Isolated Pile and to a Wall									
B	1	1/2" Sq	6"	Solid	20"	20'	Vertical	Lateral Load	
	2	Two 36" Long Walls Embedded	6"		120' Walls Embedded	20'	Vertical	Lateral Load	Loaded individually.
	3	Two 36" Long Walls Embedded	6"		120' Walls Embedded	20'	Vertical	Lateral Load	Two walls spaced 33" apart loaded simultaneously.
GROUP IV - Validity of Hrennikoff-Type Analysis									
C	1	6 @ 1/2" Rd x 21" Hollow Joined by Cap			14"	49'	2 Vertical	Lateral Load	Axial, translational and
							2 @ 3:1 Batter Forward	Lateral Load	rotational stiffness of each
							2 @ 3:1 Batter Reverse	Lateral Load	pile determined prior to test.
GROUP V - Lateral Deformations of Opposing Lock Monoliths									
D	1	3 - Lock Wall Monoliths, 1/2"x21" Rd			14"	49'	Vertical	Lateral Load	
	2	3 - Lock Wall Monoliths, 1/2"x21" Rd			14"	49'	3:1 Batter Forward; 5:1 Reverse	Lateral Load	Two walls spaced 44" apart.
	3	6 - Opposing Lock Wall Monoliths			14"	49'	Both Walls as Above	Lateral Load	Repetitious loading.
GROUP VI - Comparison of Lateral Deformations of Isolated Pile and Dam Monoliths									
E	1	3 - Dam Monoliths, 1/2" x 21" Rd			14"	49'	3:1 Batter, Forward & Reverse	Lateral Load	Repetitious loading.

Table 3

SUMMARY OF SLIDING FRICTION TESTS OF PILE MATERIALS ON SAND

Ref No.	Sample	Depth	Description	Classification		Mechanical Analysis % Sand	% Fines	Type Test	Before Test γ pcf	w %	S %	Test Result δ	c tsf
Boring LD4-1													
1a	S-12889	13.1-13.6	Brown	Sandy gravel	GP-GM	46	5	S-M	125	11	92	29	0.1
1b	↓							S-S	125	12	94	23	0.1
2a	S-12890-C	23.2-43.4	Tan	Sand	SP	--	--	S	85	9	26	32	0.0
2b								S	100	9	37	31	0.1
2c								S	110	9	48	33	0.1
2d								S-M	86	9	26	25	0.1
2e								S-M	100	9	36	32	0.0
2f								S-M	107	9	45	29	0.1
2g								S-S	84	9	24	28	0.0
2h								S-S	100	9	37	24	0.0
2i	↓							S-S	116	9	56	25	0.0
Boring LD4-10													
3	S-12893	15.0-15.5	Tan	Silty sand	SM-SP	88	12	S	100	17	71	31	0.1
4	S-12896	25.6-26.3	Tan	Sand	SP	98	2	S	100	21	84	35	0.0
5a	S-12897-C	35.5-47.0	Tan	Sand	SP-SM	--	--	S-M	90	19	60	28	0.0
5b								S-M	100	19	77	31	0.0
5c								S-M	111	19	100	35	0.0
5d								S-S	90	19	60	25	0.0
5e								S-S	100	19	77	26	0.0
5f	↓							S-S	110	19	99	28	0.0
Boring LD4-31													
6a	S-13127	32.9-33.5	Brown, numerous clay (CH) lumps	Silty sand	SM	--	--	S-S	100	15	63	30	0.0
6b	↓							S-M	100	16	64	36	0.0
7	S-13128	52.0-52.5	Brown, gravelly, few clay (CH) lumps	Sand	SP	--	--	S-S	100	13	51	23	0.0
8	S-13129	53.0-53.5	Brown	Silty sand	SM	--	--	S-S	100	14	59	29	0.0
9a	S-13130-C	62.8-82.6		Sand	SP	97	3	S	100	19	77	27	0.1
9b								S-S	89	20	62	21	0.1
9c								S-S	100	21	86	27	0.0
9d								S-S	107	21	100	24	0.0
9e								S-M	87	21	60	29	0.0
9f								S-M	99	21	83	32	0.0
9g	↓							S-M	108	21	99	30	0.0
Boring LD4-35													
10	S-12907	11.0-11.5	Brown, few clay (CH) lumps	Silty sand	SM	--	--	S	100	10	39	34	0.0
11a	S-12905-C	20.8-61.0	Brown	Sand	SP	93	3	S	101	15	62	35	0.0
11b								S-S	86	18	53	29	0.0
11c								S-S	101	15	60	25	0.0
11d								S-S	107	18	88	22	0.0
11e								S-M	86	19	55	32	0.0
11f								S-M	98	18	67	33	0.0
11g	↓							S-M	107	19	88	29	0.1

NOTES:

1. Tests were made by Corps of Engineers, Southwestern Division Laboratory, Dallas, Texas.
2. Sample numbers correspond to numbers in SWDGL Report No. 7920 and 7932.
3. All tests were made on remolded samples.

NOMENCLATURE

S - Drained direct shear test

S-S - Sliding friction test for sand on steel

S-M - Sliding friction test for sand on mortar

Table 4

PROPERTIES OF TEST PILES

Test Pile	Pile Type & Nominal Size	Modification Added	Cross Sectional Area-A ($In.^2$)	Moment of Inertia-I ($In.^4$)	Modulus of Elasticity-E (10^3 K per $In.^2$)	AE (10^3 K)	EI (10^6 K $In.^2$)
1	12.75" O.D. Pipe (0.330" Wall)	2, 4⌴7.25	17.12	--	29.0	496	--
2 & 10	16" O.D. Pipe (0.312" Wall)	4, 4⌴7.25	23.86	838.2	29.0	692	24.35
3	20" O.D. Pipe (0.375" Wall)	2, 4⌴7.25	27.36	--	29.0	793	--
4,5,11 & 14	16" Sq Concrete	None	256.00	5461.3	6.3	1550	34.5
6	Steel-H (14BP73)	2, 4⌴7.25	25.70	742.1	29.0	745	21.5
7	Steel-H (14BP73)	2, 5⌴9.00	29.33	--	29.0	851	--
8	Timber (Class A)	None	180 Butt 90 Tip	1975.0	1.6*	--	3.16
9	Steel-H (14BP73)	2, 4⌴7.25	26.28	--	29.0	763	--
11A	20" Sq Concrete	None	400.00	13330.0	6.3	2520	84.00
12	Steel-H (14BP73)	2, 1/2 x 12.6" Pls	35.40	960.2	29.0	1027	27.85
13	Steel-H (14BP73)	2, 1/2 x 12.6" Pls	36.42	992.7	29.0	1056	28.80
13A	Steel-H (14BP73)	2, 1/2 x 12.6" Pls	32.97	855.9	29.0	956	24.82
16	16" O.D. Pipe (0.312" Wall)	2; 4⌴7.25	19.62	829.2	29.0	569	24.05

* Obtained from National Lumber Manufacturers Association publication (Wood Structural Design Data).

Table 5

PILE DRIVING SUMMARY

Test Pile	Pile Type & Nominal Size	Pile Length (Ft)	Driving Hammer	Rated Hammer Energy (Ft Lb)	Steam Pressure (PSI)	Hammer Speed (Blows/Min.)	Efficiency[f] (%)	Penetration (Ft)	Blows Last Foot	Net Driving Time (Min. & Sec.)	Pile Top Damage
1	12" Pipe	55	140C	36,000	120	100	78	53.1	16	8:00	Slight bulge
2	16" Pipe	55	140C	36,000	118	-	78	52.8	38	9:12	Slight bulge
3	20" Pipe	55	140C	36,000	120	108	78	53.0	44	9:39	Slight bulge
4	16" Concrete	45	140C	36,000	130	92	81	40.2	42	5:38	None
5	16" Concrete	55	140C	36,000	130	100	81	51.0	48	12:52	Spalled 3'[a]
6	Steel-H (14BP73)	42	80C	24,450	120	91	84	40.0	17	4:30	None
7	Steel-H (14BP73)	55	80C	24,450	120	70	84	52.1	31	10:42	None
8	Timber (Class A)	40	65C	19,500	95	100	74	38.6	23	7:00	None
9	Steel-H (14BP73)	55	Bodine	--	-	-	-	53.2	-	2:17	None
10	16" Pipe	55	Bodine	--	-	-	-	53.1	-	4:04	None
11	16" Concrete	55	Bodine	--	-	-	-	38.8	-	31:37	None
11A	20" Concrete	55	Bodine	--	-	-	-	35.3	-	33:06	None
11A	20" Concrete	54.2	140C	36,000	130	80	81	51.9	130	30:39	None
12[b]	Steel-H (14BP73)	45	80C	24,450	108	75	81	43.3	29	6:30	None
13[b]	Steel-H (14BP73)	45	80C	24,450	100	102	78	43.1	23	5:00	None
13A	Steel-H (14BP73)	45	80C	24,450	125	81	84	42.5	20	8:30	None
14	16" Concrete	55	140C	36,000	118	92	78	53.0	51[d]	5:00	Insignificant
15	16" Concrete	55	140C	36,000	130	92	81	53.2	35[d]	4:00	Insignificant
16	16" Pipe	55	140C	36,000	125	96	79	52.7	24[e]	3:30	Bulged west side
17	16" Concrete	55	140C	36,000	130	90	81	52.9	38[d]	4:00	Insignificant
18	16" Concrete	55	140C	36,000	125	97	80	52.9	35[d]	4:00	Insignificant
19	16" Concrete	55	DE-40	32,000	c	45	85	53.0	90	45:30	None

a - Due to eccentric driving on pile head
b - Driven on 3 on 1 batter
c - 7.5 Ft hammer stroke
d - Pile jetted 38 ft
e - Pile jetted 40 ft
f - Manufacturer's rating x steam pressure adjustment = 0.84 x adjusted energy/rated energy

Table 6

SUMMARY OF SHEET PILE EXTRACTION TESTS

Test Pile	Penetration (Ft)	Extractor Type	Extraction Time (Min.)	Extraction Length (Ft)	Remarks
TEST SERIES 20A - MZ-32 Sheeting Driven with steam hammers					
20.1	59.2	800A	37	59.2	
20.2	59.2	800A	8	59.2	
20.3	104.5	800A	11	0	
20.4	104.5	800A	5	0	
20.5	85.0	Bodine	22	85.0	
20.6	85.0	800A-Bodine	13-13	0	
20.7	86.0	800A-Bodine	11- 7	0	
20.8	86.0	800A-Bodine	46-10	0	
TEST SERIES 20B - MZ-32 Sheeting Driven with Bodine Hammer					
20.9	52.0	Bodine	4	52.0	Driven out of interlock at 30'
20.10	60.7	Bodine	-	60.7	Pulled w/20.9
20.11	90.7	Bodine	17	90.7	
20.12	73.6	Bodine	12	73.6	Pulled 12' w/20.11
20.13	52.0	Bodine	2	52.0	Pulled 15' w/20.12
20.14	83.6	Bodine	5	83.6	
20.15	93.0	Bodine	14	0	
20.13a	53.5	Bodine	2	53.5	
20.14a	54.7	Bodine	1	54.7	
20.15a	94.0	Bodine	18	0	Driven out of interlock at 57'+
20.16a	55.5	Bodine	2	55.5	
TEST SERIES 21B - MP-112 Sheeting Driven with Bodine Hammer					
21.9	53.6	Bodine	1	53.6	Pulled 15' w/21.10
21.10	69.0	Bodine	8	69.0	
21.11	94.3	Bodine	25	0	
21.12	91.6	Bodine	13	0	
21.13	59.9	Bodine	1	59.9	Pulled 13' w/21.14
21.14	50.1	Bodine	4	50.1	
21.15	50.1	Bodine	3	50.1	
21.16	50.9	Bodine	3	50.9	

Note: Test Series 21B, MP-112 sheeting driven with steam hammers to penetrations of 90 ft ± could not be extracted with 800A extractor and 40 ft double jets.

Table 7

SUMMARY OF COMPRESSION TEST FAILURE LOADS

Test Pile	Pile Type & Nominal Size	Penetration (Ft)	Driving Hammer	Pile Failure Loads (Tons)				
				ΔS/ΔP = 0.01"	Net Set = 0.25"	Tangents	Insp.Gross	Ave
1	12" Pipe	53.1	140C	145	-	140	140	140
2	16" Pipe	52.8	140C	195	210	190	185	195
2*	16" Pipe	52.8	140C	210	230	205	195	210
3	20" Pipe	53.0	140C	220	-	215	210	215
4	16" Concrete	40.2	140C	175	185	170	160	170
5	16" Concrete	51.0	140C	250	245	250	215	240
6	Steel-H (14BP73)	40.0	80C	140	-	140	-	140
7	Steel-H (14BP73)	52.1	80C	200	175	200	-	190
8	Timber (Class A)	38.6	65C	70	85	80	-	80
9	Steel-H (14BP73)	53.2	Bodine	220	-	200	-	210
10	16" Pipe	53.1	Bodine	180	-	180	-	180
11	16" Concrete	38.8	Bodine	150	-	145	150	150
16	16" Pipe	52.7	Jet-140C	140	140	140	-	140

* Second Test

Table 8

SUMMARY OF TENSION TEST FAILURE LOADS

Test Pile	Pile Type & Nominal Size	Penetration (Ft)	Driving Hammer	Pile Failure Loads (Tons)				
				ΔS/ΔP = 0.01"	Net Rise = 0.25"	Tangents	Insp.Gross	Ave
1	12" Pipe	53.1	140C	66	78[a]	78	60	70
2	16" Pipe	52.8	140C	87	85	98	95	91
3	20" Pipe	53.0	140C	86	89[a]	98	86	90
4	16" Concrete	40.2	140C	70	73	80	60	71
7	Steel-H (14BP73)	52.1	80C	38	48	43	35	41
8	Timber (Class A)	38.6	65C	22	30	26	24	25
10	16" Pipe	53.1	Bodine	82	87[a]	92	86	87
16	16" Pipe	52.7	Jet-140C	58	--	74	58	63

a - Tip movement curves used

Table 9

SUMMARY OF LATERAL TEST RESULTS

Test Pile	Pile Type & Nominal Size	Method of Loading	Loading Point[d]	Bottom Dial[d]	Lateral Load in Kips Defl = 0.25"	Lateral Load in Kips Defl = 0.50"	EI (10^6 K In.^{2})	Remarks
2	16" Pipe	Repetitive[a]	+0.10'	+0.20'	29[e]	52[e]	24	f
5	16" Concrete	Continuous[b]	+0.50'	+0.50'	25	36	35	f
6	Steel-H (14BP73)	Repetitive	+0.20'	+0.20'	—	--	—	—
8	Timber (Class A)	Cyclic[c]	0	0	10[e]	16[e]	3.2	f
10	16" Pipe	Continuous	+0.35'	+0.35'	32	50	24	f
11A	20" Concrete	Repetitive	+0.50'	+0.20'	--	--	84	—
12	Steel-H (14BP73)	Continuous	0	0	25	42	28	3:1 Batter
13	Steel-H (14BP73)	Continuous	+0.13'	+0.50'	27	44	29	3:1 Batter
13A	Steel-H (14BP73)	Cyclic	+0.50'	+0.50'	20[e]	30[e]	25	—
14	16" Concrete	Continuous	0	+0.02'	22[e]	34[e]	35	--
16	16" Pipe	Continuous	0	+0.02'	22	35	24	Jetted 38 ft[f]

a - Repeated successive incremental loading.
b - Successive incremental loading.
c - Successive incremental loading with load release after each even increment.
d - Referenced to ground line.
e - Lateral load when indicated deflection first occurs.
f - Maximum deflection of pile head at the ground line limited to 0.5 in.

Table 10

AXIAL STIFFNESS OF TEST PILES

Test Pile	Pile Type & Nominal Size	Axial Stiffness (Tons per In. Deflection)	
		Compressive	Tensile
1	12" Pipe	690	570
2	16" Pipe	650	433
3	20" Pipe	775	485
4	16" Concrete	1130	1000
5	16" Concrete	1000	--
6	Steel-H (14BP73)	370	--
7	Steel-H (14BP73)	470	770
8	Timber	295	390
9	Steel-H (14BP73)	490	--
10	16" Pipe	670	695
11	16" Concrete	1100	--
16	16" Pipe	565	370

Note: Axial stiffness determined from gross load versus pile head deflection curve at pile working capacity (failure load/ factor safety = 1.5)

Table 11

COMPARISON OF TEST FAILURE LOADS AND PILE CAPACITIES COMPUTED FROM DYNAMIC FORMULAS

Test Pile	Pile Type & Nominal Size	Driving Hammer	Test Failure Load (Tons)	Computed Pile Capacity (Tons)			Ratio of Test Load to Computed Load		
				Pacific Coast	Janbu	ENR	Pacific Coast	Janbu	ENR
1	12" Pipe	140C	140	131	118	195	1.07	1.19	0.72
2	16" Pipe	140C	195	198	206	406	0.98	0.95	0.48
3	20" Pipe	140C	215	213	227	453	1.01	0.96	0.47
4	16" Concrete	140C	170	157	165	255	1.08	1.03	0.67
5	16" Concrete	140C	240	226	273	502	1.06	0.88	0.48
6	Steel-H (14BP73)	80C	140	112	98	151	1.25	1.43	0.93
7	Steel-H (14BP73)	80C	190	142	146	252	1.34	1.30	0.75
8	Timber (Class A)	65C	80	81	80	140	0.99	1.00	0.58
16**	16" Pipe	140C	140	165	154	203	0.85	0.91	0.69
19	16" Concrete	DE-40	265*	173	260	690	1.53	1.02	0.38

* Estimated from compressive design curves

** Comparison not valid because of effect of jetting for adjacent piles

Table 12

DENSITY OF SAND IN MODEL TESTS

Test Series	Sample	Depth to Center of Sample (In.)	Dry Density (Lb/Ft^3)	Relative Density (%)	Average Relative Density (%)
A	1	10.0	102.8	68	72
	2	4.0	103.7	71	
	3	27.5	105.2	76	
B	1	2.5	103.8	72	75
	2	2.5	104.1	73	
	3	2.5	105.5	80	
C	1	5.0	104.7	75	75
	2	6.0	105.2	76	
D	1	3.5	102.3	67	66
	2	3.5	101.8	65	
	3	3.5	102.0	66	
	4	3.5	100.4	60	
	5	3.5	102.6	68	
	6	3.5	101.0	62	
	7	3.5	102.5	67	
	8	3.5	103.0	69	
	9	3.5	103.9	72	
	10	3.5	102.0	66	
E	1	4.5	102.4	67	69
	2	5.5	103.0	69	
	3	4.5	103.0	69	
	4	9.5	103.1	69	

Table 13

PILE DATA - MODEL TEST SERIES A

Pile	Pile Section	Embedded Length (In.)	Type of Test	Corrected Failure Load (Lbs)	Deflection at Failure (In.)
1	1/2" Rd	12	Compression	8.9	0.08
2	3/4" Rd	12	"	15.5	0.08
3	1" Rd	12	"	29.0	0.08
4	1/2" Sq	12	"	13.1	0.09
5	3/4" Sq	12	"	24.0	0.10
6	1" Sq	12	"	42.0	0.10
7	1/2" Rd	24	"	26.9	0.09
8	3/4" Rd	24	"	45.7	0.09
9	1" Rd	24	"	50.1	0.10
10	1/2" Sq	24	"	28.3	0.09
11	3/4" Sq	24	"	65.0	0.10
12	1" Sq	24	"	90.1	0.12
13	1/2" Rd	36	"	45.4	0.14
14	3/4" Rd	36	"	84.9	0.11
15	1" Rd	36	"	109.2	0.11
16	1/2" Sq	36	"	50.5	0.13
17	3/4" Sq	36	"	87.0	0.16
18	1" Sq	36	"	135.0	0.15
19[a]	1/2" Sq	19	Lateral	-	-
20	1/2" Sq	24	"	-	-
21[b]	1/2"x1" Rect	24	"	-	-
22[c]	1/2" Rd	21	"	-	-

a - Hollow steel tube, instrumented with SR-4 gages.

b - Loaded normal to 1" side.

c - Hollow aluminum tube, instrumented with SR-4 gages.

Table 14

LOADING SCHEDULE - MODEL TEST SERIES C

Horizontal Load (Lbs)	Vertical Load (Lbs)	SR-4 Gages Observed	Remarks
0	0	All	Pile cap in
0	10	Top Only	contact with
11	10	All	the sand.
11	20	Top Only	
21	20	All	
21	30	Top Only	
31	30	All	
31	50	Top Only	
51	50	All	
0	50	All	
0	0	All	
0	0	All	Pile cap free
0	50	Top Only	from contact
31	50	All	with the sand.
0	50	All	
0	0	All	

Table 15

PILE DATA - MODEL TEST SERIES C

Direction of Batter	Pile	Relative Stiffness Factor-T (In.)	Axial Stiffness-N (Lb/In.)	Hrennikoff Ratios r1	r2	r3	*Horizontal Load=31 Lb; Vertical Load=50 Lb: Moment at Pile Head-M_g (In. Lb) Obser.	Theo.	Shear at Pile Head-Q_g (Lbs) Obser.	Theo.	Axial Load at Pile Head-P (Lbs) Obser.	Theo.
With the load	1	3.06	4900	0.115	0.327	1.51	11.5	11.5	5.0	3.9	18.0	16.1
	3	3.06	4000	0.141	0.400	1.86	11.2		5.2		12.8	
Vertical	5	3.22	4600	0.105	0.314	1.53	10.6	11.3	3.8	3.6	6.5	9.5
	7	3.30	5000	0.090	0.275	1.37	10.4		3.6		5.4	
Away from load	2	3.49	3600	0.106	0.341	1.81	13.2	10.9	5.2	3.3	2.75	0.4
	4	3.36	6000	0.072	0.221	1.13	10.8		3.8		3.05	

* Pile cap not in contact with the sand.

Table 16

LOADING SCHEDULE - MODEL TEST SERIES D

Monoliths Loaded	Average Load per Pile-Q_g (Lbs)	SR-4 Strains Recorded for Piles	Deflection Dials Observed	Remarks
V1 & V3	0	2, 3, 4, 5, 14	All	Initial zero
	1		"	
	2		"	
	0		"	
	2	2, 14	"	
	0		"	
V2	0		"	
	1		"	
	2	3, 4, 5	"	
	0		"	
	2		"	
	0		"	
	2		"	
	0		"	
V1,V2 & V3	0	2, 3, 4, 5, 14	"	Initial zero
	1		"	
	2	2, 3, 4, 5, 14	"	
	4	2, 3, 4, 5, 14	"	
	0		"	
	4		"	
	0		"	
	4		"	
	0		"	
B1 & B3	0	7,8,9,10,11,12,13	"	Initial zero
	1		"	
	2	7, 9	"	
	0		"	
	2		"	
	0		"	
B2	0		"	
	1		"	
	2	8, 10, 11, 12, 13	"	
	0		"	
	2		"	
	0		"	
B1,B2 & B3	0	7,8,9,10,11,12,13	"	Initial zero
	1		"	
	2	7,8,9,10,11,12,13	"	
	4	7,8,9,10,11,12,13	"	
	0		"	
	4		"	
	0		"	
	4		"	
	0		"	
Both Walls	0	All	"	Initial zero
	2	"	"	
	4	"	"	4th cycle of 4-lb loading
	4*		1 ea, V2,B2	Cycled 8 times
	4*	All	All	13th cycle
	4*		1 ea, V2,B2	Cycled 9 times
	4*		All	23rd cycle
	4*		1 ea, V2,B2	Cycled 29 times
	4	All	All	53rd cycle
	0	"	"	

* Load cycled from 0.5 lb to 4 lbs

Table 17

LOADING SCHEDULE - MODEL TEST SERIES E

Monoliths Loaded	Average Load per Pile-Q_g (Lbs)	SR-4 Strains Recorded for Piles	Deflection Dials Recorded	Remarks
M1 & M3	0	All	All	Initial zero
	1		"	
	2	1, 5, 14	"	
	0		"	
	2		"	
	0		"	
M2	0		"	
	1		"	
	2	2, 3, 4, 7	"	
	0		"	
	2		"	
	0		"	
	2		"	
	0		"	
M1, M2, M3	0		"	Initial zero
	1		"	
	2		"	
	4		"	1st cycle of 4-lb loading
	0		"	
	4		"	
	0		"	
	4*		"	Cycled 8 times
	4*		1 dial - M2	Cycled 3 times
	Overload		All	14th cycle, M1,M3=6.9 lbs
	4*		1 dial - M2	Cycled 10 times
	4*		All	25th cycle
	4	All	"	26th cycle
	0	"	"	Final zero

* Load cycled from 0.5 lb to 4 lbs.

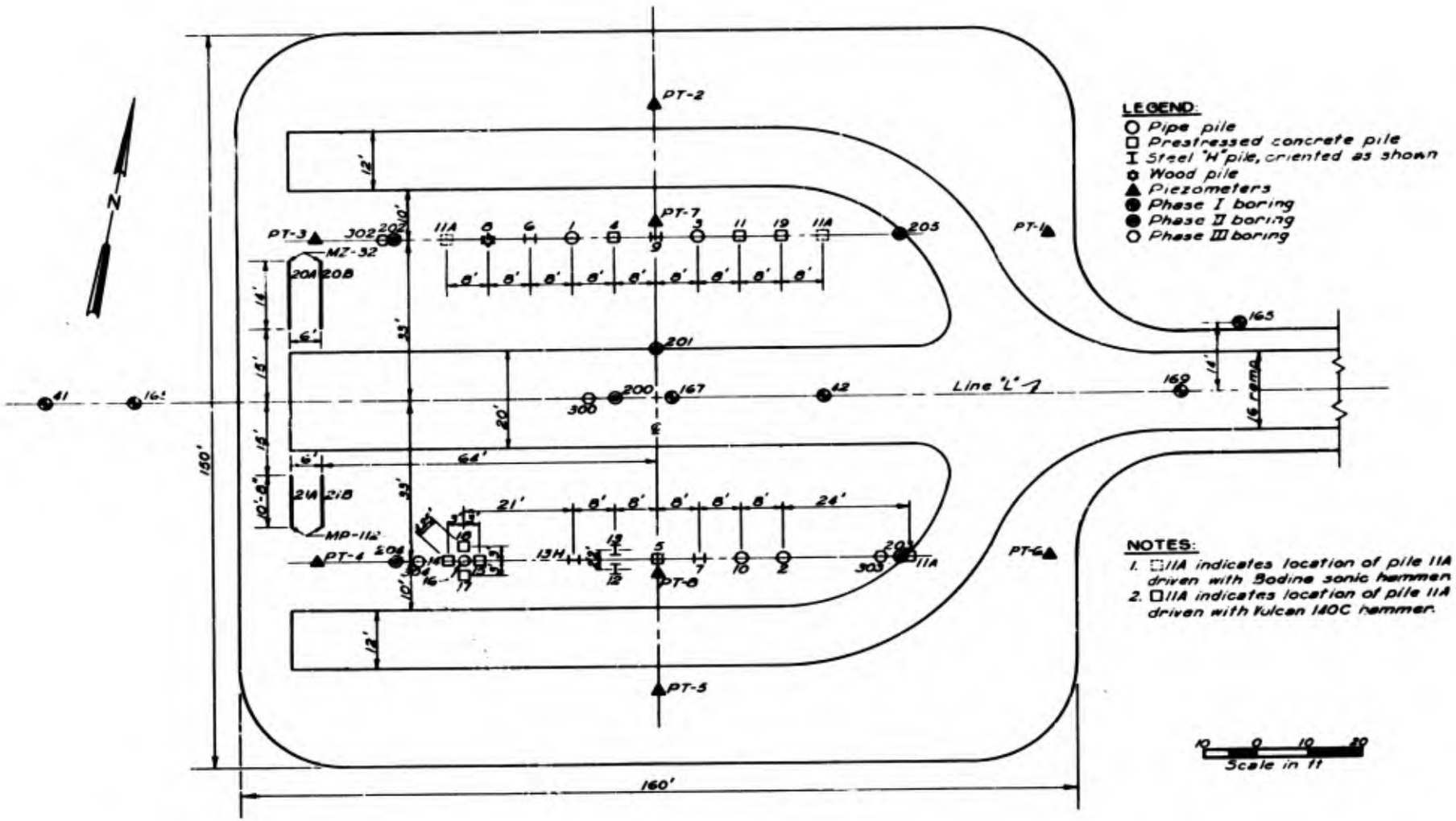

PLATE 1

PLAN OF BORINGS, PIEZOMETERS, AND TEST PILES

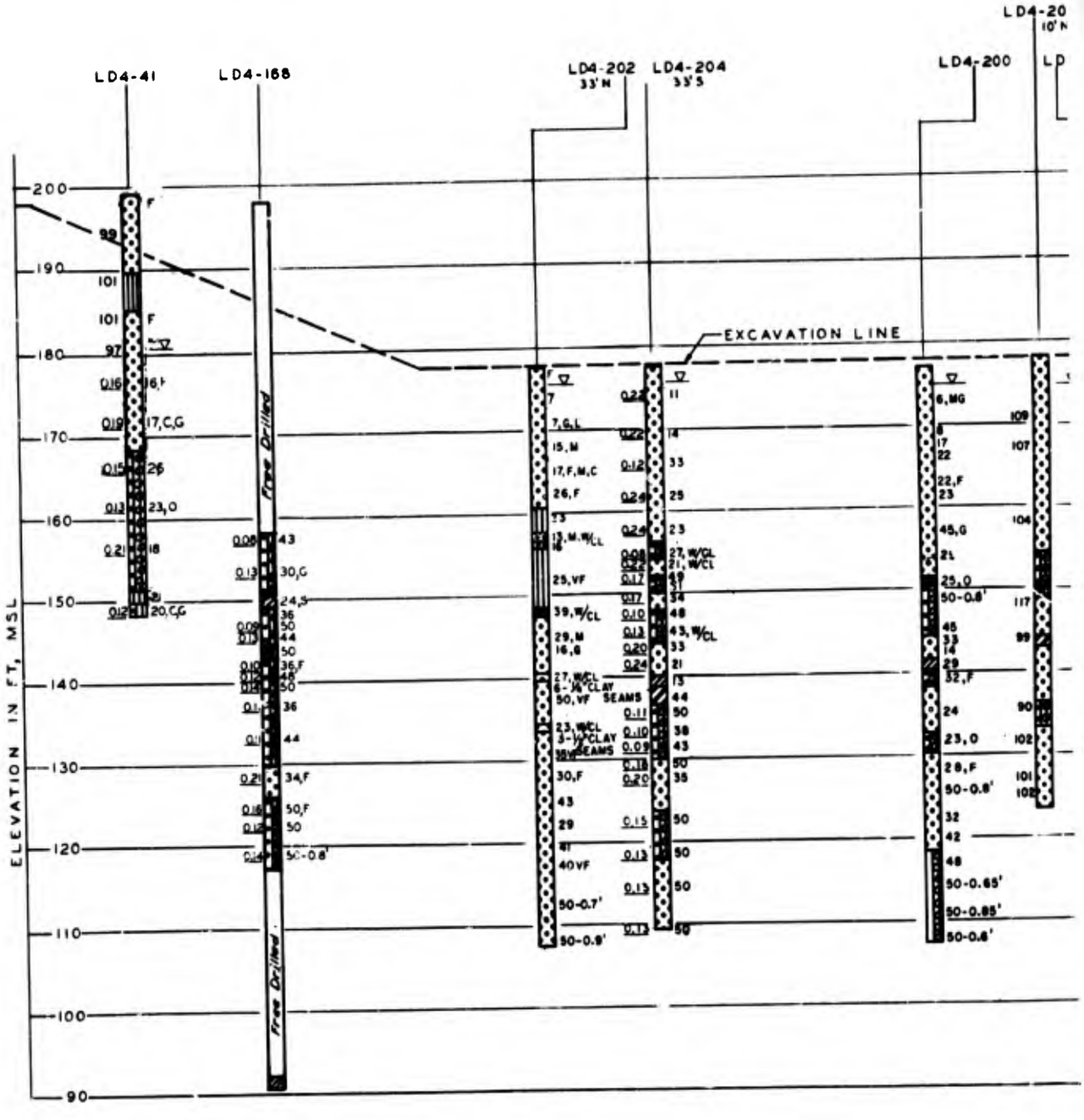

LEGEND

SYMBOLS

- GW: well-graded gravels, gravel-sand mixtures, little or no fines.
- GP: poorly-graded gravels, gravel-sand mixtures, little or no fines.
- GM: silty gravels, gravel-sand-silt mixtures.
- GC: clayey gravels, gravel-sand-clay mixtures.
- SW: well-graded sands, gravelly sands, little or no fines.
- SP: poorly-graded sands, gravelly sands, little or no fines.
- SM: silty sands, sand-silt mixtures.
- SC: clayey sands, sand-clay mixtures.
- ML: inorganic silts, silty or clayey fine sands or clayey silts with slight plasticity.
- CL: inorganic clays of low to medium plasticity.
- MH: inorganic silts of high compressibility.
- CH: inorganic clays of high plasticity.
- SP-SM: typical dual classification.

TO THE RIGHT OF LOG

VF – Very fine sand.
F – Fine sand.
M – Medium sand.
C – Coarse sand.
V – Very coarse sand.
L – With lignite particles
WSL – With sand lens or lenses
50 – Standard penetration resis
140-lb hammer, 30-inch fall, 2

TO THE LEFT OF LOG

0.10 – Effective grain size, D10
99 – Dry unit weight in lbs per

A

BORING LOGS

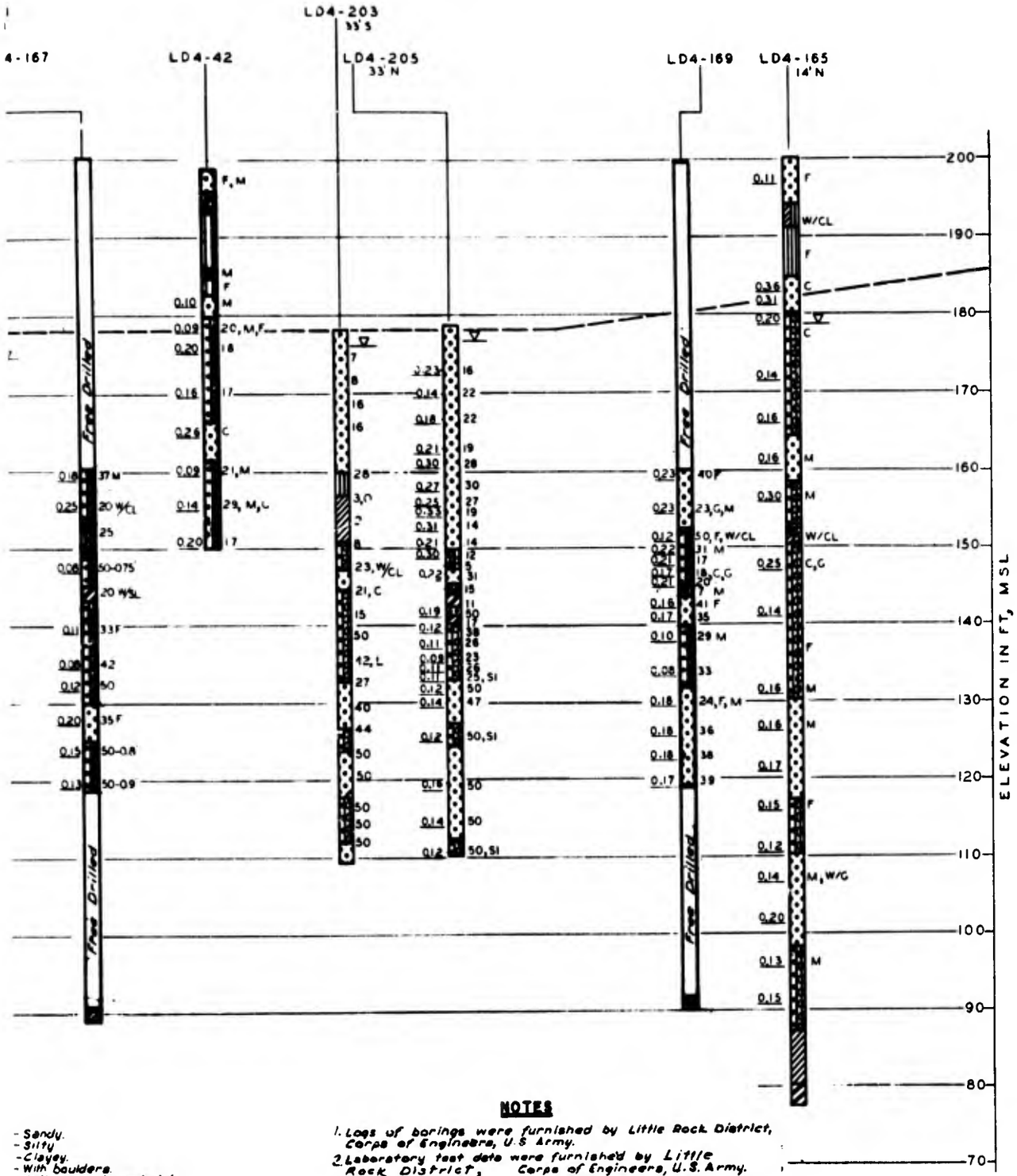

- Sandy.
- Silty
- Clayey.
- With boulders.
- With organic material
- With cobbles or gravelly.
- With clay lens or lenses.
- With gravel

Hence (blows per foot of penetration. inch O.D. split spoon)(30-08; 30 blows per 0.8

NOTES

1. Logs of borings were furnished by Little Rock District, Corps of Engineers, U.S Army.
2. Laboratory test data were furnished by Little Rock District, Corps of Engineers, U.S. Army.
3. Refer to Plate 1 for location of section and plan of borings.
4. Classification of soils is in accordance with the Corps of Engineers Unified Soils Classification System.

(mm)
u ft

B

- LINE "L"

PLATE 2

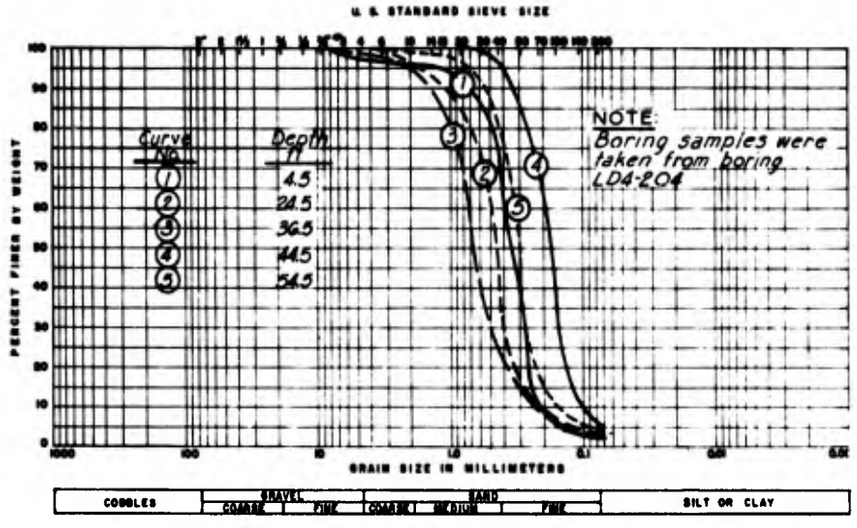

a. TYPICAL GRADATION CURVES FOR TEST SITE SANDS

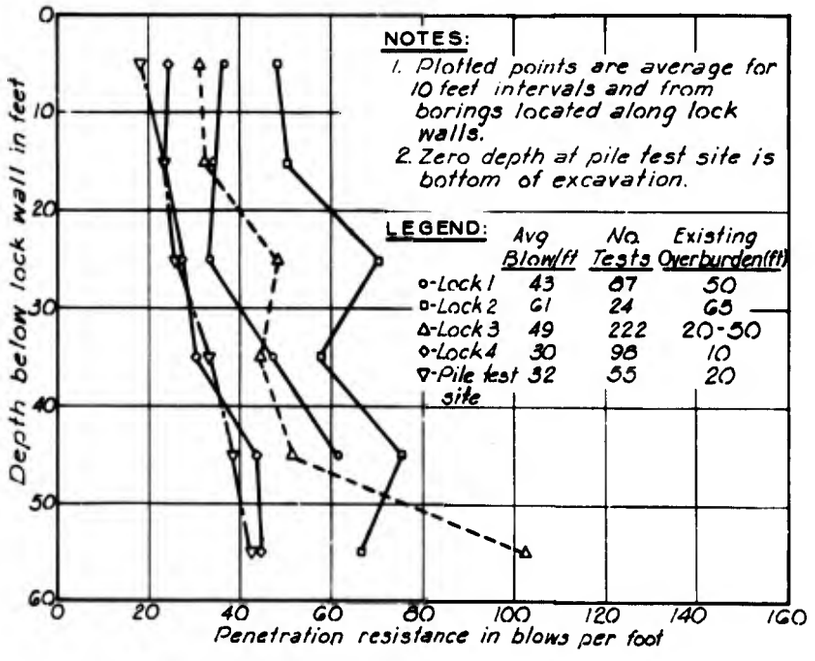

b. STANDARD PENETRATION RESISTANCE VS DEPTH FOR TEST SITE AND LOCKS AND DAMS 1 THRU 4

FIELD AND LABORATORY SOIL TEST RESULTS

PLATE 4

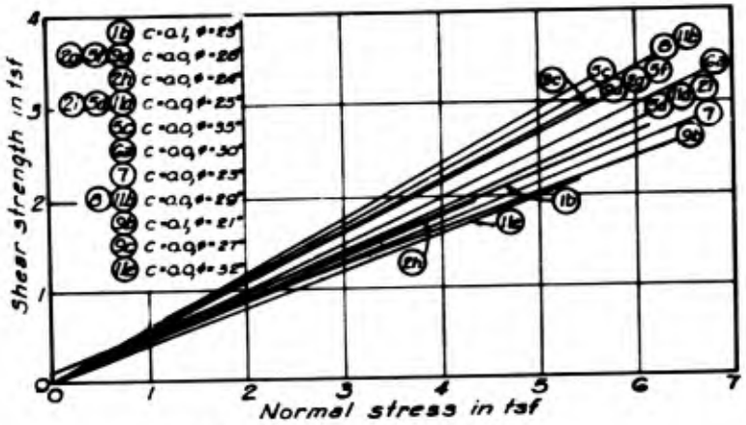

a. S - S TEST DATA

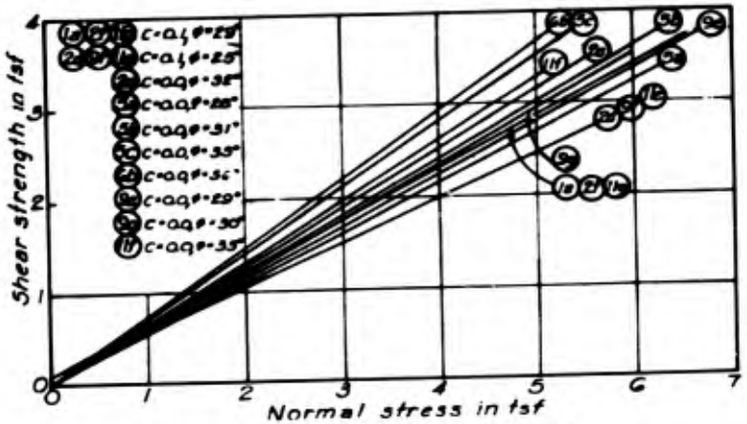

b. M - S TEST DATA

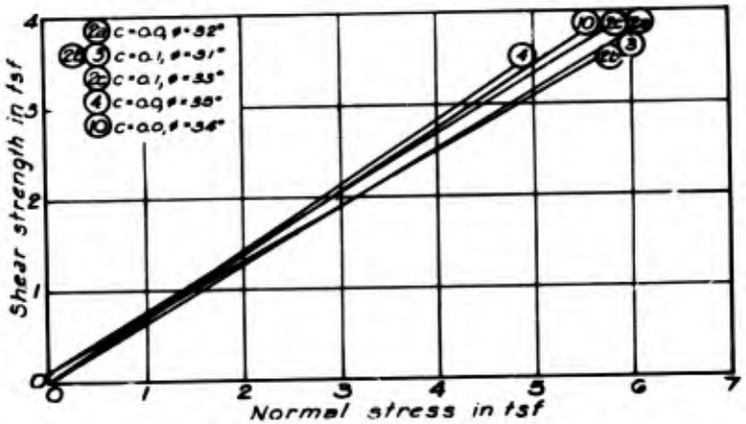

c. S TEST DATA

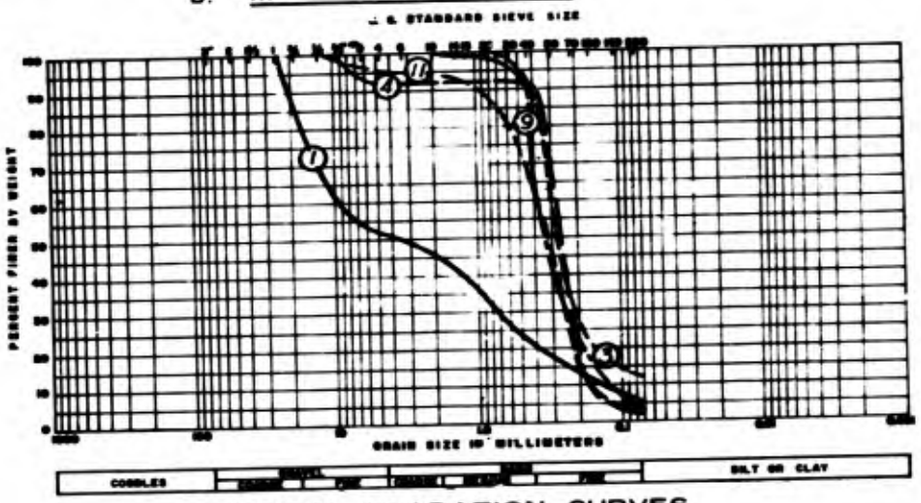

d. TYPICAL GRADATION CURVES

NOTES:

1. Tests were made by Corps of Engineers, Southwestern Division Laboratory, Dallas, Texas.
2. Sample numbers correspond to numbers in SWDGL Report No. 7920 and 7932.
3. Circled numbers by curves are reference numbers, see Table 3.
4. All tests were made on remolded samples

NOMENCLATURE:

3 — Drained direct shear test
S-S — Sliding friction test for steel on sand.
M-S — Sliding friction test for mortar on sand.

RESULTS OF GRADATION AND SLIDING FRICTION TESTS ON TYPICAL SANDS FROM LOCK AND DAM 4

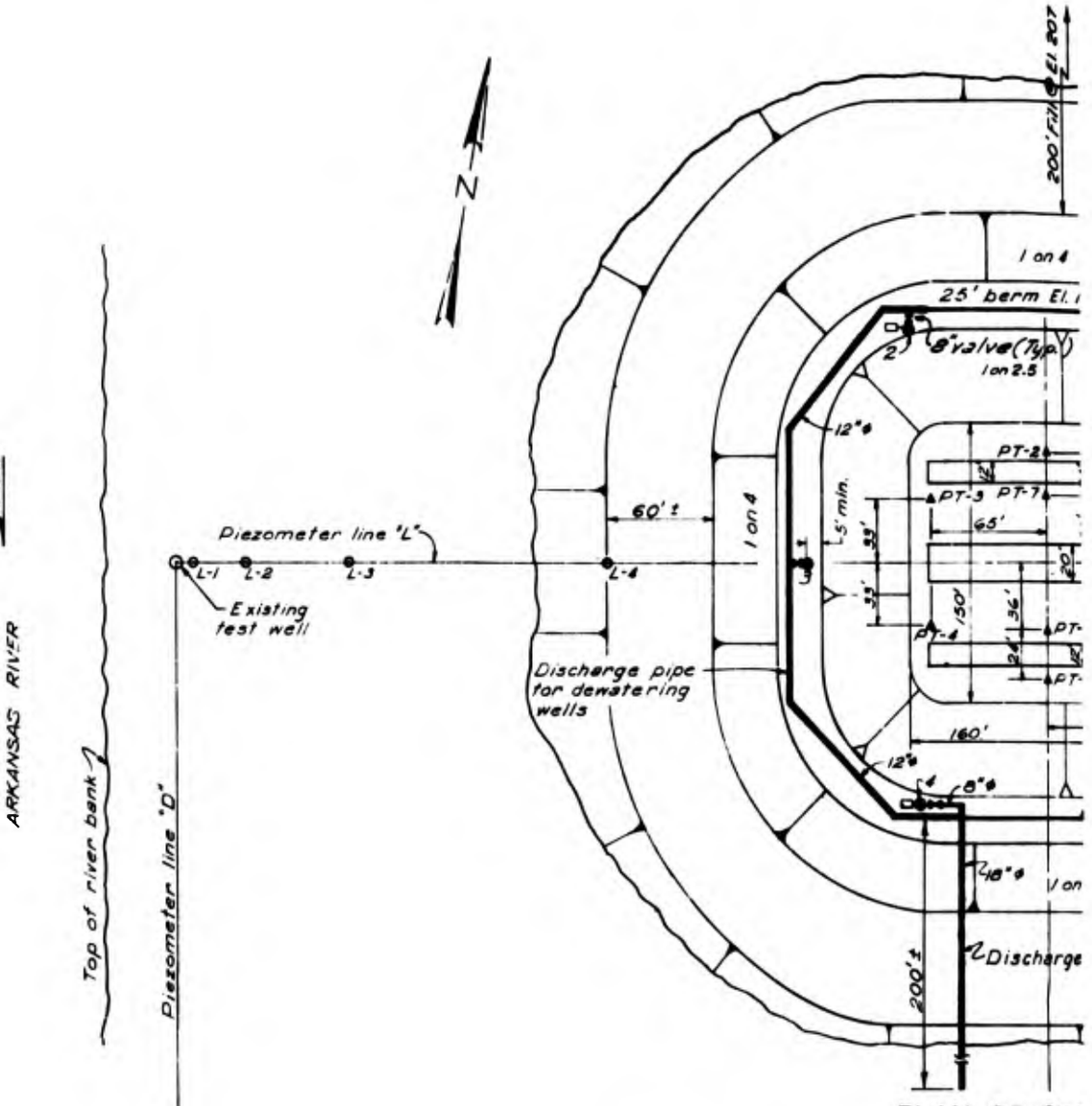

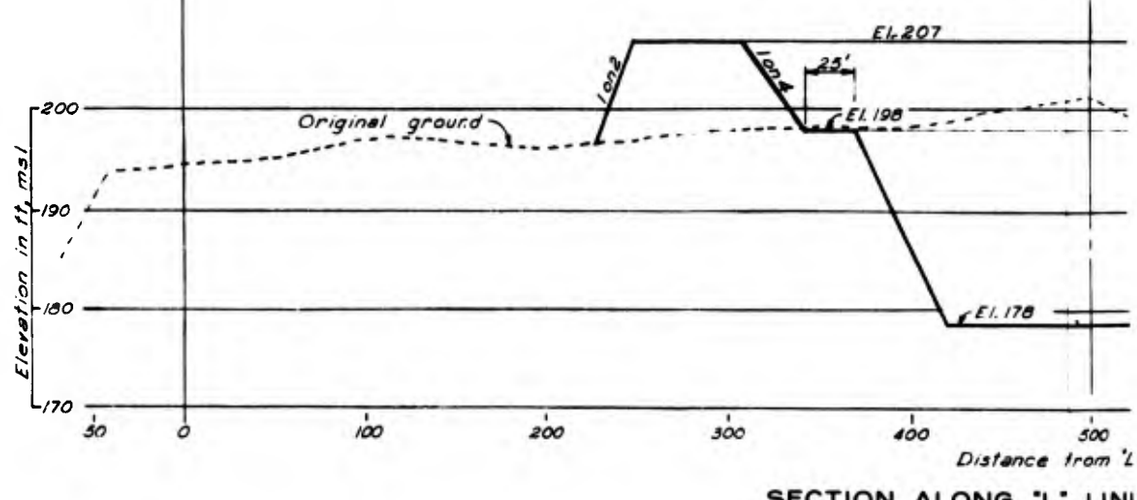

SECTION ALONG "L" LINE

TEST SITE DEVEL

A

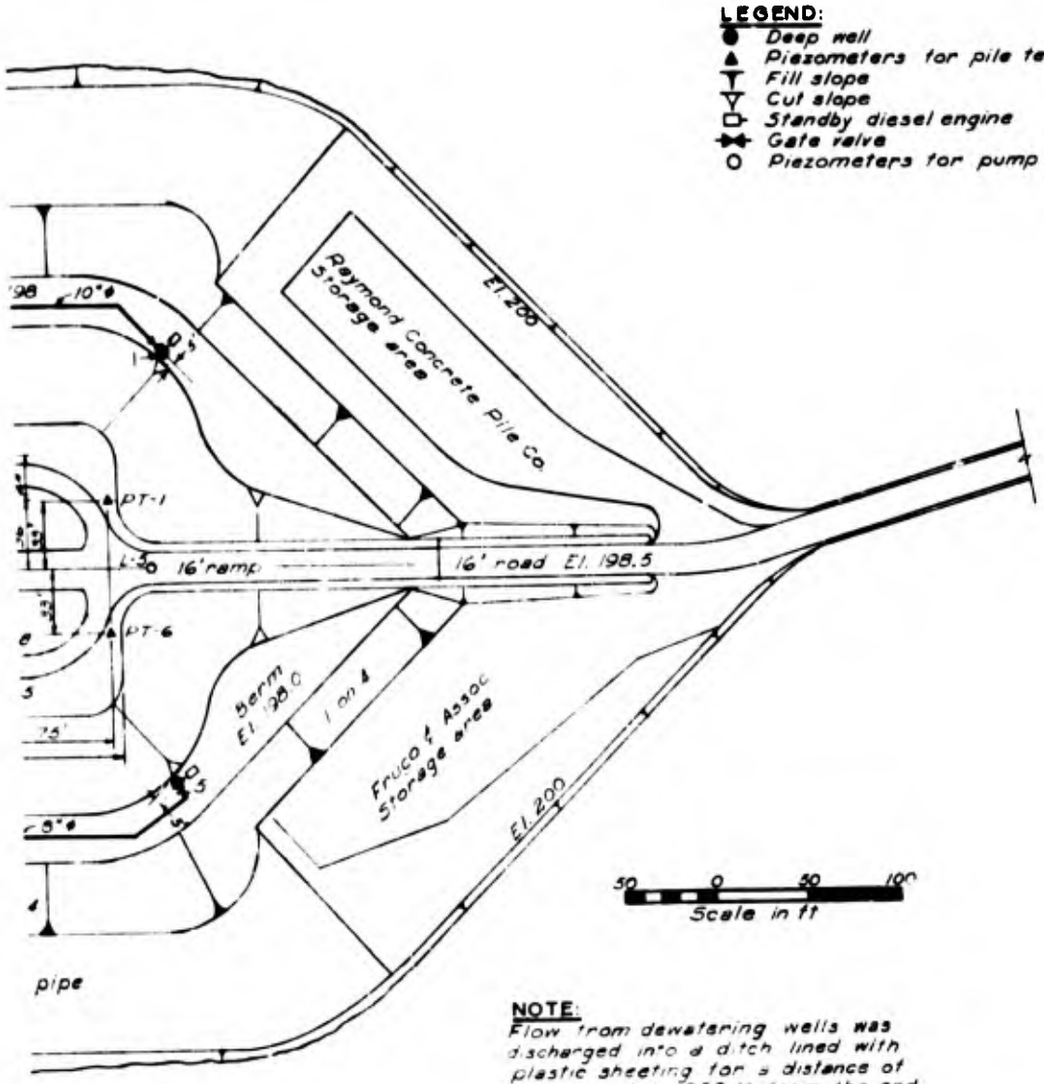

NOTE:
Flow from dewatering wells was discharged into a ditch lined with plastic sheeting for a distance of approximately 250 ft from the end of the discharge pipe.

AVATION

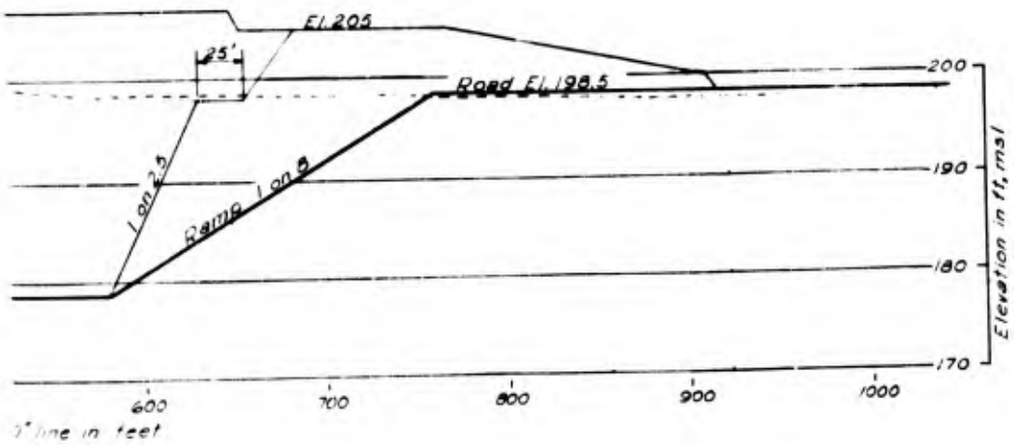

E OF PIEZOMETERS

OPMENT PLAN

B

PLATE 5

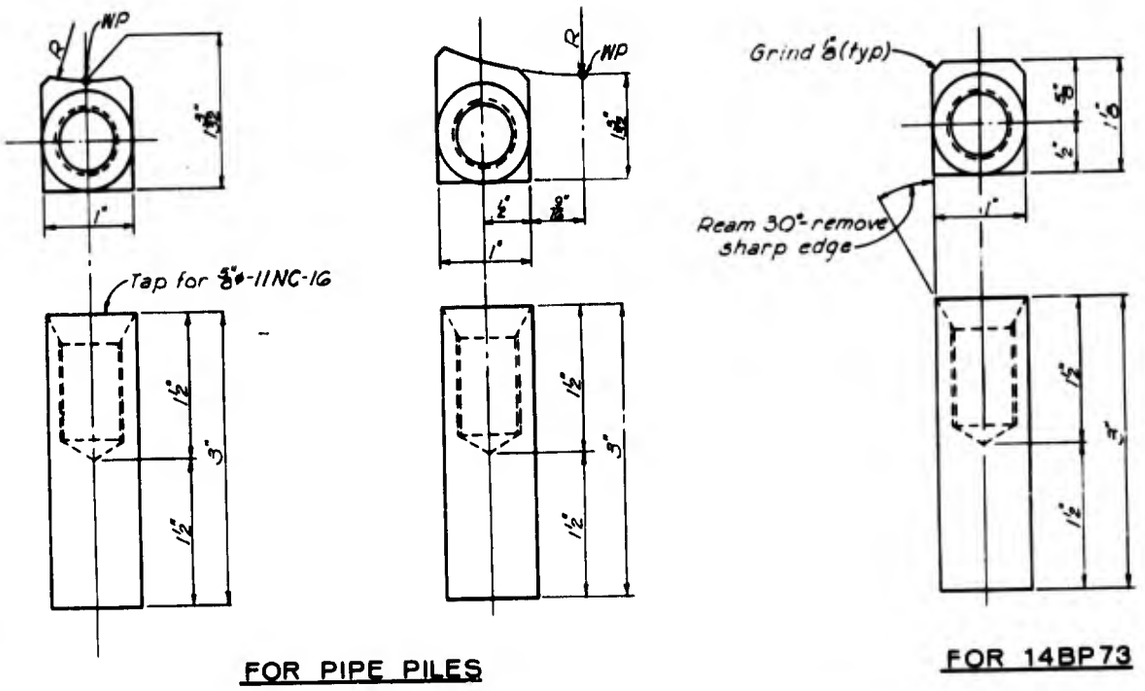

a. STRAIN ROD ANCHOR DETAILS

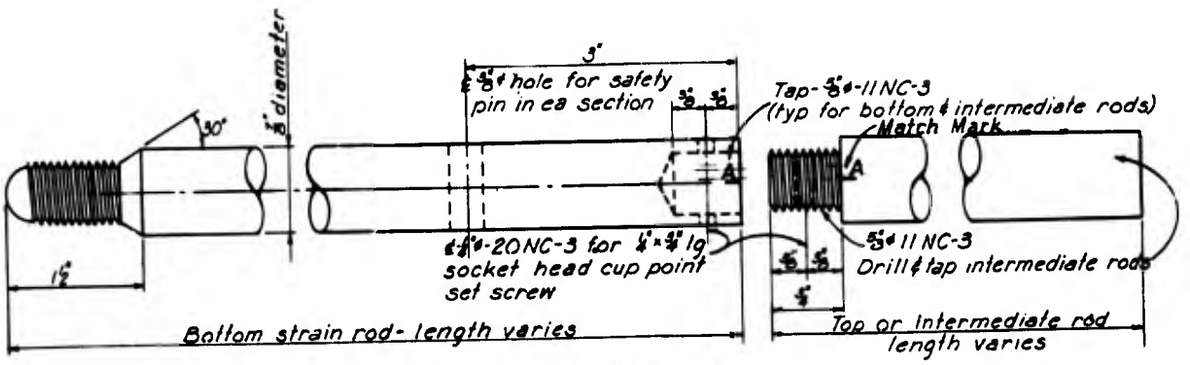

b. STRAIN ROD DETAILS

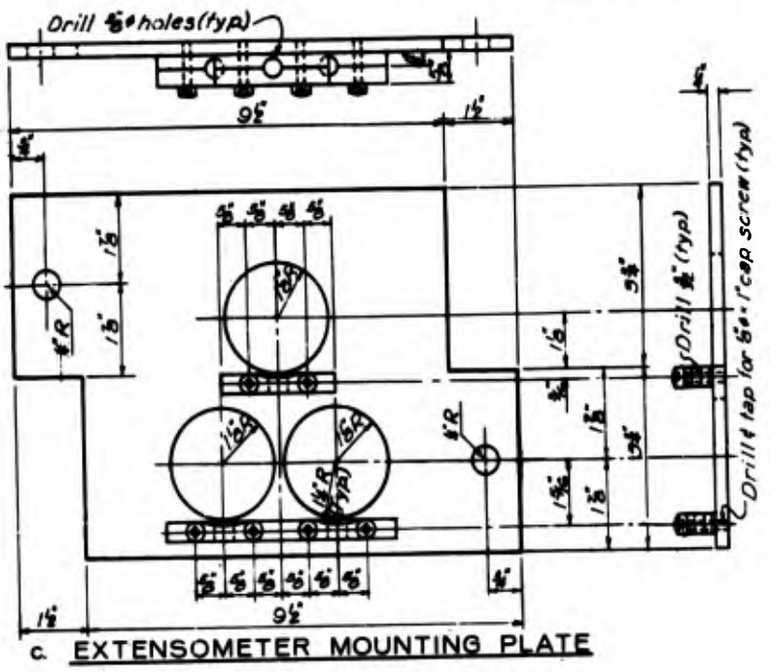

c. EXTENSOMETER MOUNTING PLATE

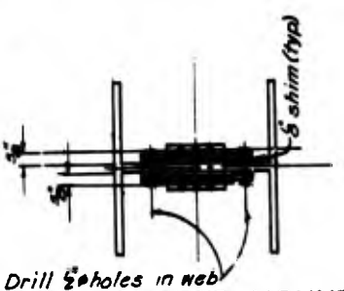

d. EXTENSOMETER MOUNTING PLATE AT H-PILES

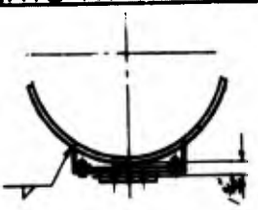

e. EXTENSOMETER MOUNTING PLATE AT PIPE PILES

STRAIN ROD, STRAIN ROD ANCHOR AND EXTENSOMETER MOUNTING DETAILS

PLATE 6

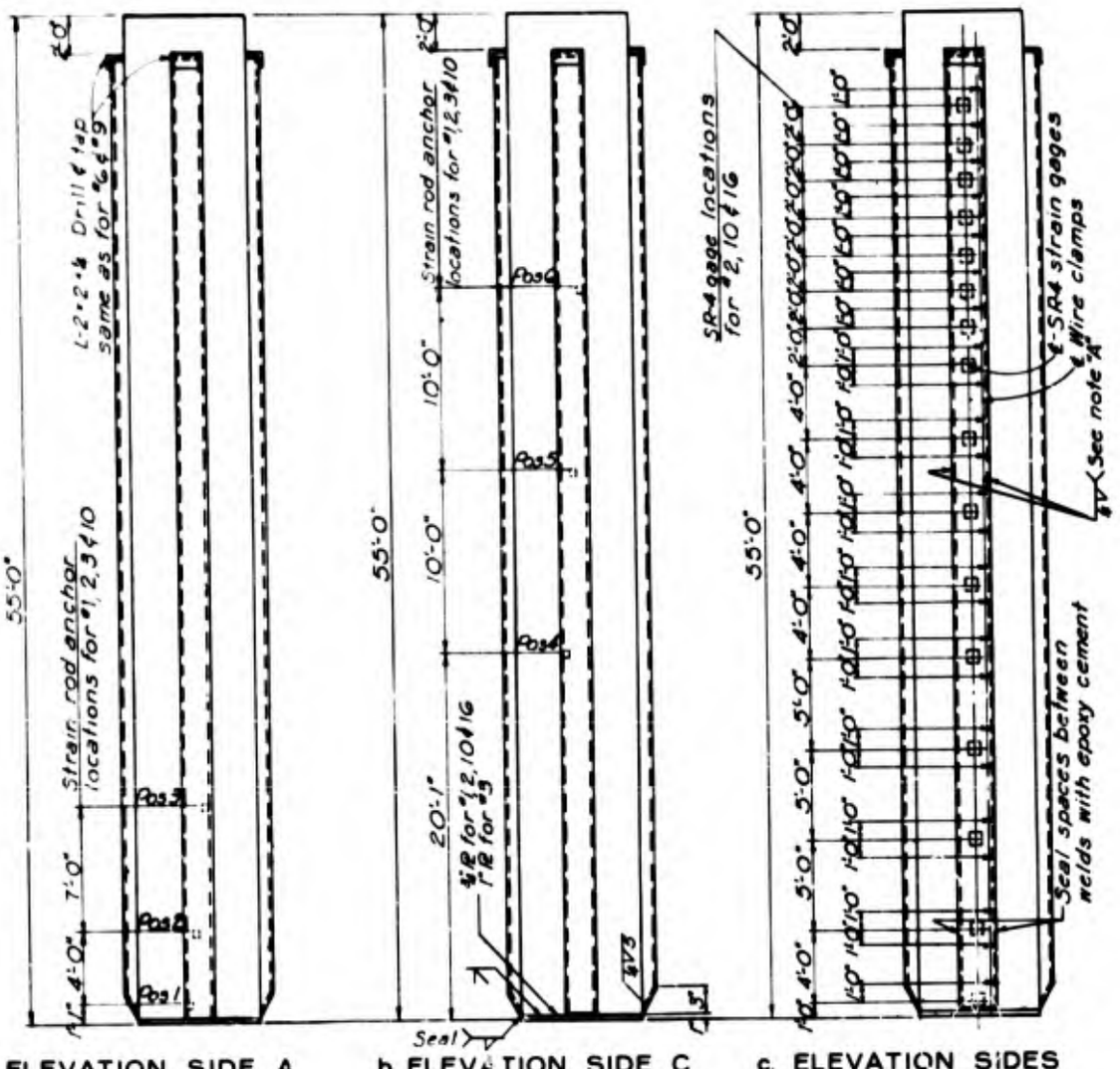

a. ELEVATION SIDE A b. ELEVATION SIDE C c. ELEVATION SIDES B AND D

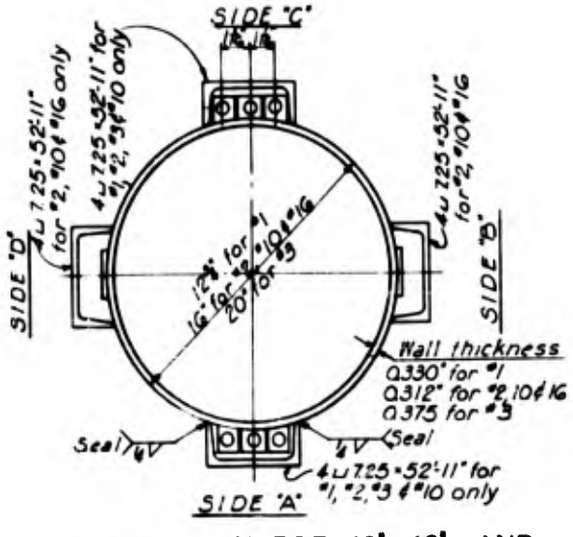

d. TYPICAL PLAN FOR 12", 16", AND 20" DIAMETER PILES

NOTE "A"

Continuous weld where there are no strain gages - Intermittent weld located midway between strain gages - End of welds 6" from gages.

NOTES:

1. No welding within 6" from any strain gage.
2. For details of strain rod anchors, see Fig. a, Plate 6.
3. All cover channels sealed with epoxy cement.

PIPE PILE INSTRUMENTATION AND FABRICATION DETAILS TEST PILES 1, 2, 3, 10 AND 16

PLATE 7

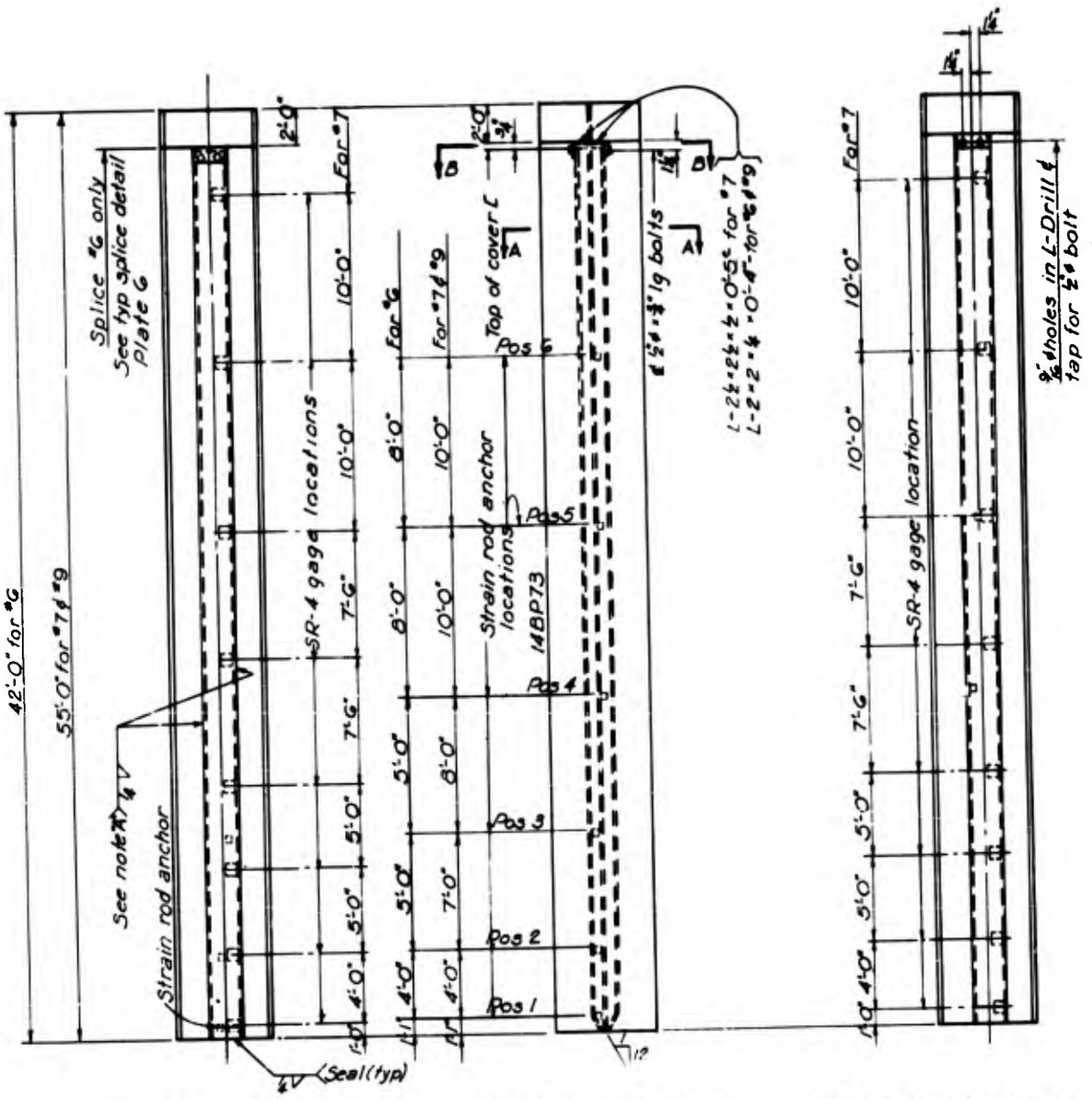

a. ELEVATION SIDE A

b. ELEVATION SIDE B

c. ELEVATION SIDE C

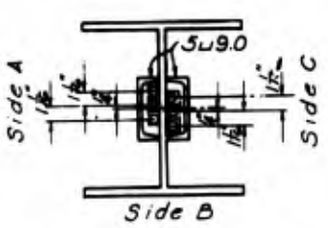

d. SECTION A - A FOR 7

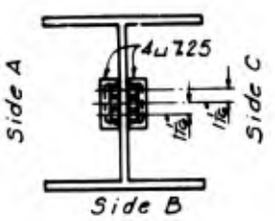

e. SECTION A - A FOR 6 AND 9

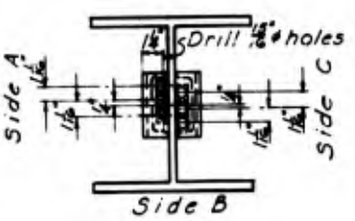

f. SECTION B - B FOR 7

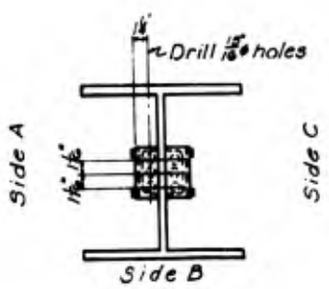

g. SECTION B - B FOR 6 AND 9

NOTE "A"

Continuous weld where there are no strain gages. - Intermittent weld located midway between strain gages - End of welds 6" from strain gages.

NOTES:

1. No welding within 6" from any strain gage.
2. For details of strain rod anchors see Plate 6.
3. All cover channels sealed with with epoxy cement.

H - PILE INSTRUMENTATION AND FABRICATION DETAILS TEST PILES 6, 7, AND 9

PLATE 8

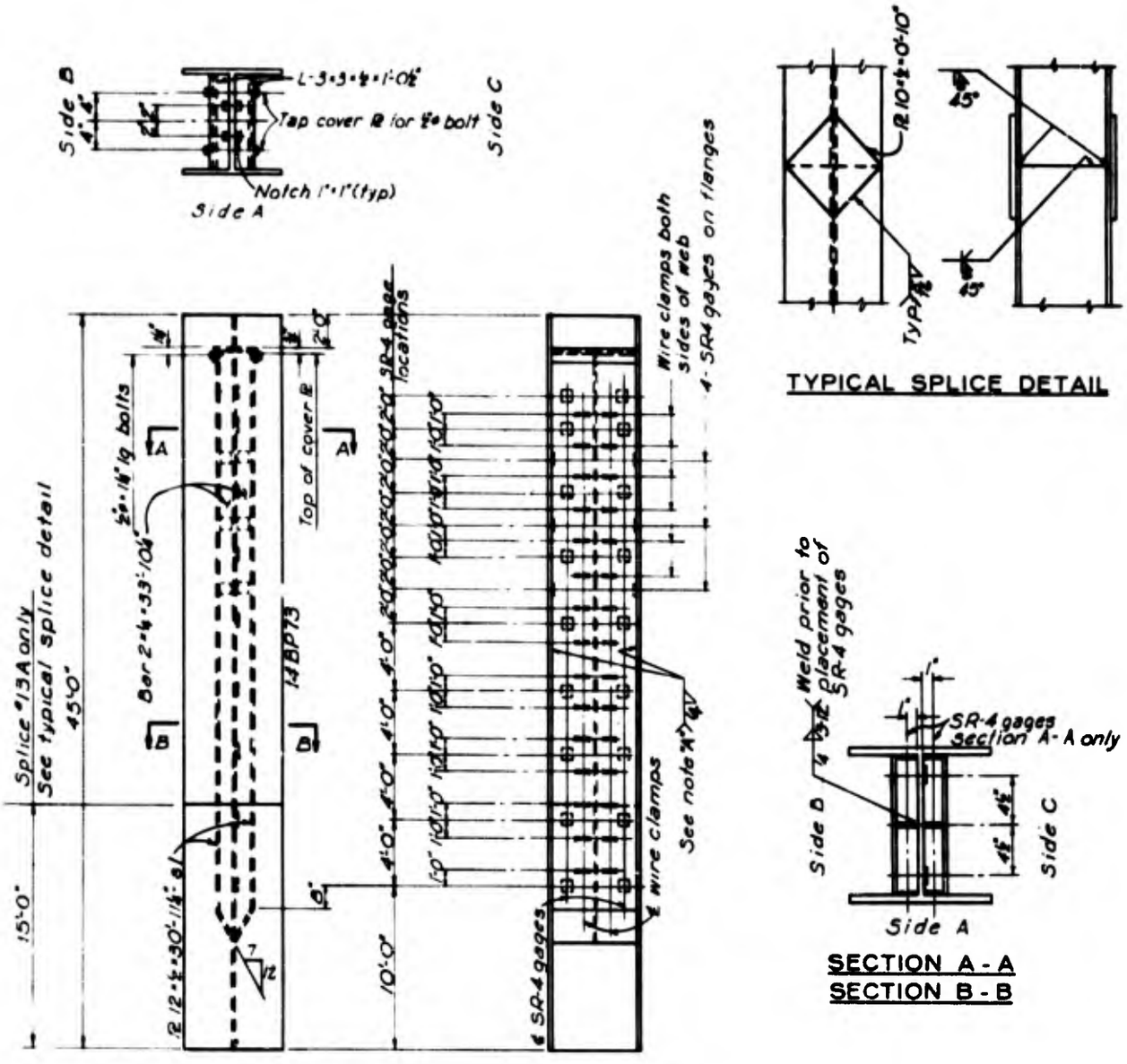

TYPICAL SPLICE DETAIL

SECTION A - A
SECTION B - B

a. ELEVATION SIDE A b. ELEVATION SIDE C

NOTE "A"

Continuous weld where there are no strain gages - Intermittent weld located midway between strain gages - End of welds 6" from gages.

NOTES:

1. *No welding within 6" from any strain gage.*
2. *For details of strain rod anchors see Fig. a, Plate 6.*
3. *All cover channels sealed with epoxy cement.*

H - PILE INSTRUMENTATION AND FABRICATION DETAILS TEST PILES 12, 13, AND 13A

PLATE 9

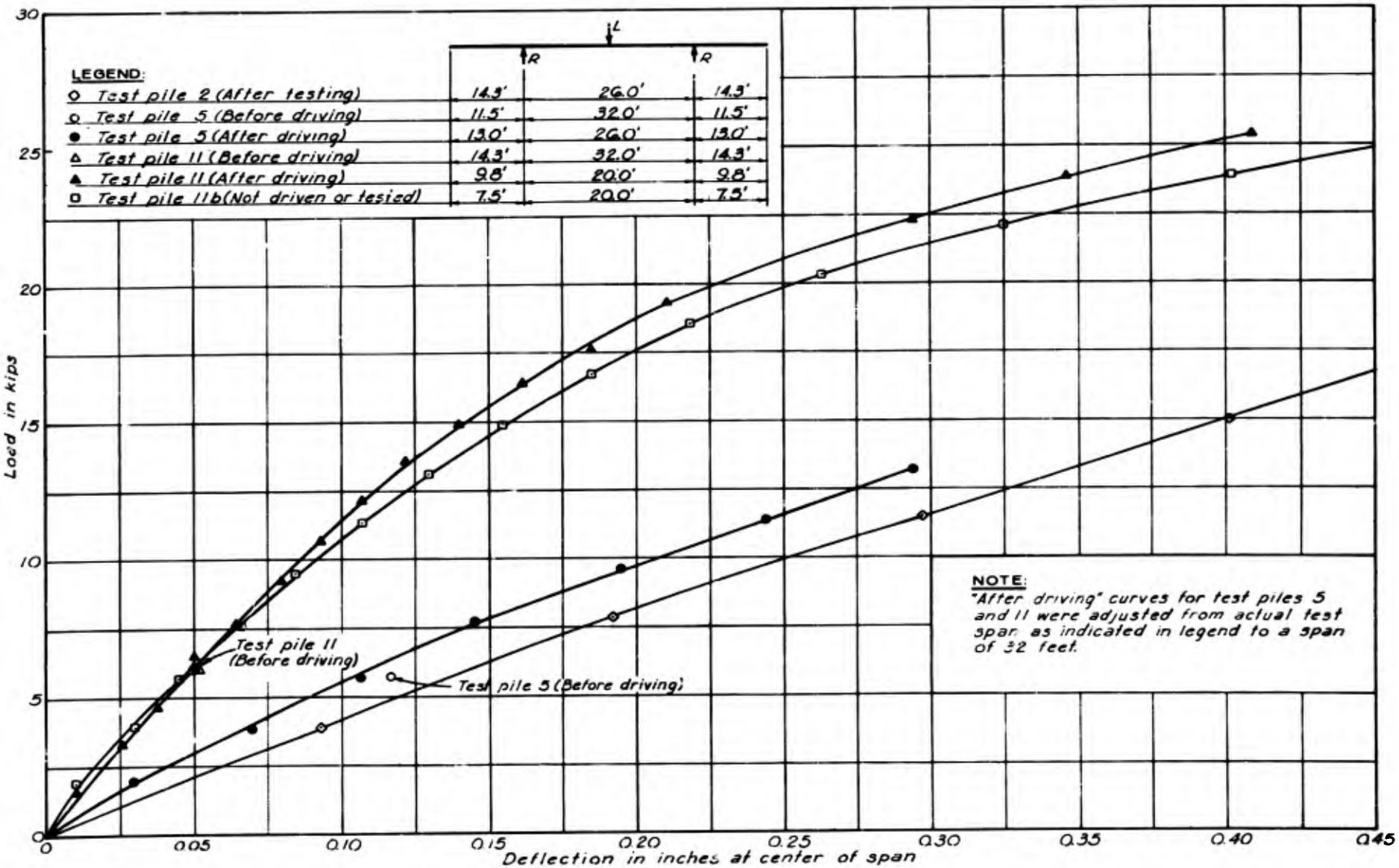

LOAD VS DEFLECTION CURVES

FIELD FLEXURE TEST RESULTS

PLATE 10

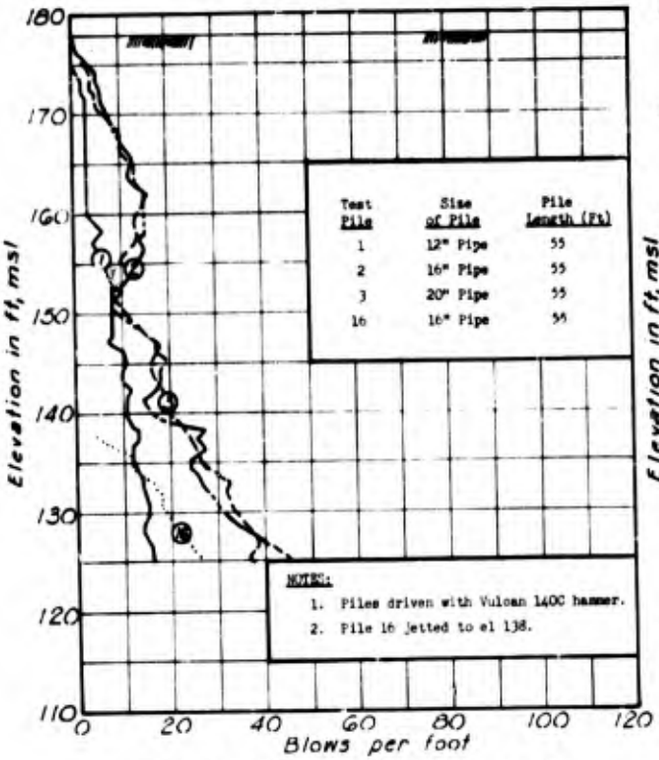

a. PIPE PILES 1, 2, 3 AND 16

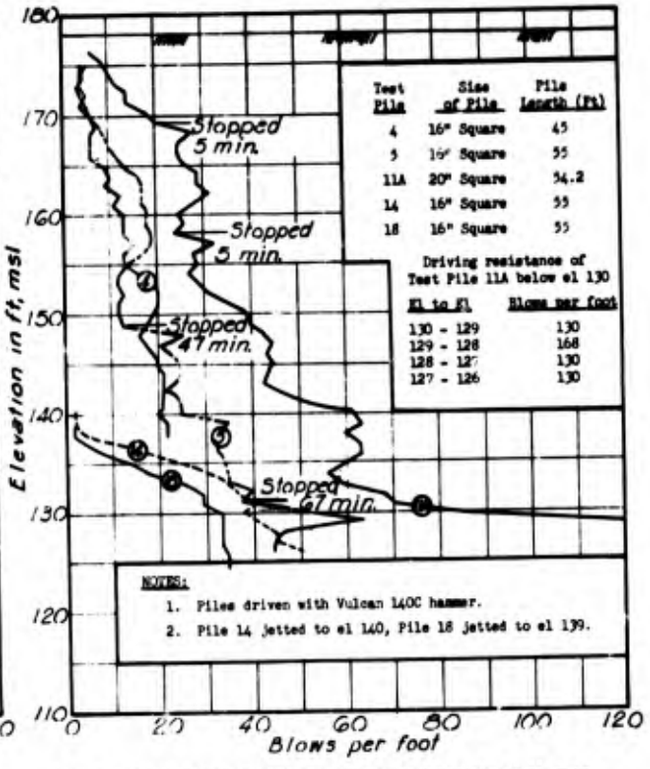

b. PRESTRESSED CONCRETE PILES 4, 5, 11A, 14 AND 18

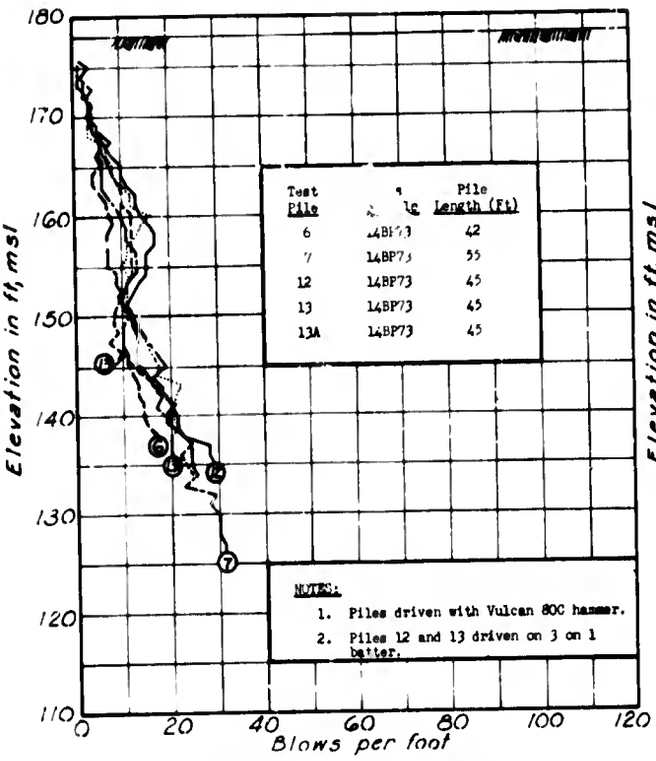

c. 14 INCH H-PILES 6, 7, 12, 13 AND 13A

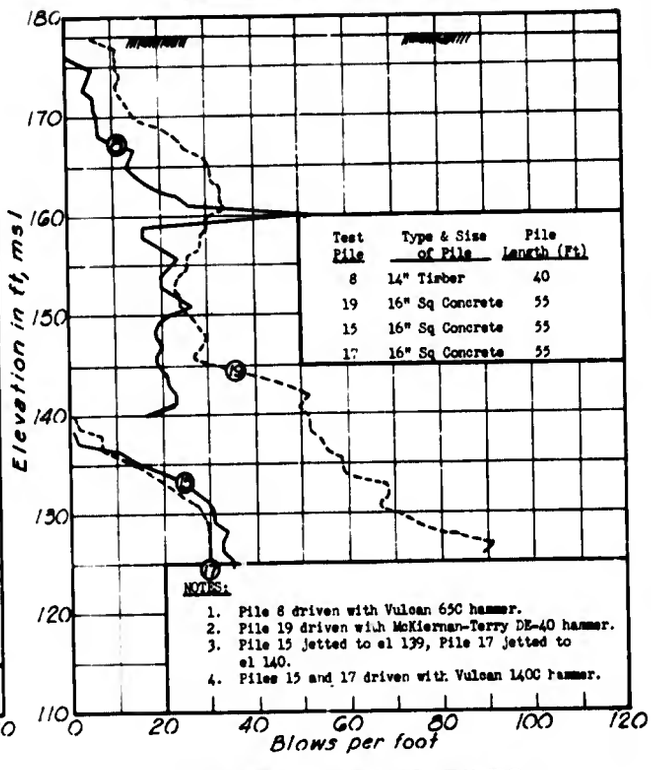

d. MISCELLANEOUS PILES 8, 15, 17 AND 19

DRIVING RECORDS FOR BEARING PILES DRIVEN WITH STEAM HAMMERS

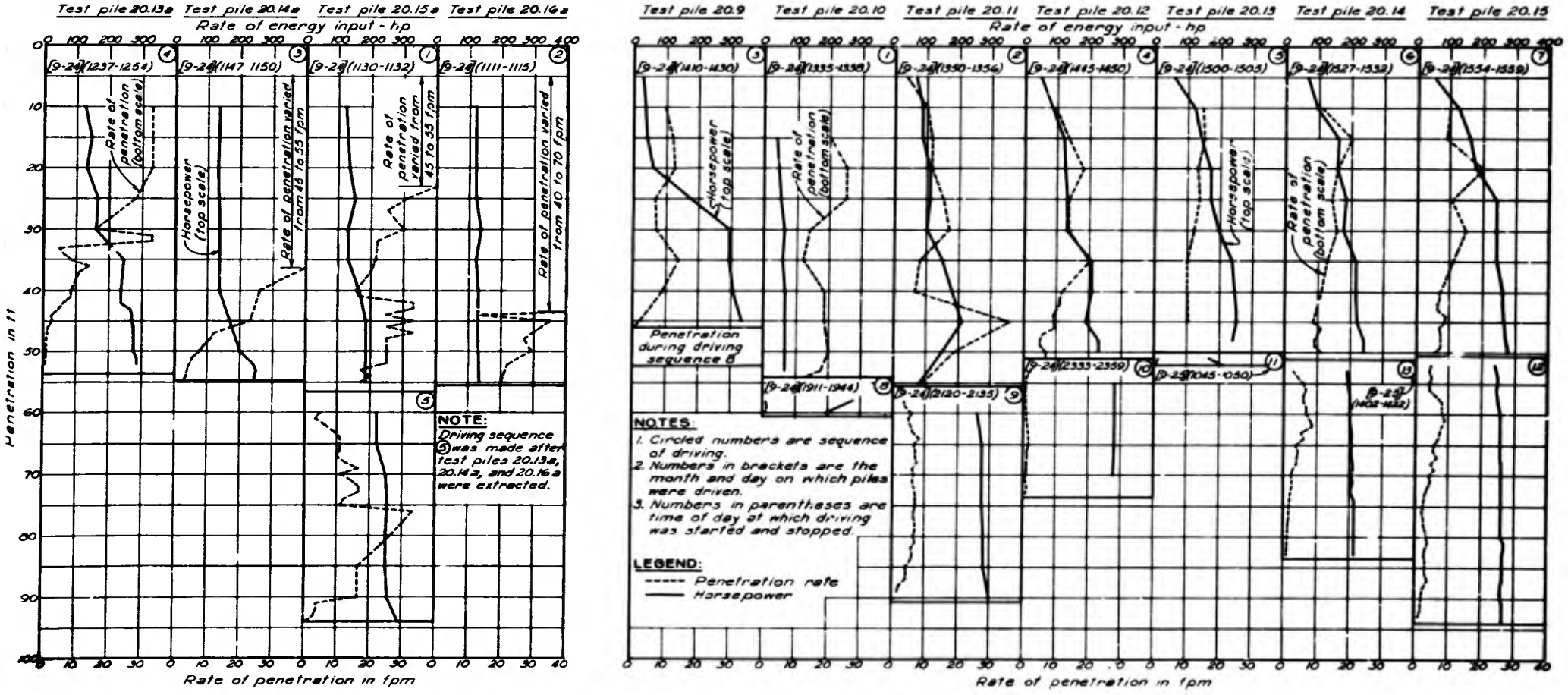

PILE DRIVING DATA FOR MZ - 32 STEEL SHEET PILING WITH BODINE HAMMER

PLATE 12

PLATE 13

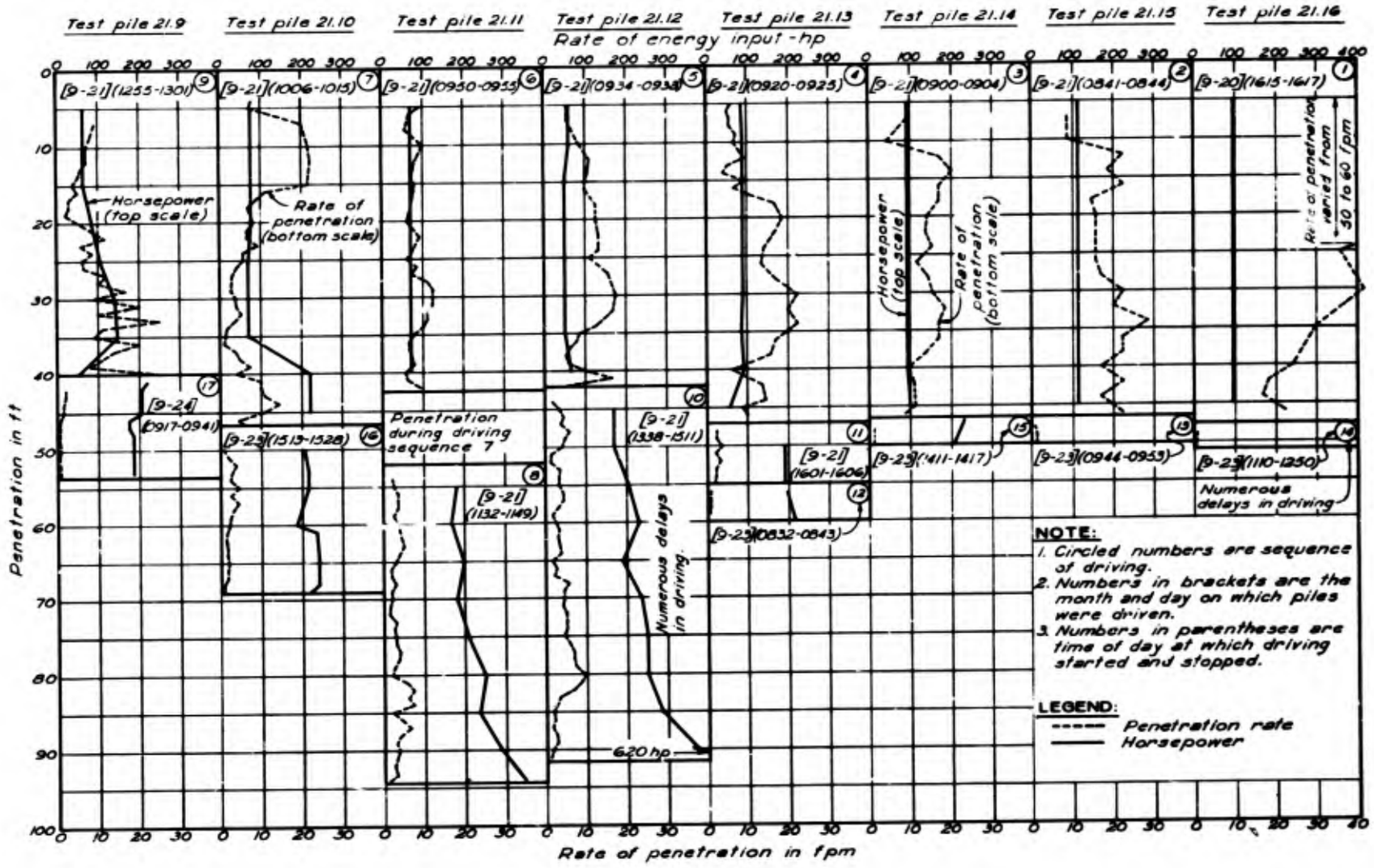

PILE DRIVING DATA FOR MP - 112 STEEL SHEET PILING
DRIVEN WITH BODINE HAMMER

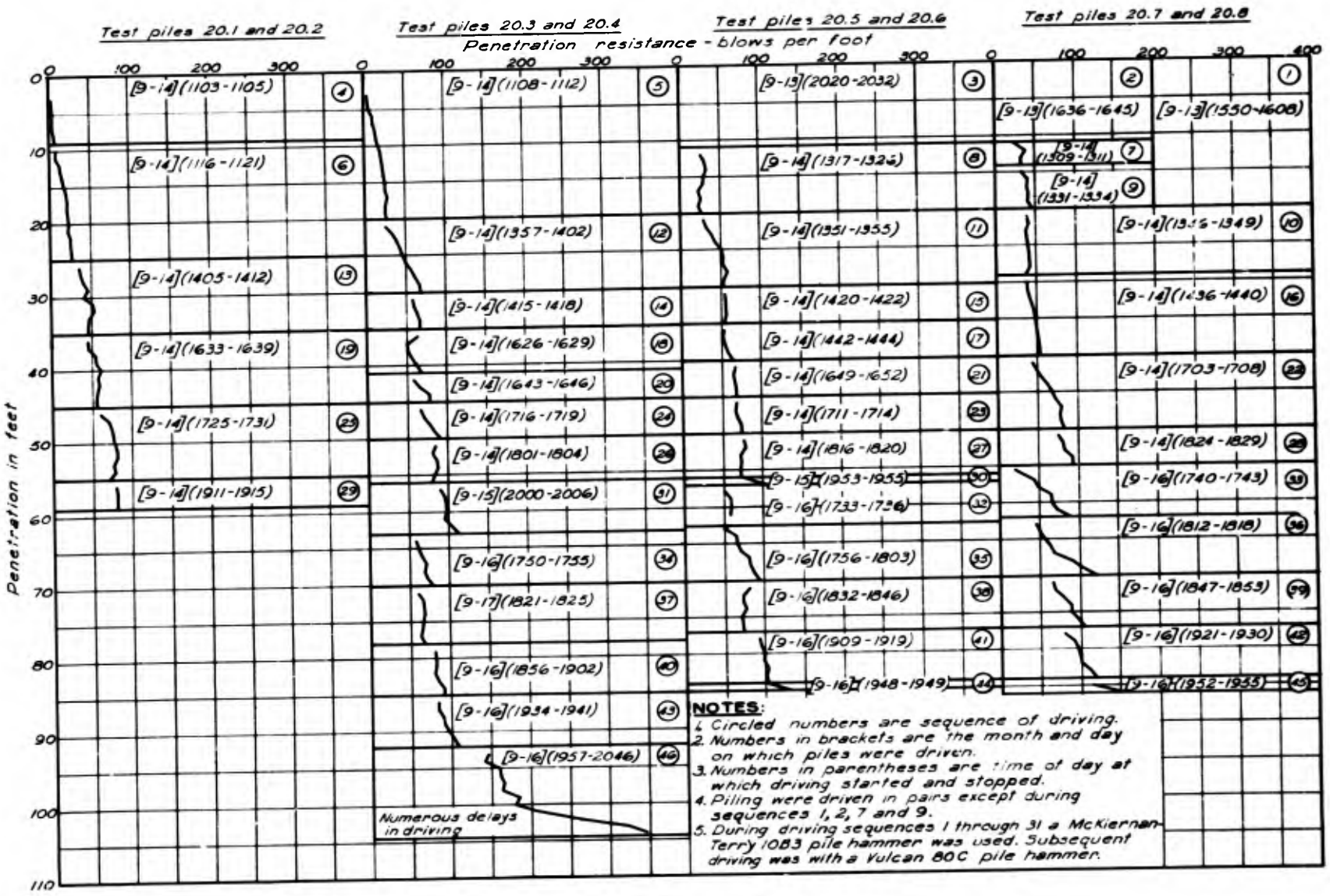

PILE DRIVING DATA FOR MZ - 32 STEEL SHEET PILING DRIVEN WITH STEAM HAMMERS

PLATE 14

PLATE 15

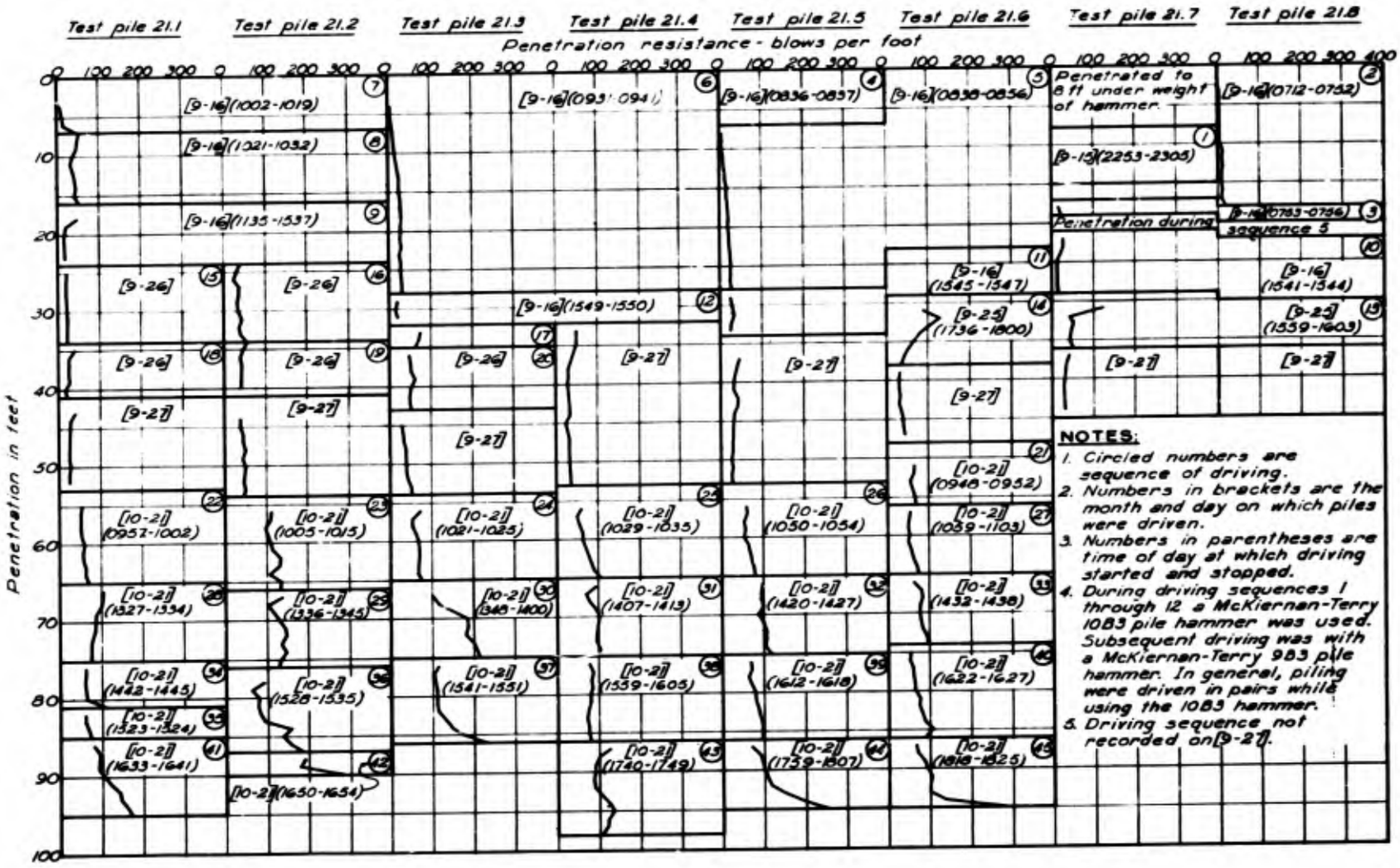

PILE DRIVING DATA FOR MP - 112 STEEL SHEET PILING WITH STEAM HAMMERS

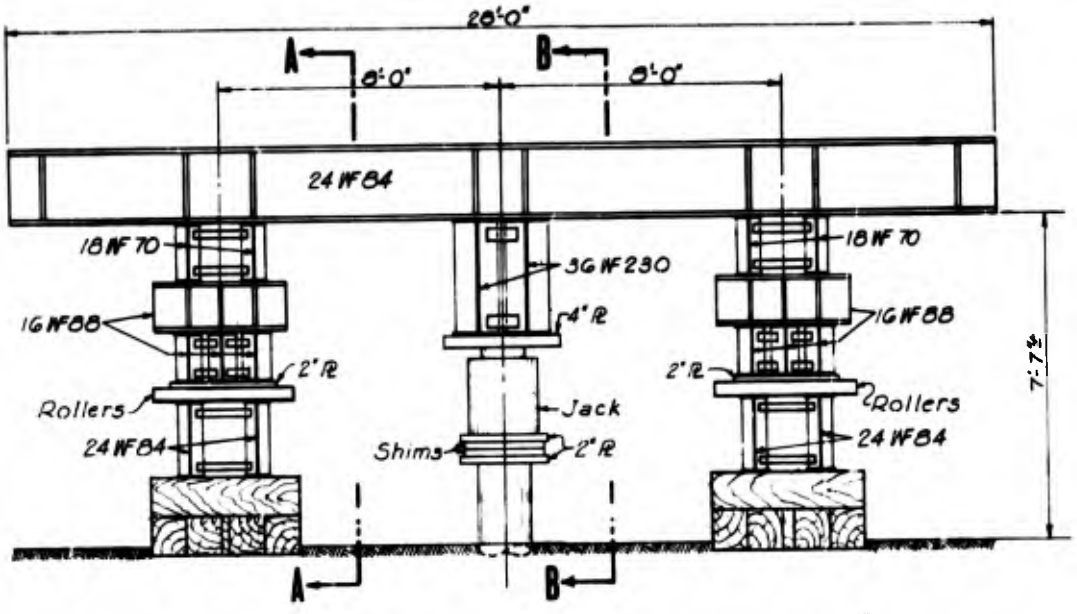

a. TYPICAL CROSS SECTION THRU LOADING FRAME

2 0 2 4
Scale in ft

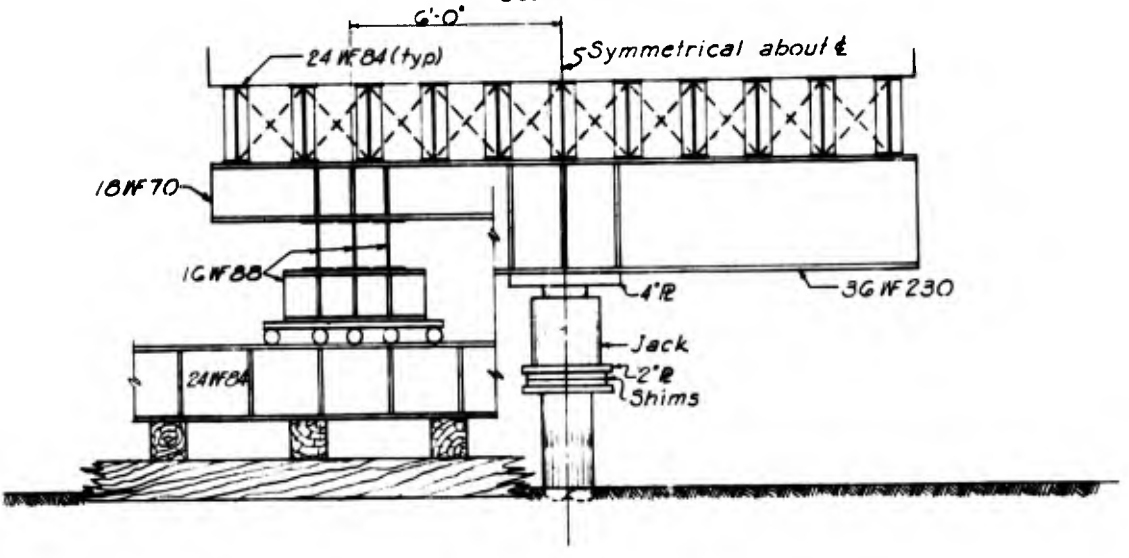

SECTION A - A

SECTION B - B

2 0 2 4
Scale in ft

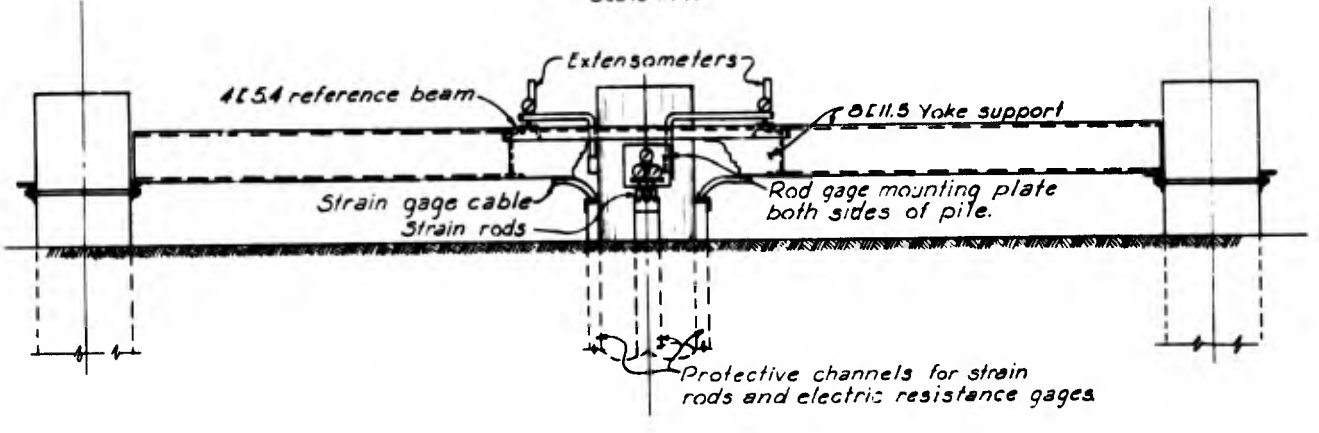

b. TYPICAL PILE HEAD INSTRUMENTATION

1 0 1 2
Scale in ft

COMPRESSION LOADING FRAME AND PILE INSTRUMENTATION

PLATE 16

PLATE 17

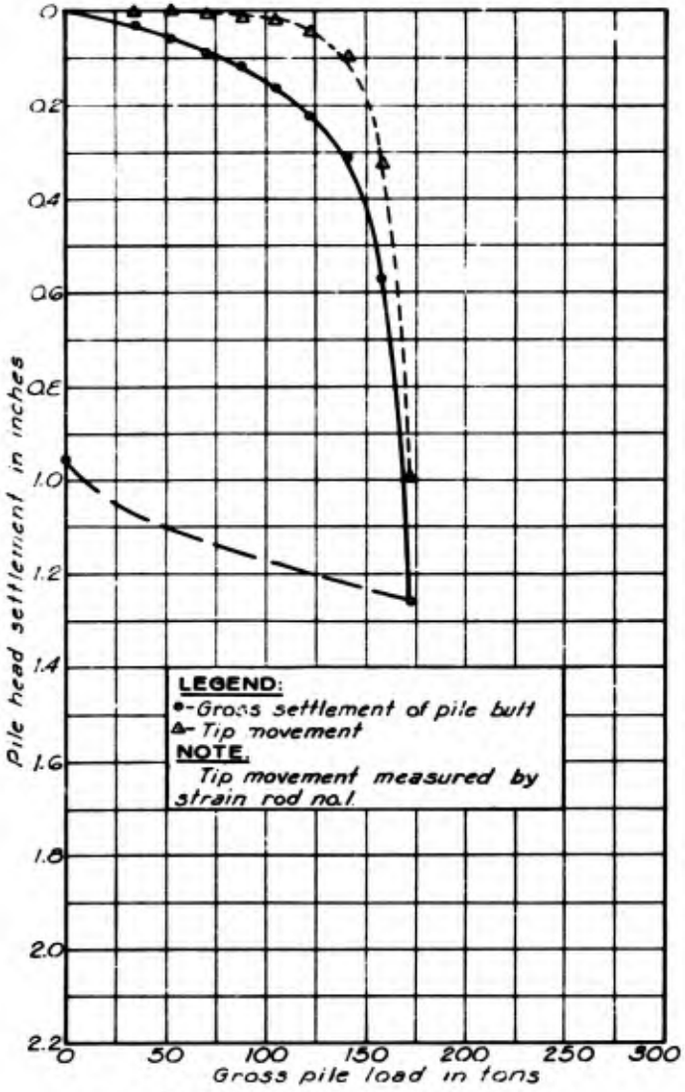

a. PILE MOVEMENT VS LOAD

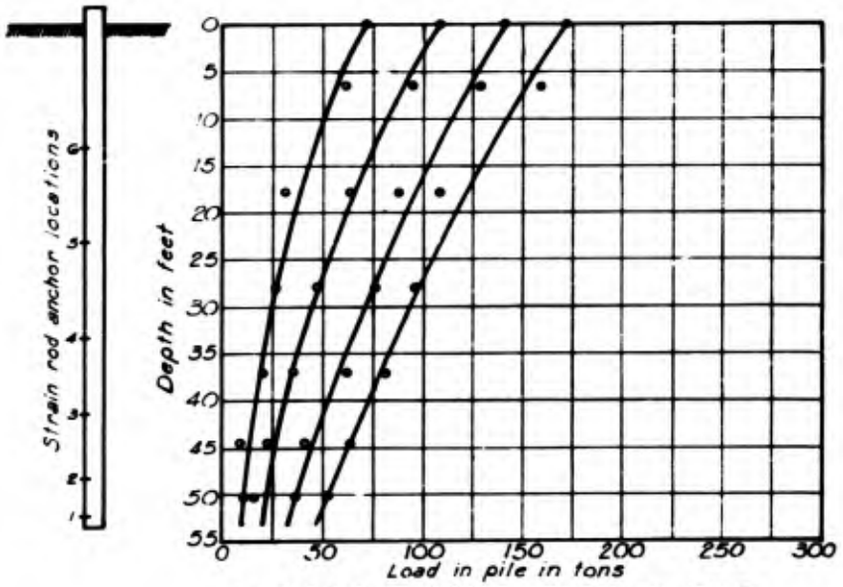

b. LOAD DISTRIBUTION IN PILE

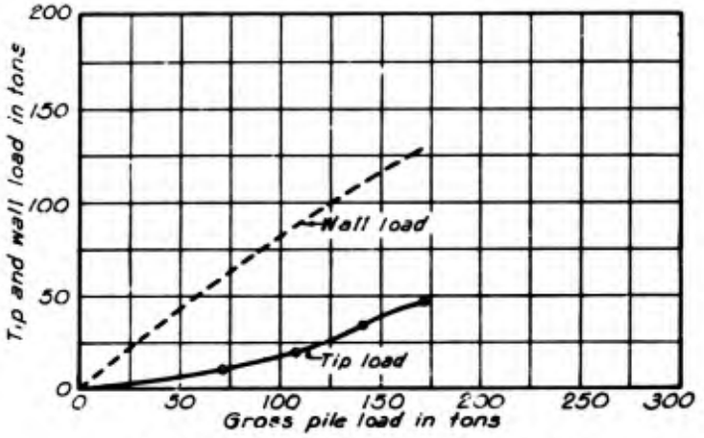

c. GROSS LOAD VS TIP AND WALL LOAD

COMPRESSION TEST RESULTS - TEST PILE 1 - 12.75-INCH DIAMETER PIPE

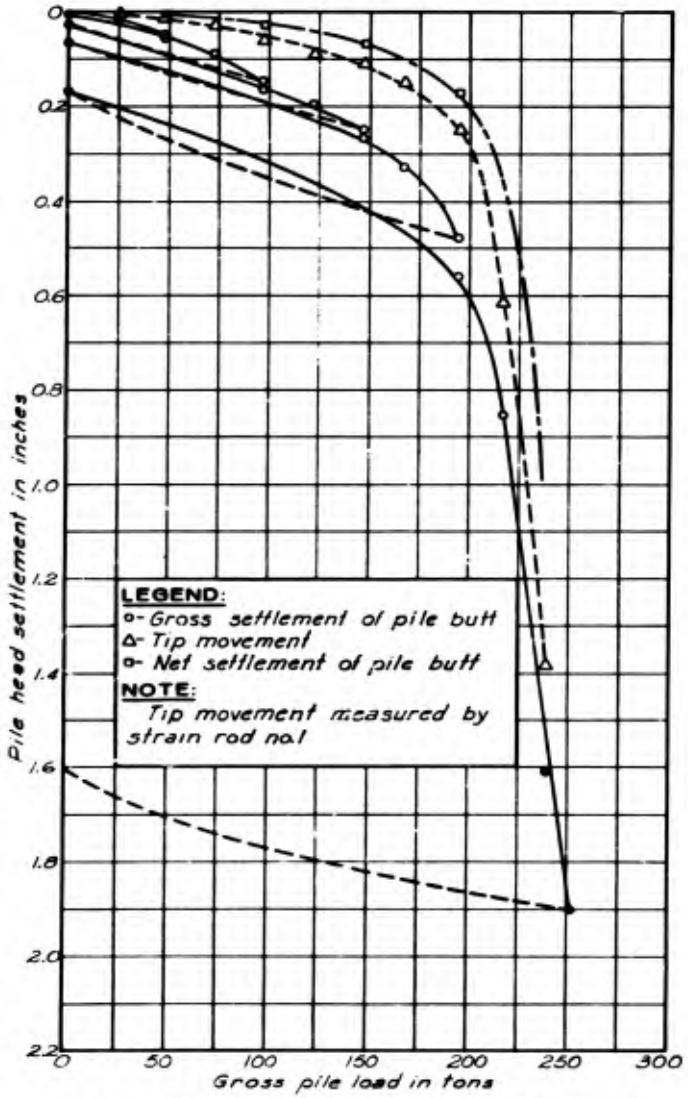

a. PILE MOVEMENT VS LOAD

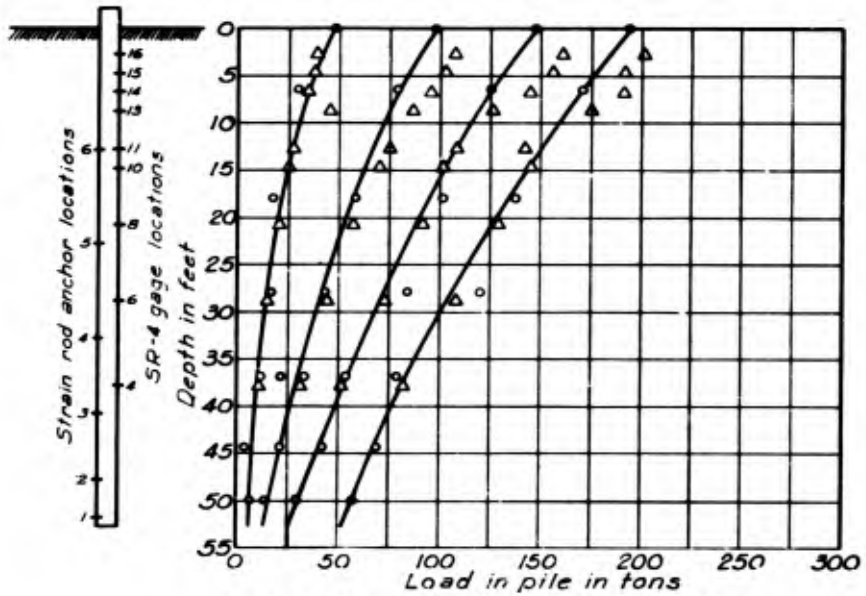

b. LOAD DISTRIBUTION IN PILE

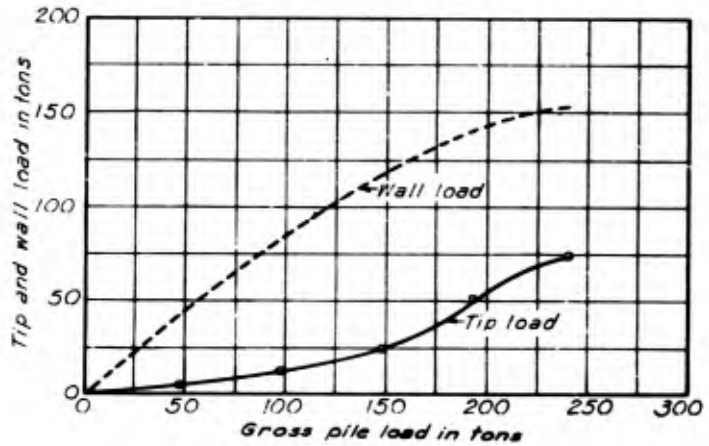

c. GROSS LOAD VS TIP AND WALL LOAD

PLATE 18

COMPRESSION TEST RESULTS - TEST PILE 2 - TEST 1 - 16-INCH DIAMETER PIPE

PLATE 19

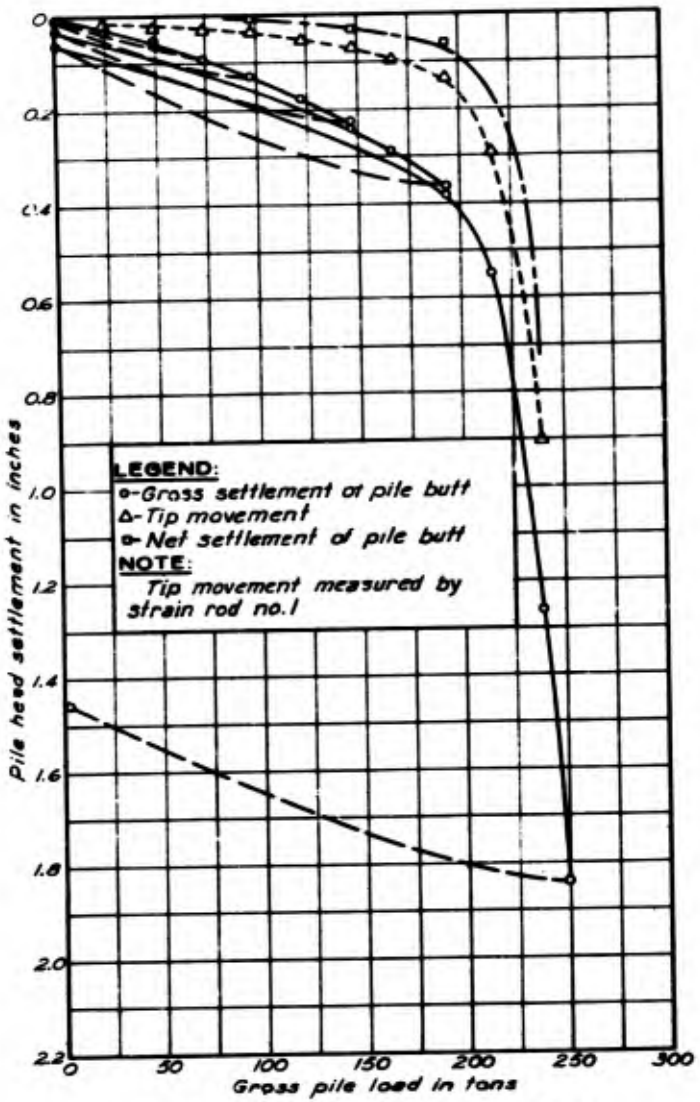

a. PILE MOVEMENT VS LOAD

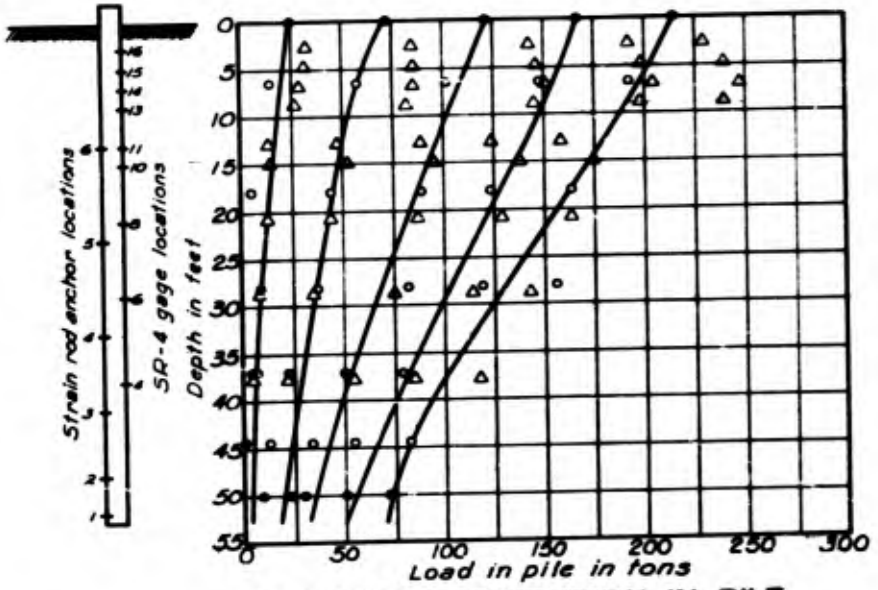

b. LOAD DISTRIBUTION IN PILE

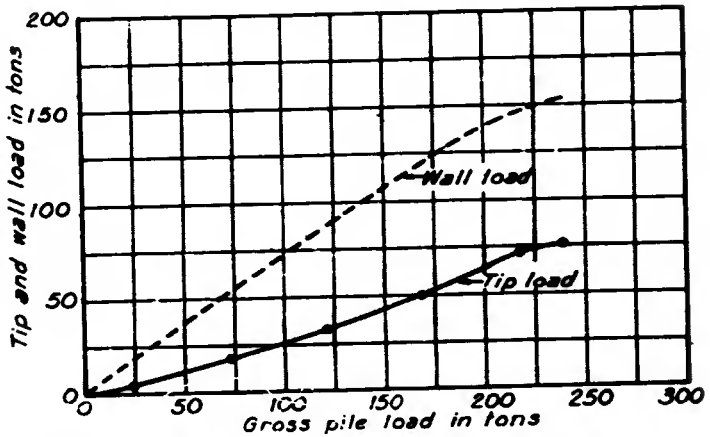

c. GROSS LOAD VS TIP AND WALL LOAD

COMPRESSION TEST RESULTS - TEST PILE 2 - TEST 2 - 16-INCH DIAMETER PIPE

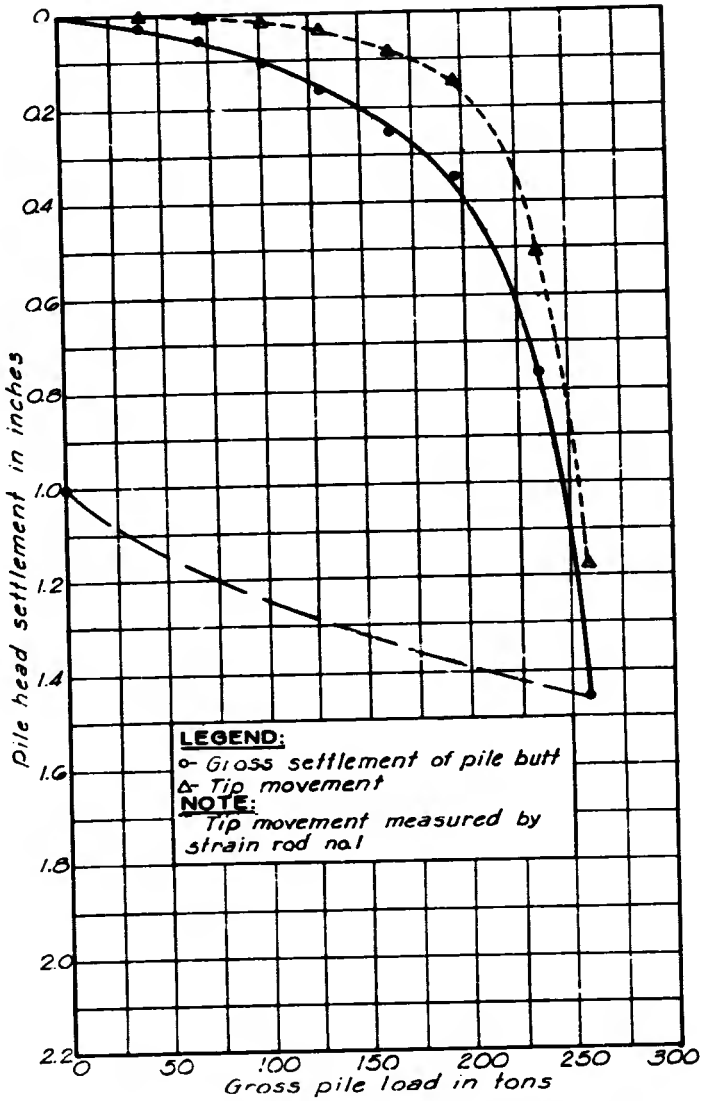

a. PILE MOVEMENT VS LOAD

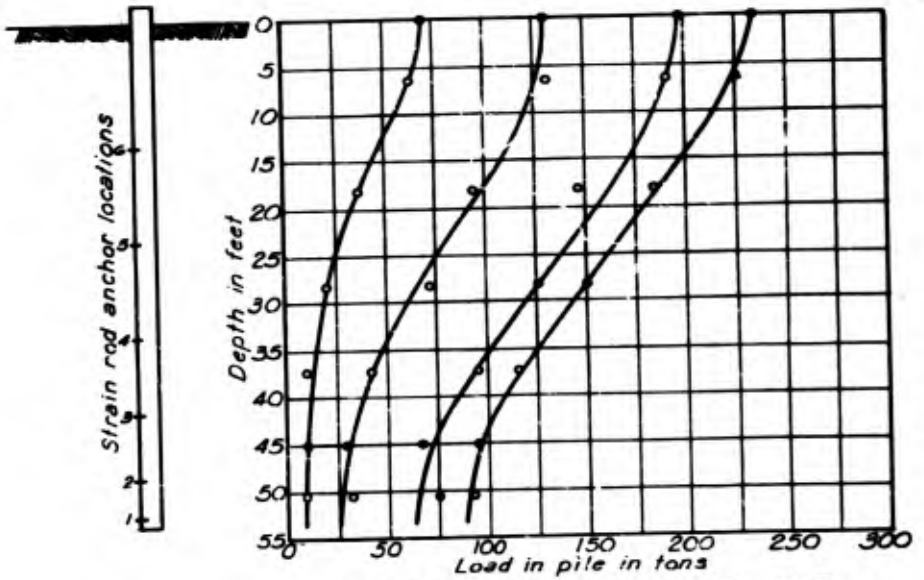

b. LOAD DISTRIBUTION IN PILE

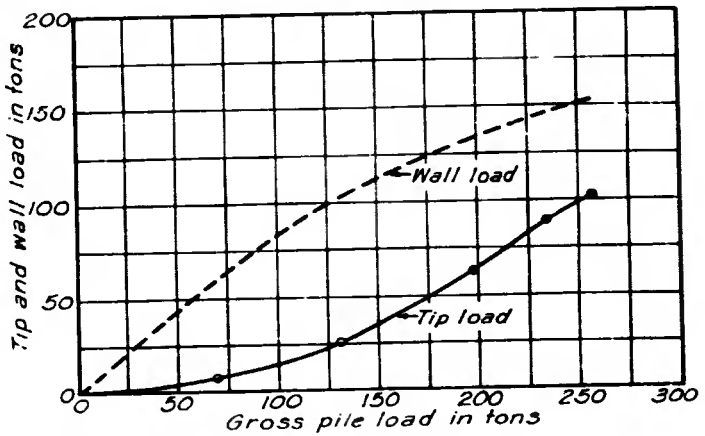

c. GROSS LOAD VS TIP AND WALL LOAD

COMPRESSION TEST RESULTS - TEST PILE3 20-INCH DIAMETER PIPE

PLATE 20

PLATE 21

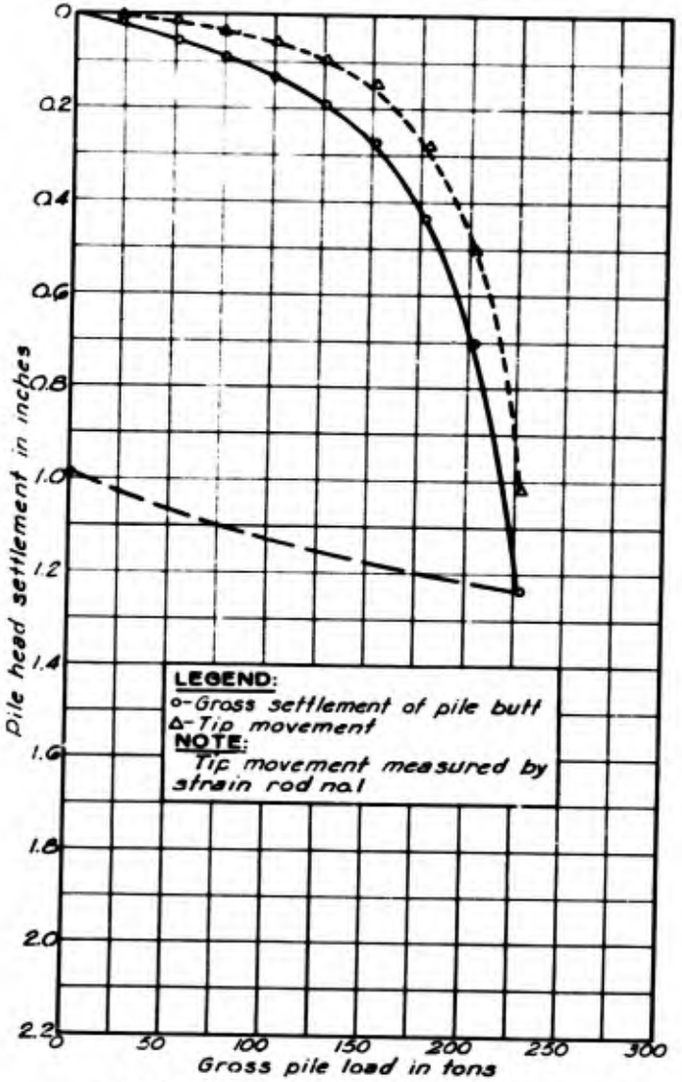

a. PILE MOVEMENT VS LOAD

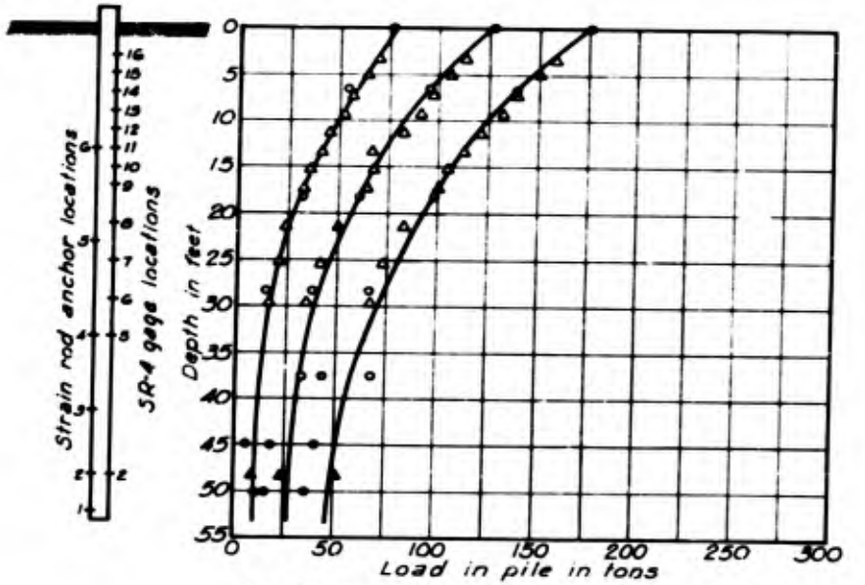

b LOAD DISTRIBUTION IN PILE

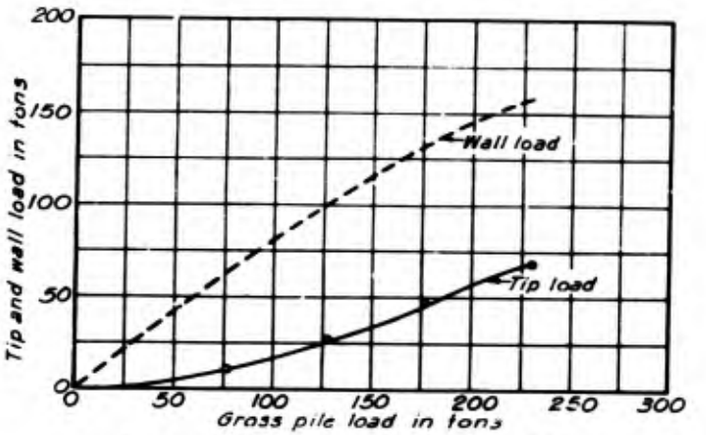

c. GROSS LOAD VS TIP AND WALL LOAD

COMPRESSION TEST RESULTS - TEST PILE 10-16-INCH DIAMETER PIPE

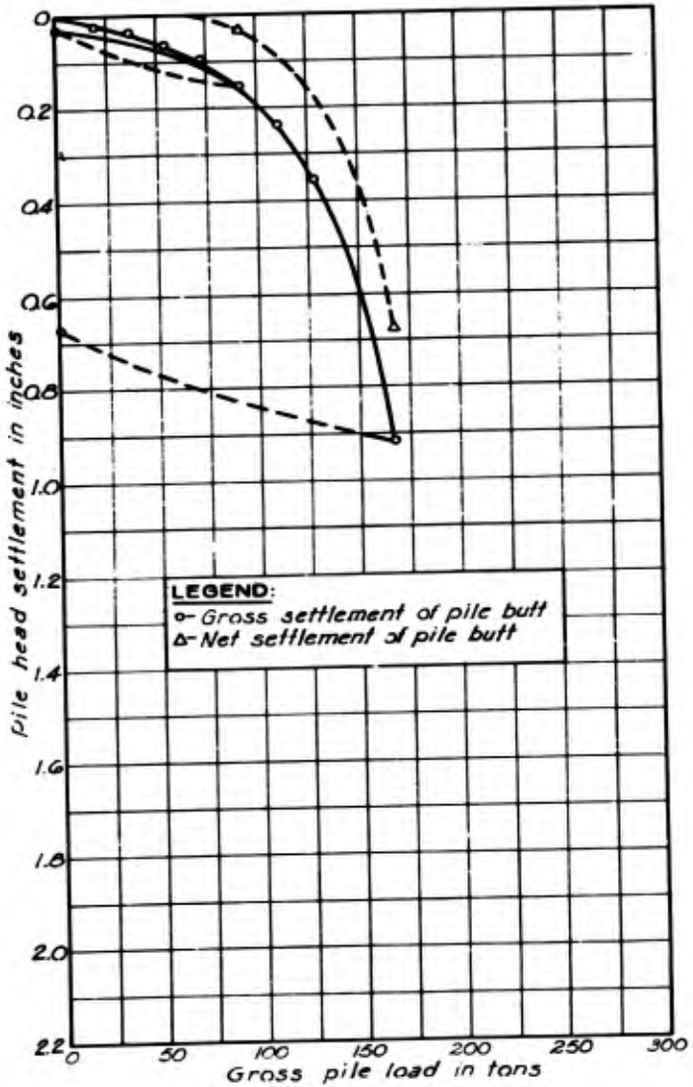

a. PILE MOVEMENT VS LOAD

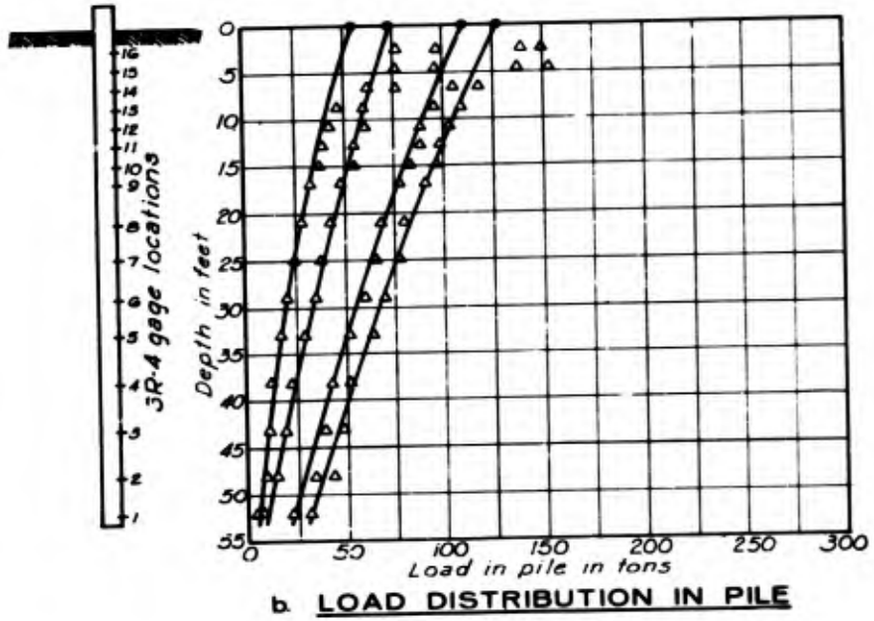

b. LOAD DISTRIBUTION IN PILE

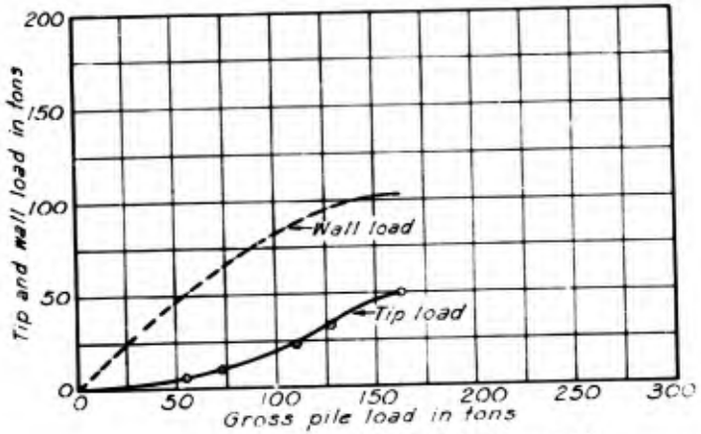

c. GROSS LOAD VS TIP AND WALL LOAD

COMPRESSION TEST RESULTS - TEST PILE 16 - 16-INCH DIAMETER PIPE

PLATE 22

PLATE 23

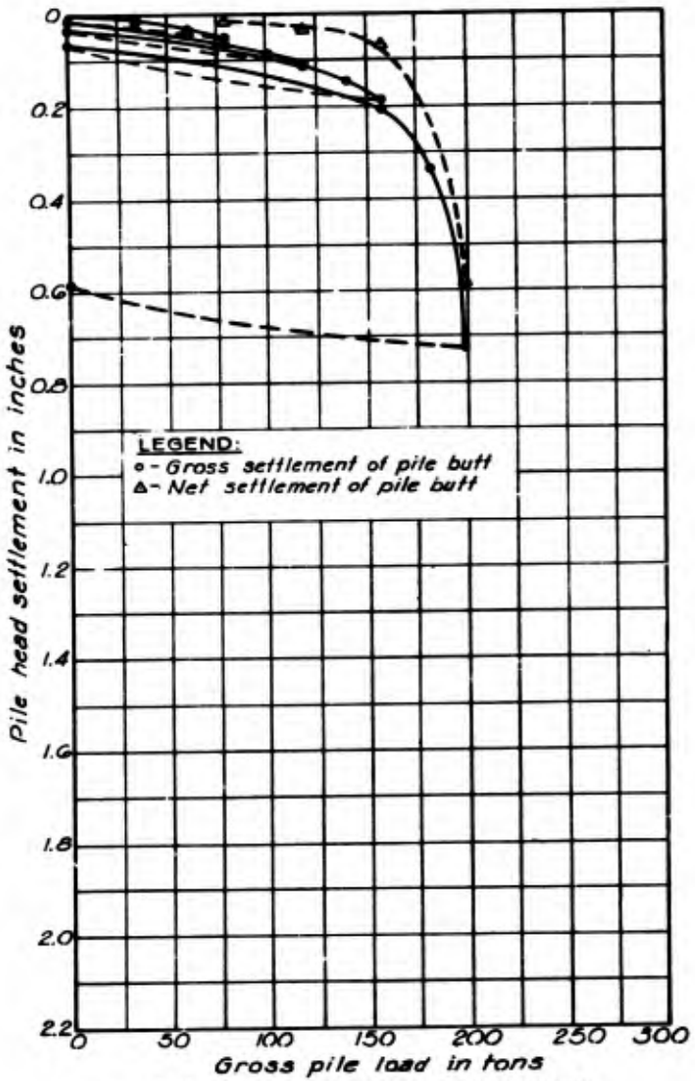

a. PILE MOVEMENT VS LOAD
TEST PILE 4

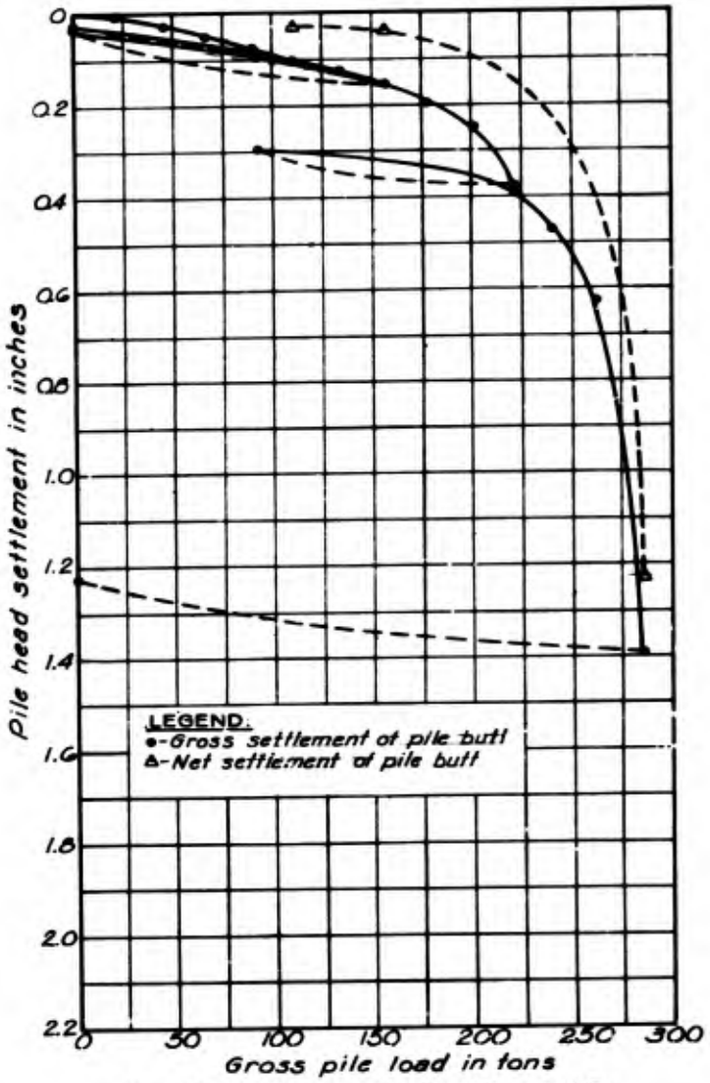

b. PILE MOVEMENT VS LOAD
TEST PILE 5

COMPRESSION TEST RESULTS
TEST PILES 4 AND 5 - 16-INCH CONCRETE

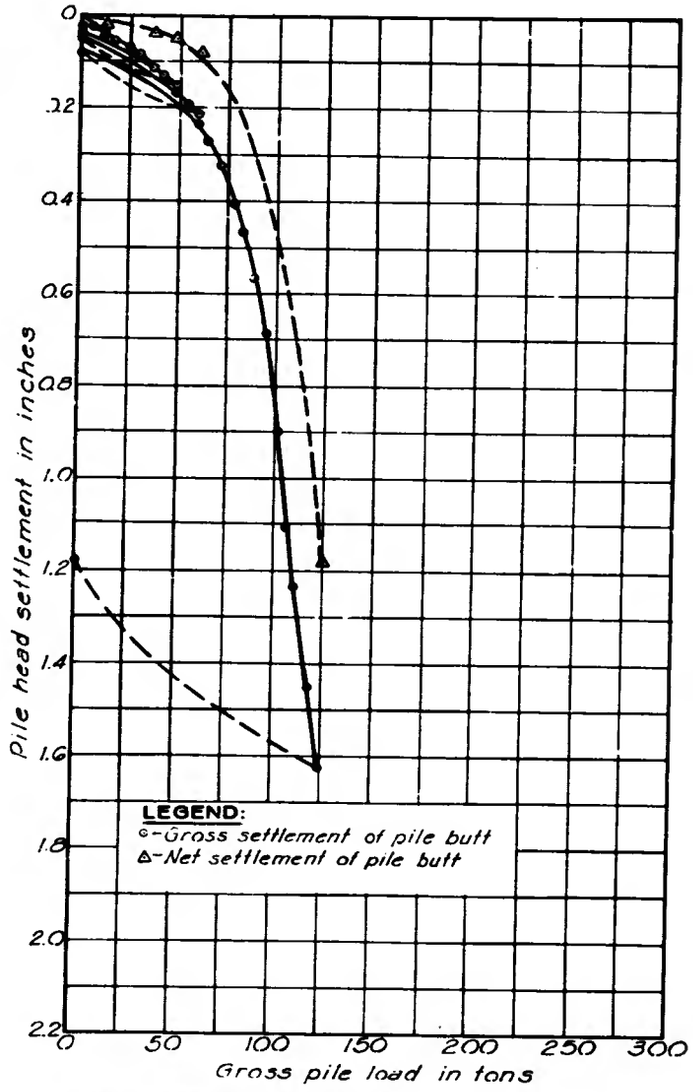

a. PILE MOVEMENT VS LOAD
TEST PILE 8

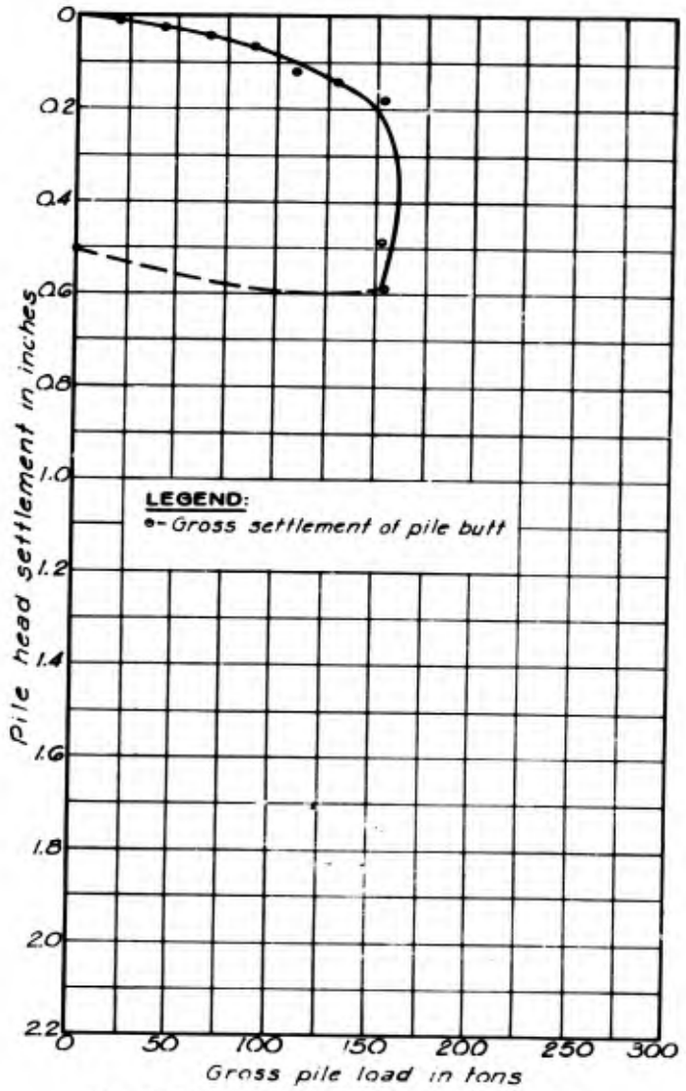

b. PILE MOVEMENT VS LOAD
TEST PILE 11

COMPRESSION TEST RESULTS - TEST PILE 8 - TIMBER
AND TEST PILE 11 - 16-INCH CONCRETE

PLATE 24

PLATE 25

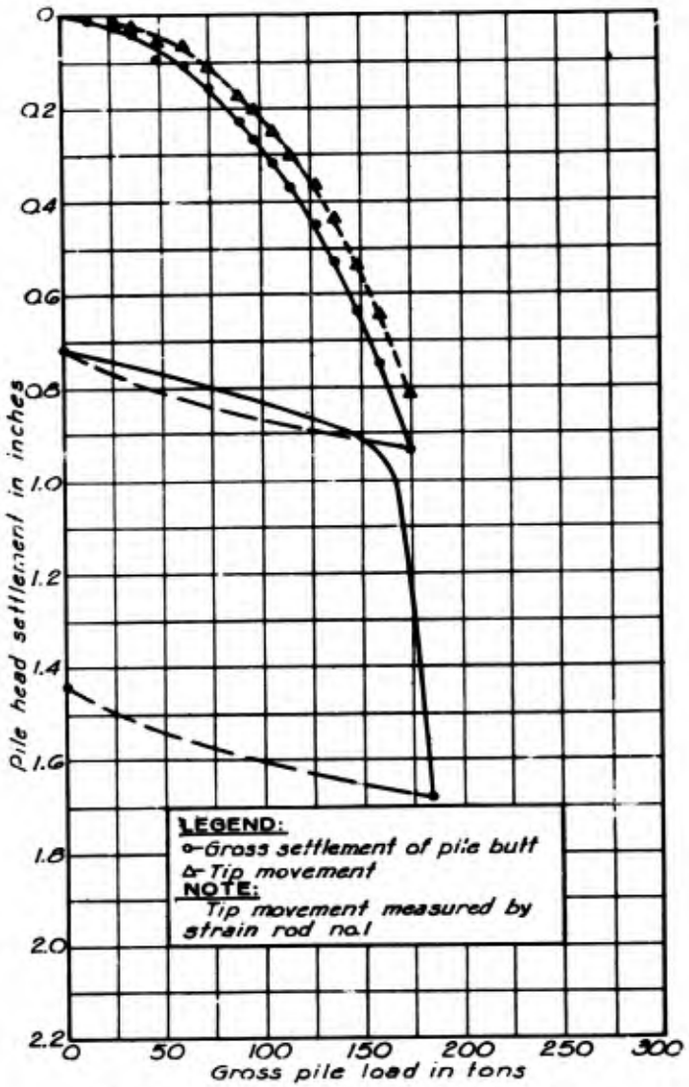

a. PILE MOVEMENT VS LOAD

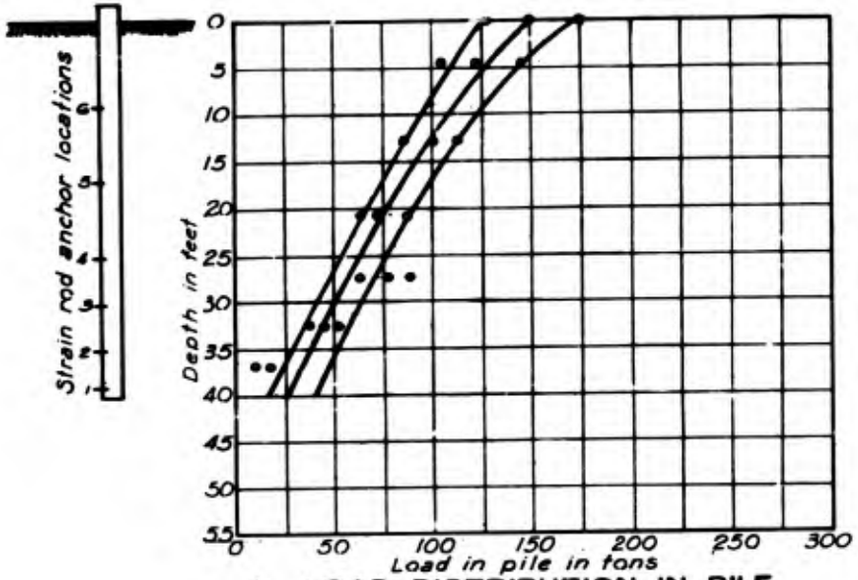

b. LOAD DISTRIBUTION IN PILE

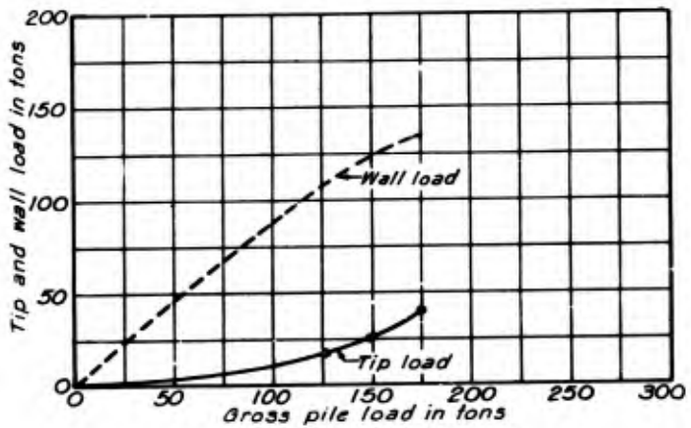

c. GROSS LOAD VS TIP AND WALL LOAD

COMPRESSION TEST RESULTS - TEST PILE 6- 14BP73

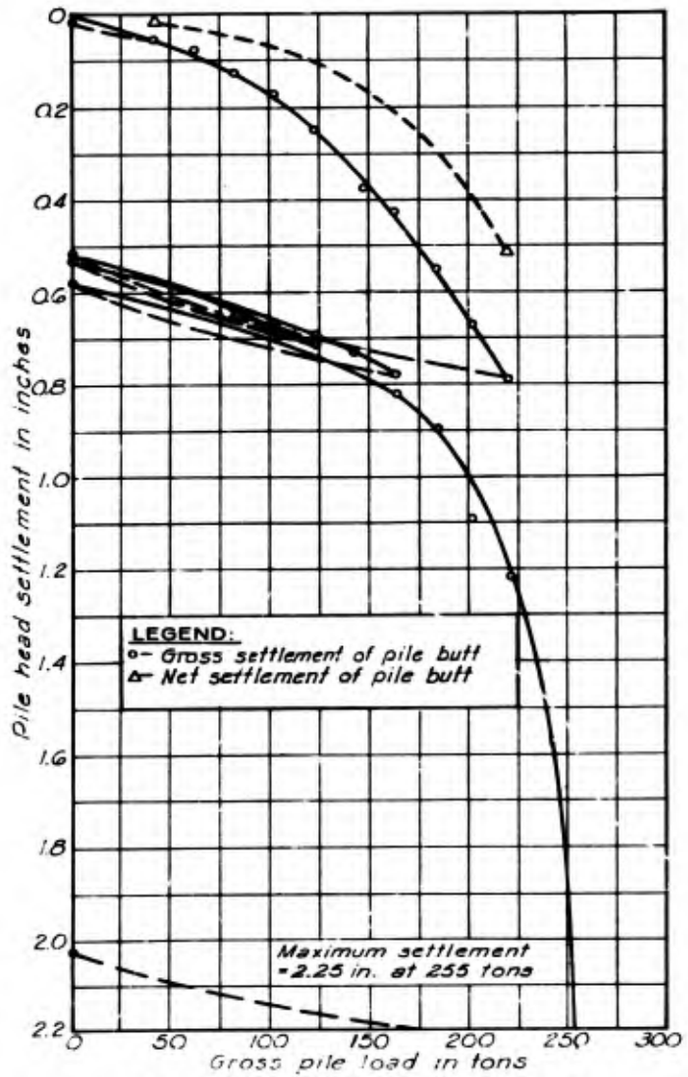

a. PILE MOVEMENT VS LOAD

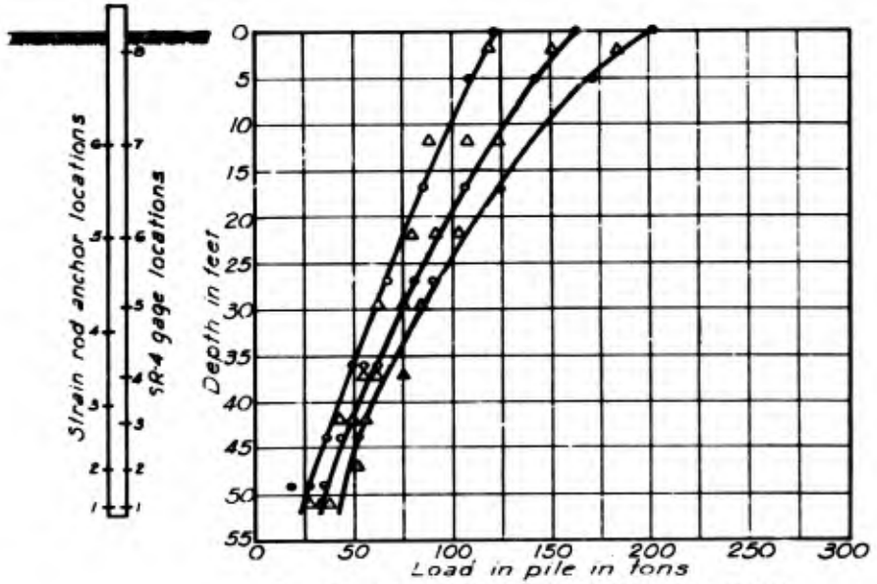

b. LOAD DISTRIBUTION IN PILE

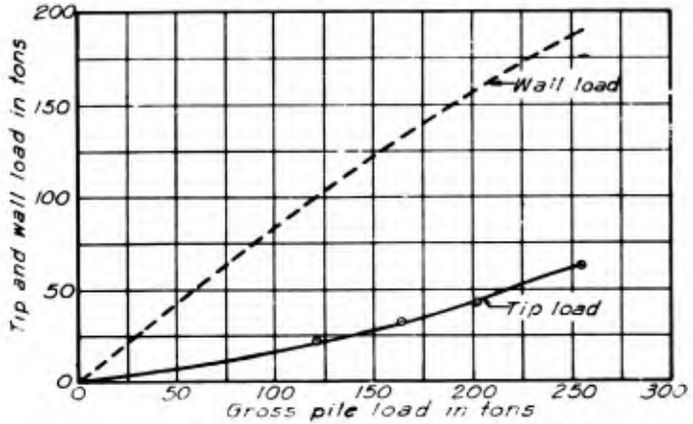

c. GROSS LOAD VS TIP AND WALL LOAD

COMPRESSION TEST RESULTS - TEST PILE 7-14BP73

PLATE 26

PLATE 27

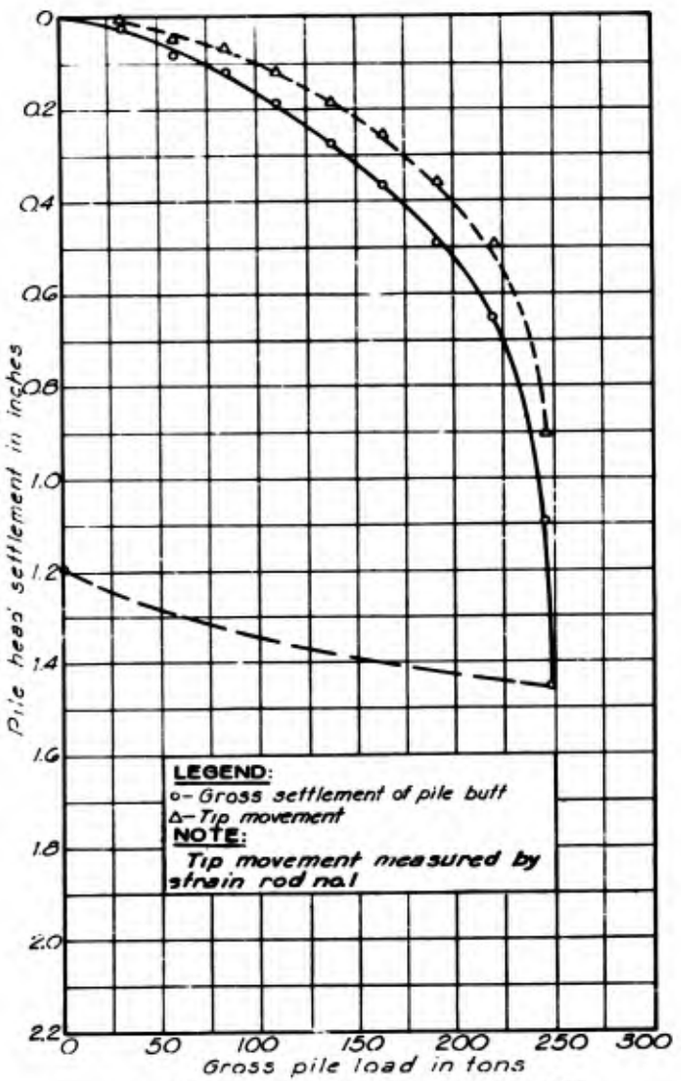

a. PILE MOVEMENT VS LOAD

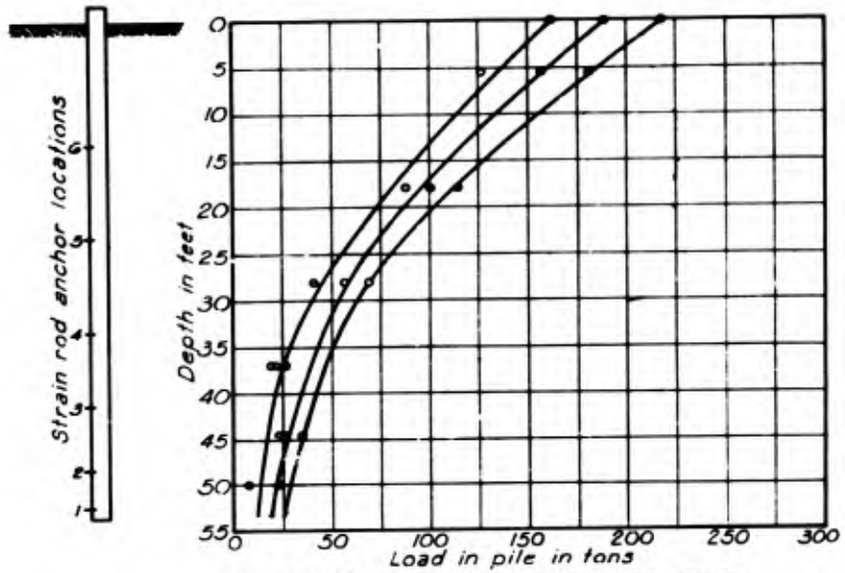

b. LOAD DISTRIBUTION IN PILE

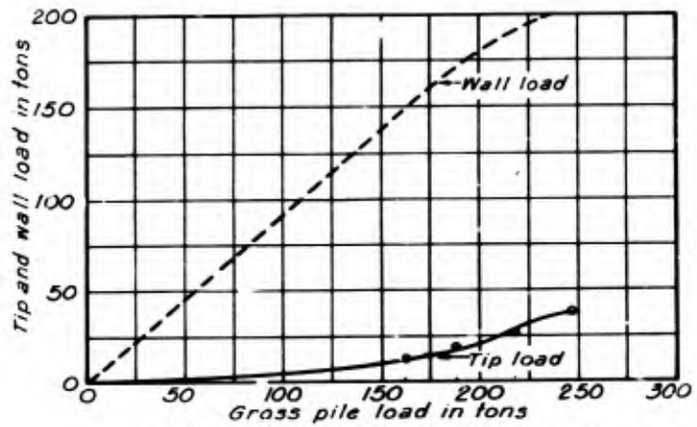

c. GROSS LOAD VS TIP AND WALL LOAD

COMPRESSION TEST RESULTS - TEST PILE 9- 14BP73

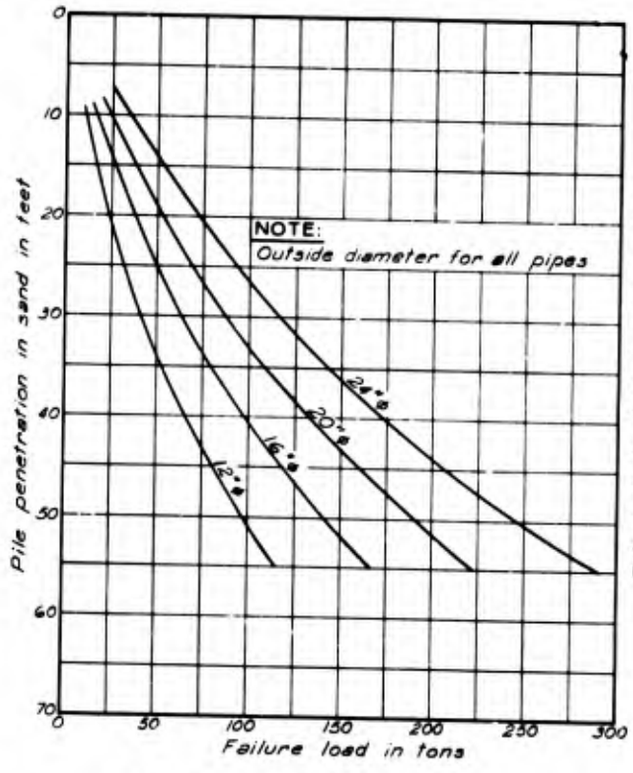

a. STEEL PIPE PILING

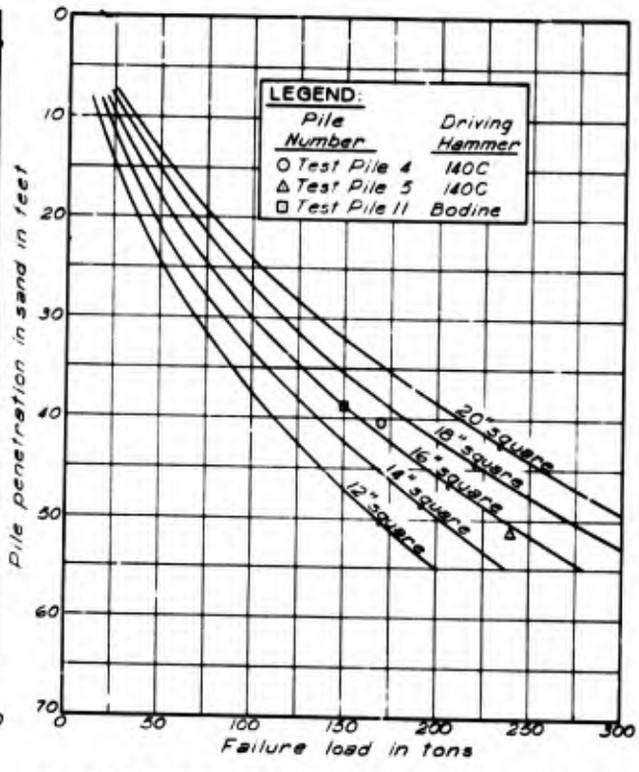

b. PRESTRESSED CONCRETE PILING

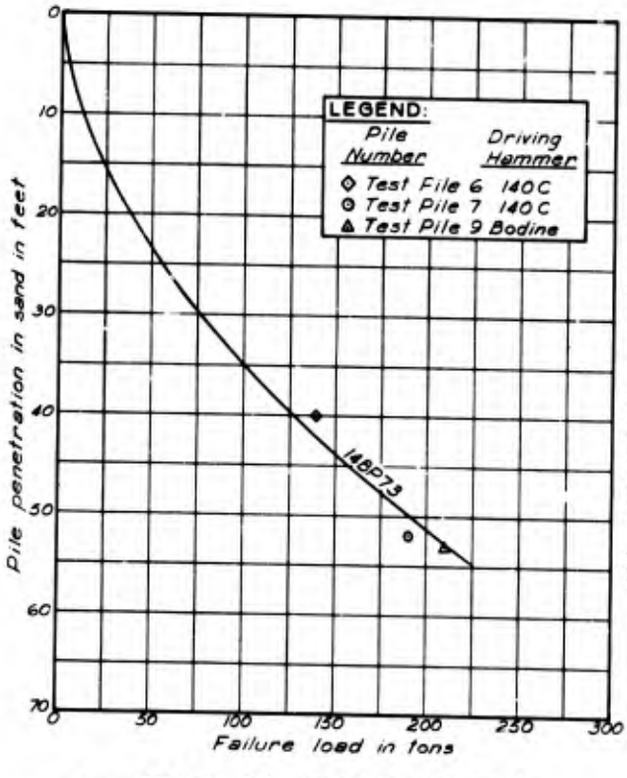

c. STEEL "H" PILING (14BP73)

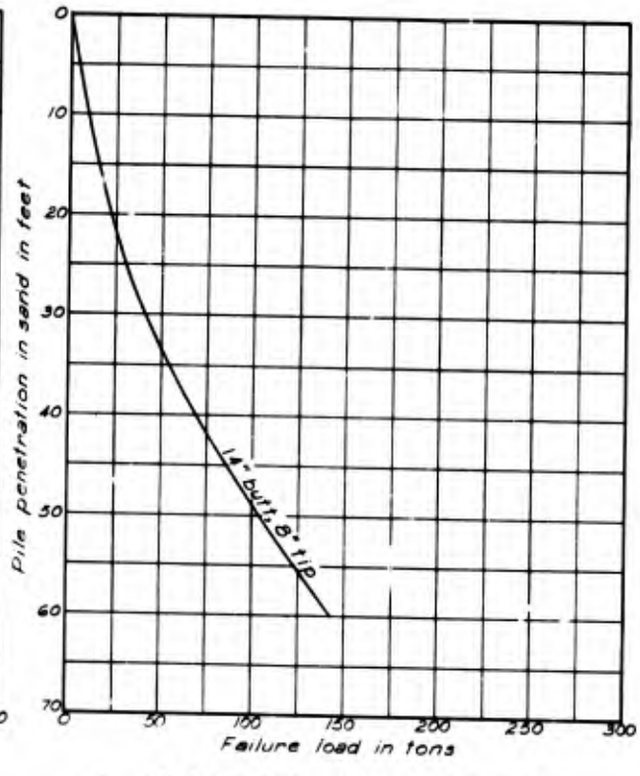

d. CLASS "A" TIMBER PILING

DESIGN CURVES FOR PILES IN COMPRESSION

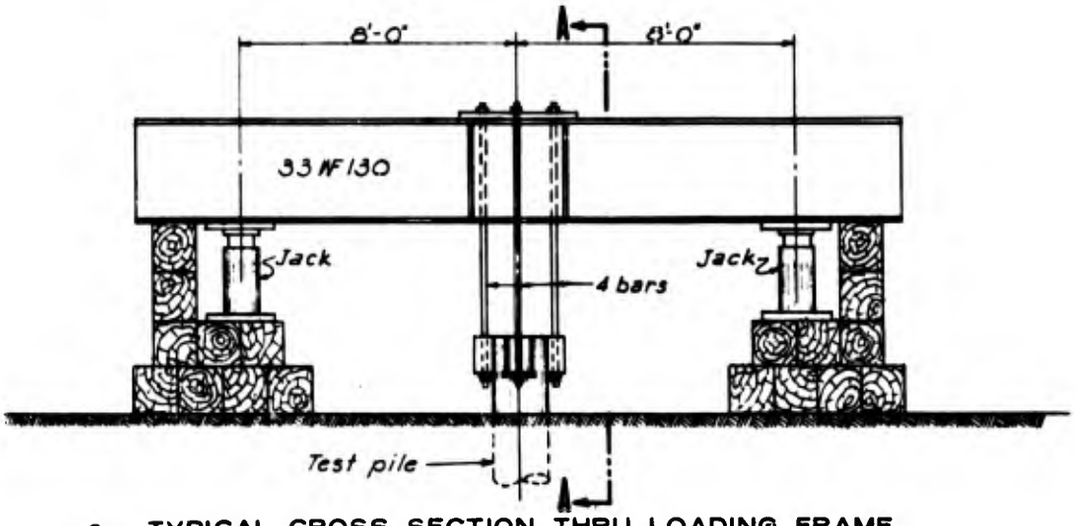

a. TYPICAL CROSS SECTION THRU LOADING FRAME

2 0 2 4
Scale in ft

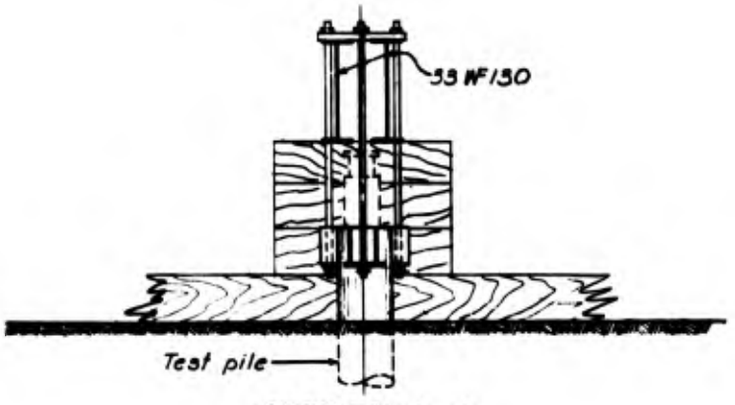

SECTION A - A

2 0 2 4
Scale in ft

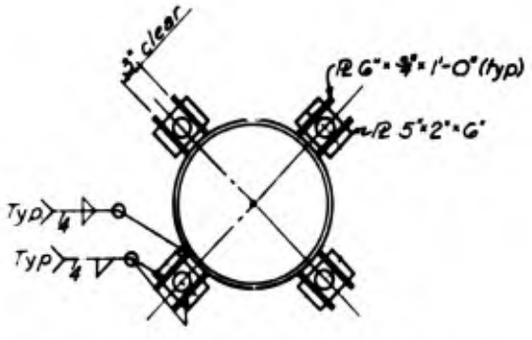

b. TYPICAL PIPE PILE

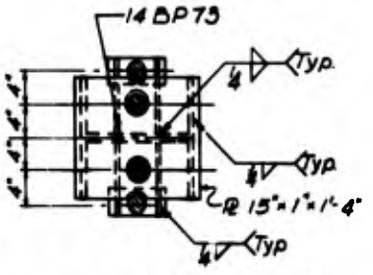

c. TYPICAL 14BP73 PILE

TENSION TEST FRAME AND PILE DETAILS

PLATE 29

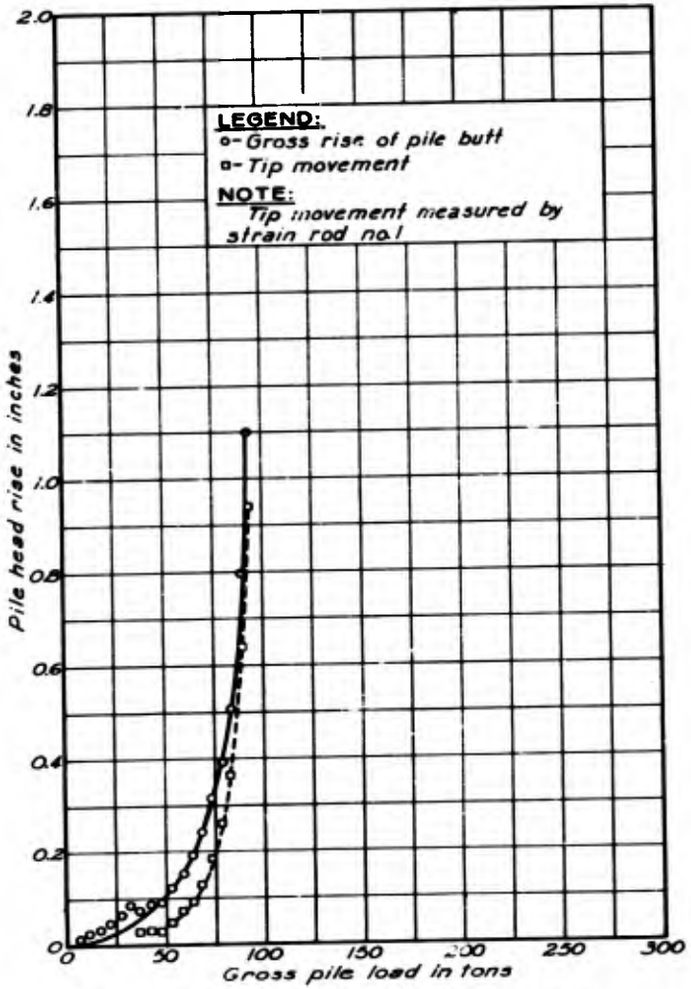

a. PILE MOVEMENT VS LOAD

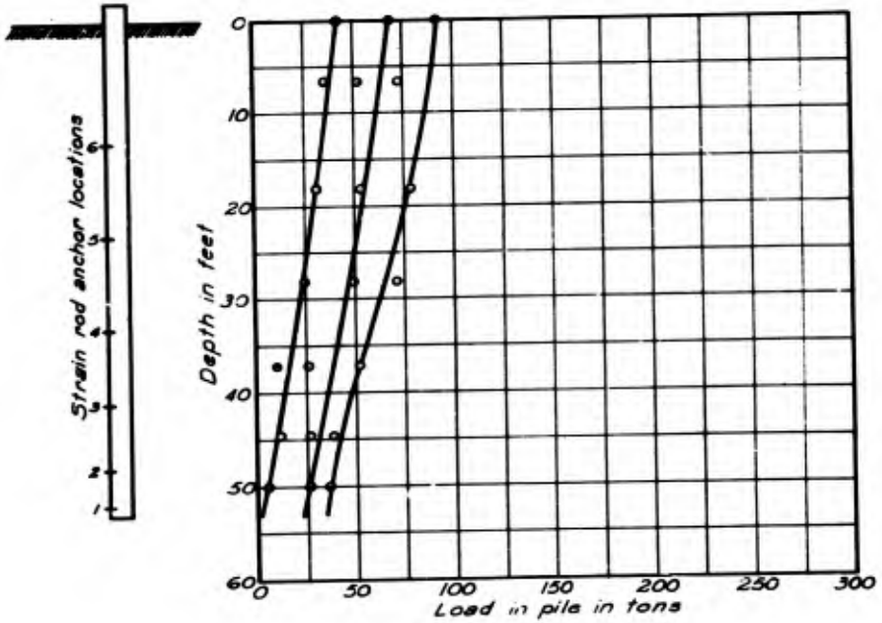

b. LOAD DISTRIBUTION IN PILE

TENSION TEST RESULTS - TEST PILE 1 - 12.75-INCH DIAMETER PIPE

PLATE 30

PLATE 31

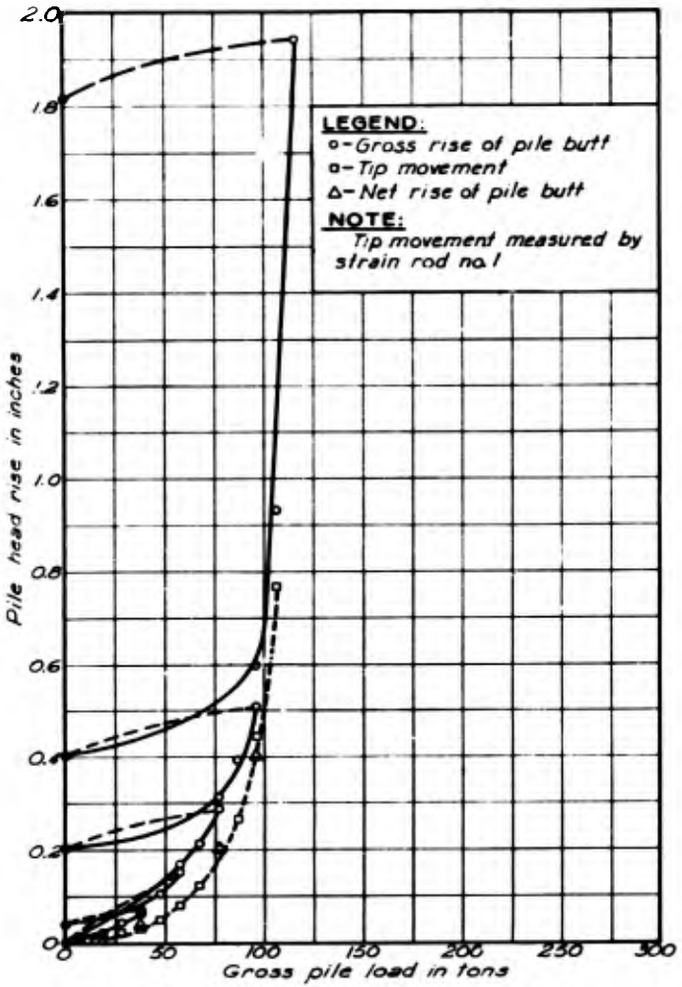

a. PILE MOVEMENT VS LOAD

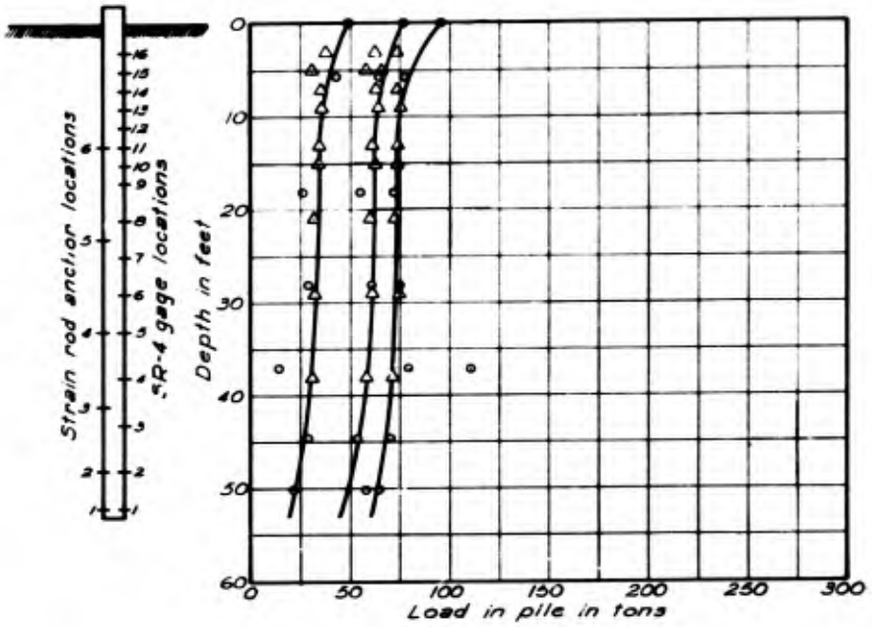

b. LOAD DISTRIBUTION IN PILE

TENSION TEST RESULTS - TEST PILE 2 - 16-INCH DIAMETER PIPE

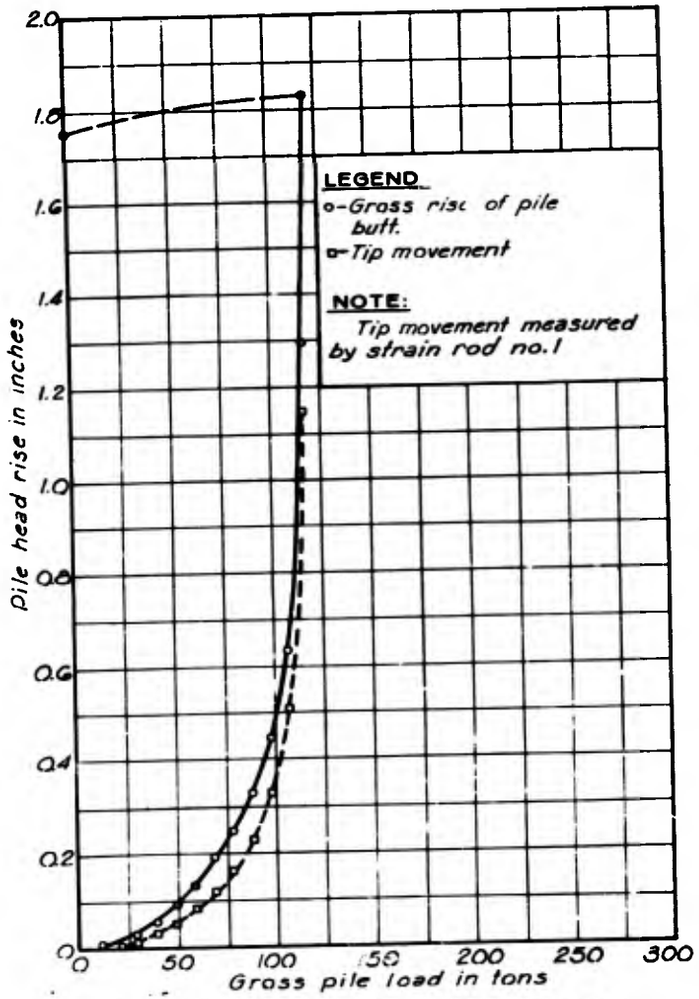

a. PILE MOVEMENT VS LOAD

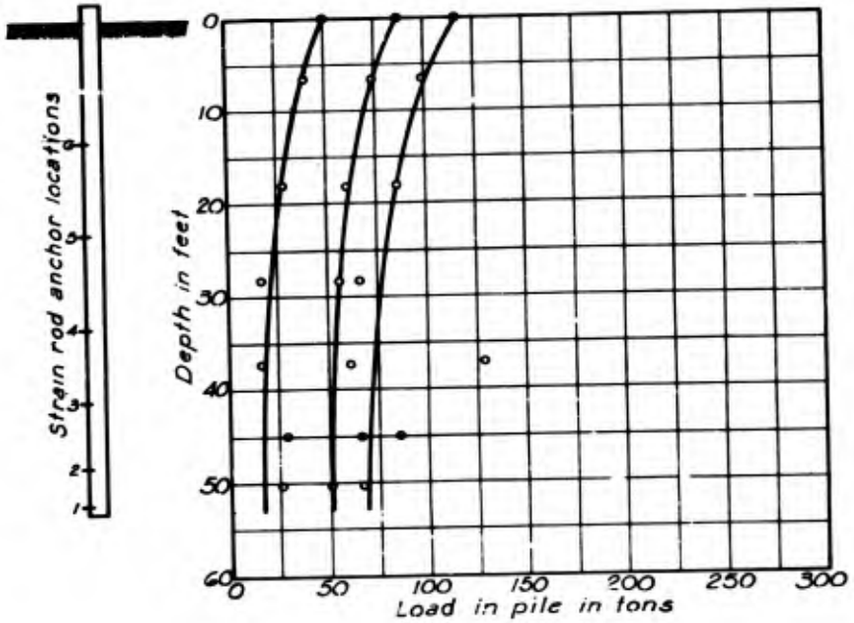

b. LOAD DISTRIBUTION IN PILE

TENSION TEST RESULTS - TEST PILE 3 - 20-INCH DIAMETER PIPE

PLATE 32

PLATE 33

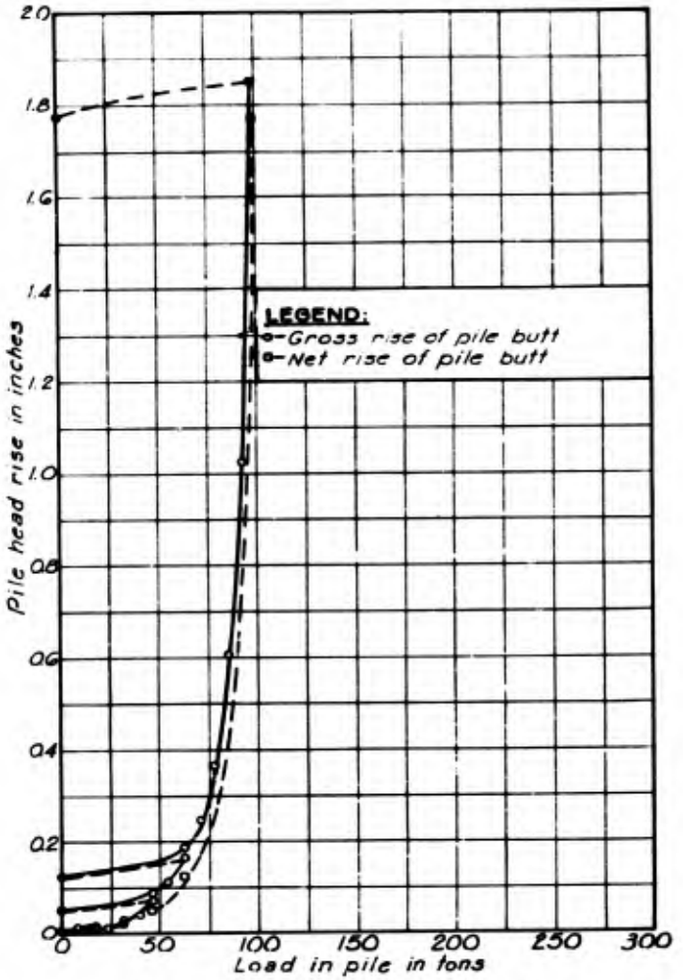

a. PILE MOVEMENT VS LOAD
TEST PILE 4 - 16 INCH CONCRETE

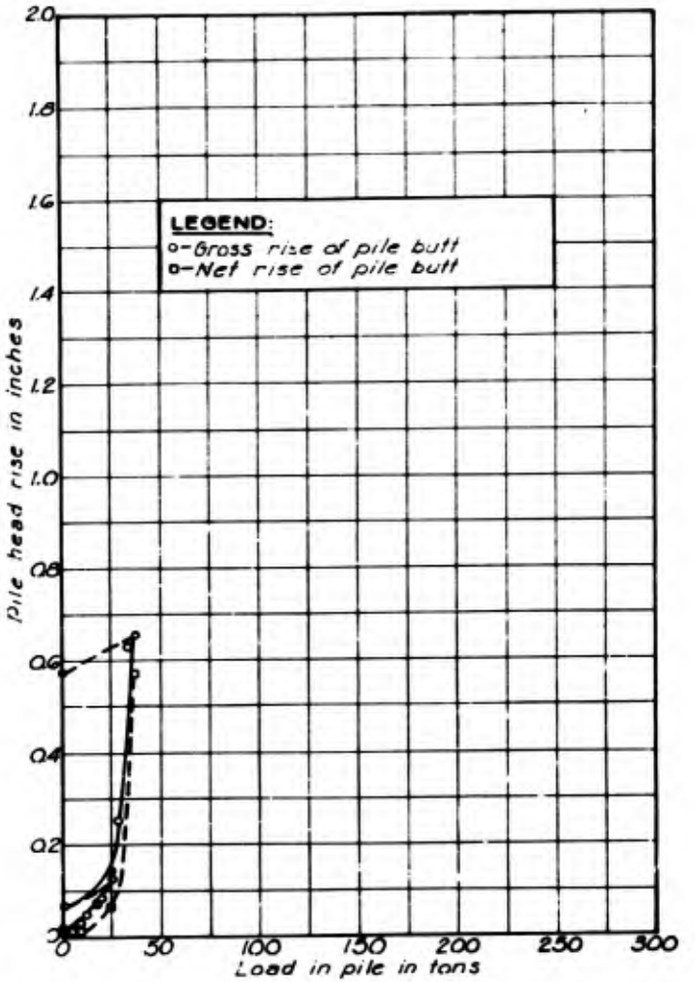

b. PILE MOVEMENT VS LOAD
TEST PILE 8 - TIMBER

TENSION TEST RESULTS - TEST PILES 4 AND 8

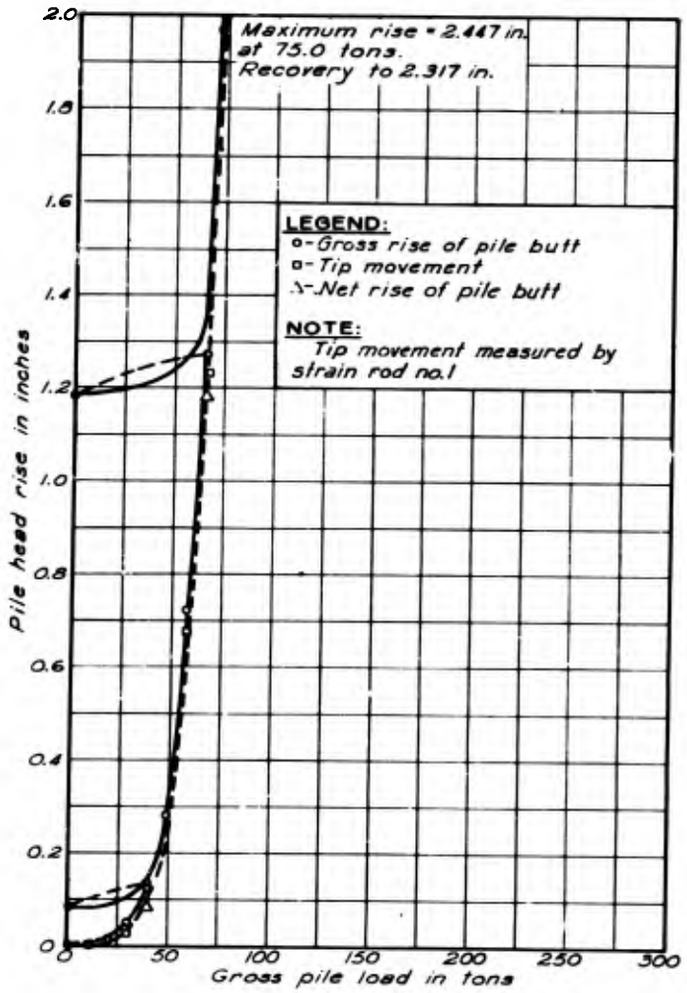

a. PILE MOVEMENT VS LOAD

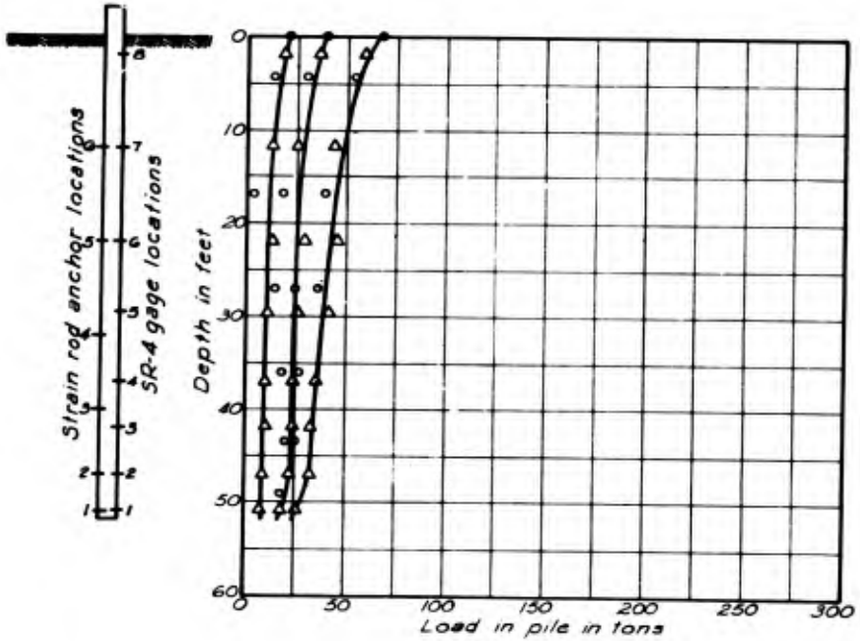

b. LOAD DISTRIBUTION IN PILE

PLATE 34

TENSION TEST RESULTS - TEST PILE 7 - 14BP73

PLATE 35

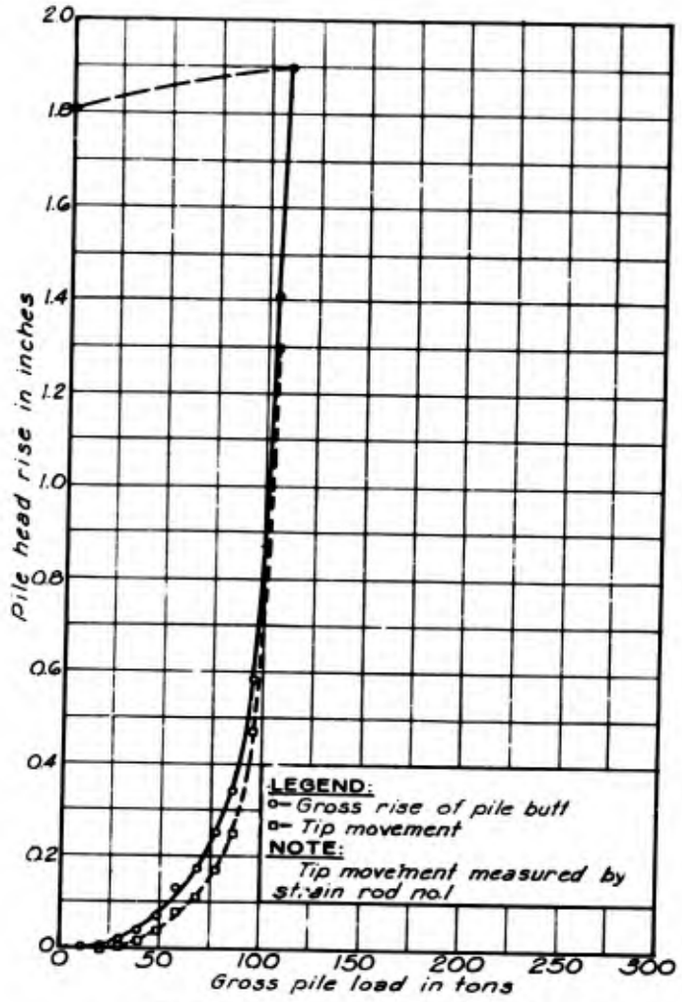

a. PILE MOVEMENT VS LOAD

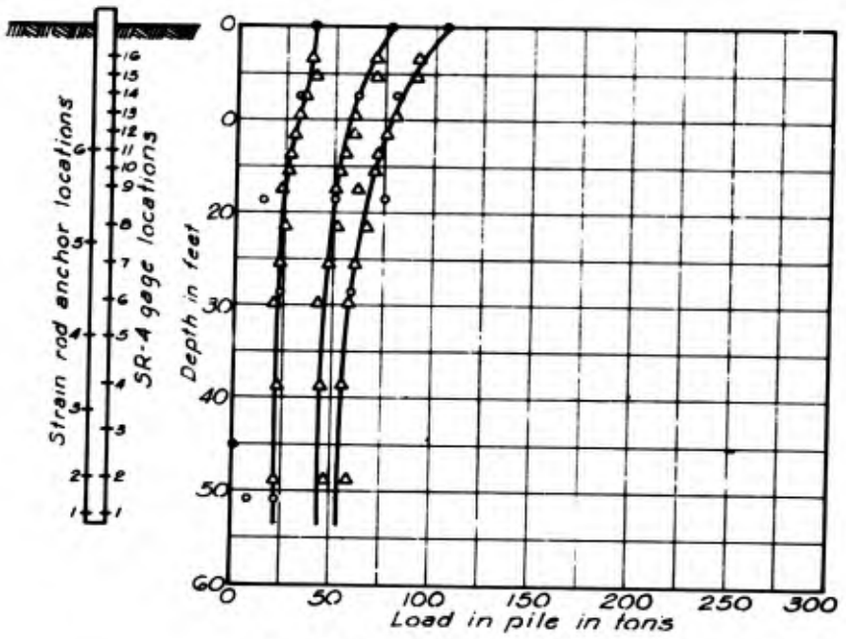

b. LOAD DISTRIBUTION IN PILE

TENSION TEST RESULTS - TEST PILE 10 - 16-INCH DIAMETER PIPE

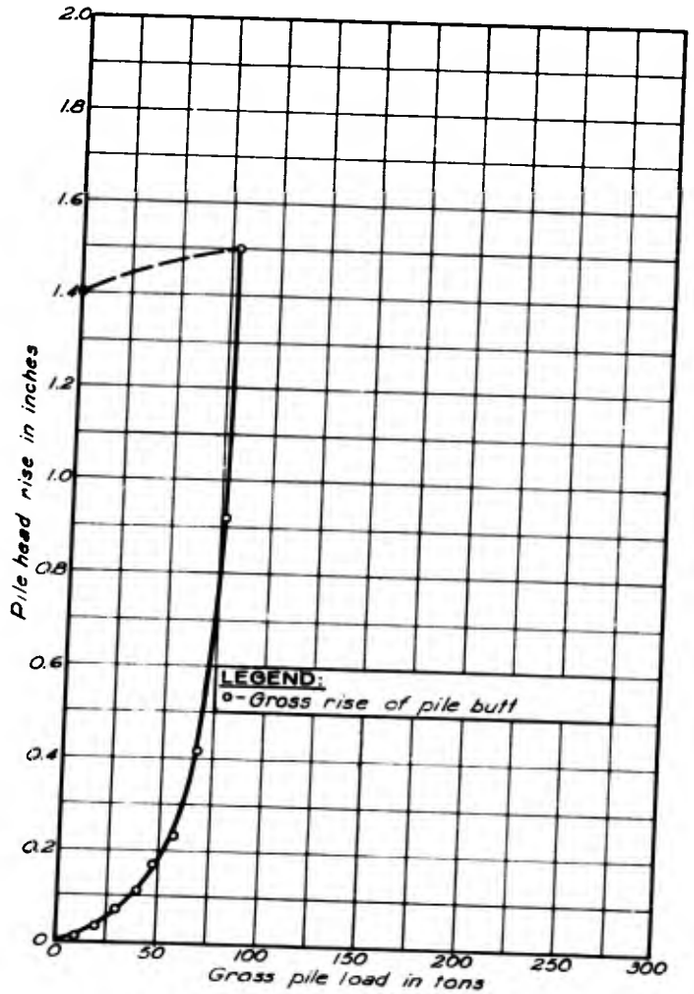

a. PILE MOVEMENT VS LOAD

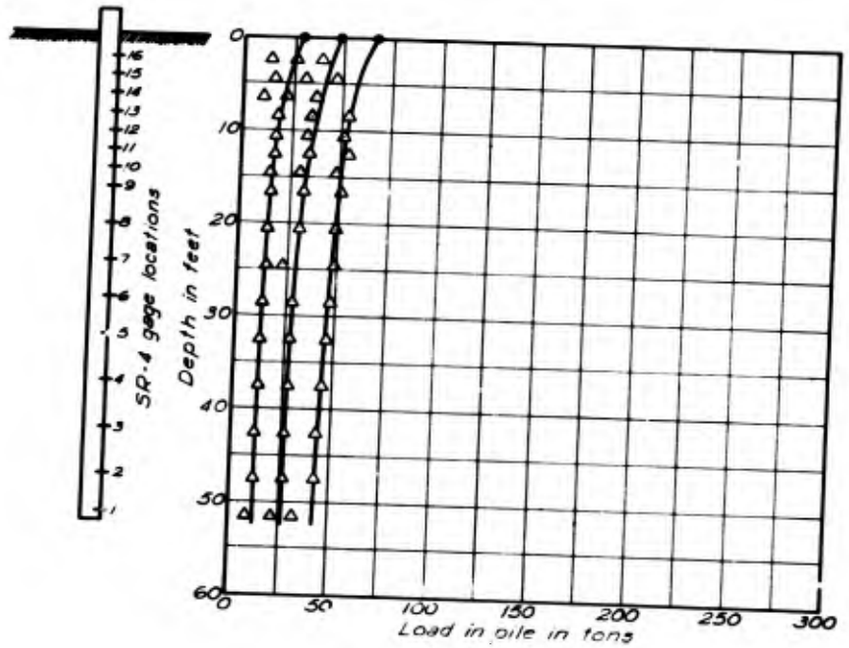

b. LOAD DISTRIBUTION IN PILE

TENSION TEST RESULTS - TEST PILE 16 - 16-INCH DIAMETER PIPE

PLATE 36

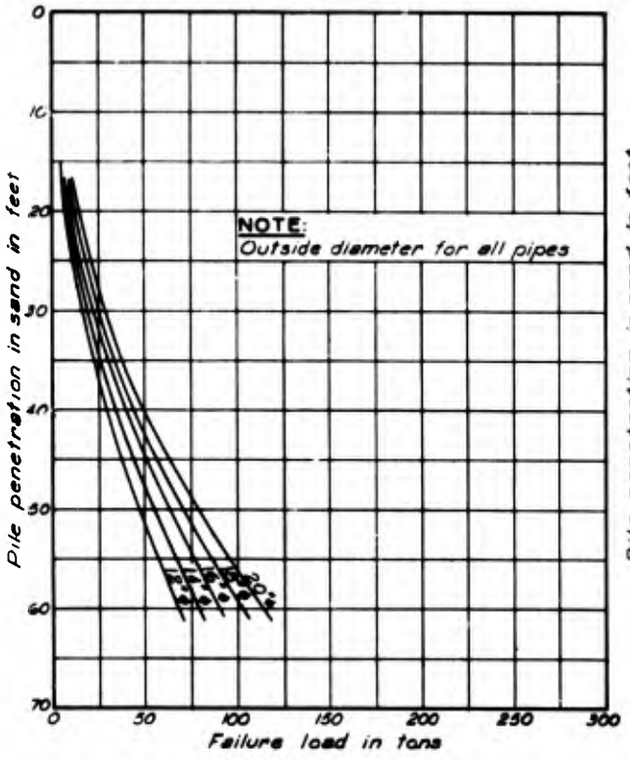

a. STEEL PIPE PILING

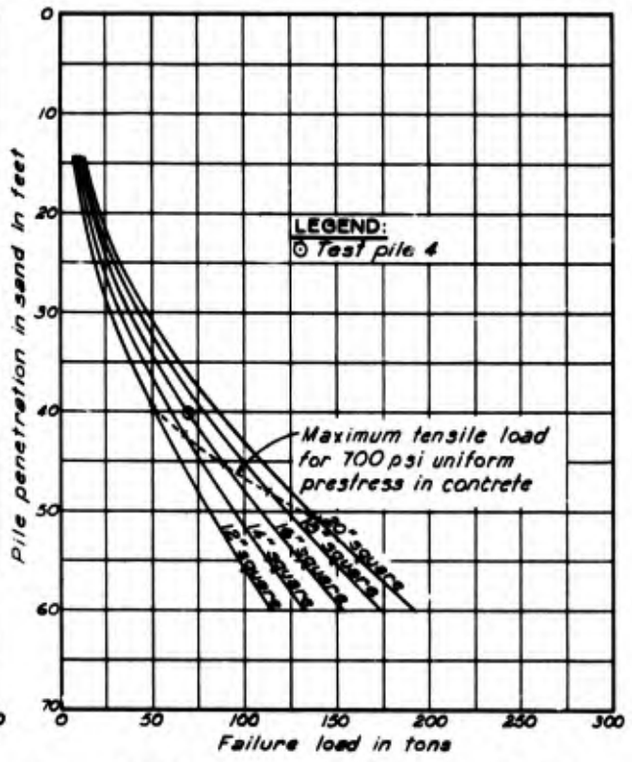

b. PRESTRESSED CONCRETE PILING

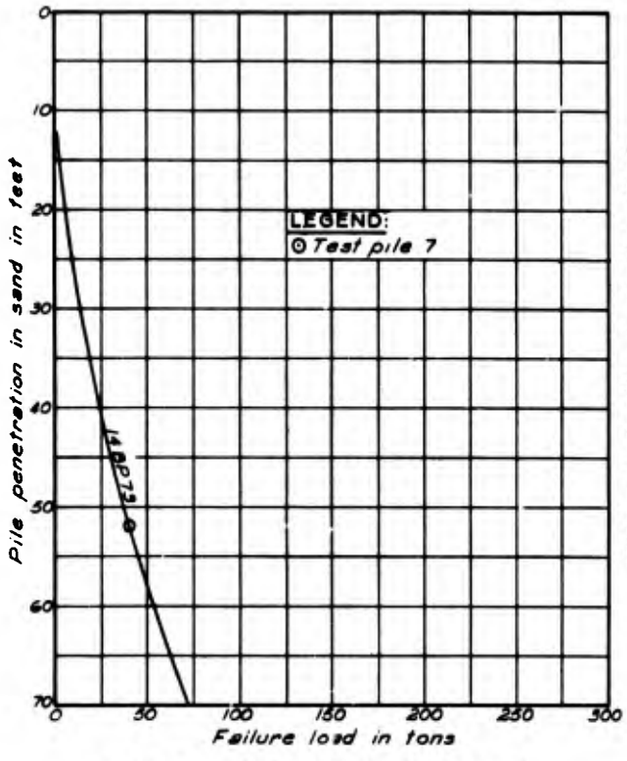

c. STEEL "H" PILING (14BP73)

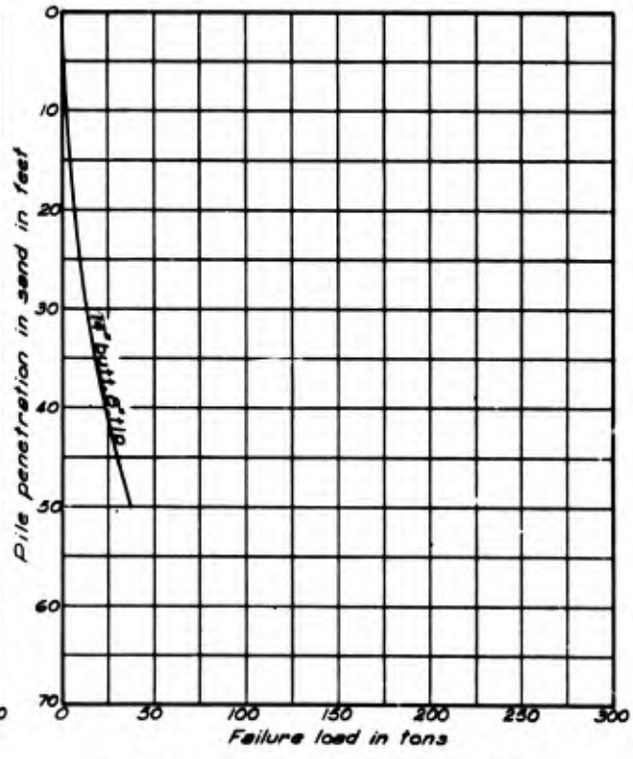

d. CLASS "A" TIMBER PILING

DESIGN CURVES FOR PILES IN TENSION

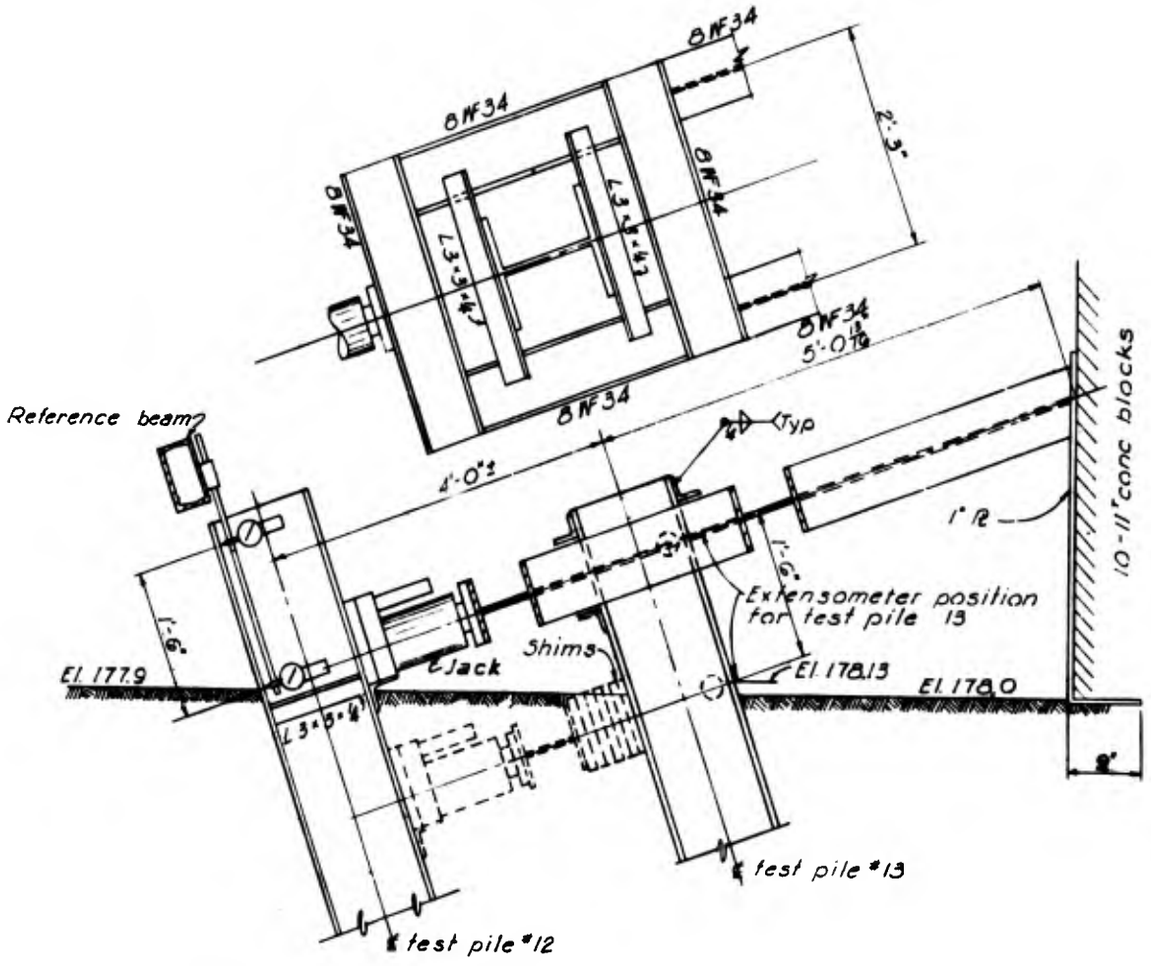

a. SECTION AT BATTERED PILES

1 0 1 2

Scale in ft

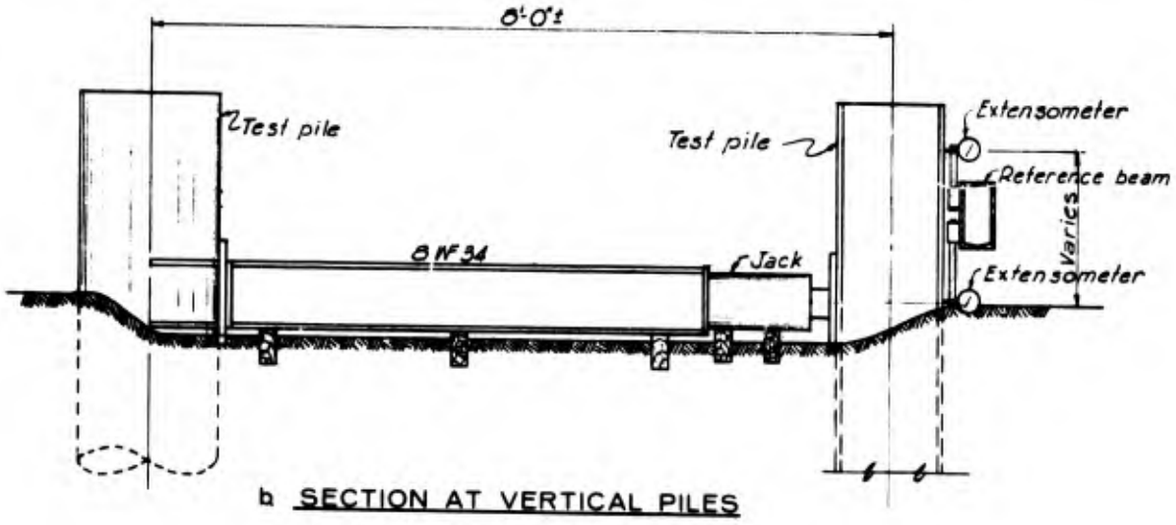

b SECTION AT VERTICAL PILES

1 0 1 2

Scale in ft

LATERAL TEST LOADING FRAMES AND DETAILS

PLATE 38

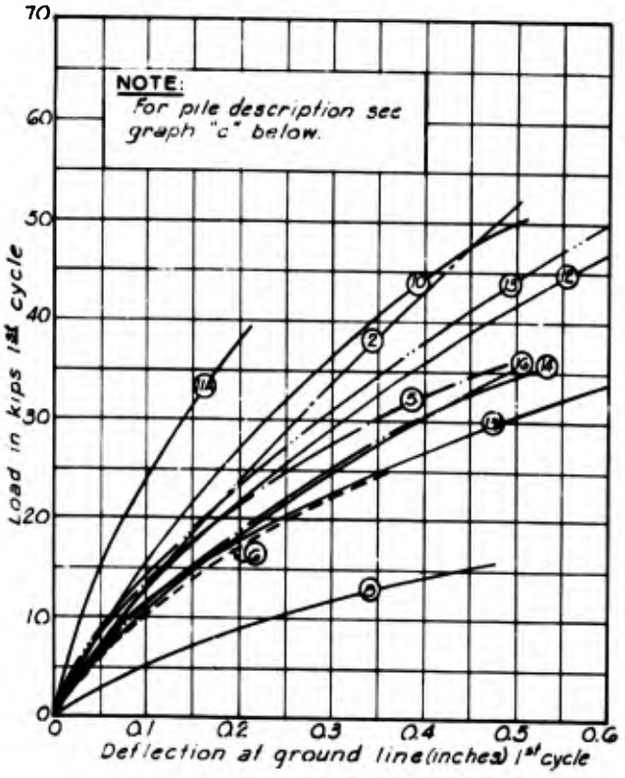

a. LOAD VS DEFLECTION-TEST PILES 2, 5, 6, 8, 10, 11A, 12, 13, 13A, 14 AND 16

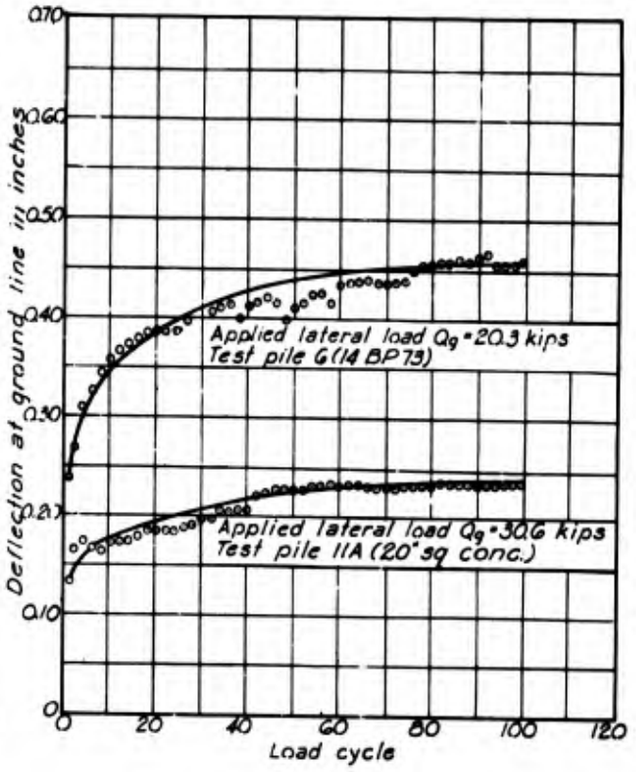

b. DEFLECTION VS. LOAD CYCLE TEST PILES 6 AND 11A

NOTE:
Water table at approximate ground surface.

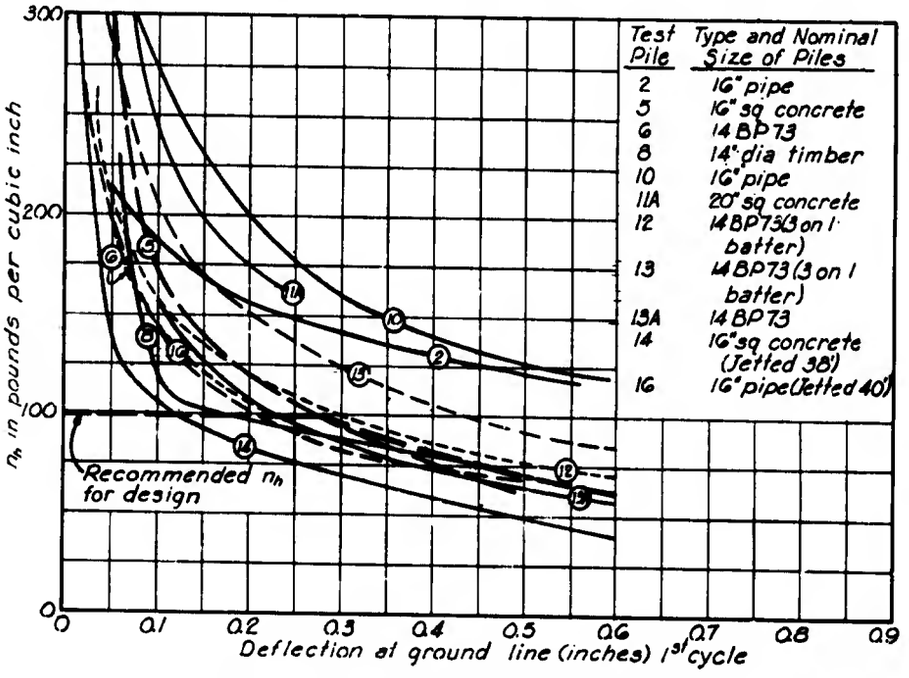

c. n_h VS DEFLECTION-TEST PILES 2, 5, 6, 8, 10, 11A, 12, 13, 13A, 14 AND 16

LATERAL TEST RESULTS

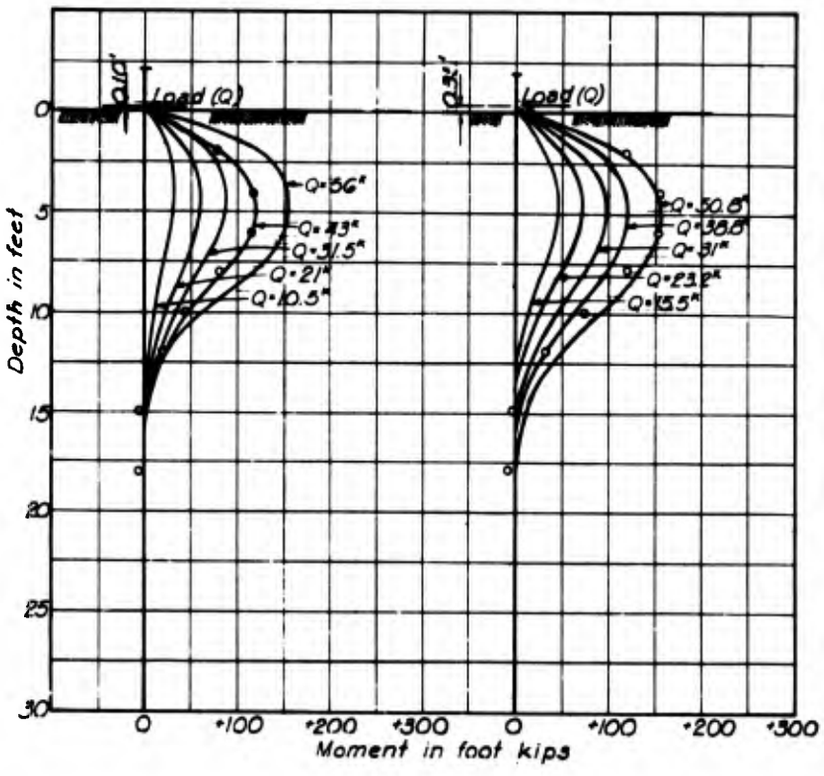

a. TEST PILE 2

b. TEST PILE 10

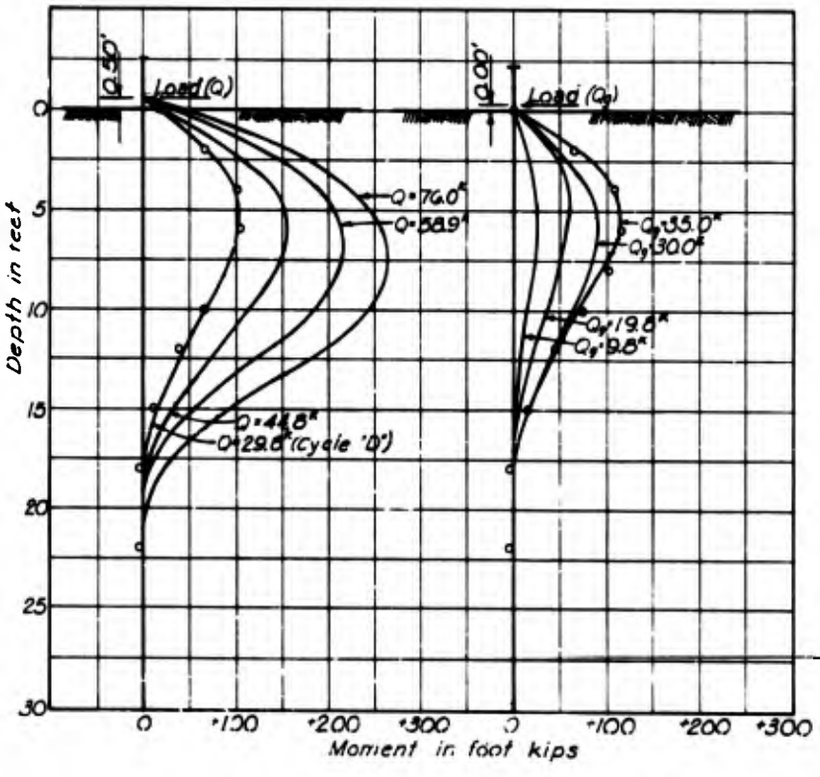

c. TEST PILE 13A

d. TEST PILE 16

LEGEND:

— Measured moment

° Theoretical moment for $k = n_h X$

LATERAL LOAD TESTS - MOMENT DIAGRAMS
TEST PILES 2, 10, 13A AND 16

PLATE 40

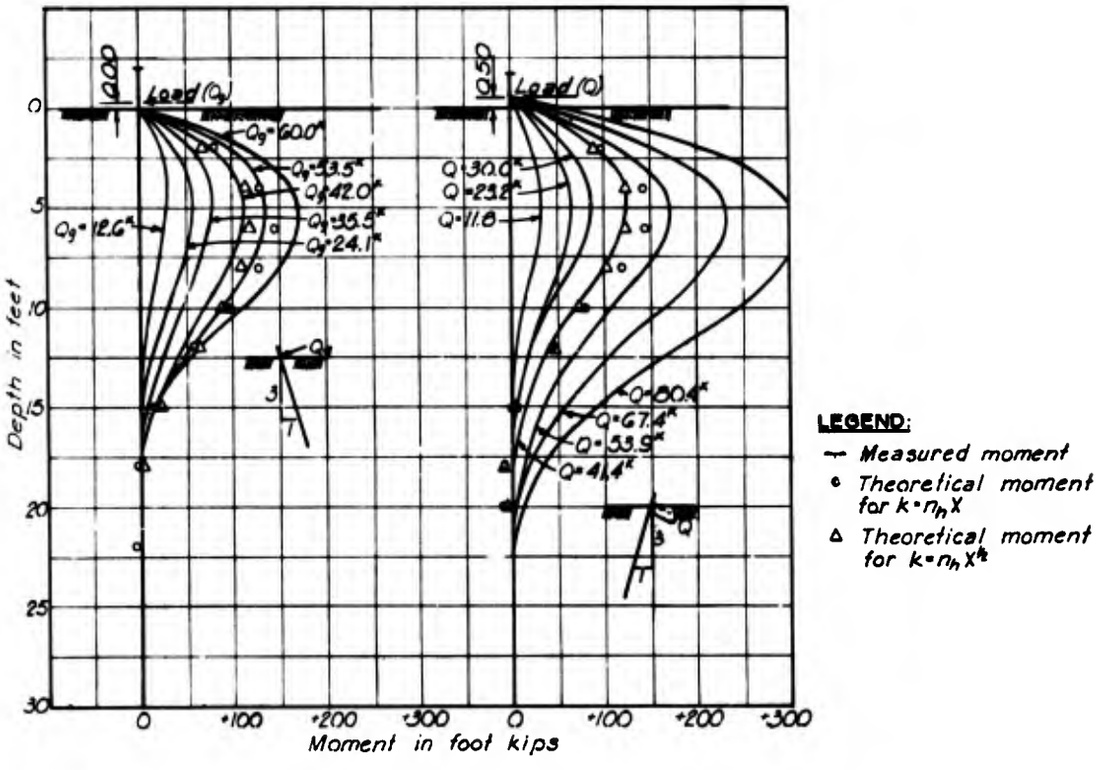

a. TEST PILE 12

b. TEST PILE 13

LEGEND:

- Measured moment
- Theoretical moment for $k = n_h X$
- Theoretical moment for $k = n_h X^{\frac{1}{2}}$

LATERAL LOAD TESTS - MOMENT DIAGRAMS
TEST PILES 12 AND 13

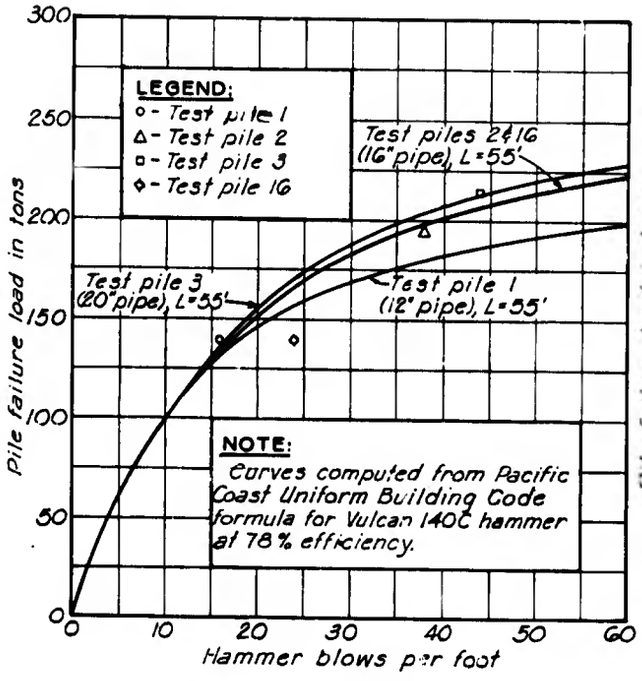

a. STEEL PIPE PILES

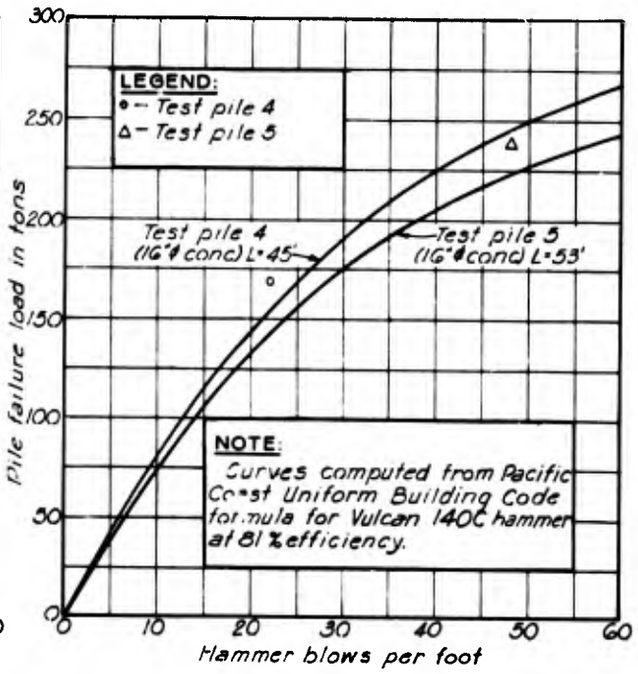

b. 16-INCH CONCRETE PILES

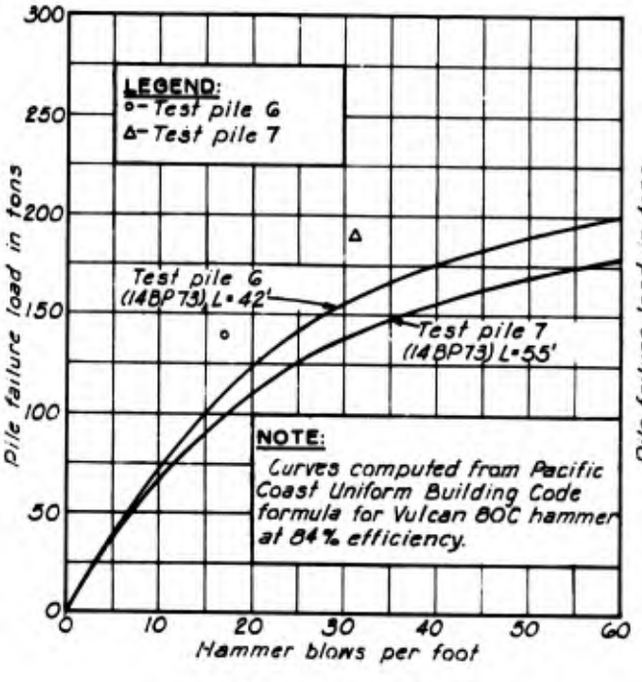

c. 14-INCH H-PILES

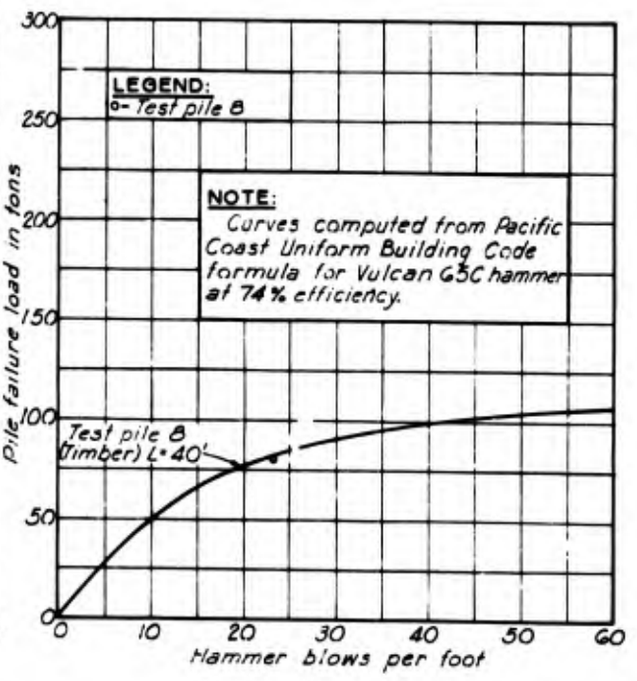

d. TIMBER PILE

CALCULATED AND MEASURED COMPRESSIVE CAPACITY OF TEST PILES

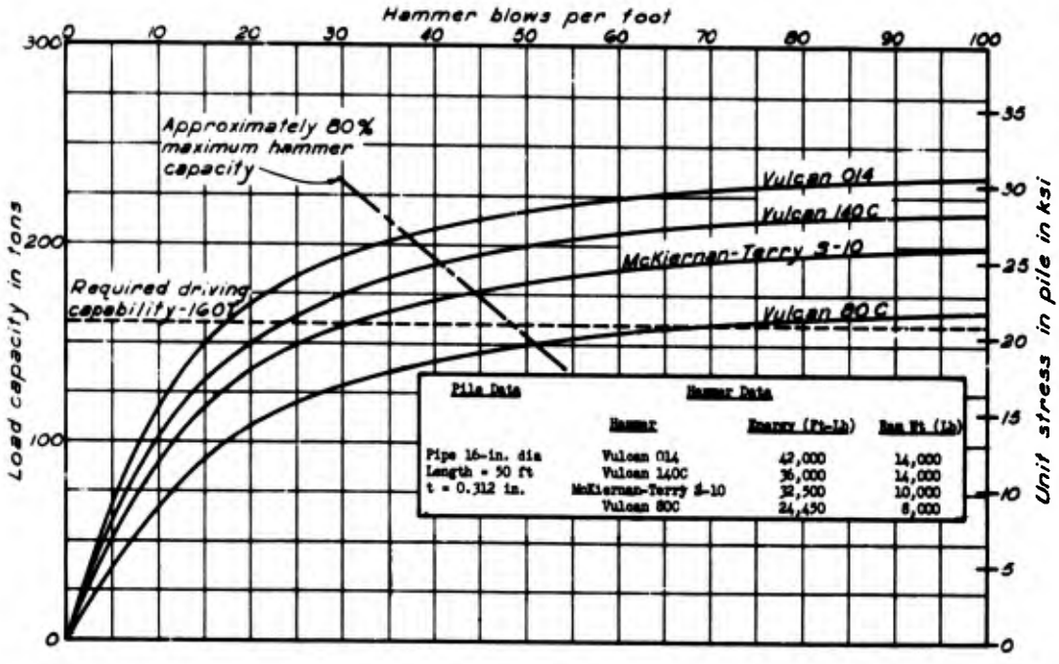

a. HAMMER SELECTION CURVES

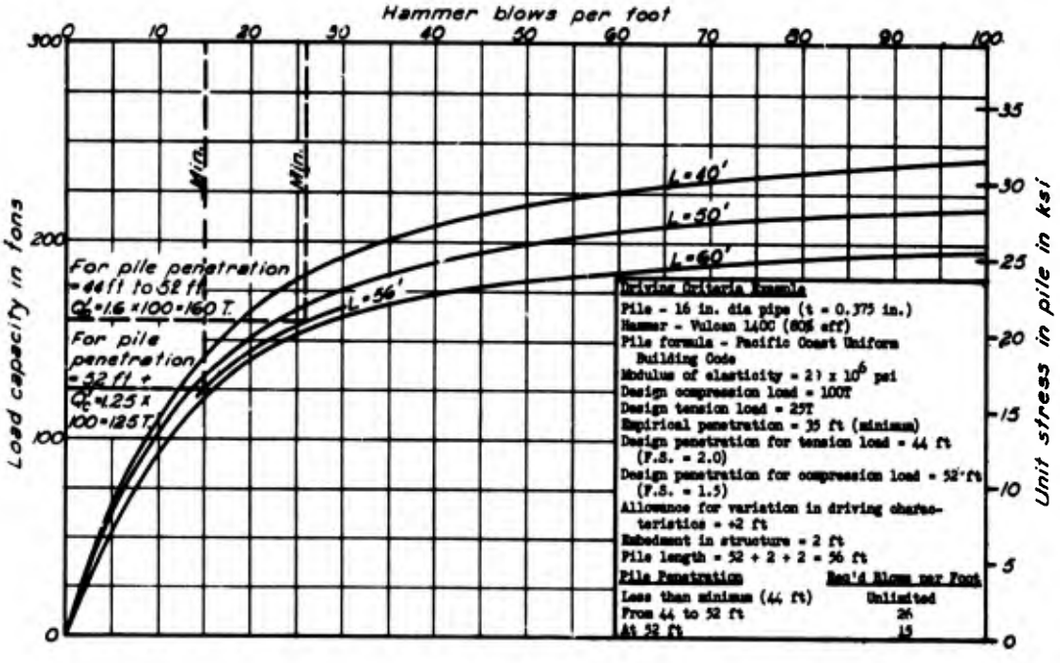

b. DRIVING CRITERIA

PILE DRIVING CURVES - 16-INCH PIPE

PLATE 43

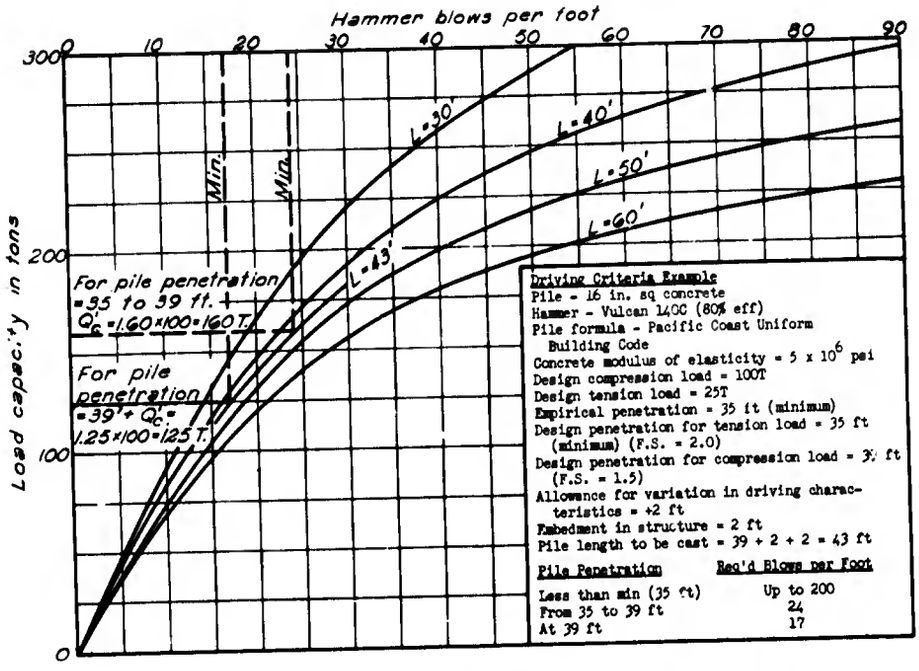

a. DRIVING CRITERIA - 16-INCH CONCRETE

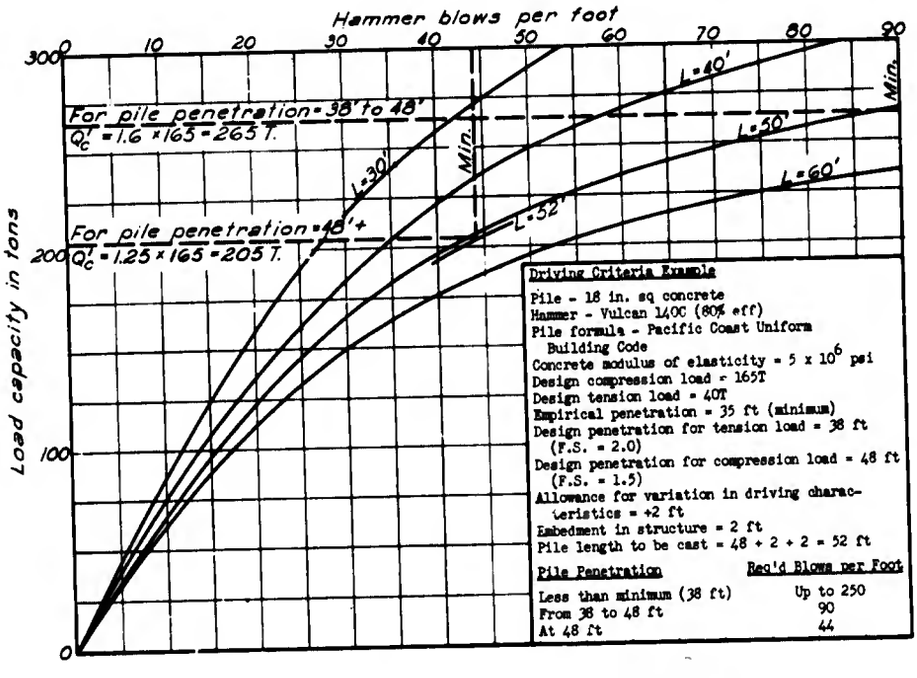

b. DRIVING CRITERIA - 18-INCH CONCRETE

PILE DRIVING CURVES - 16-AND 18-INCH CONCRETE

PLATE 44

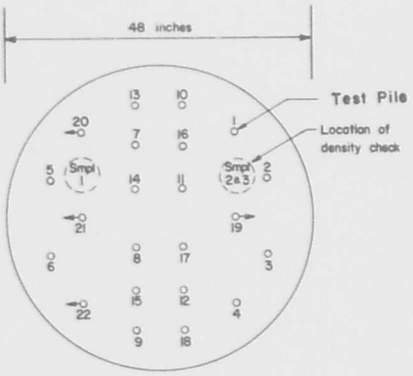

a. PLAN

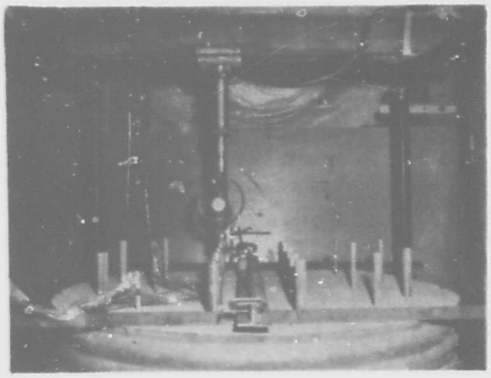

b. TEST PILES AND TANK

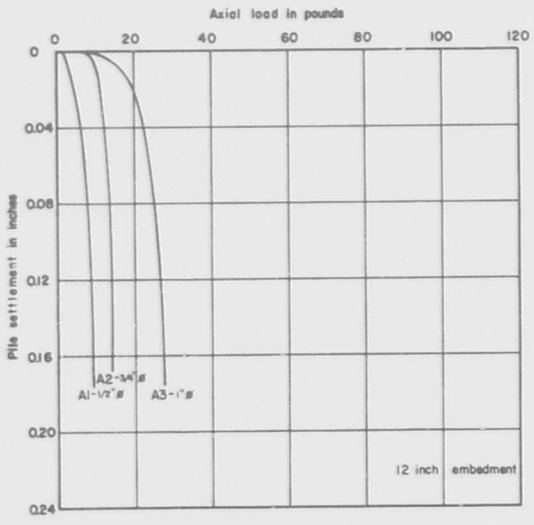

c. TESTS A1-A3

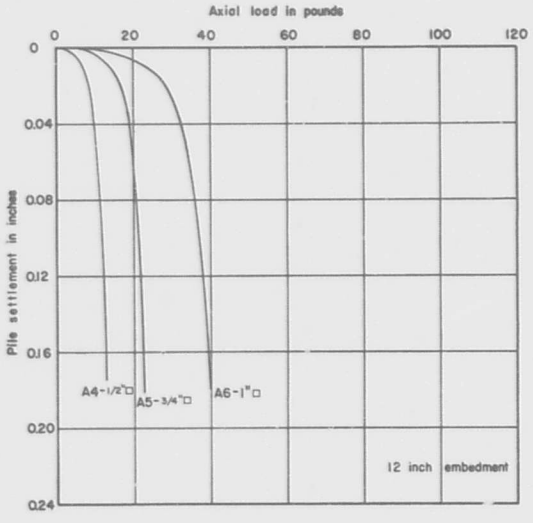

d. TESTS A4-A6

PILE SETTLEMENT VS LOAD

TEST SERIES "A"

MODEL TEST

PLATE 45

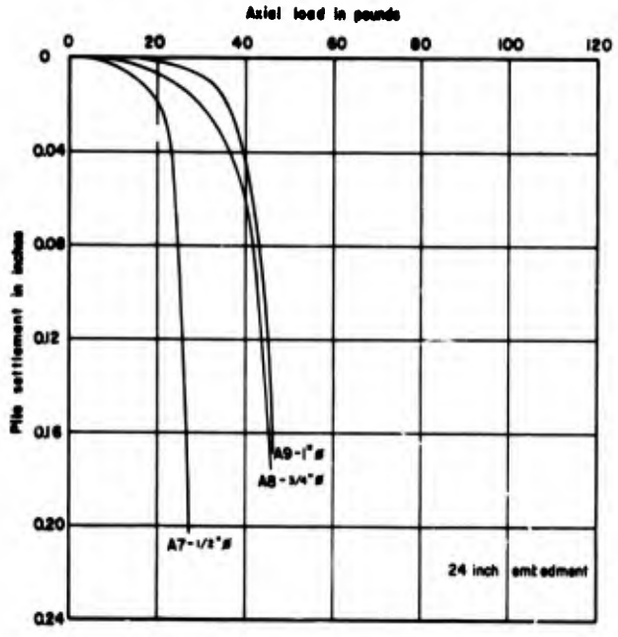

a. TESTS A7-A9

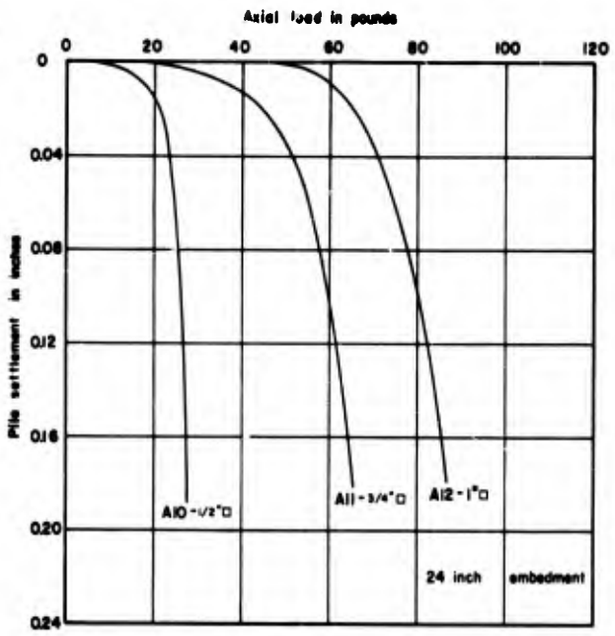

b. TESTS A10-A12

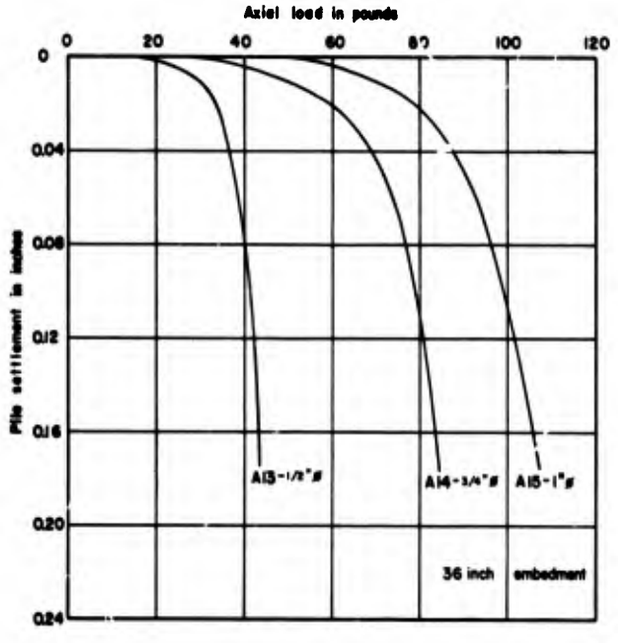

c. TESTS A13-A15

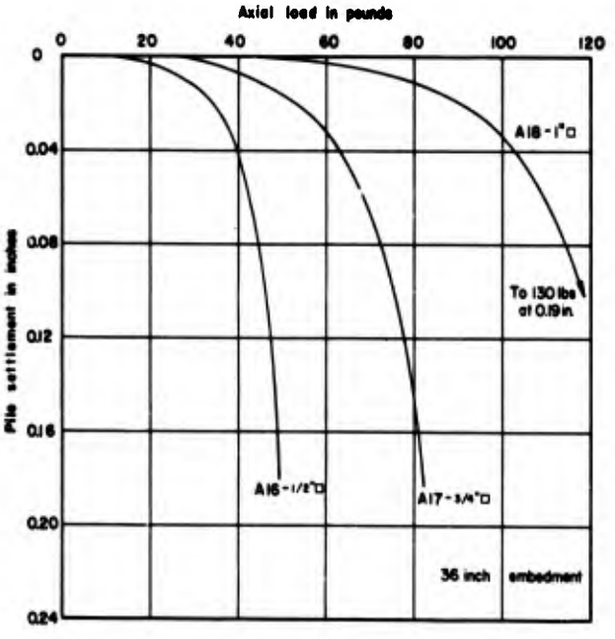

d. TESTS A16-A18

PILE SETTLEMENT VS LOAD

COMPRESSION TEST RESULTS - TEST SERIES "A"

MODEL TEST

PLATE 46

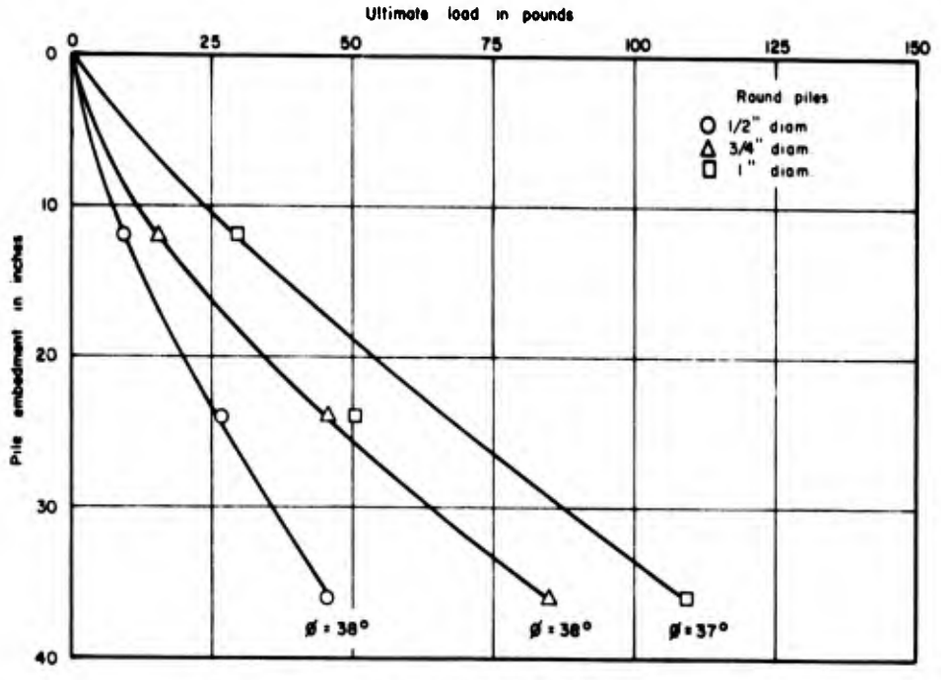

a. ROUND PILES

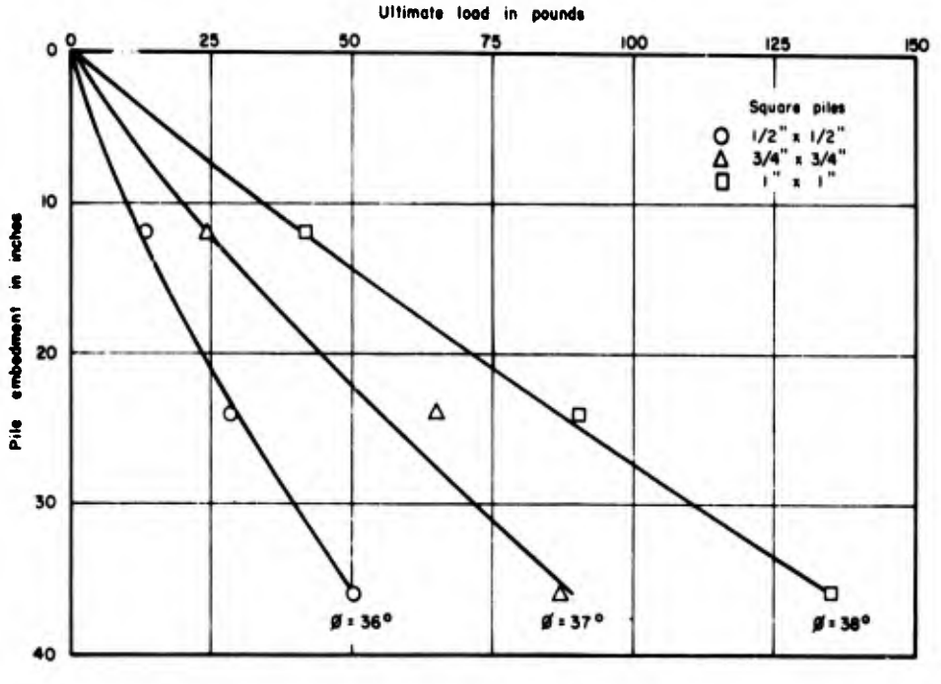

b. SQUARE PILES

BEARING CAPACITY VS DEPTH - TEST SERIES "A"

MODEL TEST

PLATE 47

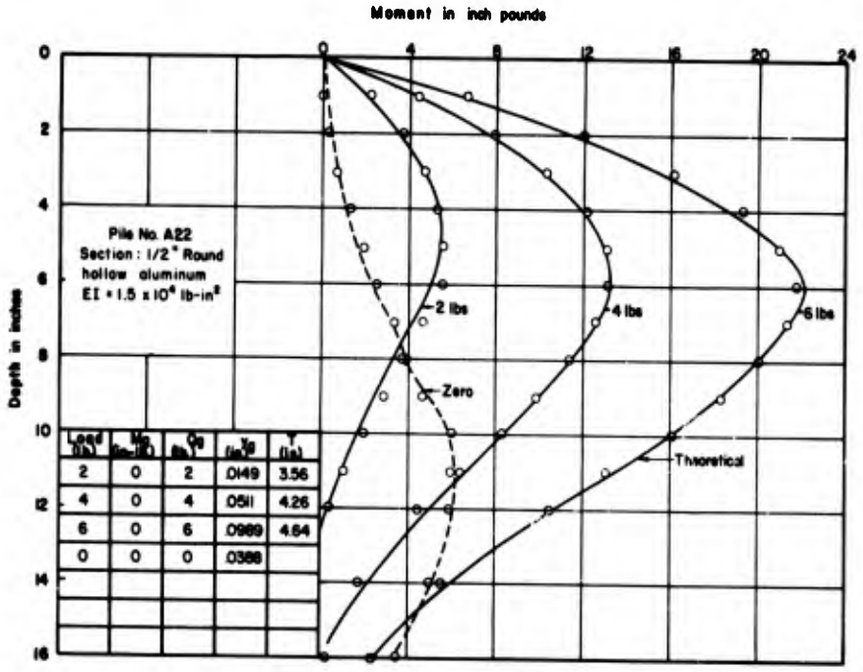

a. MOMENT VS DEPTH

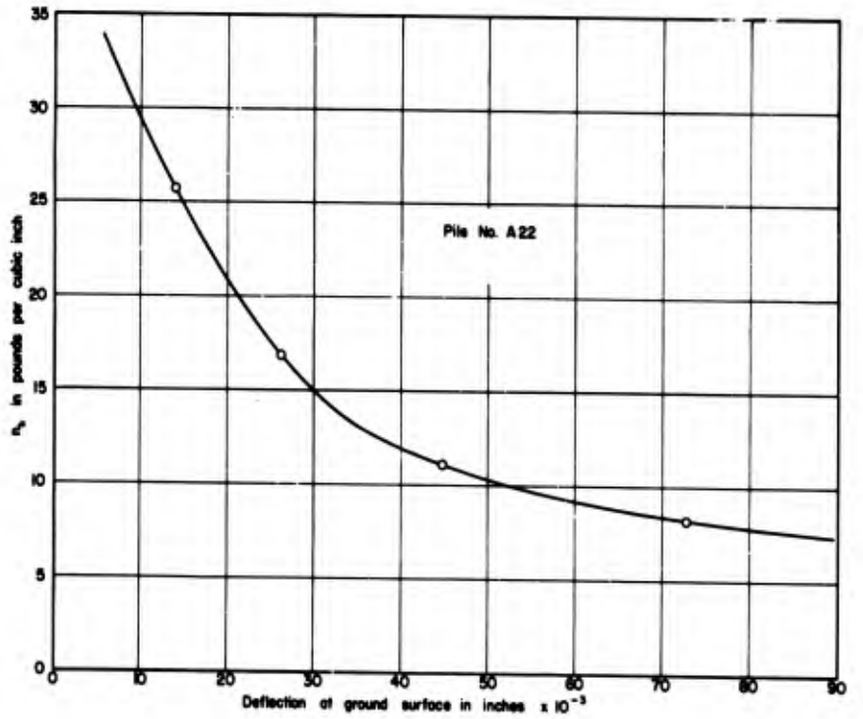

b. COEFFICIENT OF HORIZONTAL SUBGRADE REACTION VS DEFLECTION

LATERAL LOAD TEST RESULTS - MONITOR PILE A 22

MODEL TEST

PLATE 48

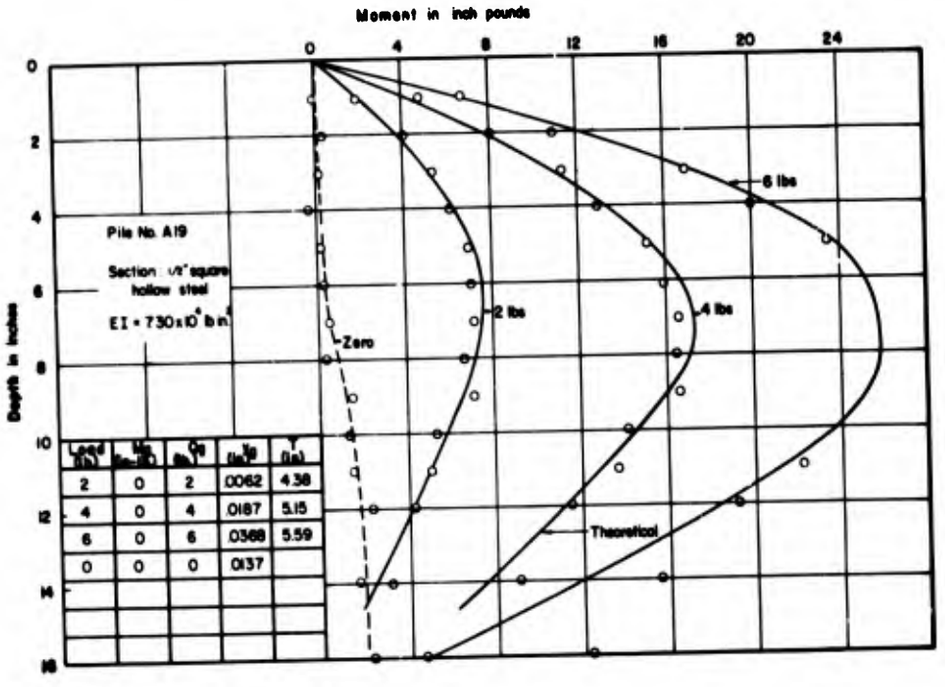

a. MOMENT VS DEPTH - PILE A19

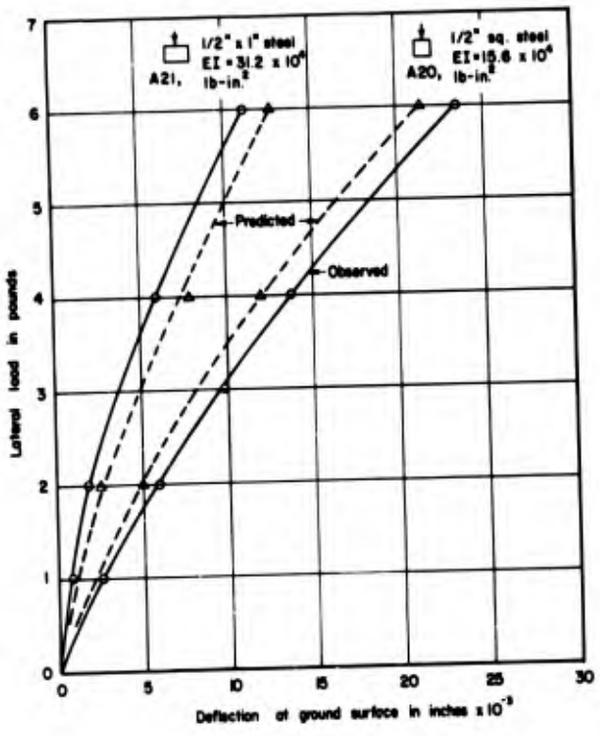

b. LATERAL LOAD VS DEFLECTION - PILES A20,A21

LATERAL LOAD TEST RESULTS - PILES A 19-A 21

MODEL TEST

PLATE 49

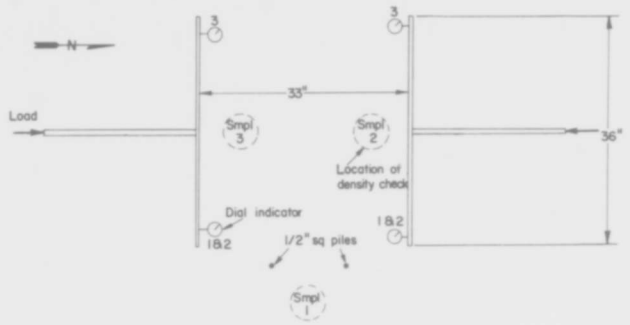

a. PLAN

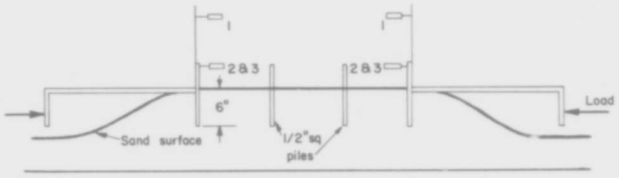

b. SECTION

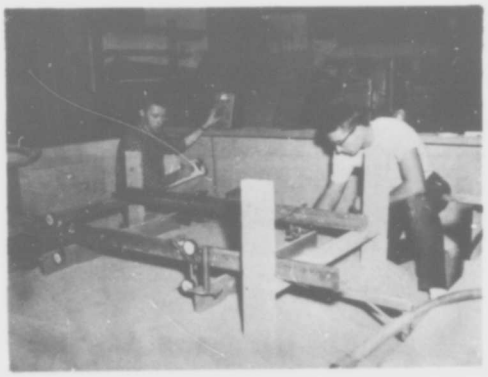

c. TEST WALLS

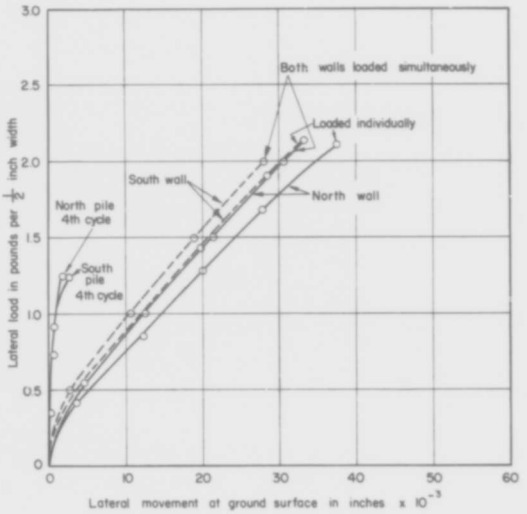

d. LATERAL LOAD VS DEFLECTION

TEST SERIES "B"

MODEL TEST

PLATE 50

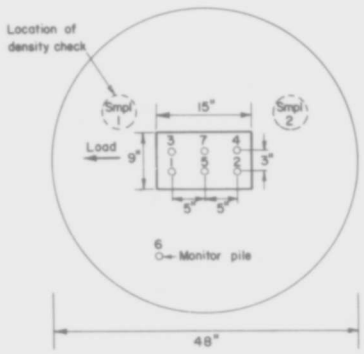

a. PLAN

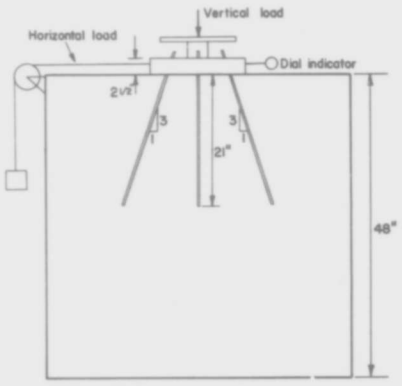

b. SECTION

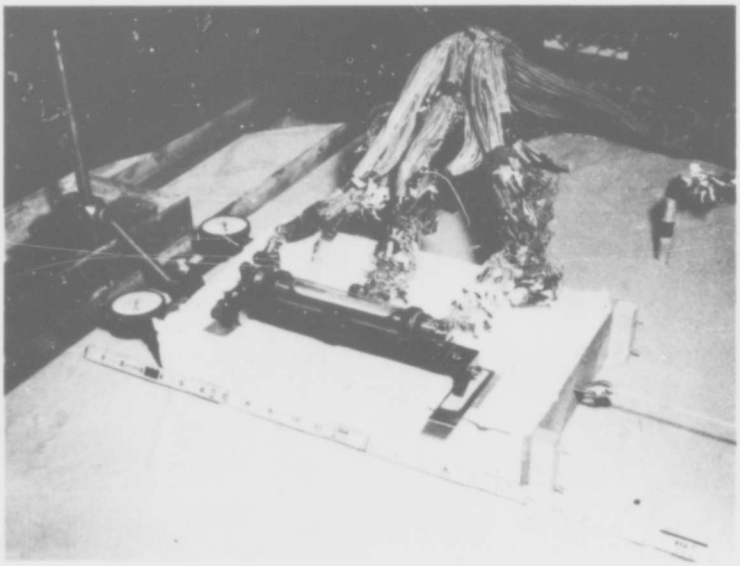

TEST SERIES "C"

MODEL TEST

PLATE 51

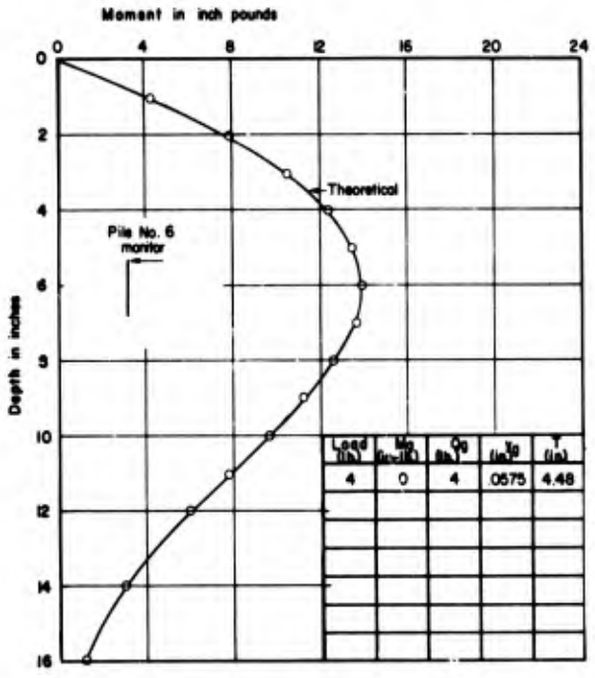

a. MONITOR PILE

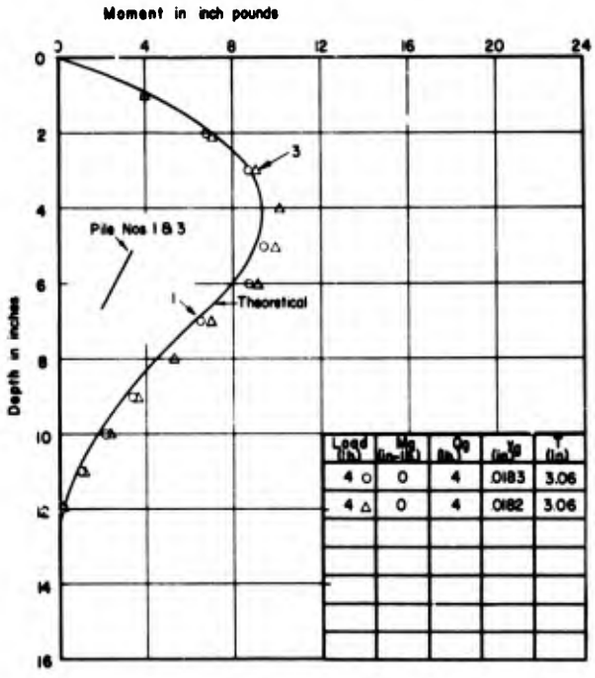

b. PILES 1 AND 3

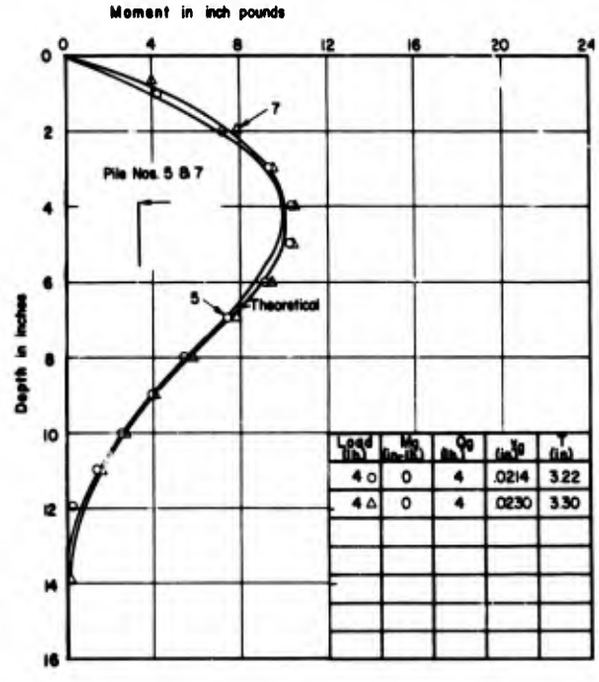

c. PILES 5 AND 7

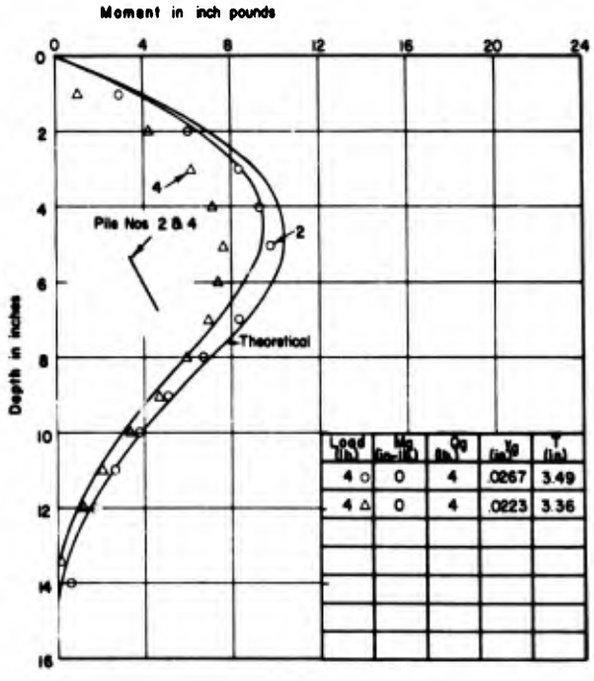

d. PILES 2 AND 4

MOMENT VS DEPTH - TEST SERIES "C"

MODEL TEST

PLATE 52

PLATE 53

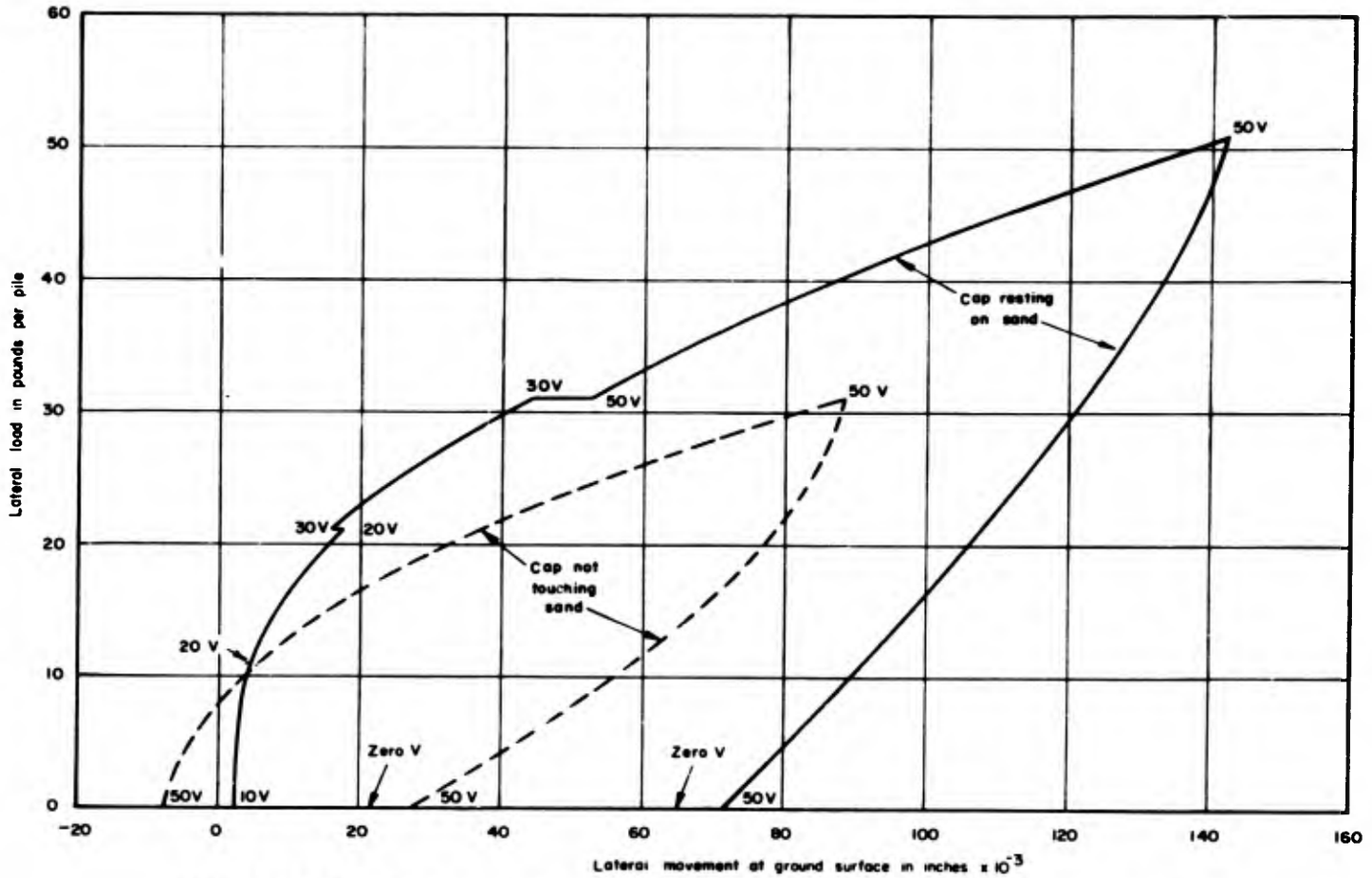

LATERAL LOAD VS DEFLECTION - TEST SERIES "C"

MODEL TEST

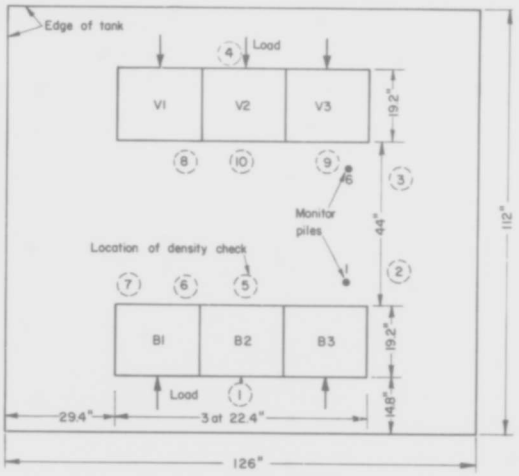

a. PLAN

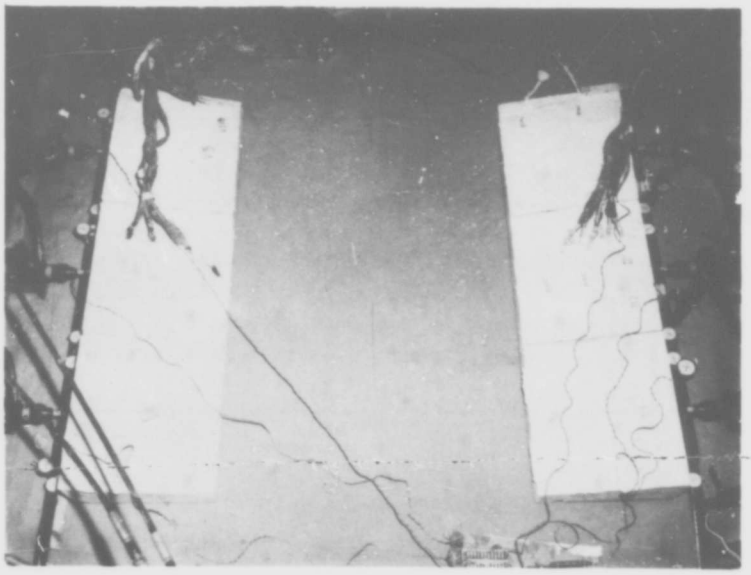

b. PILE CAPS

TEST SERIES "D"

MODEL TEST

PLATE 54

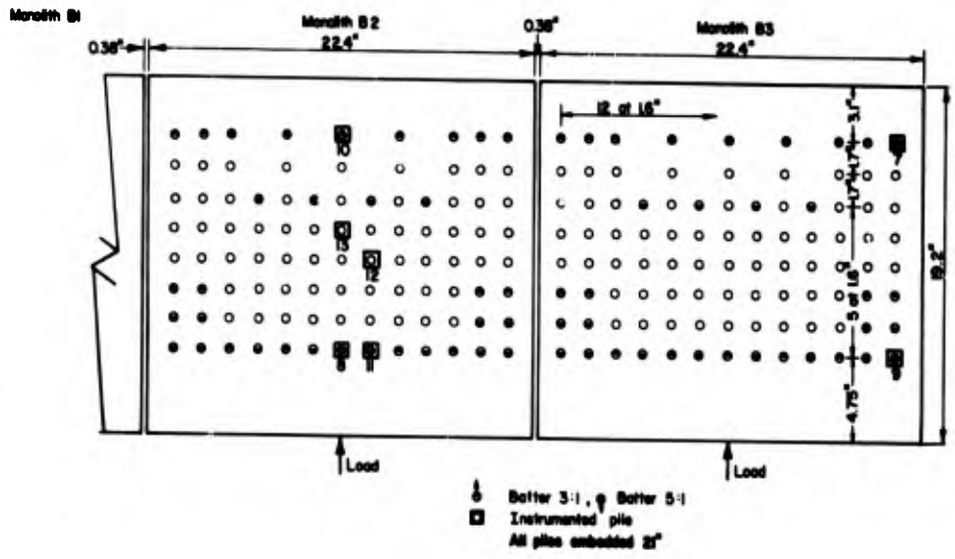

a. MONOLITHS B2 AND B3

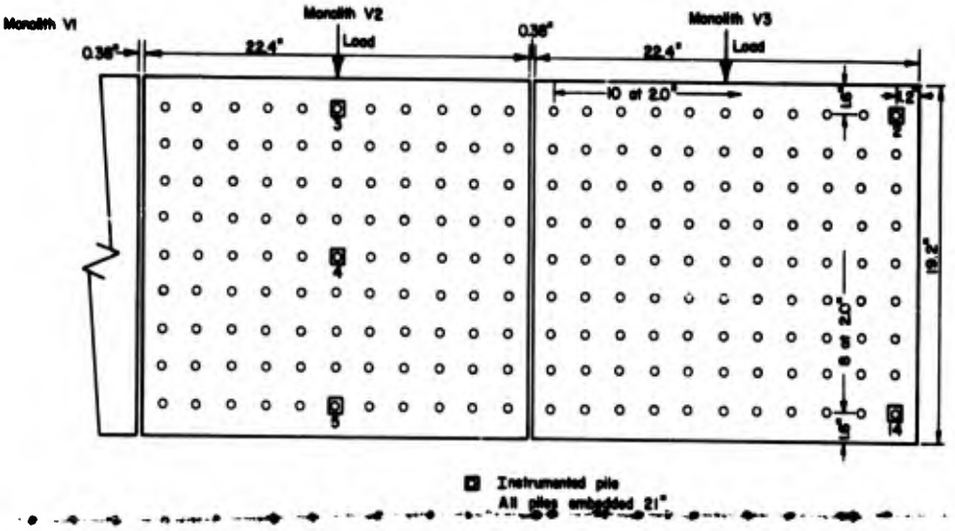

b. MONOLITHS V2 AND V3

PILE SPACING - TEST SERIES "D"

MODEL TEST

PLATE 55

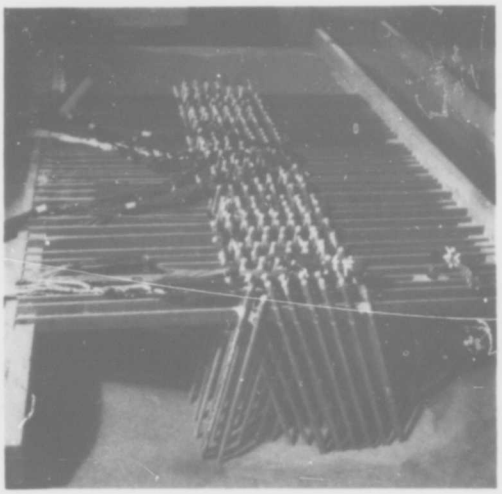

a. MONOLITHS B1 - B3

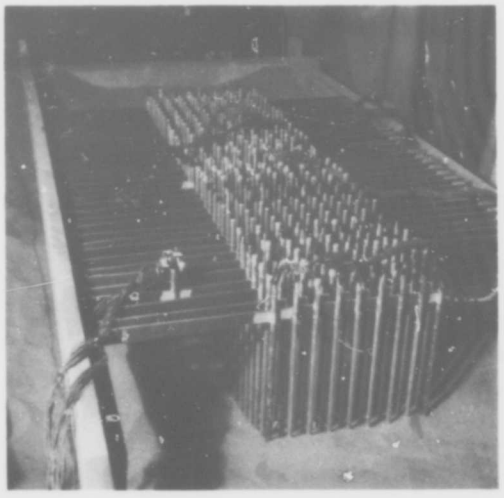

b. MONOLITHS V1 - V3

CONSTRUCTION OF MODEL – TEST SERIES "D"

MODEL TEST

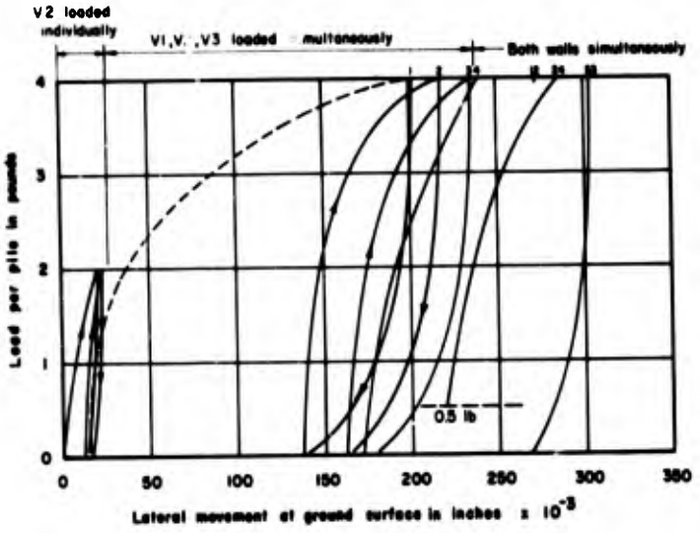

a. MONOLITH V2

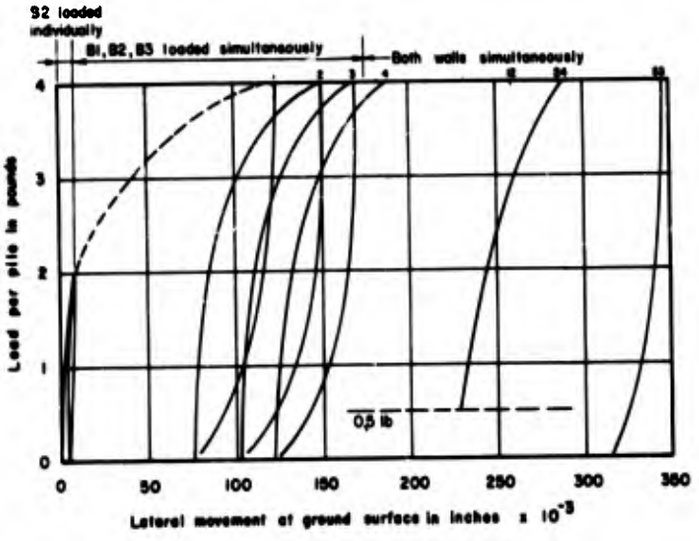

b. MONOLITH B2

LATERAL LOAD VS DEFLECTION - TEST SERIES "D"

MODEL TEST

PLATE 57

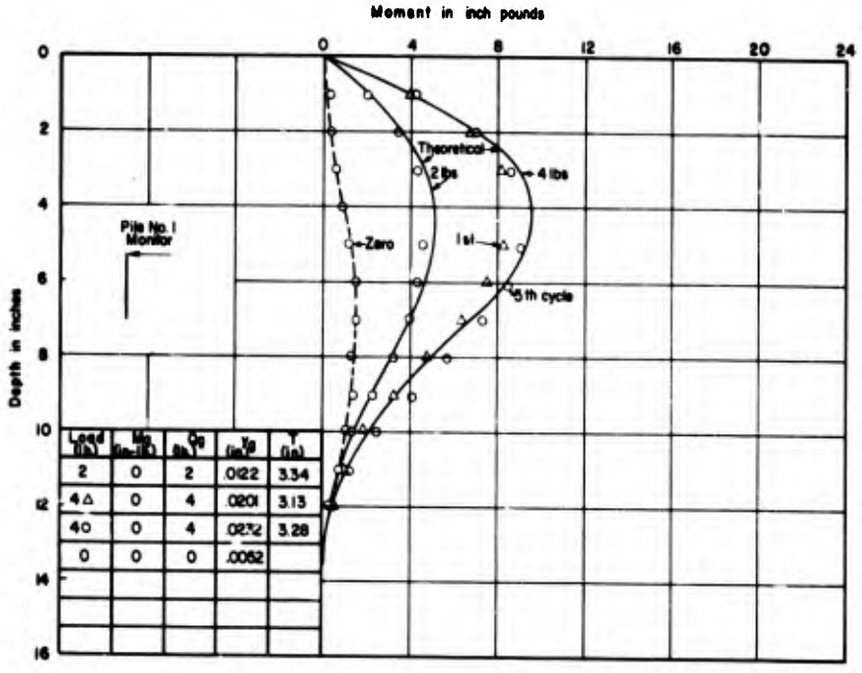

a. MONITOR PILE FOR MONOLITHS B1-B3

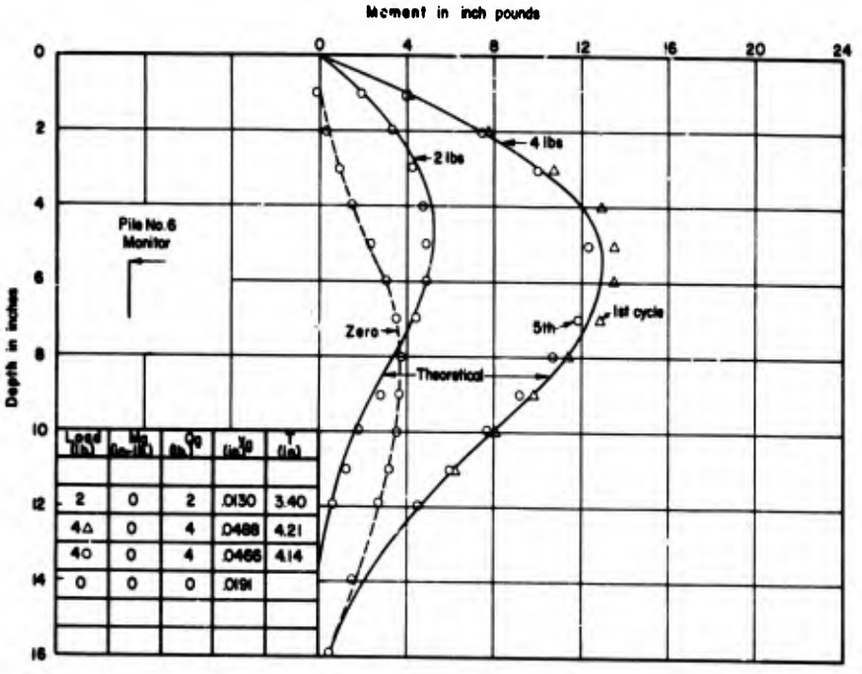

b. MONITOR PILE FOR MONOLITHS V1-V3

MOMENT VS DEPTH - TEST SERIES "D" MONITOR PILES

MODEL TEST

PLATE 58

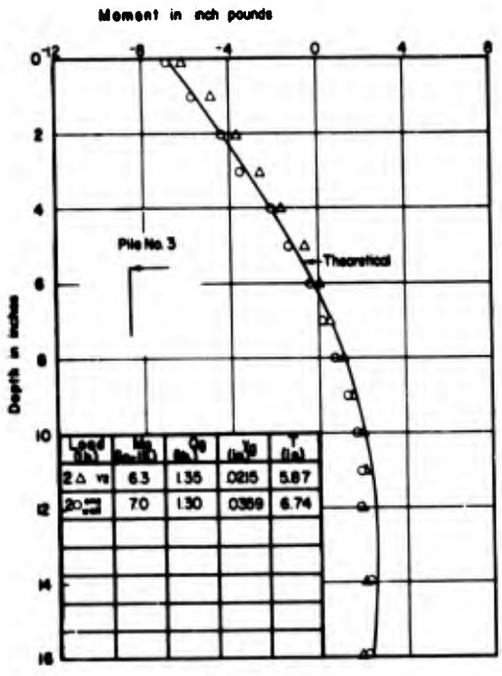

a. MONOLITH V2, PILE 3

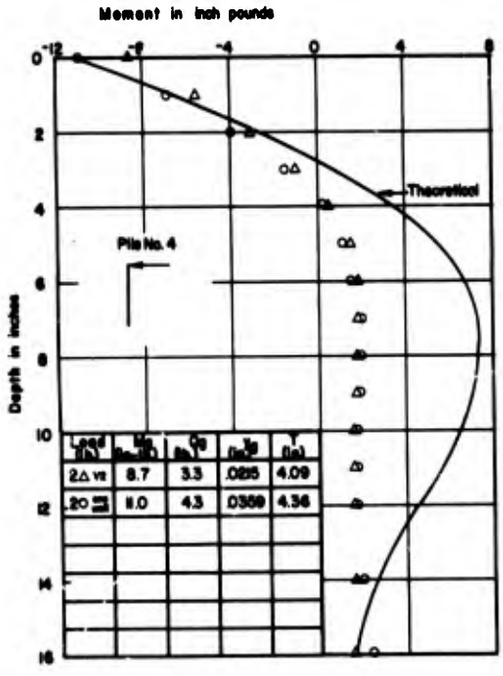

b. MONOLITH V2, PILE 4

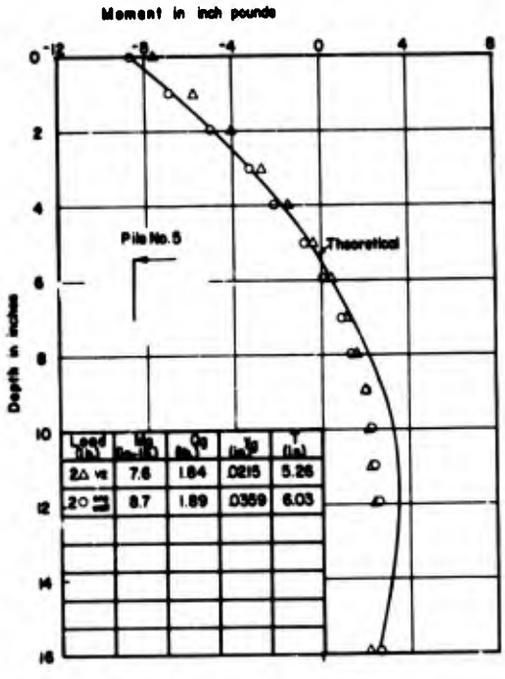

c. MONOLITH V2, PILE 5

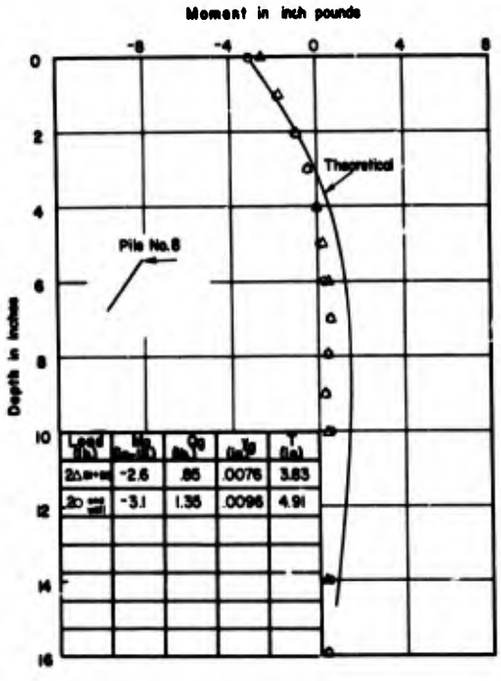

d. MONOLITH B2, PILE 8

MOMENT VS DEPTH - TEST SERIES "D"

MODEL TEST

PLATE 59

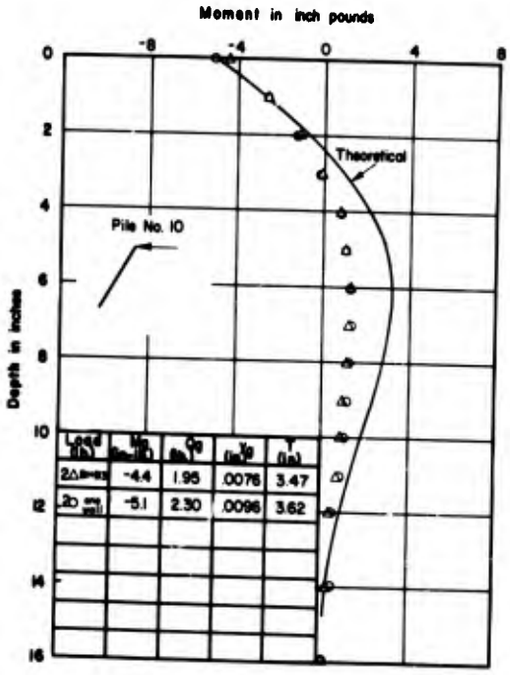

a. MONOLITH B2, PILE 10

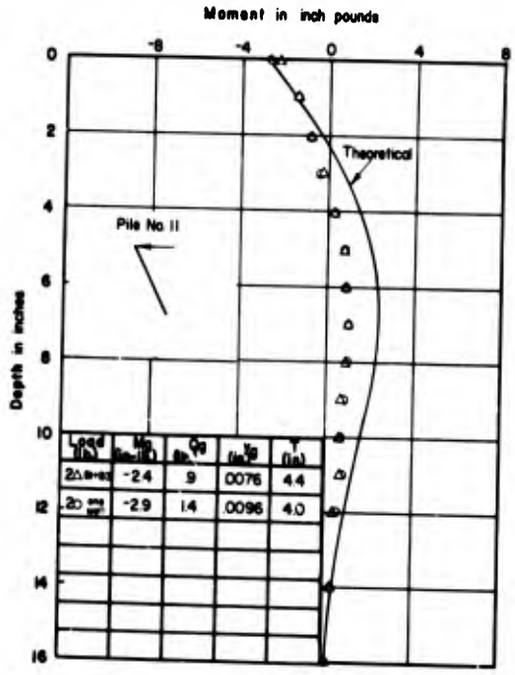

b. MONOLITH B2, PILE 11

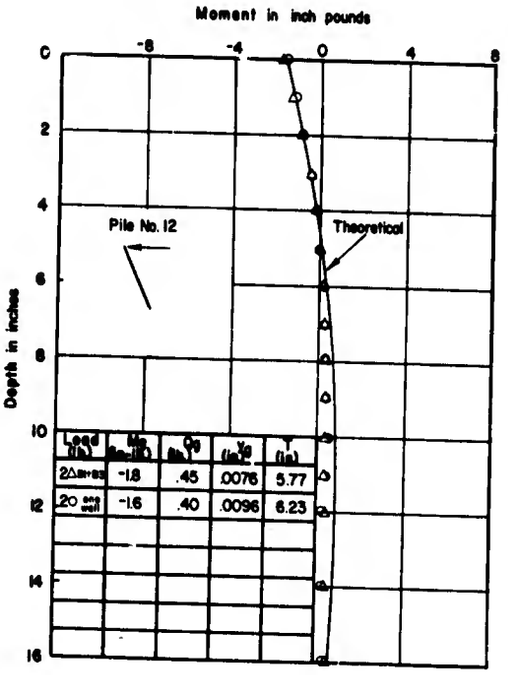

c. MONOLITH B2, PILE 12

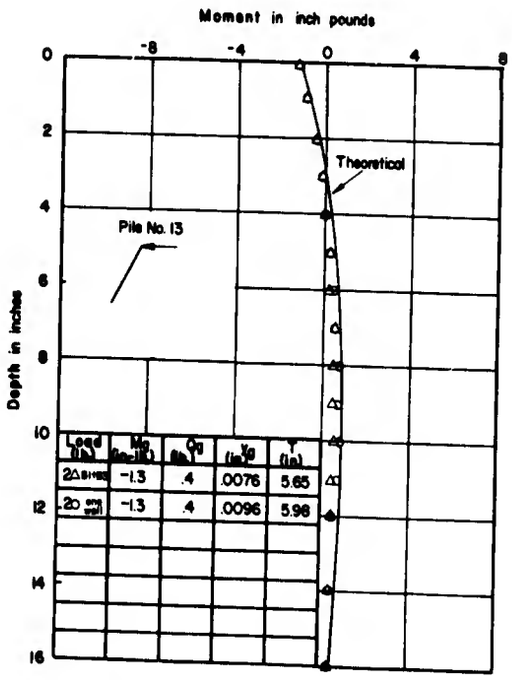

d. MONOLITH B2, PILE 13

MOMENT VS DEPTH - TEST SERIES "D"

MODEL TEST

PLATE 60

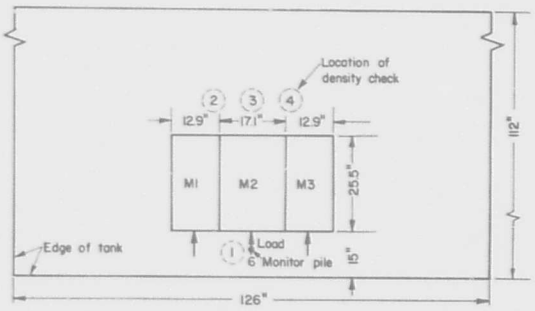

a. PLAN

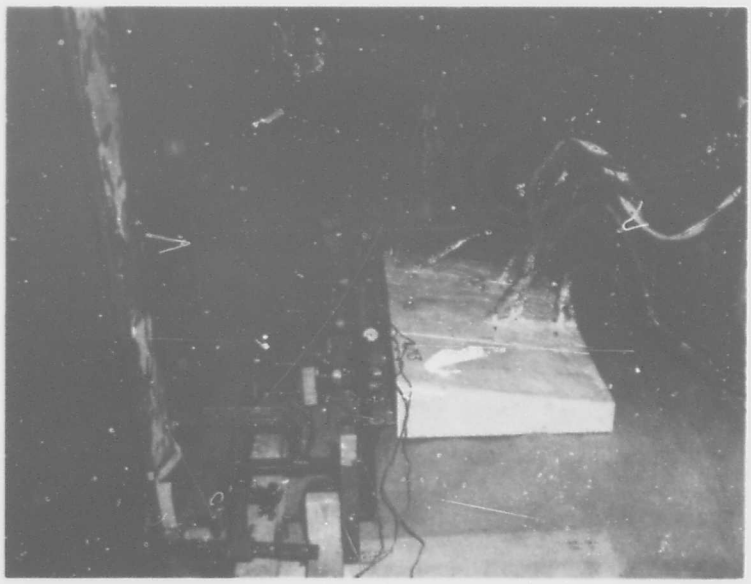

b. PILE CAPS

TEST SERIES "E"

MODEL TEST

PLATE 61

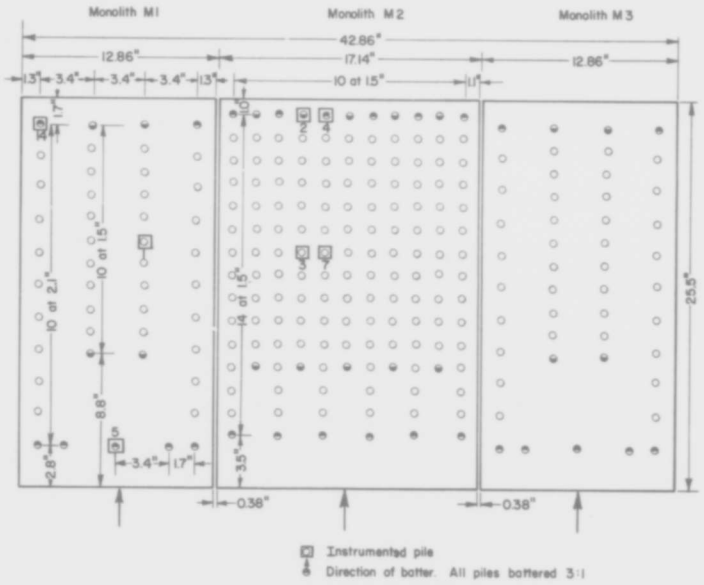

a. MONOLITHS M1 - M3

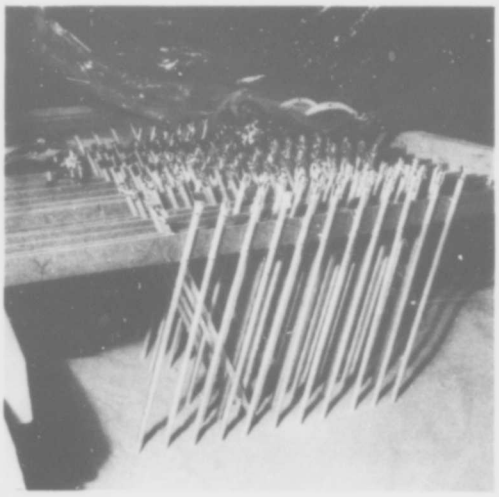

PILE SPACING - TEST SERIES "E"

MODEL TEST

PLATE 62

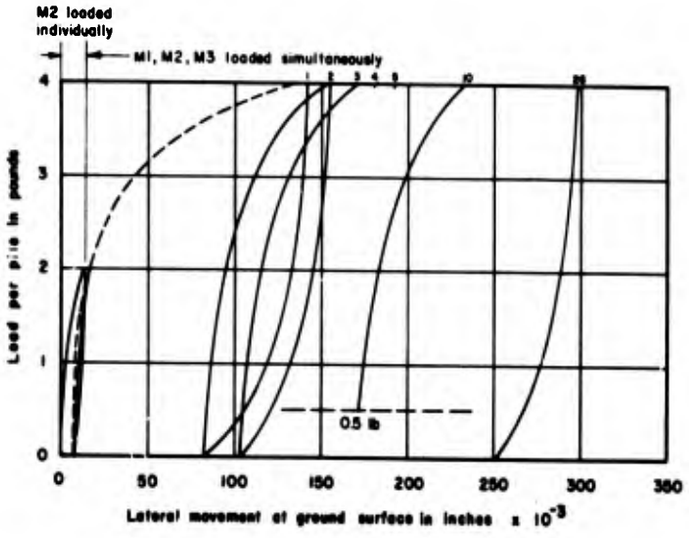

a. MONOLITH M-2

LATERAL LOAD VS DEFLECTION - TEST SERIES "E"

MODEL TEST

PLATE 63

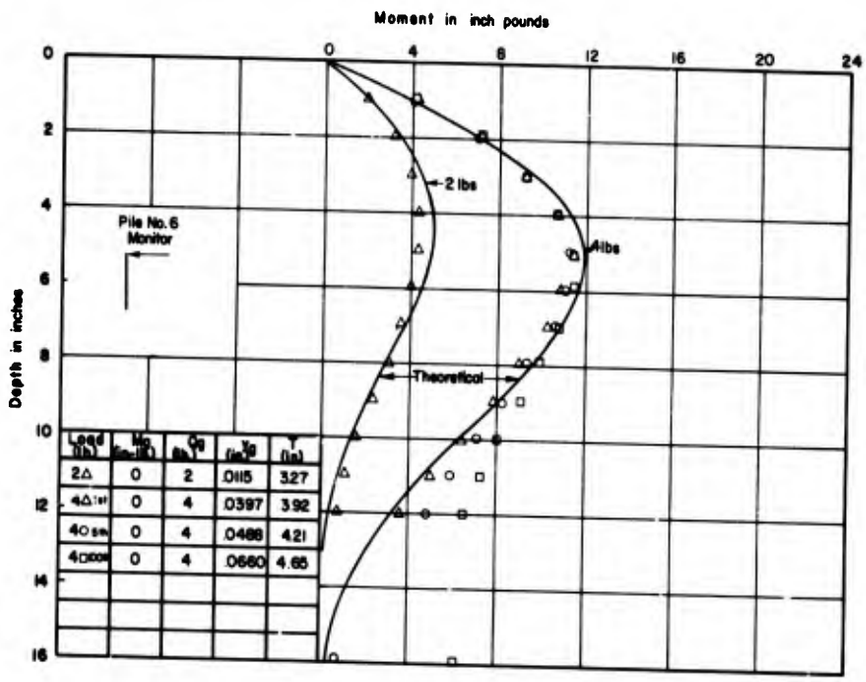

MONITOR PILE

MOMENT VS DEPTH - TEST SERIES "E"

MODEL TEST

PLATE 64

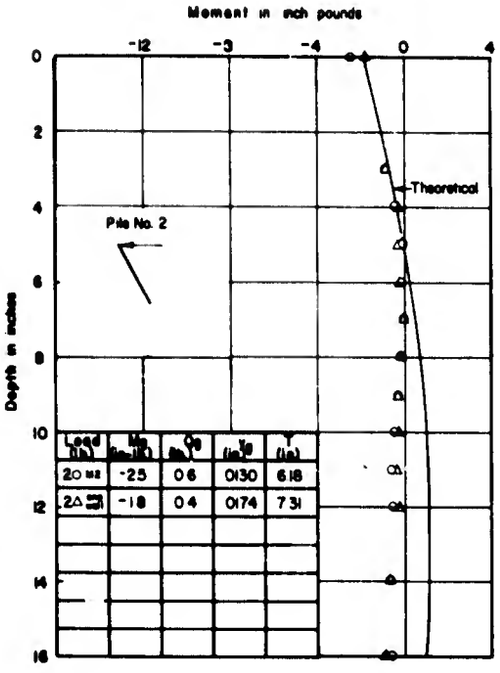

a. MONOLITH M2, PILE 2

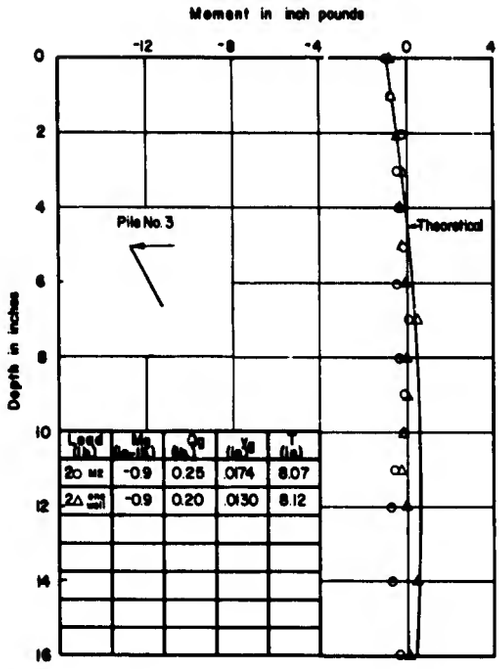

b. MONOLITH M2, PILE 3

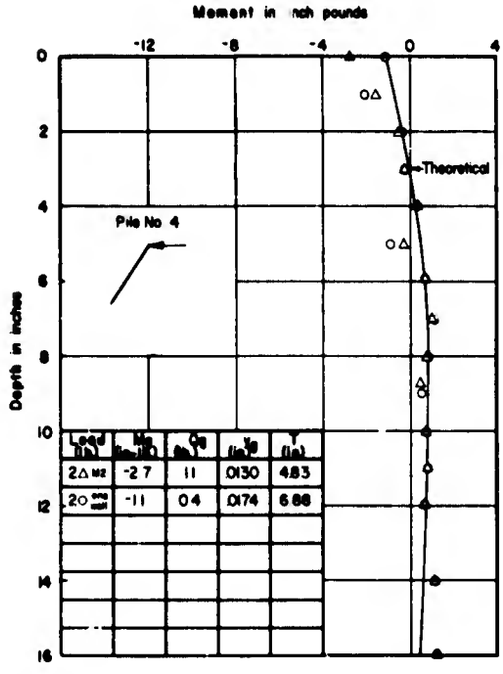

c. MONOLITH M2, PILE 4

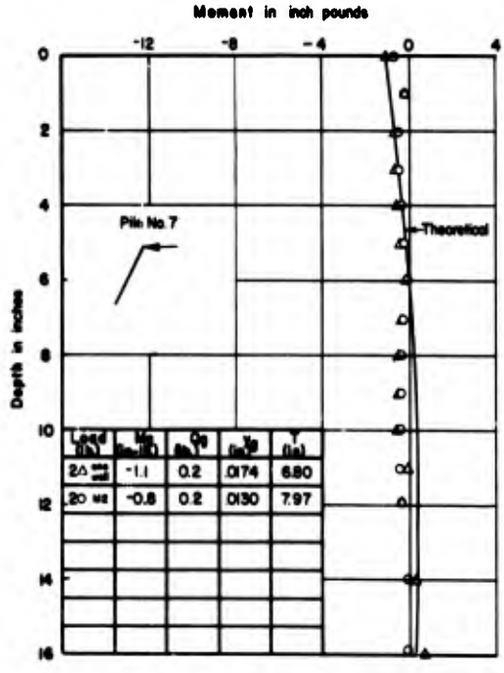

d. MONOLITH M2, PILE 7

MOMENT VS DEPTH - TEST SERIES "E"

PLATE 65

MODEL TEST

Appendix A

MODEL MATERIALS AND CONSTRUCTION

1. In a model testing program it is usually desirable to use the smallest model that will still represent the behavior of the prototype and that, in addition, can be instrumented with sufficient precision to obtain accurate test data. For the laterally loaded pile problem, the properties of the soil and the pile had to be selected in conjunction with each other because the pile behavior depended upon the mutual interaction between the soil and pile.

Sand and Placement Procedure

2. The sand used in this investigation was a fine to medium sand (graph (a), Plate A-1) from the Sangamon River, obtained from the Pontiac Stone Co., Mahomet, Illinois; it was designated as their "blend sand." It was dried by the Champaign Asphalt Company in their aggregate drier. The sand may be described as sub-angular with an effective size (D_{10}) of 0.089 mm and a uniformity coefficient (C_u) of 2.36. The maximum and minimum void ratios (e) were 0.960 and 0.462, respectively, corresponding to dry densities of 85.0 pcf and 113.8 pcf. The minimum void ratio was obtained by placing the sand in a 205 cc brass cylinder in 1/2-in. layers while the sides of the cylinder were vibrated. The maximum void ratio was obtained by placing the sand in a calibrated flask containing water. The water and sand were mixed and the volume of the sedimented sand was read directly from the calibration marks on the flask.

3. A technique was developed for placing the sand with a uniform density following the general recommendations given in Ref 15. According to this reference, a uniformly dense sand can be obtained by a raining technique, provided that each particle has a uniform fall and that a uniform rate of flow is used. It was found that a relative density of approximately 70 percent could be obtained by raining the sand from a 2-in. radiator hose and allowing it to fall 3 ft. The rate

of flow was approximately 0.3 cfm. This technique was used throughout the model testing program.

4. A summary of the sand densities obtained in each test series is presented in Table 12. The average relative density for each series varied from 66 percent for series D to 75 percent for series C, The variation in average density correlates with the interference encountered during the raining of the sand. Very little interference was encountered in Test series B and C; therefore, they have the higher densities. A large amount of falsework was used to support the model piles in Test series D and E; this interfered with the free fall of the sand and lower densities were observed. Test series A was intermediate both in interference and density.

5. The angle of internal friction (ϕ) was determined by a triaxial test on a dry specimen. For a confining pressure of 9.2 psi and a density of 104.0 pcf (72 percent relative density) a ϕ value of 36.4° was obtained.

6. The coefficient of friction of steel against sand was required for use in the analysis of the bearing capacity of the piles in Test series A. The coefficient was obtained by laying a 1-in. square steel bar (this was actually one of the piles) on the surface of the sand. A lateral load was applied to the end of the bar and the load at which sliding took place was measured. Additional tests were performed with weights placed on the bar so that the coefficient of sliding friction could be determined for varying normal pressures. An angle of sliding friction (δ) of 23° was observed.

Pile Properties and Instrumentation

7. All of the instrumented piles, with the exception of the pile used in Test A19, were made of 1/2-in. O.D. aluminum tubing with an 0.035-in, wall thickness (alloy 3003-H14), The total length of the piles was 25 in.; 21-in. was the embedded length. The flexural stiffness (EI) averaged 1.5×10^4 lb $in.^2$, as determined by calibration. A description of the non-standard piles utilized in this program is presented in the sections describing those tests.

8. A total of 28 strain gages was used on each of the 14 instrumented aluminum piles. The locations of the gages with respect to depth are shown (b) on Plate A-1. Starting at 1 in. below the ground surface, the gages were placed in diametrically opposed pairs at 1-in. intervals to a depth of 12 in., and then at 2-in. intervals to a depth of 16 in. Tatnall metal film epoxy strain gages, type No. C12-141B, were used because their 1/4-in. gage length was compatible with the small scale of the models. The gages were temperature compensated for the pile materials at normal laboratory temperatures. In addition, the strain measurement circuitry provided temperature compensation. The strain gages were obtained from the Budd Company of Phoenixville, Pa., with the requirement that the gage factor for all gages be essentially the same. The strain gage specifications are listed below:

Resistance	120± 0.2 ohms
Gage factor	2.08
Gage factor tolerance	0.5%

9. The manufacturer's instructions were carefully followed in applying the strain gages to the model piles. The gages were applied with GA-1 contact cement and allowed to dry for at least 12 hrs. The gages were then covered with two coats of epoxy, Gage Coat 5 and Gage Coat 2, manufactured by the Budd Company. The epoxy coatings served as a waterproofing and also protected the gages and exposed lead wires from direct contact with the sand.

10. The lead wires were connected in the following manner: Holes 3/32-in. in diameter were drilled in the pipe, front and back, between each pair of gages. The lead wires were put through the holes and into the inside of the tube, whence they ran to the top of the tube. No. 32 stranded phono-pick-up wire was used for this purpose, and care was taken that each wire had the same length. These wires were spliced to No. 20 stranded wire which formed the remainder of the leads.

11. Each opposing pair of strain gages was wired through switch boxes to a Baldwin type N strain indicator. The switch box consisted of rotary switches and provided a switch point for each pair of gages. A four-arm Wheatstone bridge circuit was used to permit the separate reading of strain outputs that were correlated with both flexural and

axial loads. One bridge arrangement placed both gages of each pair on the same side of the bridge as shown (c) on Plate A-1. In this case the sum of the individual gages was balanced against the two temperature compensating gages (dummy gages) on the opposite side of the bridge. This arrangement canceled the strains due to axial load, and only flexural strains were read on the strain indicator. The theoretical behavior was confirmed during the calibration of the piles described below.

12. The axial loads in the pile were read directly with the bridge circuit shown (c) on Plate A-1. In effect, the two lower arms of the bridge were reversed from the arrangement used to read moment strains, and one gage was balanced against its diametrically opposed partner. This canceled the flexural strains and only strains due to axial loading were read on the strain indicator. The direct comparison of the gages in this manner automatically compensated for temperature changes, and the dummy gages served only to complete the bridge.

13. A dummy gage was a typical strain gage mounted on a 3-in. long section of the model pile material; it was placed near the active gage so that temperature changes would affect both gages similarly. Thus, with identical resistance changes occurring in both the measuring and compensating gages, no change due to temperature would occur in the indicator reading.

Calibration

14. Gage constants for bending were determined for each pair of gages on each instrumented pile. This was accomplished by supporting each pile on a set of knife edges and placing equal loads on each of two equal cantilever projections. This introduced a condition of pure moment over the central portion of the pile. Care was taken to place the odd-numbered gages on the tension side of the pile, both in the calibration and in the tests. The gage constant was determined by comparing the observed strain with the applied moment for each pair of gages. Preliminary tests showed that the gage constant was essentially the same for different magnitudes of moment. Therefore, the calibration was performed under a moment of 12 in. lb, a moment on the order of that anticipated in the model tests.

15. The gage constants for axial load were determined for the top three pairs of gages on each instrumented pile that was subjected to axial loading. This was accomplished by placing dead weights on an upright pile.. The strain readings were compared with the applied load to obtain the gage constant. The gage constant changed very little with a change in the load level.

16. Any errors in the observed strains could be due to two causes; namely, reading errors and calibration errors. Reading errors refer to the accuracy with which the indicator can be read, estimated as 1 to 2 microinches. For bending, the gage constants were approximately 0.03 in. lb per microinch; with bending moments above 4 in. lb, the reading error would rarely exceed 2 percent. However, the axial load constants are approximately 0.3 lb/microinch, and the reading error could be 20 percent for a 2-lb load. The percentage error decreases with increasing axial load. The second main cause of error would be in the calibration. The gages were calibrated for only one load. It was found that the gage constant actually varied slightly with the load level. The errors may be as large as 4 percent, but generally are less than 2 percent.

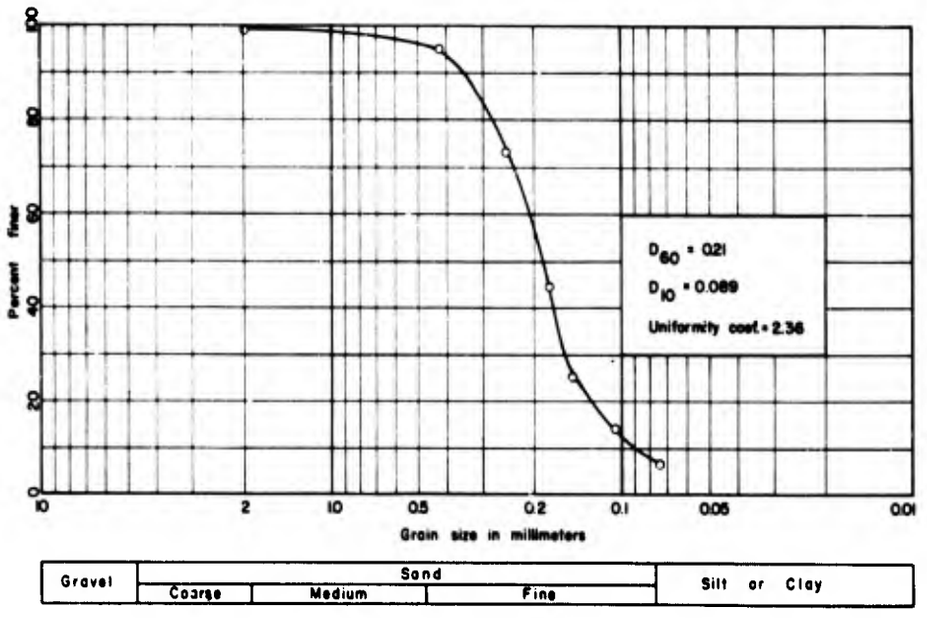

a. GRAIN SIZE CURVE OF SAND

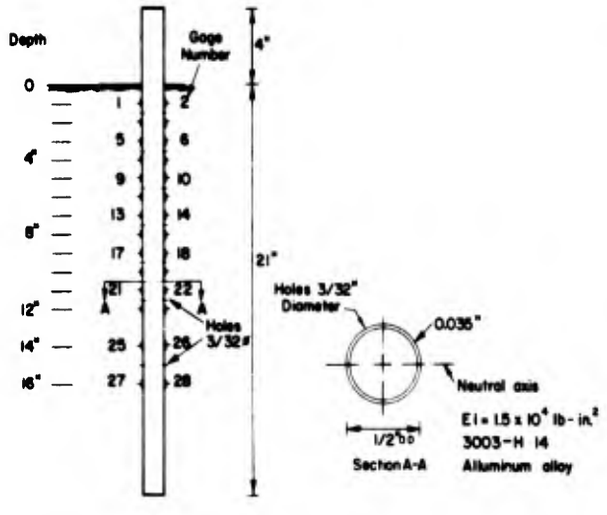

b. MODEL PILE

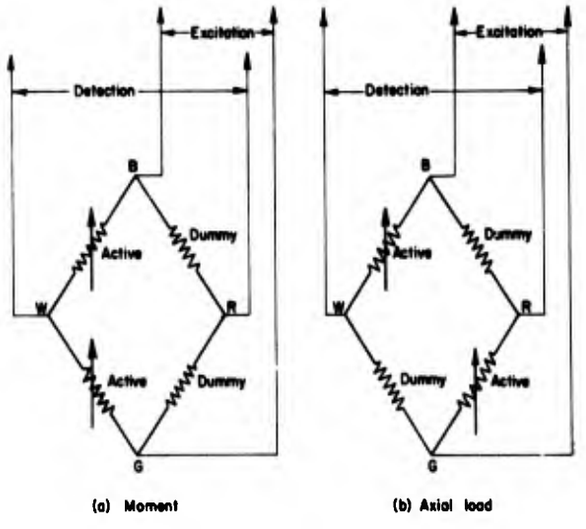

c. INSTRUMENTATION OF MODEL PILES

PROPERTIES OF MODEL MATERIALS

MODEL TEST

PLATE A-1

Appendix B

ANALYTICAL PROCEDURES FOR MODEL STUDIES

1. The procedures used to analyze the lateral load test data obtained in the model program are described in the following sections; a complete discussion of the analytical techniques is given in Ref 12. The same techniques were used to analyze the data from each of the five model test series.

2. On the basis of experience (Ref 13), the modulus of horizontal subgrade reaction applicable to a pile was assumed to be zero at the ground surface and increase linearly with depth. Non-dimensional coefficients are available (Ref 3) that facilitate the solutions for deflections, rotations, moments, shears, and soil reactions for this variation of the horizontal subgrade modulus.

Isolated Piles

3, All the isolated piles were tested with a load applied normal to the pile axis at the ground surface. The deflections were observed at the same point. Moments along the embedded portion of the pile were determined from the SR-4 strain gage instrumentation. The load-deflection relationship for the pile at the ground surface and the bending moment diagram vs embedded depth for the piles were determined from the above observed data.

4. If a triangular variation of horizontal subgrade modulus is assumed, it is possible to determine experimentally the coefficient of horizontal subgrade reaction on the basis of the load-deflection relationship that was observed at the ground surface. This is accomplished by using the analytical expressions obtained from Ref 3 which are summarized in paragraph 55, The deflection at the ground surface is related to the load at the ground surface by

$$Y_g = Y_{zq} \frac{Q_g T^3}{EI}$$

$$\text{or} \quad T = \sqrt[3]{\frac{Y_g \, EI}{Y_{zq} \, Q_g}}$$

$$\text{and} \quad n_h = \frac{EI}{T^5} = \frac{Y_{zq}^{1.667} \, Q_g^{1.667}}{Y_g^{1.667} \, (EI)^{0.667}}$$

$$n_h = \frac{4.42 \, Q_g^{1.667}}{Y_g^{1.667} \, (EI)^{0.667}} \quad \text{for} \quad \frac{\text{embedded length}}{T} > 4$$

where

Y_g = Lateral deflection of the pile at the ground surface in in.

Y_{zq} = A non-dimensional coefficient that depends on the ratio, embedded length/T. For embedded length/T > 4, $Y_{zq} = 2.435$

Q_g = Load normal to the pile axis at the ground surface in lbs

EI = Flexural stiffness of the pile in lb in.^{2}

T = Relative stiffness in in.

n_h = Coefficient of horizontal subgrade reaction in lbs per in.^{3}

T and n_h can be determined by inserting the experimental data (Y_g, Q_g, EI) into the above equations along with the appropriate value of Y_{zq} (Ref 3). Once T has been determined, it is possible to compute the deflections, rotations, moments, shears, and soil reactions with respect to depth by using the non-dimensional solutions in Ref 3.

5. The foregoing use of experimental data to determine the coefficient of horizontal subgrade reaction involves an assumption regarding the variation of subgrade reaction with respect to depth. A check on this assumption can be made by using the experimentally determined moments. On the basis of the solutions given in paragraph 55, together with a knowledge of the load at the ground surface and the magnitude of n_h determined by the above procedure, a theoretical moment diagram for the embedded depth of the pile can be computed. This theoretical moment diagram can be compared with the moment diagram determined

experimentally. If the theoretically determined moment diagram fits the experimental data, then the assumption that the subgrade modulus has a triangular variation is verified.

Piles in a Group

6. The data collected from the tests on the pile groups included the total horizontal load acting on the group, the horizontal deflection, and the bending moments in the instrumented piles in the group. Except for the instrumented piles, it is not possible to analyze each pile individually; it is possible only to treat the behavior of each pile on the basis of an average contribution to the behavior of the group because the distribution of the horizontal load to each pile in the group is unknown.

7. For the instrumented piles it is possible to extrapolate the experimentally observed bending moment diagram to the ground surface. The slope of the bending moment diagram at the ground surface is, theoretically, the shear at the ground surface. The extrapolation of the moment data and the determination of the slope have been carried out graphically. With the moment, shear, and deflection known at the ground surface, it is possible to determine the magnitude of the subgrade modulus on the basis of the assumption that the variation of the modulus is triangular. The deflection at the ground surface is related to the moment and shear acting on the pile at the ground surface by

$$Y_g = Y_{zq} Q_g \frac{T^3}{EI} + Y_{zm} M_g \frac{T^2}{EI}$$

where

Y_{zm} = A non-dimensional coefficient that depends on the ratio, embedded length/T. For embedded length/T > 4, $Y_{zm} = 1.623$

M_g = Moment in the pile at the ground surface in in, lbs

By inserting the experimental data into the above equation, a cubic equation involving T is obtained. The foregoing analysis involves the assumption, as before, that the subgrade modulus has a triangular variation with respect to depth. However, it is possible to compute the

theoretical moments with respect to depth, by using the non-dimensional solutions in Ref 3, and to compare them to the experimentally determined values. If a reasonable fit is obtained, then the assumption regarding the variation of the subgrade modulus is reasonable.

Appendix C

PHOTOGRAPHS

BLANK PAGE

Photo 1a - Timber, Steel Pipe, and Prestressed Concrete Piling at Site

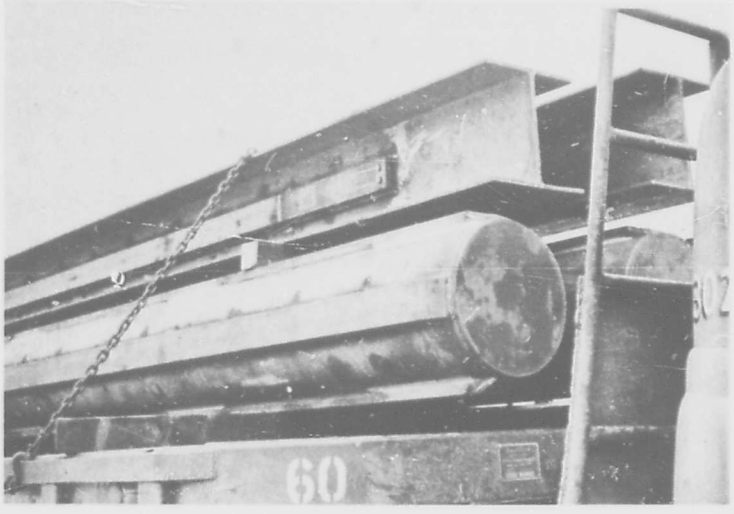

Photo 1b - Steel Pipe and H-Piles Showing Channels for Protection of Instrumentation

Photo c-1. TYPICAL TEST PILES

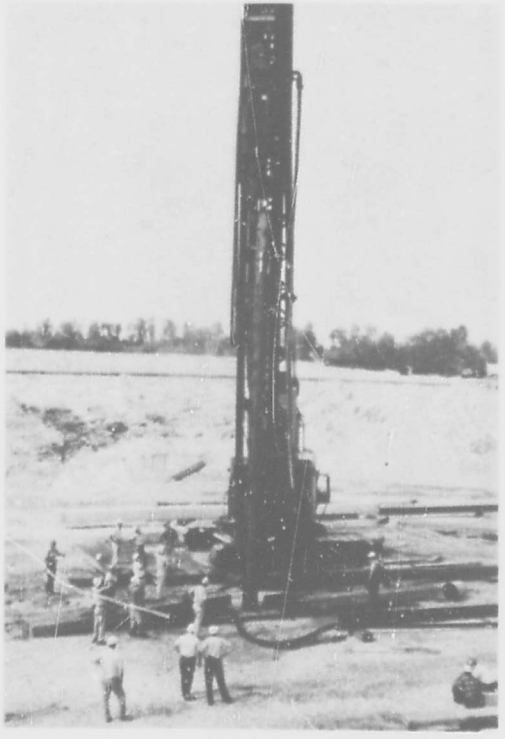

Photo 2a - Placing Timber Pile in Leads Prior to Driving with Vulcan 65C Hammer, Test Pile 8 - Class A Timber Pile

Photo 2b - Driving Steel Pipe Pile with Vulcan 140C Hammer, Test Pile 3 - 20-In. Steel Pipe Pile

Photo c-2. PILE DRIVING WITH STEAM HAMMERS

Photo 3a - Driving Pipe Pile with Bodine Sonic Hammer, Test Pile 10 - 16-In. Steel Pipe Pile

Photo 3b - Driving Steel-H Pile with Bodine Sonic Hammer, Test Pile 9 - 14BP73

Photo c-3. PILE DRIVING WITH BODINE SONIC HAMMER

Photo 4a - Head Attachment for Driving H-Piles with the Bodine Sonic Hammer

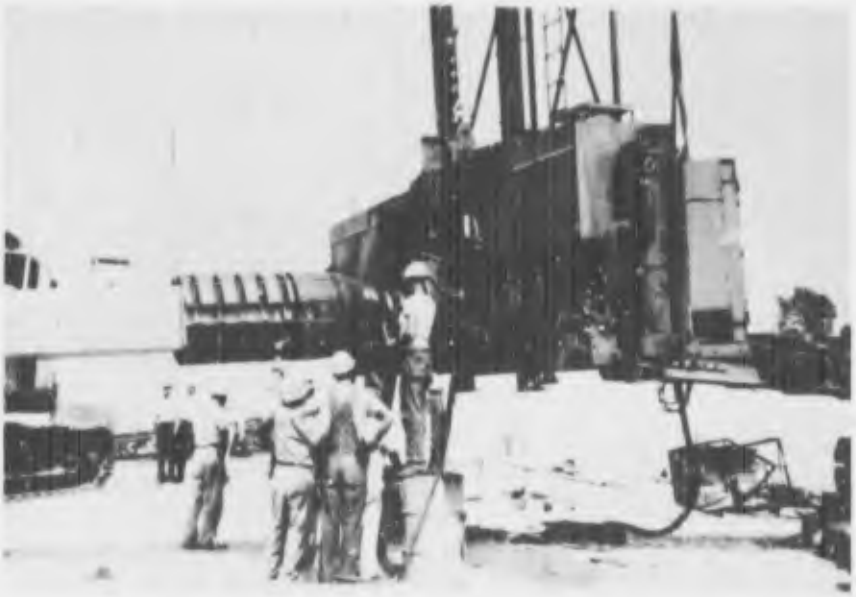

Photo 4b - Head Attachment for Driving Concrete Piles with the Bodine Sonic Hammer

Photo c-4. HEAD ATTACHMENTS FOR THE BODINE SONIC HAMMER

Photo 5a - Compression Load Testing Frame

Photo 5b - Compression Test Assembly and Apparatus, Test Pile 1 - 12-In. Steel Pipe Pile

Photo c-5. COMPRESSION LOAD TESTING

Photo 6-a - Typical Tension Test Loading Apparatus and and Instrumentation, Test Pile 16 - 16-In. Steel Pipe Pile

Photo 6-b - Typical Lateral Load Test Apparatus and Instrumentation, Test Pile 6 - 14BP73 Pile

Photo c-6. PILE TESTING SYSTEMS

Appendix D

RESIDUAL STRESSES IN TEST PILES

1. Throughout the analysis of the load distribution in the test piles as presented in the main text of this report, the assumption was made that no stresses, parallel to the axis of the pile, existed at the beginning of each test. Strain measurements of the piles indicated that this was not always the case. Test program limitations prevented an accurate determination of these stresses at the various stages in the testing sequence; however, an analysis of the load distribution data obtained for two identical steel pipe piles (2 and 10), driven with the 140C and Bodine hammers, was made to estimate residual stresses in the piles after driving and testing. The results of this analysis are presented in the following paragraphs.

General Considerations

2. The magnitude of residual stresses remaining in a pile after driving depend largely on soil conditions and method of driving. Other possible factors would be size, shape, length, and composition of the pile. Residual stresses after driving or testing a pile in sand affect the apparent distribution of stresses in the pile but probably not its total capacity.

3. Test piles 2 and 10 were selected to illustrate the possible effect of residual driving stresses on the distribution of load in the piles. Measured and estimated load distribution curves are shown on Plate D-1 for these test piles.

Test Pile 10

4. Test pile 10 was driven with the Bodine hammer. Curve 1 illustrates the measured load distribution for a compressive load of 230 tons assuming no stress in the pile at the start of the test. Upon removing the compression load, the measured compressive stresses

remaining in the test pile were as shown by curve 2. The stresses shown by curve 2 are residual stresses remaining from the compression test. Curve 3 represents the measured load distribution in the pile for a tension load of 105 tons assuming no stress in the pile at the start of the test; curve 4 represents the measured tensile stress in the pile, under no load condition, after the tension test. Curve 4 indicates an apparent tensile stress in the tip of the pile of about 50 tons. As this is not likely, the curve (4) probably represents residual compressive stresses from driving and compression loading which were released during the tension test plus tensile stresses remaining in the pile after the tension test. As it is known that the compression load test created residual compressive stresses in the pile as shown by curve 2, and as no residual compressive stress should exist after testing a pile to failure in tension, the numerical difference between curve 4 and curve 2 should represent the residual compressive stress from driving plus the residual tension stress from the tension test. There is no way of determining the portion represented by released compressive driving stresses and remaining tension. As there was a time lapse of several days between the end of the compression test and the start of the tension test, there may have been some loss of residual compressive stresses during this interval. Assuming curve 4 to represent only compressive stresses released during the tension test, the estimated distribution of tensile stress can be obtained by subtracting curve 4 from curve 3 as shown by curve 5. On the basis of the above assumption, the compressive load distribution during the compression test would equal the measured distribution (curve 1) plus the numerical difference between curves 4 and 2 as shown by curve 6. The small difference between curves 1 and 6 indicates that residual compressive stresses from driving with a Bodine hammer were small as might be anticipated because of the driving action of such a hammer.

Test Pile 2

5. Test pile 2 was driven with a 140C steam hammer. In general the load distribution curves are similar to those for test pile 10, except that the stress in the pile after the compression loading test

was the same as at the start of the test. From this, it is concluded that the compression test resulted in no increase in residual compressive stress in the pile, and that the residual stresses created by driving and load testing the pile were the same. The difference between curves 1 and 6 indicates that relatively high residual compressive stresses remained in the pile after driving with the 140C hammer. It may be noted that the estimated residual stress, from driving, at the tip of pile 2 driven with the 140C hammer approximately equals the measured residual stress after the compression loading test on pile 10 driven with the Bodine hammer, which created little or no residual stress in the tip during driving.

Other Test Piles

6. All other test piles with strain instrumentation that were loaded in both tension and compression were driven with a steam hammer. Except for test pile 16, these piles (test piles 1, 3, and 7) showed the same load distribution pattern as test pile 2. In test pile 16, which was jetted, residual stresses in the pile from driving were lower than for the other piles. This was evidenced by the increase in compressive stress in the pile from the compression load test. The lower residual driving stresses were probably due to the jetting of the pile.

Conclusion

7. The primary effect of residual compressive stresses in piles is on the measured distribution of the load in the pile. For design of piles in tension the residual driving stress or distribution of load in the pile has no effect on the computed pile capacity. In the design of piles in compression, the distribution of load in the pile may have some effect on the computed pile capacity in that the load is carried by both point bearing and wall friction. In order to check the effect of load distribution on the design curves, the compression load distribution curves for the pipe piles (test piles 1, 2, 3, and 10) were adjusted as illustrated previously and design curves were computed from the adjusted data. For the adjusted curves the average point bearing

load was 50 percent of the applied compression load and the remaining 50 percent was wall friction, and the average computed values of N_q and K were 35 and 0.88, respectively. These values compare with an average point bearing of 30 percent of the applied compression load and 70 percent wall friction as obtained from unadjusted load distribution curves, and computed values of N_q and K of 21 and 1.26, respectively. For the range of lengths and pile diameters in question, the adjusted values of N_q and K generally indicate pile capacities slightly higher than computed from unadjusted data. The maximum effect on the computed pile compression capacity is about 5 percent.

8. In view of the lack of measured data and the numerous assumptions that of necessity had to be made to estimate the residual driving stresses for the test piles, it is considered that the parameters developed from the measured distribution of loads are the most reliable for interpolating or extrapolating the compression load carrying capacity of other size and length piles.

(1) Measured compression load distribution assuming no stress in pile at start of test.

(2) Measured compression load distribution after compression test assuming no stress in pile at start of test.

(3) Measured tension load distribution assuming no stress in pile at start of test.

(4) Measured tension load distribution after tension test assuming no stress in pile at start of test.

(5) Tension load distribution adjusted by subtracting Curve 4 from Curve 3.

(6) Compression load distribution adjusted by adding Curve 4 to and subtracting Curve 2 from Curve 1.

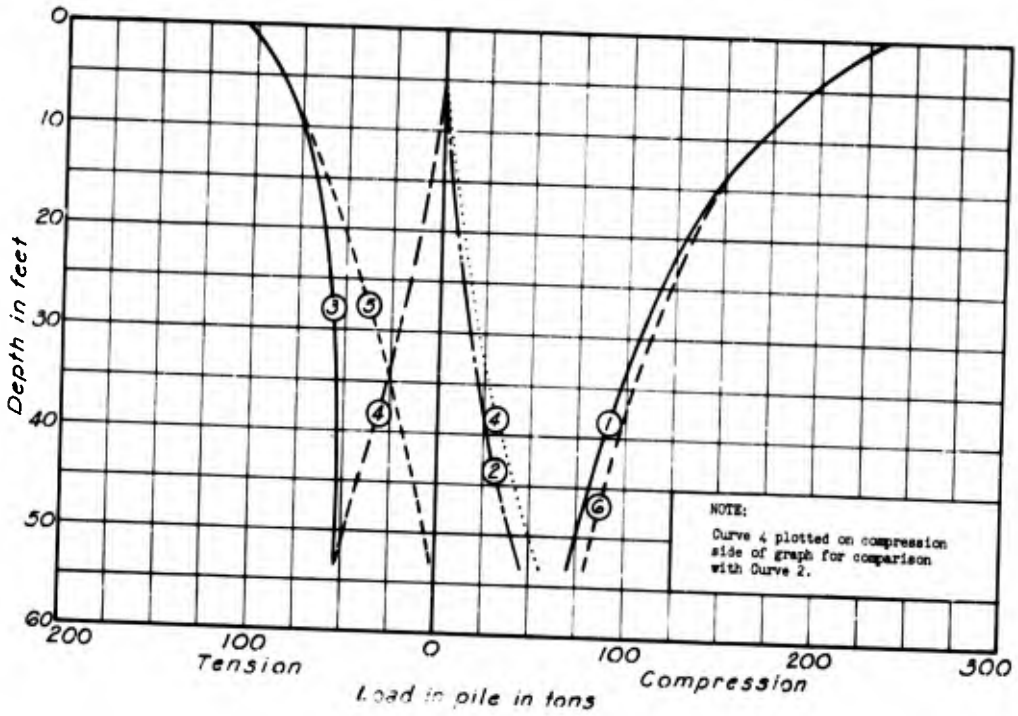

TEST PILE 10
BODINE

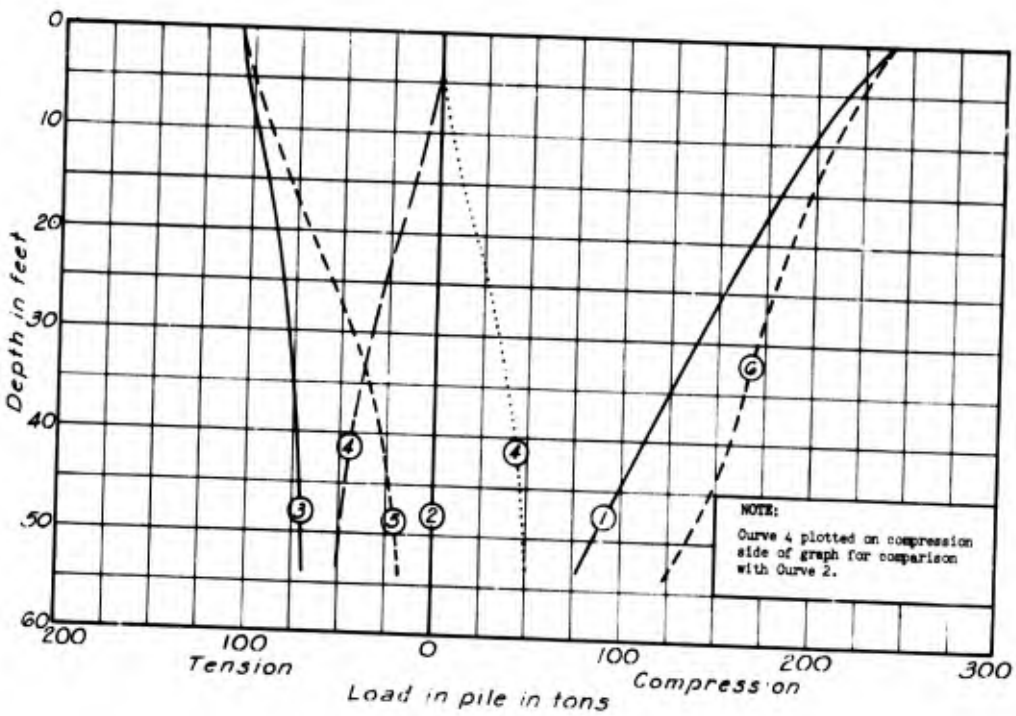

TEST PILE 2, TEST 1
VULCAN 140 C

ESTIMATED RESIDUAL STRESSES IN TEST PILES 2 AND 10

PLATE D-1

Appendix E

PILE DRIVING CRITERIA FOR WATER TABLE BELOW GROUND SURFACE

1. The pile driving criteria set forth in Part III, paragraphs 62 and 65, apply to the case where the ground water table during driving is at or close to grade. When the water table is below the ground surface, the static load capacity of a pile increases considerably; thus, the pile must be driven harder in order to achieve the required capacity under actual service conditions (ground water at or above the top of the piling).

2. Evaluation of the adequacy of driving resistance for any given size of pile, design load, and steam pressure (at hammer) for various water table depths can be made by use of the graphs plotted on Plates E-1 and E-2.

Graph (a) on Plate E-1 is a plot of penetration vs pile capacity for an 18-in. concrete pile for different assumed water table depths. This graph is based on Terzaghi's static equation for pile capacity and parameters developed from the Pile Test Program.

Graph (b) on Plate E-1 is a plot of pile penetration vs a correction factor that must be applied to indicated pile capacities at various water tables in order to obtain the capacity of the pile when the water table is at grade.

Graph (c) on Plate E-1 is a plot of driving resistance vs capacity for an 18-in. sq concrete pile and steam pressure = 120 psi for a 200C hammer for various lengths of piles regardless of depth of water table.

3. Plate E-2 is a plot of pile penetration vs required driving resistance for various water table depths. The curves on this plate are obtained from the graphs on Plate E-1 by the following procedure:

a. For various assumed penetrations obtain factor F for different water table depths from graph (b) of Plate E-1.

b. Multiply design load by factor of safety of 1.5 and factor F for each penetration depth and water table depth.

c. Obtain required driving resistance for each load obtained in step b from graph (c) on Plate E-1.

d. Plot pile penetration vs required driving resistance for various water tables.

3. Graphs similar to Plates E-1 and E-2 can be prepared for various design load, pile size, pile length, and steam pressures.

4. Required driving resistances shown on Plate E-2 do not apply to local hard driving resistances encountered due to discontinuity in the type of subgrade, capillary forces above the water table, or to driving resistances immediately after an interruption in driving.

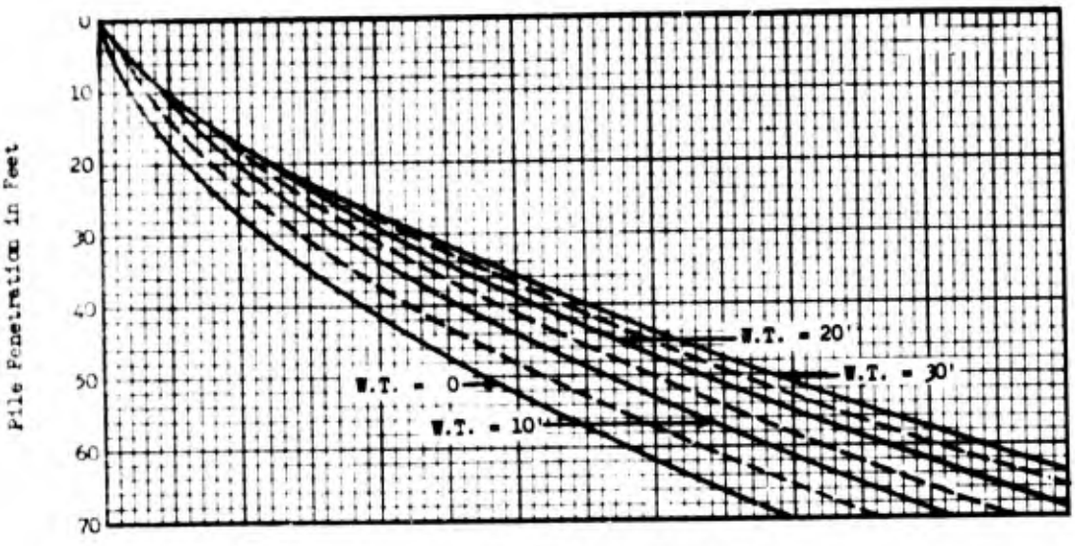

a DESIGN CURVES

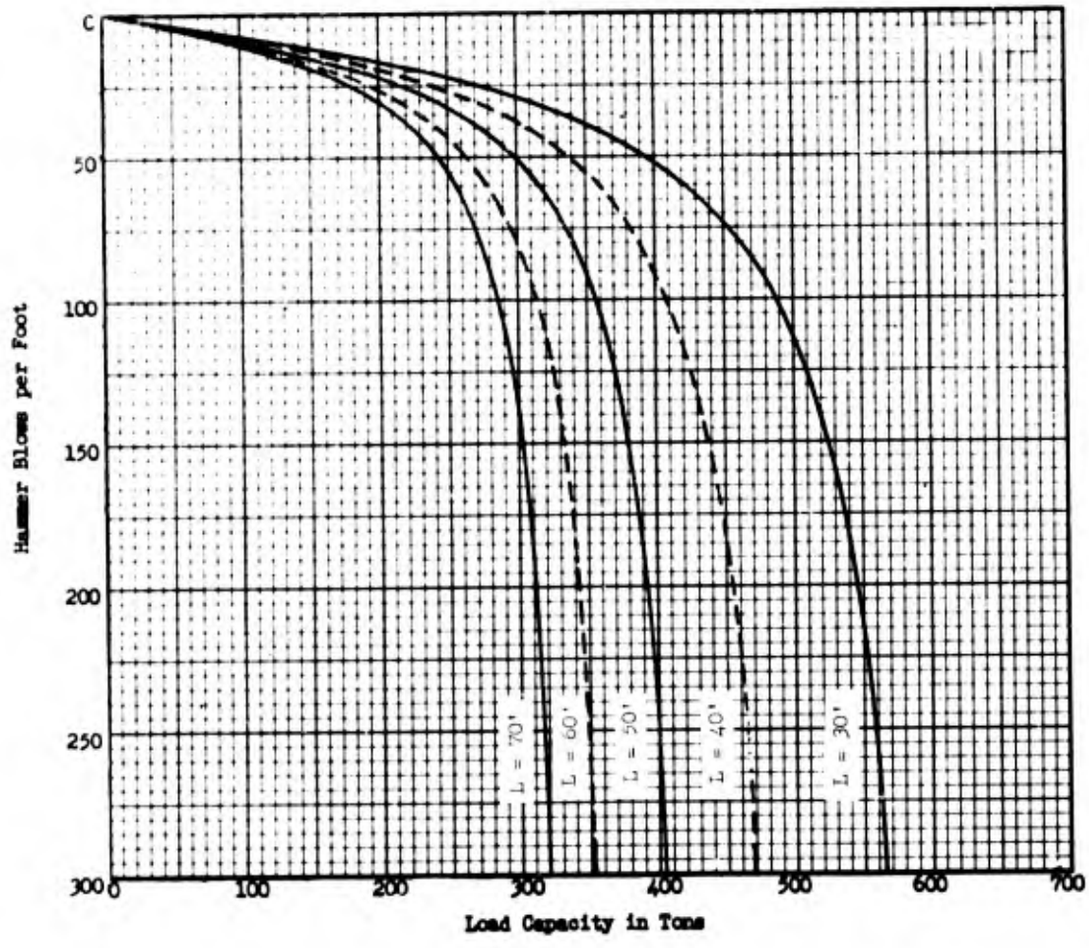

c. DRIVING CRITERIA
FOR STEAM PRESSURE = 120 psi

CRITERIA FOR DESIGN AND
CONCRETE COMPR

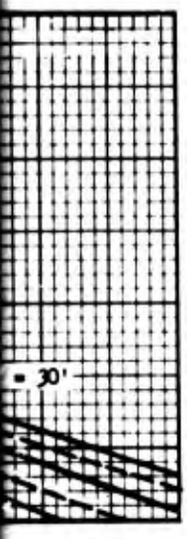

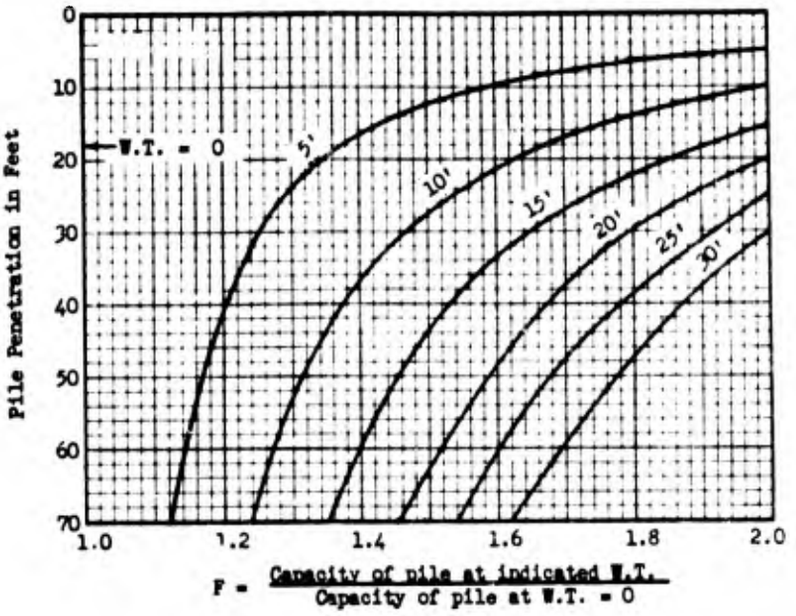

b PILE PENETRATION VS "F" FACTOR

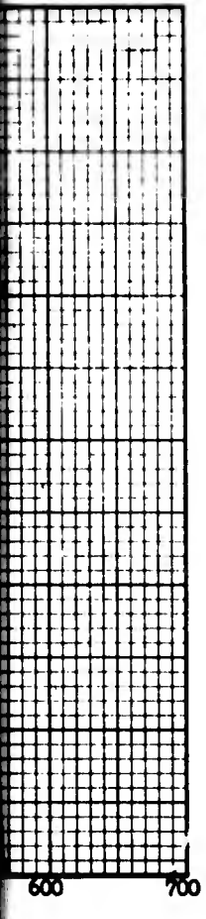

Static Formula: Terzaghi's expression for the static capacity of deep piers

Tip Bearing Capacity Factor $N_q = 21$

Lateral Earth Pressure Coefficient $K = 1.5$

Friction Angle of Concrete on Sand = 30°

Moist and Submerged Density of Sand = 124 pcf, = 62 pcf, respectively

Dynamic Formula: Pacific Coast Uniform Building Code

Hammer: Super-Vulcan 200C

Concrete Modulus of Elasticity = 5×10^6 psi

DESIGN AND DRIVING FOR 18-INCH
CRETE COMPRESSION PILE

B

PLATE E-1

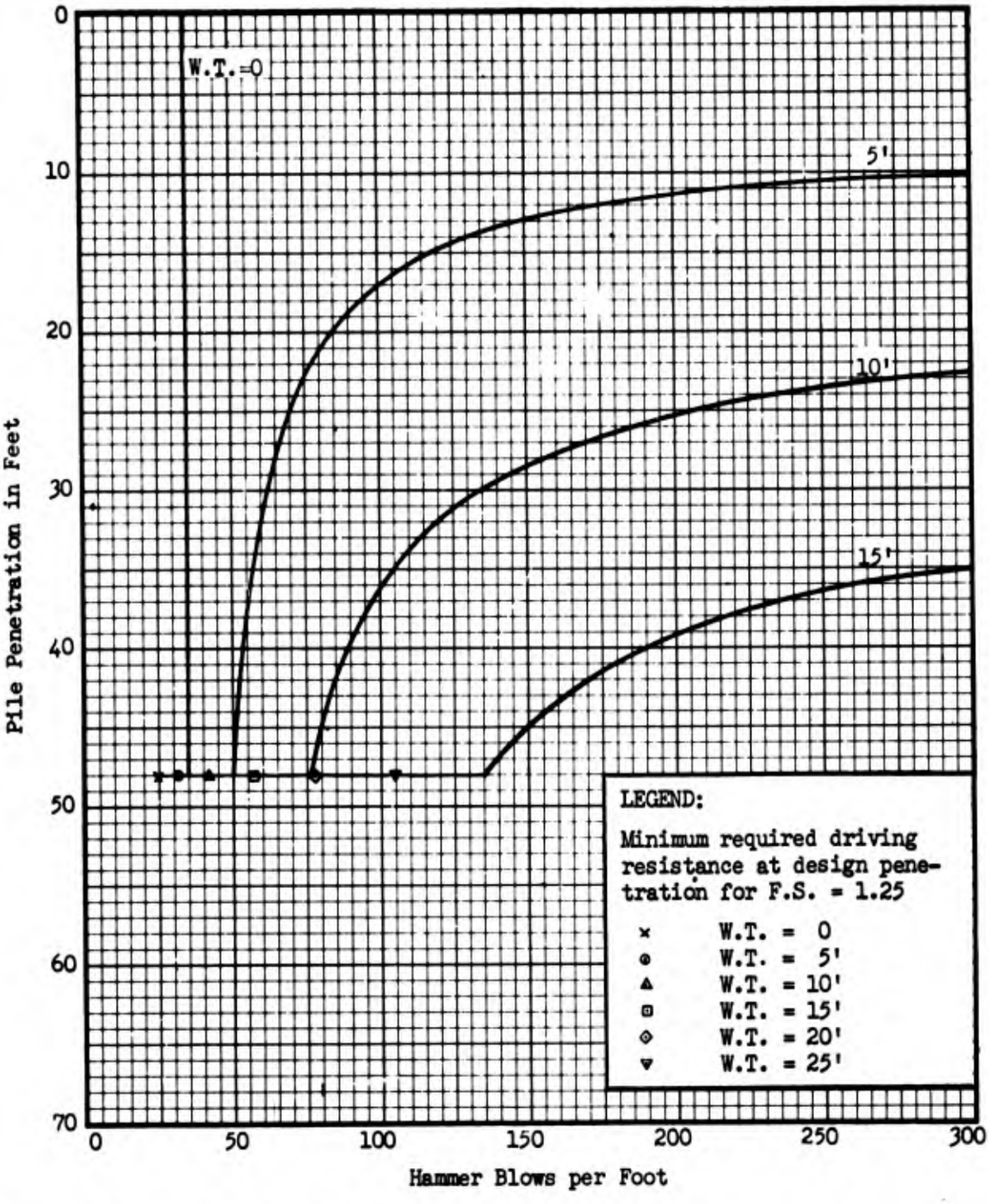

Note: Graph is based on Pacific Coast Uniform Building Code Dynamic Pile Driving Formula, and F.S. = 1.5

Concrete Modulus of Elasticity = 5×10^6 psi

Hammer = Super Vulcan 200 C

Pile Size = 18" Sq

Pile Length = 50'

Pile Design Load = 170 Tons

Steam Pressure = 120 psi

REQUIRED DRIVING RESISTANCES FOR COMPRESSION PILES

PLATE E-2

Unclassified

Security Classification

DOCUMENT CONTROL DATA - R & D

(Security classification of title, body of abstract and indexing annotation must be entered when the overall report is classified)

1. ORIGINATING ACTIVITY *(Corporate author)*
FRUCO & ASSOCIATES
1706 Olive Street
St. Louis 3, Missouri

2a. REPORT SECURITY CLASSIFICATION
Unclassified

2b. GROUP

3. REPORT TITLE
PILE DRIVING AND LOADING TESTS, LOCK AND DAM NO. 4 ARKANSAS RIVER AND TRIBUTARIES, ARKANSAS AND OKLAHOMA

4. DESCRIPTIVE NOTES *(Type of report and inclusive dates)*
Final Report

5. AUTHOR(S) *(First name, middle initial, last name)*
CHARLES I. MANSUR
A. H. HUNTER

6. REPORT DATE
September 1964

7a. TOTAL NO. OF PAGES
82

7b. NO. OF REFS
15

8a. CONTRACT OR GRANT NO.
DA-03-050-CIVENG 64-17

b. PROJECT NO.

c.

d.

9a. ORIGINATOR'S REPORT NUMBER(S)
None

9b. OTHER REPORT NO(S) *(Any other numbers that may be assigned this report)*
None

10. DISTRIBUTION STATEMENT
This document has been approved for public release and sale; its distribution is unlimited.

11. SUPPLEMENTARY NOTES

12. SPONSORING MILITARY ACTIVITY
U.S. Army Engineer District
Little Rock, Arkansas

13. ABSTRACT
Field driving and loading tests were made on a variety of piles driven with different hammers to develop criteria for the design and construction of pile foundations in sand for locks and dams on the lower Arkansas River. The effect of jetting on the capacity of a pile was determined. Steel pipe and H-piles were instrumented to measure strains produced by compression and tension loadings to determine the distribution of stress in the piles. Load tests were also made on piles driven during construction of some of the locks in the lower valley. The pile tests showed that 12-in. to 16-in. 50-ft long displacement piles driven into the alluvial sands in the Arkansas River Valley have capacities in excess of 100 tons in compression, and 50 tons in tension. The pile capacity was the same regardless of hammer used to drive the pile. Compression test failure loads checked capacities calculated from the Pacific Coast Uniform Building Code and the Janbu equation except for H-piles.

DD FORM 1 NOV 65 1473 REPLACES DD FORM 1473, 1 JAN 64, WHICH IS OBSOLETE FOR ARMY USE.

Unclassified

Security Classification

14. KEY WORDS	LINK A		LINK B		LINK C	
	ROLE	WT	ROLE	WT	ROLE	W
Pile foundations						
Pile structures						
Soil mechanics						
Foundations						
Locks & Dams (Waterways)						
Compression pile tests						
Tension pile tests						
Lateral pile tests						